UNIVERSIDAD DE MÁLAGA

FACULTAD DE CIENCIAS

DEPARTAMENTO DE QUÍMICA FÍSICA

Tesis Doctoral

Birradicales Kekulé: Espectroscopía Raman en la Transición Singlete-Triplete

José Luis Zafra Paredes

Málaga, 2014

Publicaciones y
Divulgación Científica

AUTOR: José Luis Zafra Paredes

EDITA: Publicaciones y Divulgación Científica. Universidad de Málaga

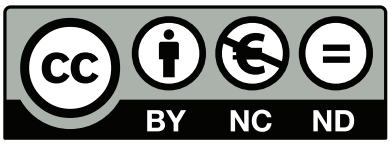

Agradecimientos

Tras unos meses ajetreados, llenos de plazos y urgencias, me alegra poder hacer un alto en el camino para mirar atrás. Significa que se acerca el momento de cerrar una etapa, no por dura y llena de esfuerzo menos gratificante. Porque en estos cuatro años mal contados ha sido mucho lo aprendido y muchos los buenos momentos vividos, es hora de dar las gracias.

A mis directores de Tesis, Teo y Juan. A nadie se le escapa que este trabajo, del que me siento orgulloso, no es más que una nueva muestra de su enorme nivel científico, fruto de la pasión, tenacidad y brillantez con la que día a día afrontan los vaivenes propios de la investigación. A ellos les debo muchas cosas pero, sobre todo, les doy gracias por su apoyo y confianza, y por haberme hecho sentir siempre "como en casa". Me siento muy afortunado de haber trabajado con vosotros.

Del buen recuerdo que me llevo de esta etapa predoctoral son en gran medida responsables las personas con las que he compartido sobremesas, café, viajes y sobre todo risas. A mis compañeros de "fatigas": Belén, María, Cris, Rafa, Dani, Miriam, Guzmán, Iratxe, Estefanía, Sandra, Reyes y Gwen, muchas gracias por estar siempre ahí. Gracias también a Rocío, a quien pude ver partir recién doctorada y volver como Ramón y Cajal, sin perder ni un ápice de naturalidad y ganas de ayudar. Muchas gracias también a Mª Carmen, una de esas personas de las que sólo escuchas cosas buenas y que es mejor todavía cuando la conoces. Para el final he querido dejar a mi debilidad (con permiso de Dani) y la fan número uno de mis canturreos en el laboratorio: muchas gracias por tu cariño Paula, sé lo mucho que has sufrido por mi naturaleza tranquila, "destartalá" y distraída pero no te preocupes, que me he comprado una agenda y amenazo con usarla.

No me puedo olvidar de agradecer a los demás miembros del grupo de investigación y del Departamento de Química-Física, en especial a Javier quien, hace ya seis años, me introdujo en la espectroscopia vibracional y siempre me ha echado una mano en todo lo que he necesitado; y a Víctor, capaz siempre de arrancarme una sonrisa y que me ha enseñado a cambiar el desecante del Tensor 27, entre otras muchas

cosas. Gracias también a Joaquín, Juan Carlos Otero, Juan Soto, Juan Francisco Arenas, Juan Antonio, Rosa, Silvia, Isabel, Cristina Ruano, Jessica y Paco. Del resto de la Facultad, ha habido mucha gente que me ha ayudado en diversas situaciones, como Ezequiel y Dani, de Química Orgánica; José María, con el que he compartido largos ratos de Fluorímetro; Augusto, de Análisis Elemental; Goyo, de SEM, o la gente de Catálisis, en especial Cristina, Enrique y Juan, a todos ellos, muchas gracias.

He de agradecer también a los profesores *Jishan Wu*, del *π- and Supramolecular Space Research Group* (Universidad Nacional de Singapur) y *Kazuo Takimiya*, del *Emergent Molecular Function Research Group* (RIKEN Advanced Science Institute) por suministranos los materiales objeto de estudio en esta Tesis.

Una de las experiencias más gratificantes de estos cuatro años ha sido la posibilidad de viajar y conocer cómo se trabaja y vive en otras partes del mundo. En este aspecto, tuve la oportunidad de pasar tres meses en el *Surface/Interface Laboratory* bajo la supervisión del Prof. *Antoine Kahn* en la Universidad de Princeton, a quien agradezco la oportunidad que me dio para aprender técnicas de caracterización de superficies en esa magnífica institución, también a Christoph, Yenting y Nyan, por hacerme pasar muy buenos ratos por allí. También tuve la oportunidad de pasar tres meses en Bolonia trabajando en espectroscopia Raman de fonones en el Grupo de Estado Sólido. Por el cariño con el que me acogieron y por todo lo que allí aprendí, me siento profundamente agradecido a los profesores Aldo Brillante, Raffaele Guido Della Valle y Elisabetta Venuti. Especialmente, quiero dar las gracias a Tommaso, que me enseñó de arriba abajo a manejar el famoso T6400 y con el que compartí innumerables bocadillos de mortadela y *taralli* de todos los sabores. También agradecer a Marco, Mattia, Tiziana, Enzo, Michelle, Laura, Joanna y al pequeño fan del Real Madrid, Mathew.

Aunque la vida nos haya alejado físicamente, o las circunstancias hagan menos frecuente coincidir, hay amigos que uno siempre lleva consigo y que de una forma u otra me han ayudado a llegar hasta aquí,

gracias especialmente a Danielo, Chelu, Jacde, Iván, Anto, Moi, Esther, Can y Marta.

Haciendo balance de este periodo, puedo decir que de lo que más orgulloso me siento es del esfuerzo, algo que he de agradecer a mis padres, a quienes debo tantas y tantas cosas. Porque todo es más fácil cuando sientes el apoyo de quien más quieres, quien te impulsa para superar los obstáculos y amortigua tus caídas. No hay palabras para expresar mi gratitud. Gracias también a mi hermana María, que se me ha hecho mayor, y a Jorge. Por supuesto también a mis abuelos Luis y Obdulia, tíos y primos, en especial a mi primo David, que siempre está el primero para todo, gracias por la portada.

Quien posiblemente más me haya sufrido en los malos momentos ha sido Aroa. No sabes lo agradecido que estoy por el ánimo y la comprensión que siempre me has transmitido, esto hubiera sido mucho más duro sin ti.

Por último, quisiera dar las gracias a mi abuela Eloisa, a cuya memoria va dedicada esta Tesis.

Gracias a todos, de corazón.

ÍNDICE

1. Introducción

1. Introducción

1.1 BIRRADICALES

Según el Compendio de Terminología Química de la IUPAC (*Gold Book*), un sistema de capa abierta es aquel átomo o molécula en el que sus electrones no se asignan completamente a los orbitales formando pares [1]. En el contexto de la Teoría de Orbitales Atómicos, una capa abierta consiste en una capa de valencia que no está completamente llena o que no comparte todos sus electrones mediante el enlace con otros átomos o moléculas. En el ámbito de la Teoría de Orbitales Moleculares, este concepto implicaría la existencia de electrones desapareados y por tanto, la presencia de orbitales moleculares semiocupados, en contraste con la configuración de capa cerrada, que se caracteriza por tener todos sus orbitales moleculares doblemente ocupados o vacíos.

Desde finales del siglo pasado, el desarrollo de la química de moléculas de capa abierta se ha incrementado notablemente, centrándose principalmente en dotar a este tipo de sistemas de un grado de estabilidad razonable para su caracterización y aplicación práctica [2]. Una de las propiedades que hacen interesantes a este tipo de sistemas es el inherente carácter birradical que presentan muchos de ellos y que los dota de propiedades electrónicas, ópticas y magnéticas poco convencionales, con una más que futurible aplicabilidad en dispositivos para electrónica orgánica, principalmente en Óptica No Lineal [3-6], Fotovoltaica Orgánica [7] o Espintrónica [8]. Sin embargo, este carácter birradical es, a su vez, el mayor inconveniente que la síntesis de sistemas de capa abierta se encuentra en el camino, debido a la alta reactividad que lleva asociada.

En la literatura científica es común usar indistintamente los términos birradical y dirradical para hacer referencia a moléculas que poseen dos electrones desapareados. Desde una aproximación química, la nomenclatura establecida en el Compendio de Terminología Química de la IUPAC y adoptada por *Abe* en su revisión sobre dirradicales, establece que un birradical será aquella molécula en la que los dos electrones desapareados actúen de manera prácticamente independiente [9], es decir, aquellos sistemas en los que la interacción de canje entre los dos electrones desapareados sea despreciable como consecuencia de la distancia que los separa y en los que, por tanto, cada uno de ellos se pueda considerar que actúa como un monorradical o doblete aislado [10]. A los casos en que la interación dipolo-dipolo entre los electrones desapareados es suficiente como para dar lugar a dos estados de espín diferentes, singlete y triplete, se les denomina con el término dirradical. Durante el desarrollo de la presente Tesis Doctoral, sin embargo, se ha decidido aplicar una nomenclatura simplificada y de corte más físico en la que el término birradical engloba a todos los sistemas con dos electrones desapareados. En la **Figura 1.1** se muestran algunos ejemplos de birradicales de base orgánica.

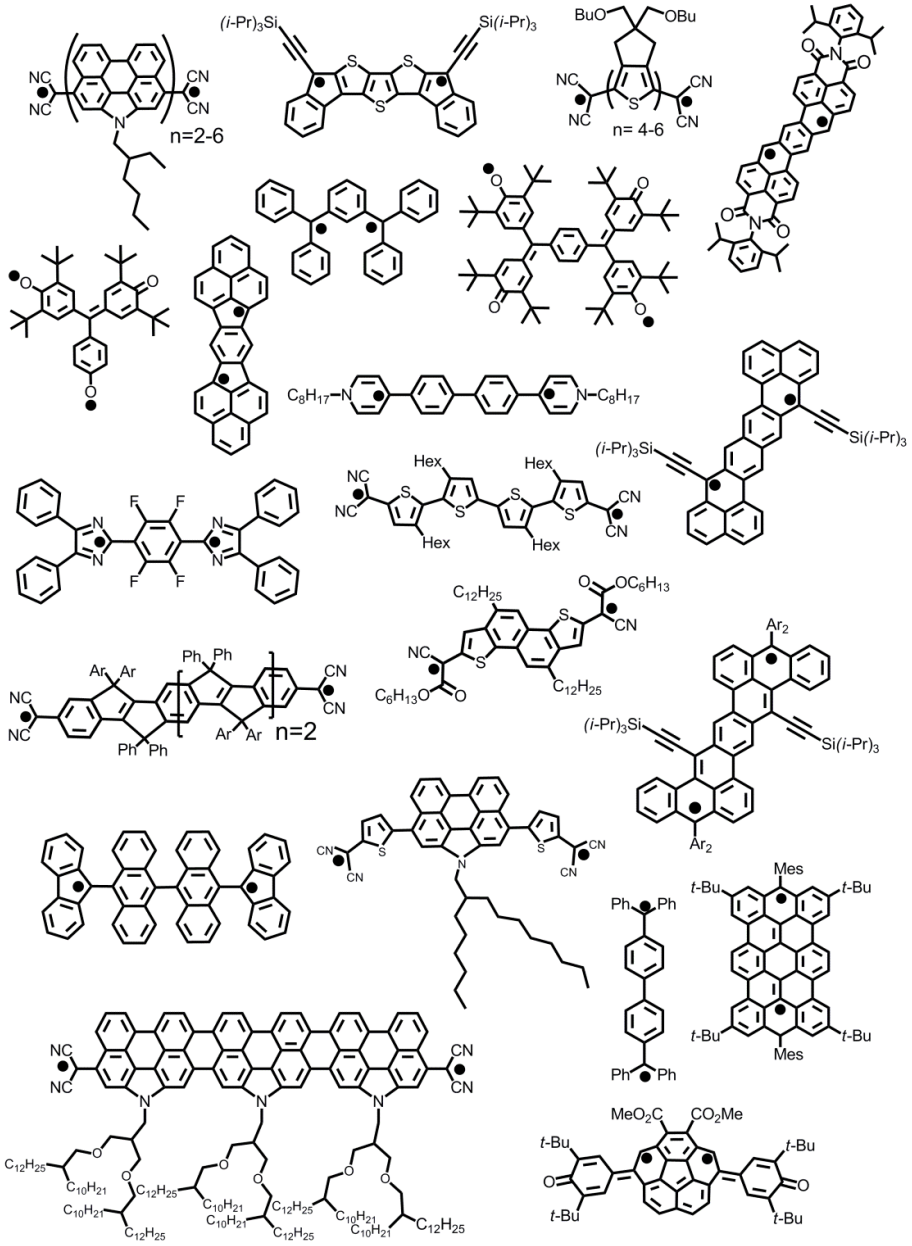

Figura 1.1 Ejemplos de birradicales orgánicos. (Ph=fenilo, Ar= 4-octilfenilo, *i*-Pr=*iso*-propilo, *t*-Bu=*tert*-butilo, Mes= Mesitilo).

1.1.1. CLASIFICACIÓN

Dentro de los birradicales, en los sistemas con dos electrones desapareados que se sitúan en dos orbitales moleculares no enlazantes de parecida o igual energía en los que la integral de canje electrónico (*J*) es pequeña pero distinta de cero, se puede considerar que existen tres tipos principales: moléculas antiaromáticas, birradicales tipo *No-Kekulé* y birradicales tipo *Kekulé* **(Figura 1.2)**.

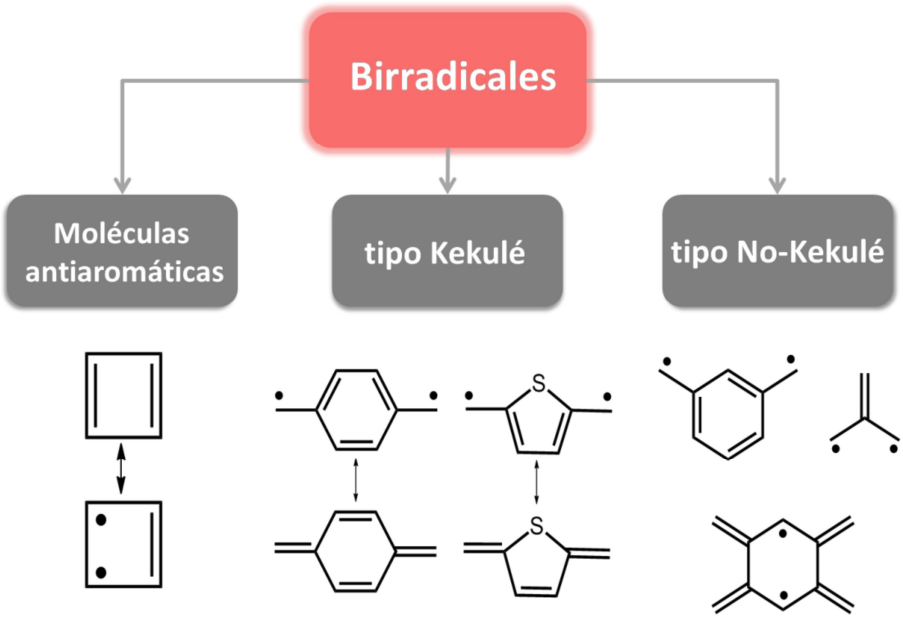

Figura 1.2 Origen de los distintos tipos de birradicales orgánicos.

1.1.1.1. MOLÉCULAS ANTIAROMÁTICAS

El término antiaromático se aplica a hidrocarburos cíclicos planos que constan de un número par de dobles enlaces en alternancia con enlaces simples. Se trata de sistemas que presentan 4*n* electrones π (con n=1, 2, 3...), a diferencia de los compuestos aromáticos, que constan de 4*n*+2 electrones π [11,12]. Este *déficit* de un par electrónico con respecto a los compuestos aromáticos hace que la configuración electrónica del estado fundamental pase de una situación en la que los electrones ocupan únicamente orbitales enlazantes a una en la que se produce la ocupación de orbitales antienlazantes [13,14]. Con objeto de mitigar esa inestabilidad, éstos pueden evolucionar distorsionando su estructura molecular o, en el caso de que la distorsión se viera restringida, dando lugar a una especie birradical [15]. Este último es el caso del ciclobutadieno (**Figura 1.3**), que constituye el prototipo de estructura antiaromática y se caracteriza por su planaridad. Además, muestra una reactividad muy alta en comparación con otros sistemas antiaromáticos (ciclooctatetraeno) que permiten una cierta distorsión de la estructura molecular, inestabilidad que recientemente se ha relacionado con su extraordinaria tensión estructural [16].

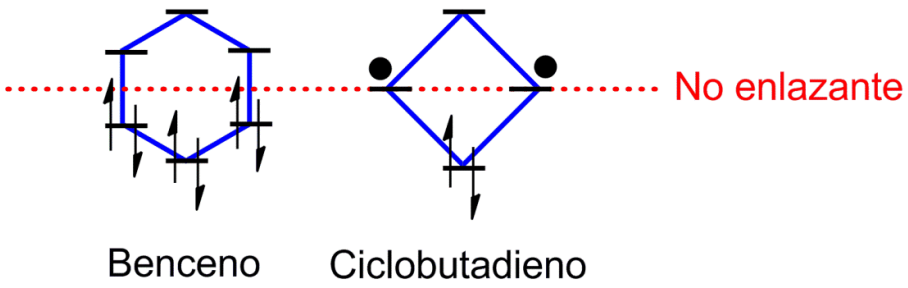

Figura 1.3. Distribución de electrones π en las moléculas de benceno y ciclobutadieno.

1.1.1.2. BIRRADICALES TIPO NO-KEKULÉ

Los birradicales tipo *No-Kekulé* se definen como sistemas conjugados cuyas estructuras de *Kekulé* contienen al menos dos átomos que no están π-enlazados o, en otras palabras, moléculas para las cuales no se puede establecer ninguna estructura de *kekulé* en la que sus 2*n* electrones π se encuentran acomodados en *n* enlaces dobles. No son pocos los ejemplos de este tipo de sistemas en bibliografía [17-19]. Uno de los primeros y más conocidos surge cuando en 1917, *W Schlenk y M. Brauns*, asumiendo que para obtener birradicales estables lo más sencillo era conectar dos monorradicales mediante unidades de transferencia de espín, sintetizaron el conocido como *birradical de Schlenk* [20] (**Figura 1.4**). Éste, aunque casi por completo oligomerizado a temperatura ambiente, presentaba una minoría de especies con estado fundamental birradical triplete.

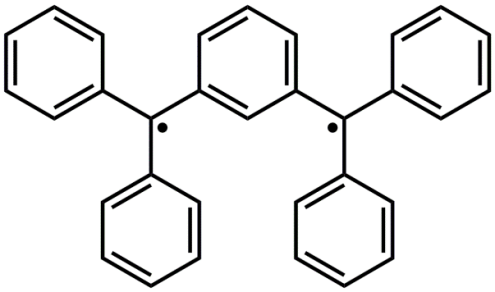

Figura 1.4 Birradical de Schlenk.

Otros ejemplos clásicos del desarrollo de la química de birradicales *No-Kekulé* durante el siglo XX son los sintetizados por *Yang* en 1960 o por *Coppinger* en 1962 (**Figura 1.5**) [21,22].

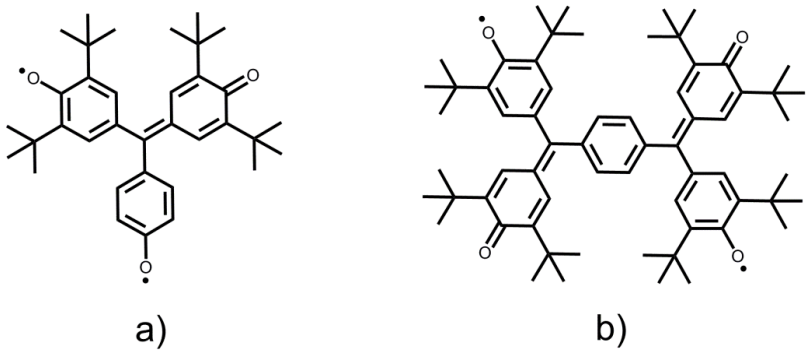

Figura 1.5 a) Birradical de Yang; **b)** Birradical de Coppinger.

1.1.1.3. BIRRADICALES TIPO KEKULÉ

El rasgo característico de este tipo de moléculas consiste en que pueden ser representadas mediante diversas estructuras resonantes, incluyendo la correspondiente a una configuración electrónica de capa cerrada (**Figura 1.2**). Esto implica que los electrones desapareados en la forma resonante birradical estén formando parte de un doble enlace, lo que constituye la diferencia fundamental con respecto a los birradicales tipo *No-Kekulé*, que solamente pueden ser descritos mediante una estructura de capa abierta, con los electrones desapareados ocupando orbitales no enlazantes [10,23].

A comienzos del siglo XX, se sintetizaron dos de los primeros birradicales tipo *Kekulé* suficientemente estables como para poder ser caracterizados. El primero de ellos data de 1904, cuando *J. Thiele y H. Balhorn*, publicaron la síntesis del que posteriormente se conocería como *Hidrocarburo de Thiele* (**Figura 1.6a**) [24,25]. En 1907, el químico ruso *A. E Tschischibabin* iría un paso más adelante y sintetizaría el célebre *Hidrocarburo de Chichibabin* que consta de una unidad central de bifenilo y que serviría como plataforma molecular para la síntesis de numerosos birradicales en el futuro [24,26] (**Figura 1.6b**).

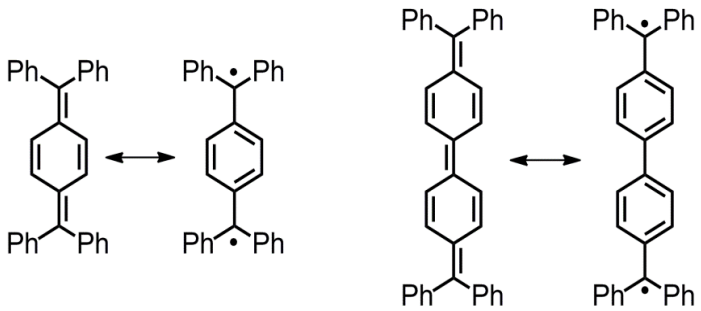

Figura 1.6 Estructuras resonantes de: **a)** Birradical de Thiele y **b)** Birradical de Chichibabin.

Ambas moléculas resultaron ser altamente inestables. Concretamente, la molécula de Chichibabin ha sido objeto de gran interés durante los últimos cien años desde el punto de vista de la particular configuración electrónica que cabe esperar para su estado fundamental. Sin embargo, tanto ella como gran parte de sus derivados, reaccionan ávidamente con oxígeno y descomponen, dimerizan, polimerizan, etc. Esto hace que su caracterización resulte compleja, quedando limitada por completo su aplicación práctica, lo que explica que la elucidación de la multiplicidad de espín del estado electrónico fundamental en moléculas tipo Chichibabin haya sido objeto de debate durante mucho tiempo.

La química de heterociclos también ha jugado un papel relevante en el desarrollo de nuevos birradicales estables. Ya en 1966, *Zimmerman et al.* sintetizaron la molécula *BDPY-2Y* (**Figura 1.7a)** introduciendo grupos imidazol entre la unidad de para-quinodimetano (*p-QDM)* central y los grupos exometileno de la *molécula de Thiele* [27]. El resultado fue un sólido verdoso y con brillo metálico que presentaba un 0.1% de especies paramagnéticas en disolución a temperatura ambiente, porcentaje que se veía aumentado al incrementar la temperatura. Esto hacía pensar en la existencia de un equilibrio térmico entre un estado fundamental

diamagnético de capa cerrada y un estado birradical paramagnético. Sin embargo, la falta de evidencias experimentales que demostraran la contribución del carácter birradical al estado electrónico fundamental de este tipo de moléculas mantenía la incertidumbre sobre su estructura electrónica básica, algo que ha venido siendo una constante en este tipo de sistemas durante largo tiempo. No sería hasta 2004 cuando *J. Abe et al.* [28] consiguieran aclarar esta cuestión mediante la detección del dímero formado por el derivado tetrafluorinado de *BDPY-2Y*, *tF-BDPY-2Y* (**Figura 1.7b**).

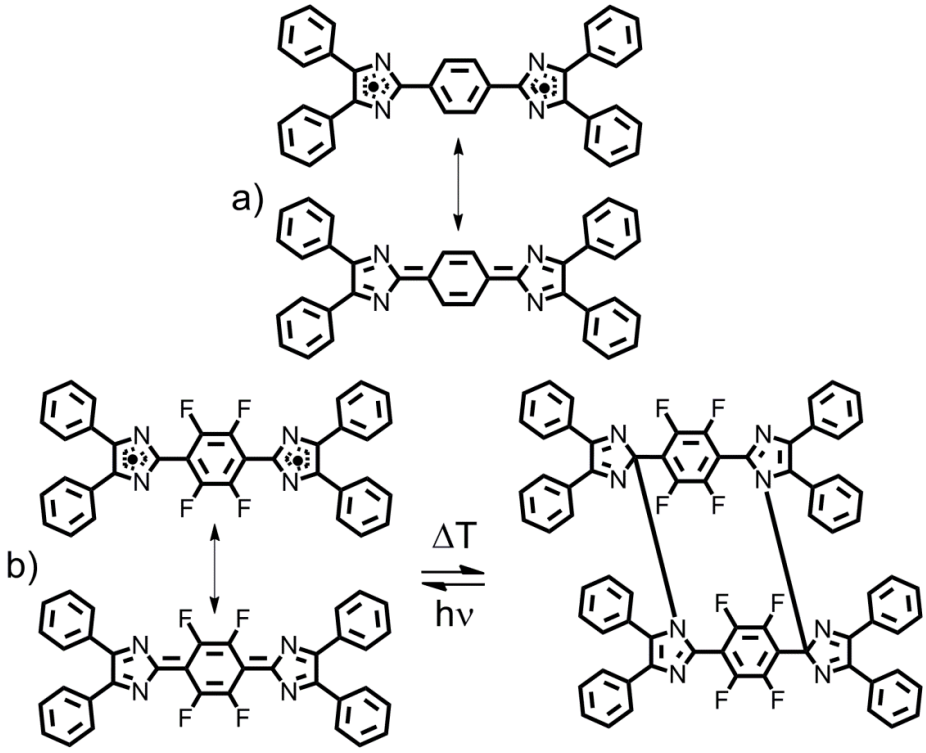

Figura 1.7 a) Estructuras resonantes de *BDPY-2Y*; **b)** Estructuras resonantes de *tf-BDPY-2Y* y dímero detectado.

Otro ejemplo reciente lo constituye el viológeno extendido sintetizado por *Porter et al.* [29] (**Figura 1.8**). Se trata de una molécula que guarda similitud estructural con la *molécula de Chichibabin*, al constar de la unidad central bifenilo sustituida por unidades de piridina en las posiciones *para*-. Esta molécula fue estudiada por nuestro grupo de investigación en 2008 [30], trabajo que permitió caracterizar el estado fundamental como un birradical singlete en equilibrio térmico con un estado triplete gracias a la información que la espectroscopia Raman y los cálculos químico-cuánticos proporcionaron acerca de la interconversión quinoide-aromática del bifenilo central.

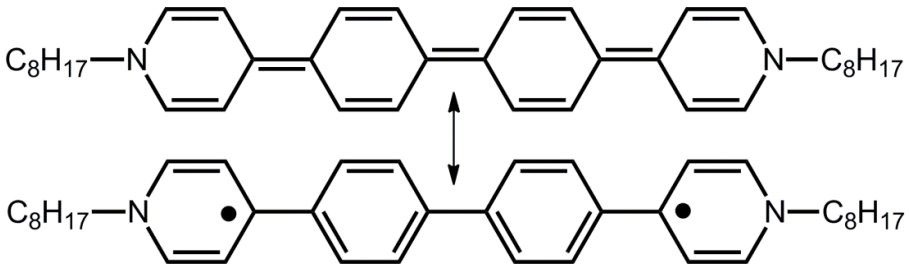

Figura 1.8 Estructuras resonantes de un viológeno extendido.

También existen ejemplos de birradicales orgánicos de base tiofénica, de entre los que destacan algunas familias de oligotiofenos tetracianosustituidos [31]. En este tipo de sistemas se pretendía jugar con la menor aromaticidad del anillo de tiofeno con respecto al benceno para obtener birradicales y, al mismo tiempo, observar el efecto que la inclusión de grupos fuertemente aceptores, promotores de estructuras quinoides, pudieran tener sobre la estructura electrónica del estado fundamental. En la **Figura 1.9** se muestran algunas de ellas, estudiadas previamente por nuestro grupo de investigación [32].

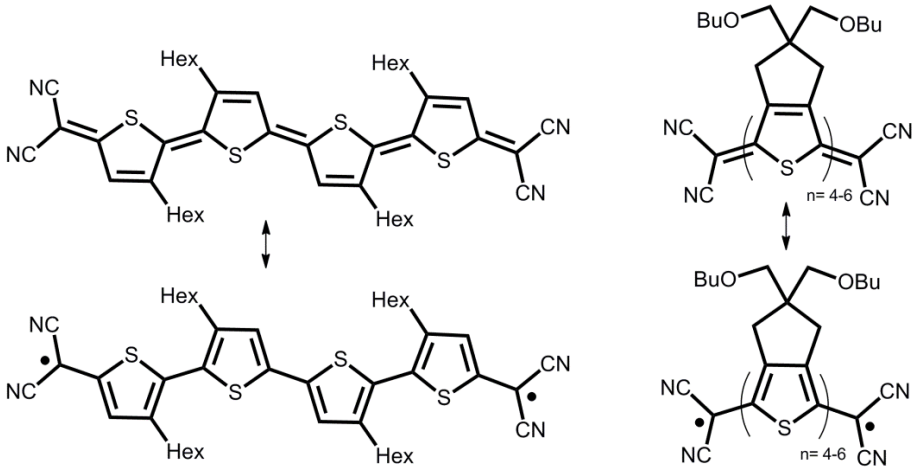

Figura 1.9 Oligotiofenos tetracianosustituidos con carácter birradical.

Otro ejemplo muy interesante lo constituye el derivado de *tri-p-QDM* sintetizado por *Nakamura et al.* [33] (**Figura 1.10**), que explota el concepto de rigidez estructural y consiste en tres unidades de *p-QDM* conectadas por vinilenos y rigidificadas por puentes de carbono. Esta molécula se caracteriza por ser estable al aire durante meses y por su resistencia a temperaturas de hasta 160 ^{o}C en atmósfera inerte, lo que la convierte en uno de los birradicales más estables descubiertos hasta la fecha.

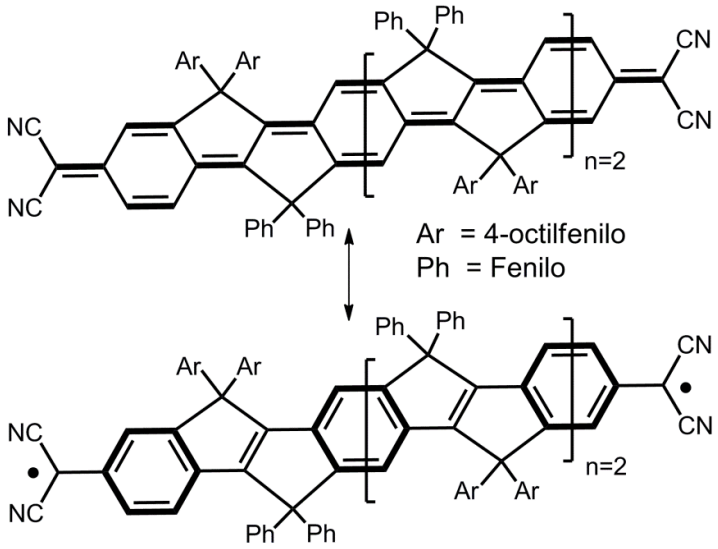

Figura 1.10 Estructuras resonantes del derivado *tri-p-QDM*.

Todos estos sistemas moleculares se sitúan en la interfase entre teoría y ciencia experimental. Esto les confiere un enorme interés ya que permiten profundizar en conceptos de química fundamental como la Teoría de Enlace y presentan propiedades prometedoras de cara a su aplicabilidad en ciencia de materiales. Además, a diferencia de los birradicales *No-Kekulé*, su estructura electrónica ha sido menos estudiada, por lo que a día de hoy sigue siendo un reto caracterizar la configuración electrónica de este tipo de birradicales y continúan llevándose a cabo numerosos esfuerzos dirigidos a sintetizar sistemas que permitan entender los fenómenos que en ellos tienen lugar, así como a obtener nuevas potencialidades y mejorar las ya conocidas.

1.1.2 Multiplicidad de espín en el estado fundamental. Doble Polarización de Espín (DSP).

En sistemas birradicalarios en los que la interacción dipolo-dipolo es de suficiente magnitud como para dar lugar a dos estados de espín, singlete y triplete, elucidar cuál de ellos es más estable para una molécula dada y obtener reglas empíricas y teóricas, extrapolables a distintos sistemas, que permitan tener una idea de la naturaleza del estado electrónico fundamental más probable de los mismos, es de vital importancia de cara al diseño de nuevas plataformas moleculares con vistas a su aplicación en electrónica orgánica. Por ello, el estudio de estos sistemas ha venido siendo objeto de una intensa actividad investigadora desde principios de los 90.

Cuando dos electrones ocupan dos Orbitales Moleculares No Enlazantes (NBMOs) dando lugar a un birradical, éstos suelen ser degenerados. Así, en ausencia de correlación electrónica (repulsión) existen seis configuraciones electrónicas posibles: $\mathbf{T_{1,2}}$, $\mathbf{T_{1,2'}}$, $\mathbf{S_{1,2}}$, $\mathbf{S_{1,2'}}$, $\mathbf{S_{1,1}}$ y $\mathbf{S_{2,2}}$, que dan lugar a cuatro estados energéticos posibles al imponer las condiciones de simetría molecular (**Figura 1.11**).

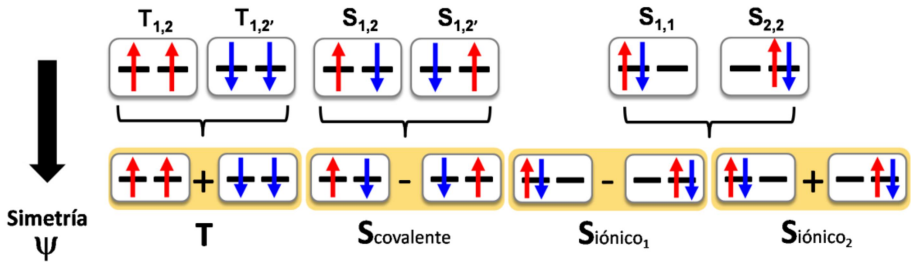

Figura 1.11 Configuraciones y estados de espín posibles para un birradical.

La configuración electrónica más estable en átomos y moléculas se puede predecir, de modo general, haciendo uso de la Regla de Hund [34]. Ésta establece que, al añadir electrones a orbitales atómicos de la misma energía, primero se han de ocupar todos los orbitales posibles con electrones de espín paralelo, para evitar la repulsión electrónica. Así, al llenar dos orbitales equivalentes con dos electrones, la configuración electrónica triplete estará favorecida energéticamente con respecto al estado singlete. En general, la Regla de Hund puede aplicarse para determinar la multiplicidad de espín en birradicales. Por tanto, la introducción de correlación electrónica estabiliza las configuraciones de alto espín (**Figura 1.12**).

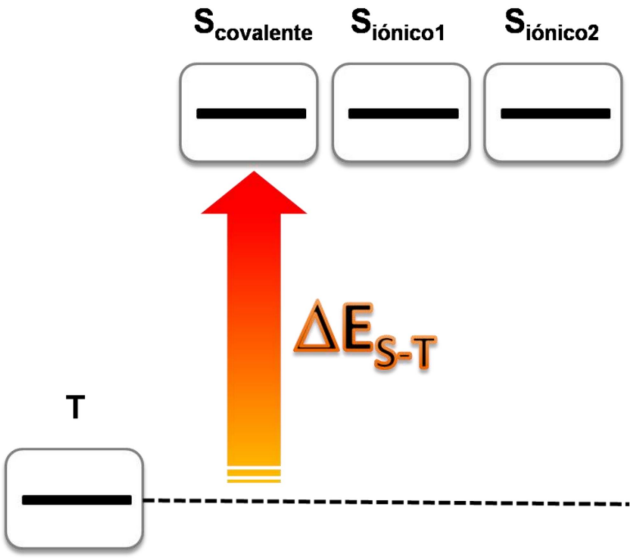

Figura 1.12 Modelo de los cuatro estados de espín posibles para un birradical teniendo en cuenta el efecto de correlación electrónica. ($\Delta E_{S-T} = E_S - E_T$, diferencia de energía entre estados singlete y triplete).

Haciendo uso del Hamiltoniano molecular de orden cero (monoelectrónico o *h*) y de orden uno (con repulsión), se puede obtener una descripción cuantitativa de la disposición energética relativa para los distintos estados de espín, que llevaría a establecer el orden de estabilidad para las cuatro configuraciones posibles en ausencia de campo magnético externo (**Figura 1.13)**, donde j_{ij} es la integral de Coulomb para dos centros, *k* la integral de canje magnético y j_{ii} la integral de Coulomb para un único centro ($j_{ii} >> j_{ij}$).

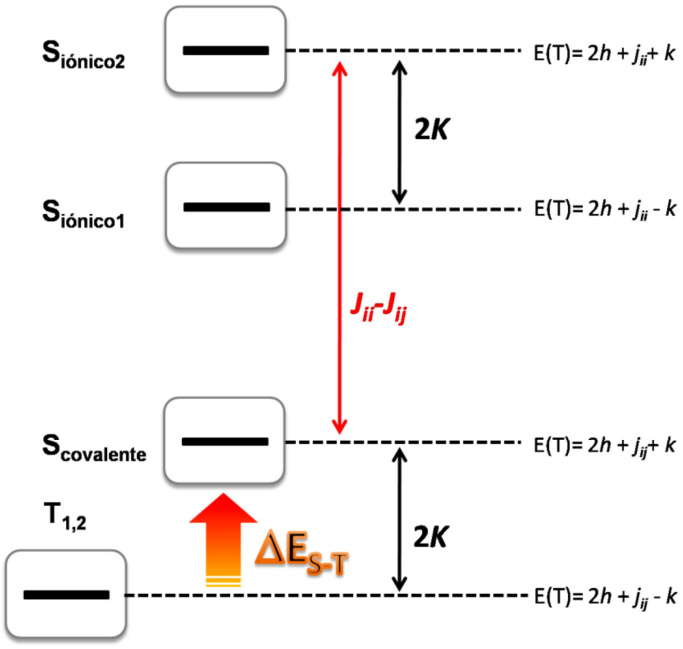

Figura 1.13 Energías de los cuatro estados posibles para un birradical.

En la **Figura 1.14** se puede visualizar el significado de las magnitudes relevantes en la distribución de energías detallada con anterioridad. Si se considera una situación de dos electrones en dos orbitales ϕ_A (azul) y ϕ_B (rojo), la integral de Coulomb, j_{ij}, indica la repulsión electrón-electrón entre zonas que no se solapan en el espacio (zonas

azules y rojas); la integral de canje magnético, *k*, por su parte, da cuenta de la repulsión electrón-electrón en el volumen de solapamiento entre ambos orbitales (zona blanca) y la integral de Coulomb para un centro, j_{ii}, tiene que ver con la repulsión electrón-electrón que ocurre en el volumen de cada orbital individual.

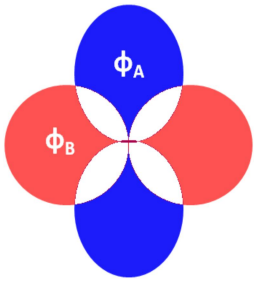

Figura 1.14 Representación esquemática del solapamiento de dos orbitales *p* ocupados cada uno por un electrón.

Esta situación en la que el triplete se ve energéticamente favorecido con respecto al singlete es característica de birradicales tipo *No-kekulé*. Por tanto, este tipo de sistemas presentan estados fundamentales de alto espín (**Figura 1.15**), en línea con lo que determina la Regla de Hund.

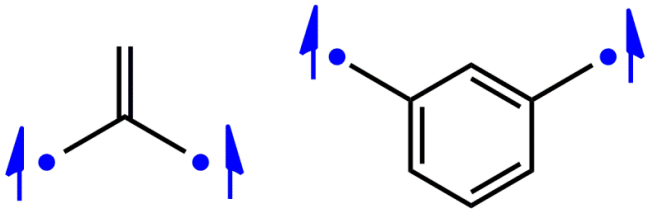

Figura 1.15 Multiplicidad de espín del estado fundamental en birradicales *No-Kekulé*.

Partiendo de la **Figura 1.13**, la diferencia energética entre triplete y singlete ($\Delta E_{S\text{-}T}$) se puede determinar a partir de la **eq[1],** la cual establece su dependencia lineal con la interacción de canje magnético (k) y ésta, a su vez, es proporcional a la integral de solapamiento entre los NBMOs que ocupan los electrones desapareados.

$$\Delta E_{S\text{-}T} = -2k \quad \textbf{eq[1]}$$

Cabe preguntarse entonces qué ocurriría en función del grado de solapamiento entre NBMOs, ¿podrían darse excepciones a la Regla de Hund en situaciones en las que el solapamiento fuera mínimo?

Esta cuestión ya comenzó a plantearse a raíz de los trabajos de *Dowd* de principios de los 90 [35,36], en los que estudiaba moléculas que posteriormente se confirmarían como las primeras excepciones a la concepción que, sobre la multiplicidad de espín del estado fundamental en birradicales, imponía la Regla de Hund. En este contexto, cabe destacar las predicciones de *Borden* [37-39] y su clasificación de birradicales atendiendo a la distribución de sus NBMOs sobre el esqueleto molecular. Así, se consideran birradicales tipo *disjoint* aquellos en los que los NBMOs se encuentran separados en el espacio, y birradicales tipo *Non-disjoint* los que muestran un cierto grado de solapamiento entre orbitales. Ejemplos clásicos de este tipo de sistemas los constituyen el trimetilenmetano (TMM) y el tetrametilenetano (TME) [40]. En el primero de ellos, como se puede observar en la **Figura 1.16**, existe una distribución de NBMOs de modo que coiciden en algunas zonas del espacio (*Non-disjoint*) mientras que en el TME los NBMOs están restringidos a zonas separadas de la molécula *(disjoint)*.

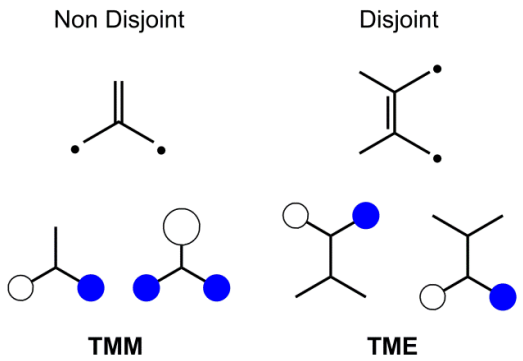

Figura 1.16 Ejemplos de birradicales Disjoint y *Non Disjoint*.

Los estudios de Dowd anteriormente citados mostraban evidencias de un estado fundamental triplete en ambos casos. Sin embargo, mientras que la multiplicidad de espín del estado fundamental para el TMM no albergaba dudas, en el caso del TME y otros derivados con una distribución de NBMOs tipo *disjoint*, la cuestión de si el estado fundamental era de alto o bajo espín se mantuvo abierta durante largo tiempo, generando numerosos estudios teóricos que contradecían los iniciales datos experimentales [41-45]. No sería hasta 1996 cuando *Iwamura et al.* [46] caracterizaran inequívocamente el estado fundamental del TME como birradical singlete, prácticamente degenerado con un estado birradical triplete excitado a unas 0.02 Kcal/mol.

En este contexto, con las predicciones teóricas y evidencias experimentales en buena sintonía, cobra sentido profundizar en el mecanismo responsable de esta violación de la Regla de Hund. Atendiendo a la física subyacente a ésta, se ha de traer a colación el Principio de Exclusión de Pauli, que establece la imposibilidad de que dos electrones de espines paralelos ocupen simultáneamente la misma región del espacio. Teniendo en cuenta que este Principio permite que electrones con espines antiparalelos aparezcan en una misma región, éstos presentan una mayor energía de repulsión mutua que los electrones

con el mismo espín. Aquí entra en juego la diferencia entre NBMOs tipo *disjoint* y *Non-disjoint* ya que, en el primer caso, independientemente de que los dos electrones desapareados tengan o no el mismo espín, no existe probabilidad de que ambos electrones ocupen el mismo orbital. Esto, en un principio, llevaría a considerar isoenergéticos los estados triplete y singlete, sin embargo, en el caso del singlete existe la posibilidad de que los electrones de los orbitales π-enlazantes se localicen parcialmente en el mismo par de carbonos donde se encuentran los electrones desapareados. Este tipo de correlación entre electrones en orbitales enlazantes y no enlazantes es energéticamente favorable, y no es posible en el estado triplete, lo que implica la estabilización del estado capa abierta de bajo espín. En el caso de NBMOs tipo *Non-disjoint*, el estado fundamental será triplete en base a la aplicación del Principio de Exclusión de Pauli a las zonas que los NBMOs tienen en común [18].

En pocas palabras, la capacidad que los dos electrones desapareados en birradicales singlete tienen para conjugar con los electrones enlazantes del puente molecular que los conecta, en sistemas tipo *disjoint*, donde la *k* es pequeña, pueden hacer que esta configuración electrónica se vea favorecida frente a la configuración de birradical triplete que cabría esperar tras la aplicación de la Regla de Hund, como muestra la **Figura 1.17**.

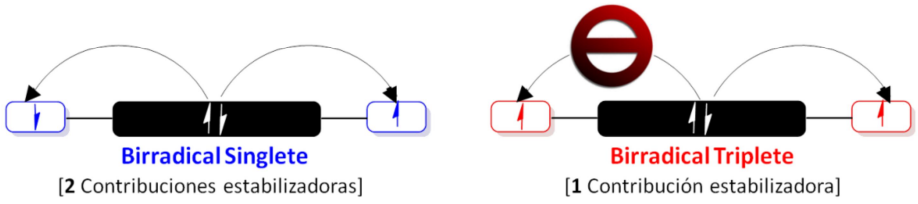

Figura 1.17 Influencia de la conjugación sobre la estabilización de birradicales tipo *disjoint*.

Para estos sistemas, el modelo de cuatro estados tomaría la forma que se muestra en la parte derecha de la **Figura 1.18,** cuya distribución se basa en las energías de segundo orden obtenidas mediante la interacción de configuraciones entre los estados capa cerrada y los estados capa abierta bajos en energía que se obtenían a partir del Hamiltoniano molecular de primer orden. Como puede observarse, el balance entre el término *2K* y el término *IC* (interacción de configuraciones) es el que, en principio, determinaría la preferencia hacia un estado fundamental de alto o bajo espín.

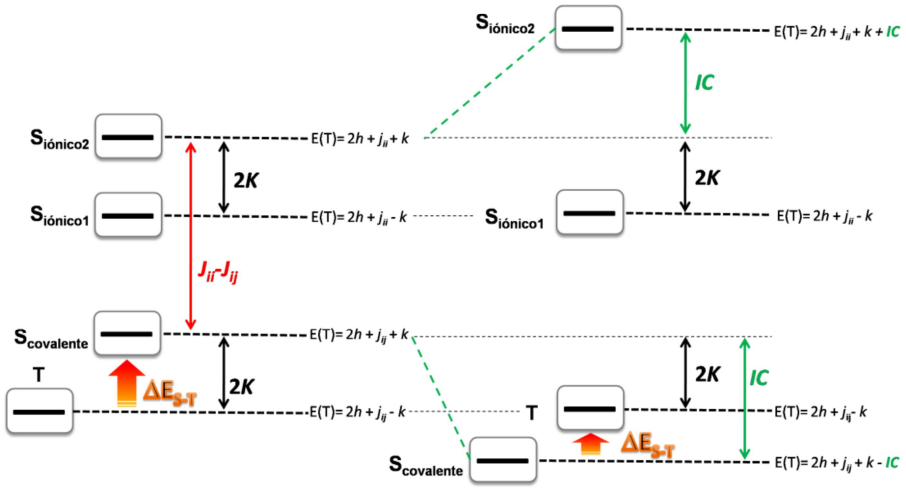

Figura 1.18 Modelo de cuatro estados antes y después de introducir el efecto de la interacción de configuraciones.

El término *IC* tiene que ver con la integral híbrida de Coulomb, la cual, si se retrocede a la **Figura 1.14**, daría cuenta de la repulsión electrón-electrón entre las zonas en las que las funciones de onda solapan (zonas blancas) y aquellas en donde no hay solapamiento (zonas rojas y azules). Por su parte, la integral de canje (*k*) indica la repulsión electrón-electrón en las zonas que solapan, es decir, es la cantidad de energía que el sistema ahorraría al disponer los electrones formando un triplete, por

tanto, a menor grado de solapamiento, se favorecería la estabilización de configuraciones capa abierta de bajo espín.

Este es el caso de birradicales tipo *Kekulé* que presentan NBMOs tipo *disjoint*, en los que el bajo valor de *k* y el carácter enlazante de la estructura resonante de capa cerrada, pueden llegar a estabilizar estados fundamentales birradical singlete de capa abierta. Se trata de sistemas muy interesantes desde el punto de vista práctico ya que, debido a las particulares características de su estado fundamental y primeros estados excitados, pueden ser útiles en aplicaciones relacionadas con fisión de singletes, reactividad química, absorción de dos fotones o *switching* magnético (**Figura 1.19**) [3-8, 47-53].

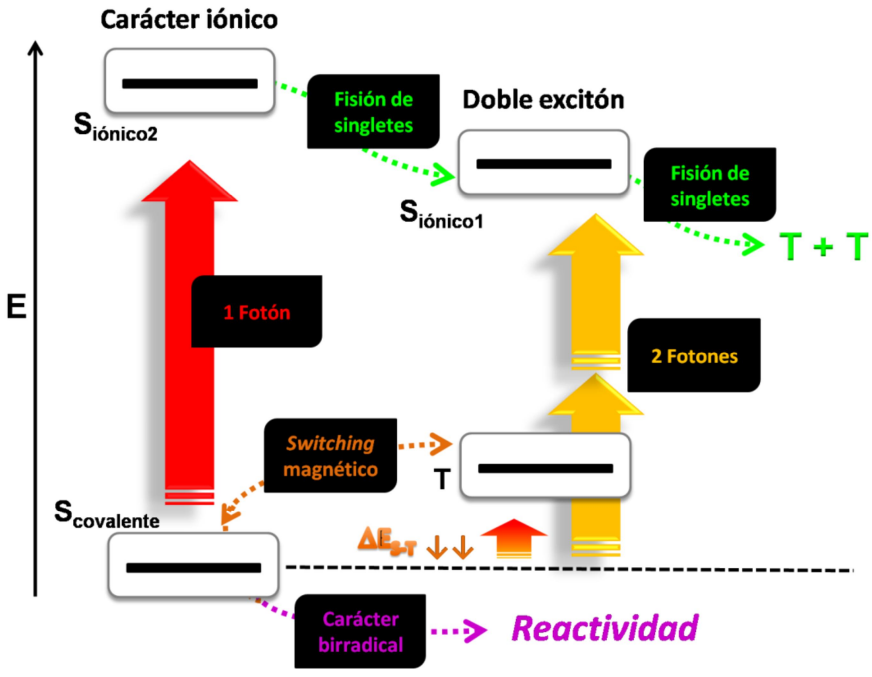

Figura 1.19 Posibles aplicaciones de un birradical singlete

Se puede decir, por tanto, que este fenómero de estabilización de especies singlete de capa abierta, tiene que ver con el concepto de polarización de espín en radicales (SP), consecuencia directa de la Regla de Hund y que en birradicales, debido a la presencia de dos electrones desapareados, ocurre dos veces, en lo que se conoce como *Mecanismo de Doble Polarización de Espín* o *Polarización Dinámica de Espín* (*DSP*) [37,54,55].

1.1.2.1. Mecanismo de Doble Polarización de Espín. Base Molecular

La *DSP* es un factor que explica la repulsión electrón-electrón en sistemas de capa abierta con S > ½ y que juega un papel determinante en la multiplicidad de espín del estado fundamental en birradicales π-conjugados [56], condicionando así el comportamiento ferromagnético o antiferromagnético de los mismos, como se ha visto con anterioridad. En un birradical de este tipo, con *n* electrones, cada electrón desapareado polariza a los restantes (*n*-2)/2 pares de electrones. La cuestión a tener en cuenta aquí, y que a la postre será crítica para que se estabilice el estado de alto o bajo espín, es si la polarización individual que cada centro radical ejerce sobre la nube π-conjugada es competitiva o aditiva. La DSP será aditiva cuando los dos electrones desapareados del birradical polaricen los orbitales llenos del puente conjugado en el mismo sentido, mientras que si lo hacen en sentidos opuestos estaremos ante un mecanismo *DSP* competitivo. Estas dos modalidades determinarán la multiplicidad de espín del estado fundamental en función de la estructura molecular del puente con respecto a los centros radicales.

El conjunto de los tres isómeros del benzoquinodimetano (*orto-, meta- y para-*) constituye un modelo ideal para entender el mecanismo

DSP [55] a nivel molecular. En la parte superior de la **Figura 1.20a**, se muestran los NBMOs para nuestros sistemas, de tipo bencílico.

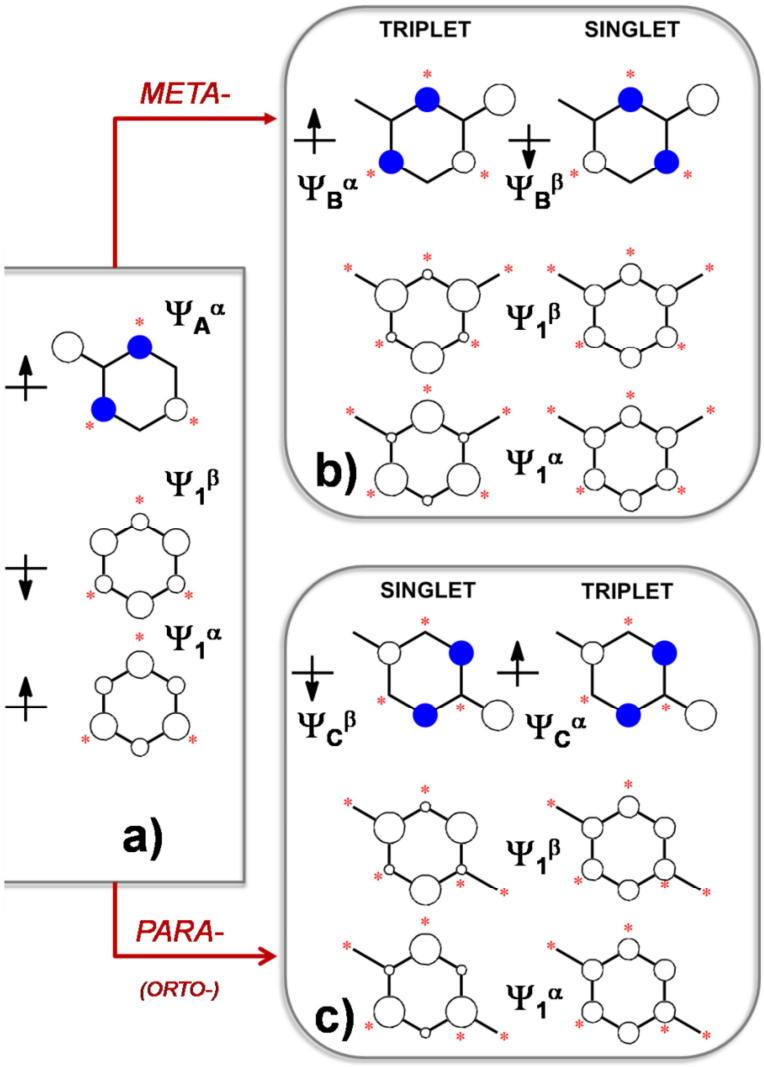

Figura 1.20 a) Polarización de espín en un orbital molecular doblemente ocupado, **b)** Electrón de espín α (izquierda) y β (derecha) en Ψ_B para la configuración *meta-*, **c)** Electrón de espín β (izquierda) y α (derecha) en Ψ_C para la configuración *para-*.

Si nos fijamos en el isómero *meta* **(Figura 1.20b)**, los dos NBMOs se orientan hacia las posiciones marcadas (*) y, por tanto, ambos presentan la misma paridad (muestran LCAOs no nulos en las posiciones señaladas del anillo de benceno). La **Figura 1.20a** muestra el fenómeno de SP en un orbital molecular (MO) doblemente ocupado Ψ_1 inducido por el primer electrón desaparado de espín α que ocupa un NBMO Ψ_A^{α}. El efecto de la polarización del par de electrones en Ψ_1 busca minimizar la repulsión electrostática y, por tanto, el electrón de espín β que ocupa el MO Ψ_1^{β} disminuye sus coeficientes LCAO en las posiciones donde el electrón desapareado de espín α situado en el NBMO Ψ_A^{α} tiene amplitudes distintas de cero. Ocurre lo contrario en el caso de un electrón de espín α que ocupa Ψ_1^{α}, cuyo efecto hace que los coeficientes LCAO aumenten en esas posiciones. En otras palabras, la **Figura 1.20a** muestra la menor repulsión entre electrones con espines paralelos, de acuerdo con la Regla de Hund.

Ahora, si se considera una segunda SP inducida por el electrón desapareado que ocupa el NBMO Ψ_B, existen dos posibilidades: que ese electrón tenga espín α o que su espín sea β. Un electrón de espín α en Ψ_B **(Figura 1.20b, izquierda)**, en base a las razones físicas expuestas con anterioridad, afectaría a los MOs Ψ_1^{α} y Ψ_1^{β} ya polarizados aumentando, aún más, los coeficientes de las posiciones marcadas en Ψ_1^{α}, disminuyéndolos en Ψ_1^{β}. Es decir, el efecto de la SP del primer electrón va en el mismo sentido que el del segundo, por tanto, estamos ante un mecanismo de *DSP* aditivo. Por el contrario, si el electrón que se aloja en Ψ_B tiene espín β **(Esquema 1.20b, derecha)**, la segunda SP que éste genera disminuye los coeficientes LCAO de las posiciones marcadas en el MO Ψ_1^{α} y los aumenta en Ψ_1^{β} como resultado de un mecanismo DSP competitivo, ya que el efecto de la SP ejercida por cada electrón desapareado es opuesto. Estos resultados indican una estabilización del estado birradical triplete sobre el biradical singlete, y por tanto, la preferencia hacia un estado fundamental de alto espín.

En el caso del isómero *para-*, los dos NBMOs se orientan en las posiciones no marcadas del anillo de benceno, con la correspondiente distinta paridad de los mismos (uno de ellos tiene los coeficientes LCAO no nulos en las posiciones marcadas del anillo de benceno y el segundo los tiene en las restantes). El efecto de la SP del primer electrón desapareado es igual en todos los casos pero, al introducir el efecto de la SP del segundo electrón, los efectos varían. Si el espín del electrón que se sitúa en el NBMO Ψ_C es α **(Figura 1.20c, derecha)**, los MOs Ψ_1^{α} y Ψ_1^{β} aumentan y disminuyen sus coeficientes en las posiciones no señaladas respectivamente, dando lugar a un mecanismo DSP competitivo. En caso de que el espín fuera β **(Figura 1.20c, izquierda)**, ocurriría al contrario, y el mecanismo DSP sería aditivo, con el correspondiente resultado de la estabilización del estado birradical singlete para el isómero *para-*.

1.1.3 Proaromaticidad y Carácter Birradical en PAHs. La unidad p-QDM.

Actualmente, uno de los enfoques que más interés suscita en el contexto de la síntesis de sistemas π-conjugados extendidos o Hidrocarburos Policíclicos Aromáticos (*PAHs*), es el dirigido a la obtención de sistemas moleculares de bajo gap, debido principalmente a su potencial como semiconductores en OFETs, cromóforos NIR para absorción de luz en células solares fotovoltaicas orgánicas [57] o marcadores fluorescentes NIR para aplicaciones de imagen y detección en tejidos biológicos [58], así como para cromóforos en óptica no líneal [50,51,59-61]. Además, estos materiales son valiosos también como modelos para estudiar las relaciones estructura-propiedad en grafenos desde una perpectiva *Bottom-up* (Nanografenos) [62,63].

El estado fundamental electrónico de estos sistemas es generalmente de capa cerrada, pero a medida que el *gap* HOMO-LUMO se estrecha, comienzan a estabilizarse soluciones de capa abierta para la función de onda. Es conocida la influencia que la minimización del *gap HOMO-LUMO* tiene en la génesis del carácter birradical en este tipo de sistemas, al facilitar la mezcla de una configuración de doble excitación en la configuración electrónica del estado fundamental [64] por lo que este tipo de PAHs de bajo gap pueden encontrar también interesantes aplicaciones en el campo de la espintrónica orgánica.

Dentro de los PAHs de bajo gap, resultan especialmente interesantes los birradicales tipo *Kekulé* con estado fundamental singlete de capa abierta debido a las singulares propiedades que presentan (**Figura 1.21**). Existe una considerable variedad de este tipo de sistemas, algunos de los cuales ya se mostraban en la **Figura 1.1**. Sin embargo, un rasgo común a muchos de ellos es que comparten la unidad p-quinodimetano (*p-QDM*) como *building block* fundamental. En la **Figura 1.21** se muestran las estucturas resonantes de capa abierta y capa cerrada para algunos de ellos.

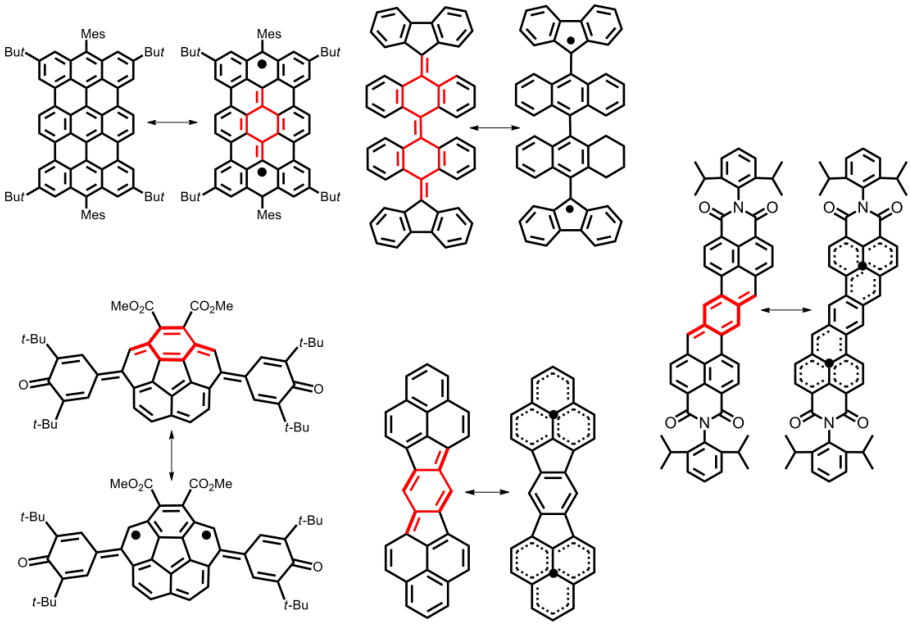

Figura 1.21 PAHs de bajo gap HOMO- LUMO basados en *p-QDM*.

Como se ha visto en apartados anteriores, la unidad *p-QDM* es, en si misma, un birradical de *Kekulé*, ya que se puede representar por sus estructuras resonantes de capa abierta y quinoide de capa cerrada. La estabilización de la forma birradical surge como consecuencia de la ganancia de un anillo aromático al pasar de la estructura resonante de capa cerrada a la correspondiente estructura de capa abierta (**Figura 1.22**). Por tanto, la estabilización de birradicales derivados de *p-QDM* se puede relacionar con la proaromaticidad del mismo, y es esta característica la que lo convierte en una de las más comunes unidades estructurales en química de *PAHs* de bajo *gap* con carácter birradical [65-67].

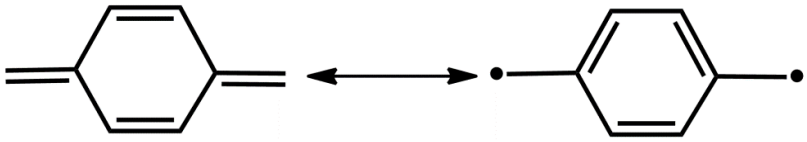

Figura 1.22 Estructuras resonantes de la unidad de p-QDM

Investigaciones recientes han demostrado que, a través de la incorporación de unidades de *p-QDM* en esqueletos π-conjugados, se pueden generar sistemas *PAHs* quinoides con estado fundamental singlete capa abierta, gracias a la anteriormente citada recuperación de la aromaticidad de la unidad pro-aromática que ocurre en la forma resonante birradicalaria. Sin embargo, obtener derivados de *p-QDM* de una cierta extensión es todavía un reto debido al aumento de la reactividad con la longitud de la cadena, además de a problemas de solubilidad propios de sistemas poliaromáticos de gran tamaño. Todo esto hace que la necesidad de entender la conexión estructura-carácter birradical y sus implicaciones en las propiedades físicas aflore, necesariamente, a la hora de proponer alternativas sintéticas en la búsqueda de este tipo de sistemas.

Tres son las principales vías de estabilización usadas en la síntesis de sistemas birradicalarios de bajo gap estables y con estructuras quinoides tipo *kekulé* de base *p-QDM*:

i) Termodinámica, mediante deslocalización de los electrones desapareados en el esqueleto de la molécula.
ii) Aromática, via ganancia de unidades aromáticas en la forma resonante birradical.
iii) Cinética, a través del bloqueo de los sitios más reactivos con sustituyentes voluminosos.

En base a esto, los sistemas fusionados proporcionan una excelente plataforma para incorporar la unidad *p-QDM* y generar birradicales estables, ya que la intrínseca planaridad y rigidez del esqueleto aromático facilita la deslocalización de los radicales y, además, gracias a la accesibilidad de métodos sintéticos, los sitios reactivos se pueden bloquear cinéticamente de manera relativamente sencilla. Estos conceptos de diseño químico, han ayudado a sintetizar diversos tipos de *PAHs* quinoides y con carácter birradical en los últimos años (**Figura 1.21**), de entre los cuales, uno de los sistemas más destacados lo constituye la familia de los bisfenalenilos.

Los trabajos de *Nakasuji y Kubo et al* [68,69], a partir de la conexión de dos radicales fenalenilo mediante un sistema π-conjungado, han dado lugar a una serie de moléculas quinoides de capa cerrada y con carácter birradical (**Figura 1.23**) muy interesantes a la hora de estudiar la estructura electrónica del estado fundamental y que presentan, además, propiedades muy particulares y novedosas.

El primer indacenodifenaleno (*IDPL*) se sintetizó en 1991 [70-72]**,** y han ido apareciendo diversos derivados desde entonces (**Figura 1.23a**), todos ellos con estados fundamentales birradical singlete.

En 2005, *Kubo et al.* publicaron el derivado **a5** comprobando, por primera vez en este tipo de sistemas, la presencia de interacciones intermoleculares fuertes en estado sólido [72]. Este último y novedoso fenómeno, abrió la puerta a una candente discusión sobre los motivos que generaban este tipo de interacciones, ya que la estructura de rayos X mostraba la formación de cadenas 1D en escalera mediante la superposición de los centros radicales uno a uno y mostrando distancias intermoleculares propias de enlaces de centros múltiples. Esto sería confirmado por el mismo grupo tras el estudio de los derivados **a6, b1 y b2** (**Figura1.23a, b**) [73] que les permitió relacionar el mayor carácter

birradical de éstos con una menor distancia intermolecular en el empaquetamiento [74].

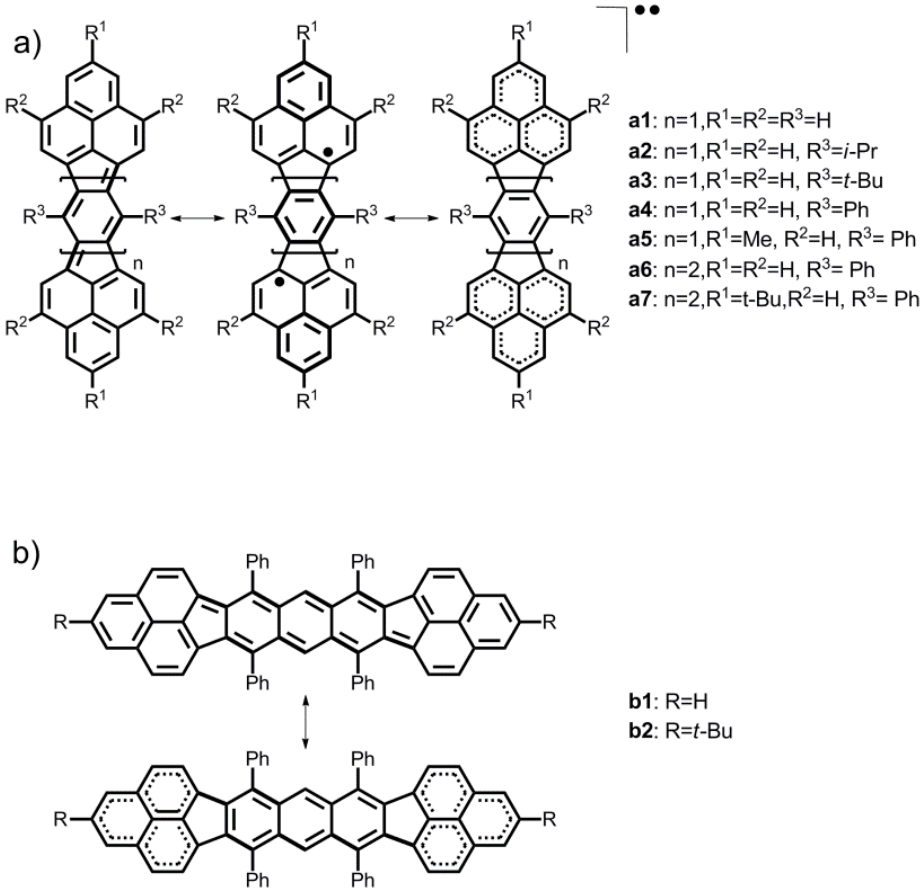

Figura 1.23 Estructuras resonantes para distintos derivados de indacenofenaleno: **a)** IDPL; **b)** IDPL-Ph_4.

1.1.4 BIBLIOGRAFÍA

1. *IUPAC Compendium of Chemical Terminology*. release 2.3.2 ed. 2012. 168.
2. Hicks, R.C., *Stable Radicals. Fundaments and Applied Aspects of Odd-Electron Compounds*. 2011: John Wiley & Sons. 606.
3. Nakano, M., Kishi, R., Nitta, T., Kubo, T.Nakasuji, K.,Kamada, K., Ohta, K., Champagne, B., Botek, E., Yamaguchi, K. *J. Phys. Chem. A*, 2005. **109**(5): p. 885-891.
4. Nakano, M.; Minami, T.; Yoneda, K.; Muhammad, S.; Kishi, R.; Shigeta, Y.; Kubo, T.; Rougier, L.; Champagne, B.; Kamada, K.; Ohta, K. *J. Phys. Chem. Lett.*, 2011. **2**(9): p. 1094-1098.
5. Nakano, M.; Kishi, R.; Nakagawa, N.; Ohta, S.; Takahashi, H.; Furukawa, S.; Kamada, K. ;Ohta, K.; Champagne, B. ;Botek, E ;Yamada, S.; Yamaguchi, K., *J. Phys. Chem. A*, 2006. **110**(12): p. 4238-4243.
6. Nakano, M. ;Kishi, R.; Ohta, S.; Takahashi, H.; Kubo, T.; Kamada, K.; Ohta, K.; Botek, E.; Champagne, B., *Phys. Rev. Lett.*, 2007. **99**(3): p. 033001.
7. Smith, M.B. and Michl, J. *Chem. Rev.* 2010. **110**(11): p. 6891-6936.
8. Coronado, E. and Epstein, A.J., *J. Mat. Chem. 2009.* **19**(12): p. 1670-1671.
9. *IUPAC Compendium of Chemical Terminology*. release 2.3.2 ed. 2012. 427.
10. Abe, M. *Chem. Rev.*, 2013. **113**(9): p. 7011-7088.
11. Breslow, R., *Chem. & Eng. News.,* 1965. **43**(26): p. 90-100.
12. Dewar, M.J.S., *Advan. Chem. Phys.*1965. **8**: p. 65.
13. Zilberg, S. and Haas, Y., *J. Phys. Chem. A* 1998. **102**(52): p. 10843-10850.
14. Shi, X; Burrezo, P. M.; Lee, S.; Zhang, W.; Zheng, B.; Dai, G.; Chang, J: Lopez Navarrete, J. T.; Huang, K-W.; Kim, D.; Casado, J.; Chi, C. *Chem. Sci.,* 2014. **5**(11): p. 4490-4503.
15. Breslow, R. *Acc. Chem. Res.* 1973. **6**(12): p. 393-398.
16. Wu, J. I. C.; Mo, Y.; Evangelista, F. A.; Von Rague Schleyer, P., *Chem, Comm.* 2012. **48**(67): p. 8437-8439.

17. Carl-Lineberger, W. and Borden, W. T., *Phys. Chem. Chem. Phys*, 2011. **13**(25): p. 11792-11813.
18. Berson, J.A., *Acc. Chem. Res.*, 1997. **30**(6): p. 238-244.
19. J. Cramer, C. *J., Chem. Soc., Perkin Trans. 2*, 1998(5): p. 1007-1014.
20. Schlenk, W. and Brauns, M., *Chem. Ber.* 1915. **48**(1): p. 661-669.
21. Yang, N.C. and Castro, A. J., *J. Am. Chem. Soc.,* 1960. **82**(23): p. 6208-6208.
22. Coppinger, G.M., Tetrahedron, 1962. **18**(1): p. 61-65.
23. Baumgarten, M., *High Spin Molecules Directed Towards Molecular Magnets*, in *EPR of Free Radicals in Solids II*, A. Lund and M. Shiotani, Editors. 2012, Springer Netherlands. p. 205-244.
24. Montgomery, L. K.; Huffman, J. C. ;Jurczak, E. A.; Grendze, M. P., *J. Am. Chem. Soc*, 1986. **108**(19): p. 6004-6011.
25. Thiele, J. and Balhorn, H., *Ber. Chem.*, 1904. **37**(2): p. 1463-1470.
26. Tschitschibabin, A.E., *Ber. Chem.*, 1907. **40**(2): p. 1810-1819.
27. Mayer, U.; Baumgärtel, H.; Zimmermann, H., *Angew. Chem. Int. Ed.*, 1966. **5**(3): p. 311-311.
28. Kikuchi, A.; Iwahori, F.; Abe, J., *J. Am. Chem. Soc.*, 2004. **126**(21): p. 6526-6527.
29. Porter, W.W.; Vaid, T.P.; Rheingold, A.L., *J. Am. Chem. Soc.*, 2005. **127**(47): p. 16559-16566.
30. Casado, J.; Patchkovskii, S.; Zgierski, M. Z.; Hermosilla, L.; Sieiro, C.; Moreno Oliva, M.; López Navarrete, J. T., *Angew. Chem. Int. Ed.*, 2008. **47**(8): p. 1443-1446.
31. Higuchi, H.; Nakayama, T.; Koyama, H.; Ojima, J.; Wada, T.; Sasabe, H., *Bull. Chem. Soc. Jpn.*, 1995. **68**(8): p. 2363-2377.
32. Ponce Ortiz, R.; Casado, J.; Hernández, V.; López Navarrete, J. T.; Viruela, P. M.; Ortí, E.; Takimiya, K-; Otsubo, T., *Angew. Chem. Int. Ed.,* **119**(47): p. 9215-9219.
33. Zhu, X.; Tsuji, H.; Nakabayashi, K.; Ohkoshi, S.; Nakamura, E., *J. Am. Chem. Soc.*, 2011. **133**(41): p. 16342-16345.
34. a) Hund, F., 1925. **33**: p. 345.; b) Levine, I. N. (1991). *Quantum Chemistry* (4th ed.). Prentice-Hall. pp. 303–304.
35. Dowd, P.; Chang, W.; Paik, Y.H*., J. Am. Chem. Soc.*, 1986. **108**(23): p. 7416-7417.
36. Dowd, P.; Chang, W.; Paik, Y.H., *J. Am. Chem. Soc.*, 1987. **109**(17): p. 5284-5285.

37. Borden, W.T., *Diradicals*, ed. W. Interscience. Vol. 1. 1982, New York.
38. Borden, W.T., *J. Am. Chem. Soc.*, 1975. **97**(21): p. 5968-5970.
39. Borden, W.T. and Davidson, E.R., *J. Am. Chem. Soc.*, 1977. **99**(14): p. 4587-4594.
40. Borden, W. T.; Iwamura, H.; Berson, J. A., *Acc. Chem. Res.*, 1994. **27**(4): p. 109-116.
41. Du, P. and Borden, W.T., *J. Am. Chem. Soc.*, 1987. **109**(3): p. 930-931.
42. Nachtigall, P. and Jordan, K.D., *J. Am. Chem. Soc.*, 1992. **114**(12): p. 4743-4747.
43. Pranata, J., *J. Am. Chem. Soc.*, 1992. **114**(26): p. 10537-10541.
44. Nachtigall, P. and Jordan, K.D., *J. Am. Chem. Soc.*, 1993. **115**(1): p. 270-271.
45. Prasad, B.L.V. and Radhakrishnan, T.P., J. Phys. Chem., 1992. **96**(23): p. 9232-9235.
46. Matsuda, K. and Iwamura, H., *J. Am. Chem. Soc.*, 1997. **119**(31): p. 7412-7413.
47. Lee, J.; Jadhav, P.; Reusswig, P. D.; Yost, S. R.; Thompson, N. J.; Congreve, D. N.; Hontz, E.; Van Voorhis, T.; Baldo, M. A., *Acc. Chem. Res.*, 2013. **46**(6): p. 1300-1311.
48. Wilson, M.; W. B. Rao, A.; Ehrler, B.; Friend, R. H., *Acc. Chem. Res.*, 2013. **46**(6): p. 1330-1338.
49. Zimmerman, P. M.; Musgrave, C. B.; Head-Gordon, M., *Acc. Chem. Res.*, 2013. **46**(6): p. 1339-1347.
50. Kamada, K. ; Ohta, K.; Kubo, T.; Shimizu, A.; Morita, Y.; Nakasuji, K.; Kishi, R.; Ohta, S.; Furukawa, S.; Takahashi, H.: Nakano, M., *Angew. Chem. Int. Ed.*, 2007. **46**(19): p. 3544-3546.
51. Masayoshi N.; Kyohei Y.; Ryohei K.; Hideaki T.; Takashi K.; Kenji K.; Koji O.; Botek, E.; Champagne, B., *J Chem. Phys.*, 2009. **131**(11): p. 114316.
52. Ko, K.C., D. Cho, Lee, J.Y., *J. Phys. Chem. A*, 2012. **116**(25): p. 6837-6844.
53. Matsuda, K., Matsuo, M.; Irie, M., *J. Org. Chem.*, 2001. **66**(26): p. 8799-8803.
54. Salem, L. Rowland, and C., *Angew. Chem. Int. Ed.*, 1972. **11**(2): p. 92-111.

55. Karafiloglou, P., *J. Chem. Ed.*, 1989. **66**(10): p. 816.
56. Karafiloglou, P., *J. Chem. Phys.*, 1985. **82**(8): p. 3728-3740.
57. Imahori, H.; Umeyama, T.; Ito, S., *Acc. Chem. Res.*, 2009. **42**(11): p. 1809-1818.
58. Kiyose , K.; Kojima, H.; Nagano T., *Chem. Asian. J.*, 2008. **3**(3): p. 506-515.
59. Motomura, S.; Nakano, M.; Fukui, H.; Yoneda, K.; Kubo, T.; Carion, R.; Champagne, B., *Phys. Chem. Chem. Phys.*, 2011. **13**(46): p. 20575-20583.
60. Fukuda, K. and Nakano, M., *J. Phys. Chem. A*, 2014. **118**(19): p. 3463-3471.
61. Nakano, M.; Champagne, B.; Edith, B.; Ohta, K.; Kamada, K.; Kubo, T., *J. Chem. Phys.*, 2010. **133**(15): p. 154302- 154317.
62. Chen, L.; Hernandez, Y.; Feng, X.; Müllen, K., *Angew. Chem. Int. Ed.*, 2012. **51**(31): p. 7640-7654.
63. Wu, J.; Pisula, W.; Müllen, K., *Chem. Rev.*, 2007. **107**(3): p. 718-747.
64. Michl, J. and Bonačić-Koutecký, V., *Tetrahedron*, 1988. **44**(24): p. 7559-7585.
65. Konishi, A.; Hirao, Y.; Nakano, M.; Shimizu, A.; Botek, E.; Champagne, B.; Shiomi, D.; Sato, K.; Takui, T.; Matsumoto, K.; Kurata, H.; Kubo, T., *J. Am. Chem. Soc.*, 2010. **132**(32): p. 11021-11023.
66. Sun, Z.; Ye, Q.; Chi, C.; Wu, J, *Chem. Soc. Rev.*, 2012. **41**(23): p. 7857-7889.
67. Sun, Z.; Zeng, Z.; Wu, J., *Acc. Chem. Res.*, 2014. **47**(8): p. 2582-2591.
68. Kubo, T.; Yamamoto, K.; Nakasuji, K.; Takui, T.; Murata, I., *Bull. Chem. Soc. Jpn.*, 2001. **74**(11): p. 1999-2009.
69. Kubo, T.; Yamamoto, K.; Nakasuji, K.; Takui, T.; Murata, I., *Angew. Chem. Int. Ed.*, 1996. **35**(4): p. 439-441.
70. Murata, I.; Sasaki, S.; Klabunde, K-U.; Toyoda, J.; Nakasuji, K., et al., *Angew. Chem. Int. Ed.*, 1991. **30**(2): p. 172-173.
71. Ohashi, K.; Kubo, T.; Masui, T.; Yamamoto, K.; Nakasuji, K.; Takui, T.; Kai, Y.; Murata, I., *J. Am. Chem. Soc.*, 1998. **120**(9): p. 2018-2027.

72. Kubo, T.; Shimizu, A.; Sakamoto, M.; Uruichi, M.; Yakushi, K.; Nakano, M.; Shiomi, D.; Sato, K.; Takui, T.; Morita, Y.; Nakasuji, K., *Angew. Chem.Int. Ed.*, 2005. **44**(40): p. 6564-6568.
73. Kubo, T.; Shimizu, A.; Uruichi, M.; Yakushi, K.; Nakano, M.; Shiomi, D.; Sato, K.; Takui, T.; Morita, Y.; Nakasuji, K., *Org. Lett*., 2006. **9**(1): p. 81-84.
74. Shimizu, A.; Kubo, T.; Uruichi, M.; Yakushi, K.; Nakano, M.; Shiomi, D.; Sato, K.; Takui, T.; Hirao, Y.; Matsumoto, K.; Kurata, H.; Morita, Y.; Nakasuji, K., *J. Am. Chem. Soc.*, 2010. **132**(41): p. 14421-14428.

2. Objetivos

2. OBJETIVOS

En la presente Tesis Doctoral se propone la caracterización del estado electrónico fundamental y de los estados electrónicos excitados de naturaleza triplete cercanos o casi degenerados en energía con el fundamental en moléculas policíclicas extendidas de naturaleza quinoide o pro-aromática. Estas moléculas son elegidas pues son susceptibles de, en función del tamaño de la cadena, presentar una apertura de la capa cerrada (o singlete capa cerrada) para dar lugar a un cierto carácter birradical modulable con la extensión o tamaño molecular y convertible de bajo a alto espín, o de singlte a triplete. Para ello se relacionarán los cambios en los espectos Raman vibracionales con la necesaria participación del mecanismo de doble polarización de espín cuando se estabiliza el singlete capa abierta. Se pretende obtener adicionales relaciones estructura-propiedad que puedan ser de utilidad para proponer nuevas plataformas moleculares en el contexto de la química de Hidrocarburos Policíclicos Aromáticos (*PAHs*). Dicha caracterización se lleva a cabo en base a tres sub-objetivos principales:

- ✓ Elucidación de la configuración electrónica de los sistemas objeto de estudio que permita clasificarlos como capa cerrada o capa abierta.

- ✓ En sistemas capa abierta, determinación de la multiplicidad de espín del estado fundamental.

- ✓ Estudio de la relación entre las características estructurales de los sistemas y la configuración electrónica del estado fundamental.

Para poder lograr los objetivos propuestos, se hace uso, fundamentalmente, de la espectroscopia vibracional Raman, técnica de contrastada utilidad en la caracterización de birradicales π-conjugados y sistemas π-conjugados en general. El uso de la espectroscopía Raman en sus variantes de resonancia Raman, pre-resonancia Raman y termo-espectroscopía Raman representa uno de los pocos casos donde esta técnica espectroscópica se utiliza para el análisis de este tipo de moléculas capa abierta o birradicales.

El conjunto de moléculas objeto de estudio se puede dividir en cuatro bloques, que corresponden con cuatro capítulos. Cada uno de ellos permite abordar los tres objetivos enumerados anteriormente desde distintas perspectivas:

Bloque 1: Derivados de perileno con sustituyentes bis(dicianometileno) sintetizados por el grupo del Prof. *Jishan Wu,* de la Universidad Nacional de Singapur. El conjunto de moléculas que constituye este bloque permite estudiar el efecto que sobre la estabilización de especies capa abierta tienen:

a) El aumento de la longitud de cadena a través del estudio de una serie de oligómeros derivados de perileno con sustituyentes bis(dicianometileno) en los extremos, desde el monómero al hexámero, *nPer-CN* (*n=1-6*), ver Figura 2.1:

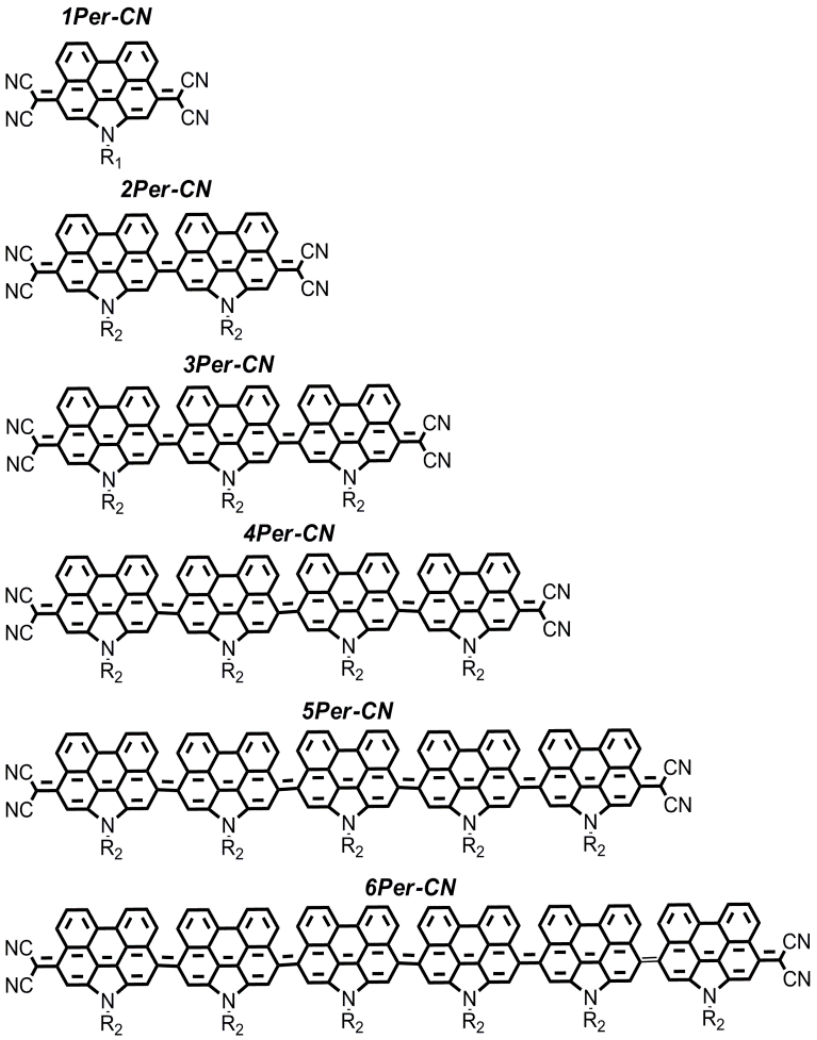

Figura 2.1 Estructura química de la serie *nPer-CN* (*n=1-6*), con R= C_8H_{17} para *n=1* y R= $C_{24}H_{49}$ para *n=2-6.*

b) La rigidificación del esqueleto conjugado mediante el estudio de los derivados de rileno quater- y hexa-rileno con sustituyentes bis(dicianometileno) en los extremos, *QR-CN* y *HR-CN*:

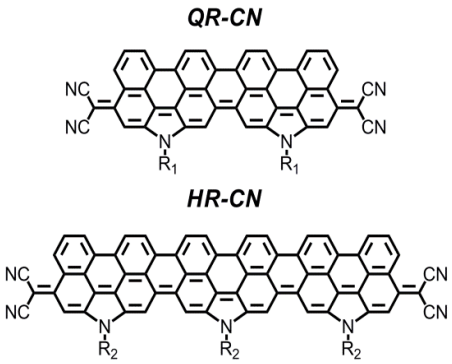

Figura 2.2 Estructura química de las moléculas *QR-CN* y *HR-CN*, con R_1= C_8H_{17} y R_2= $C_{52}H_{103}O_2$.

c) La inclusión de anillos de tiofeno entre el esqueleto conjugado y los grupos aceptores bis(dicianometileno), para lo cual se estudia la pareja de derivados *RyTh$_2$-CN* y *Ry$_2$Th$_2$-CN*.

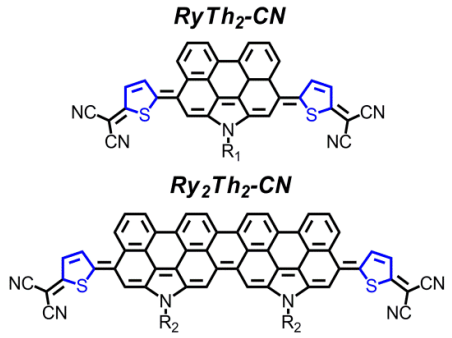

Figura 2.3 Estructura química de las moléculas *RyTh$_2$-CN* y *Ry$_2$Th$_2$-CN*, con R_1=$C_{16}H_{33}$ y R_2= $C_{24}H_{49}$.

Bloque 2: Derivados cetrénicos.

En este bloque se caracterizan tres nuevos derivados cetrénicos, *HZ-TIPS*, *OZ-TIPS* y *HZ-DI* sintetizados por el grupo del Prof. *Jishan Wu,* de la Universidad Nacional de Singapur. Éstos permiten determinar el papel que el aumento de la longitud de cadena, la inclusión de grupos aceptores y el carácter pro-aromático del puente tipo aceno tienen sobre la estabilización de especies neutras capa abierta. También se estudiaron las correspondientes especies cargadas para indagar en su relación con el carácter pro-aromático.

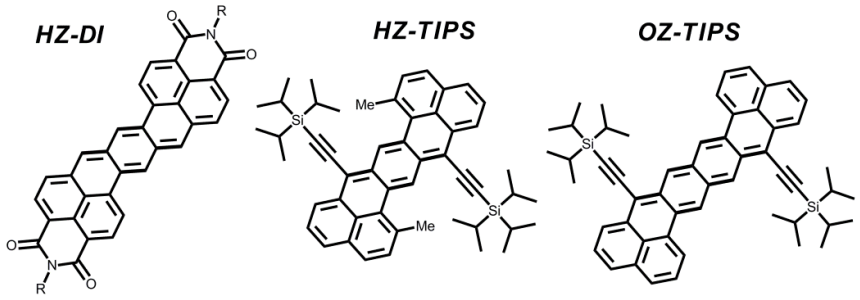

Figura 2.4 Estructura química de las moléculas *HZ-TIPS, OZ-TIPS* y *HZ-DI*, con R=$C_{11}H_{23}$.

Bloque 3: Derivados tetrabenzo-chichibabin.

La pareja de moléculas que integran este apartado, también sintetizados por el grupo del Prof. *Jishan Wu,* de la Universidad Nacional de Singapur, permite abordar el estudio de la influencia que tiene la inclusión de unidades tipo fluoreno o bencénico, deslocalizadoras de centros radicales, sobre la estabilización de especies capa abierta y especies cargadas, y, además, comprobar el efecto de la distorsión de la estructura molecular sobre la multiplicidad de espín en dos nuevos derivados tetrabenzo-chichibabin, *1-CS* y *2-OS*.

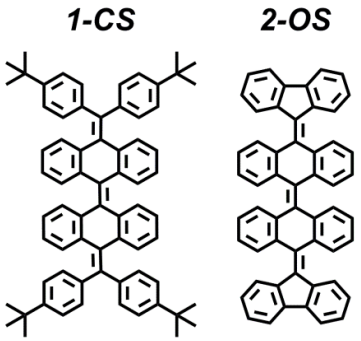

Figura 2.5 Estructura química de las moléculas *1-CS y 2-OS*.

Bloque 4: Derivados de naftoditiofeno con sustituyentes bis(dicianometileno) y bis(ciano-acilmetileno) sintetizados por el grupo del Prof. *Kazuo Takimiya* del *RIKEN Advanced Science Institute en Japón*.

En este último bloque se pretende analizar la influencia del carácter birradical de los sistemas objeto de estudio sobre la formación de enlaces σ débiles intermoleculares, asi como la caracterización de la evolución que sufre la estructura electrónica y molecular de las unidades monoméricas al formarse las correspondientes entidades supramoleculares.

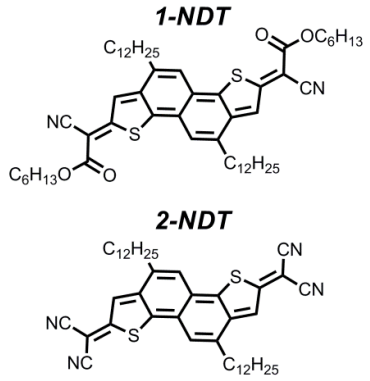

Figura 2.6 Estructura química de las moléculas *1-NDT y 2-NDT*.

Una vez caracterizados todos los sistemas estudiados y, a modo de objetivo transversal de esta Tesis Doctoral, se tratará de racionalizar, en términos del mecanismo DSP, los efectos que ejercen las distintas variaciones estructurales introducidas sobre el estado fundamental de cada una de las familias estudiadas y que se manifiestan directamente en la huella vibracional Raman, o lo que denominaremos en la transición desde el singlete birradical al birradical triplete, título elegido para la Tesis Doctoral.

3. Metodología

3. METODOLOGÍA

3.1 TÉCNICAS ESPECTROSCÓPICAS

La espectroscopia es la rama de la ciencia que estudia la interacción de la radiación electromagnética con la materia y por tanto, permite analizar propiedades estructurales a través del resultado de dicha interacción. Para ello, se analiza la distribución de intensidad de la radiación electromagnética, emitida, absorbida o dispersada por la muestra, en función de la longitud de onda o frecuencia de dicha radiación o espectro [1,5].

La naturaleza de la luz ha venido siendo objeto de debate desde la antigüedad en los ámbitos científico y filosófico pero la comprensión moderna de la misma surge con el célebre experimento que Newton realizó en 1665 sobre la dispersión de la luz blanca con un prisma triangular. En este experimento, se comprobaba como cualquier haz incidente de luz blanca se descomponía en el espectro del arcoiris. Más tarde cada color sería asignado a un único valor de longitud de onda o frecuencia.

Hacia 1815, Fraunhofer descubrió que el espectro de la luz solar estaba dividido por una serie de líneas oscuras, algo que Kirchoff relacionaría con la absorción, a ciertas frecuencias características, por parte de los elementos químicos presentes en las capas más externas del Sol. Se concluye entonces que cada elemento emite y absorbe luz a ciertas frecuencias fijas y características, con lo que los espectros de absorción y emisión atómicos se pueden considerar como la "huella dactilar" de los mismos. Este hallazgo da pie al desarrollo de la espectroscopia como ciencia práctica.

El desarrollo de la mecánica cuántica y la consiguiente propuesta de cuantización de la energía permitieron explicar los fenómenos de absorción y emisión de luz observados en átomos y moléculas. Una vez asumida la cuantización de la energía, la absorción de radiación electromagnética a una determinada frecuencia se relaciona con los niveles de energía implicados en la transición cuántica.

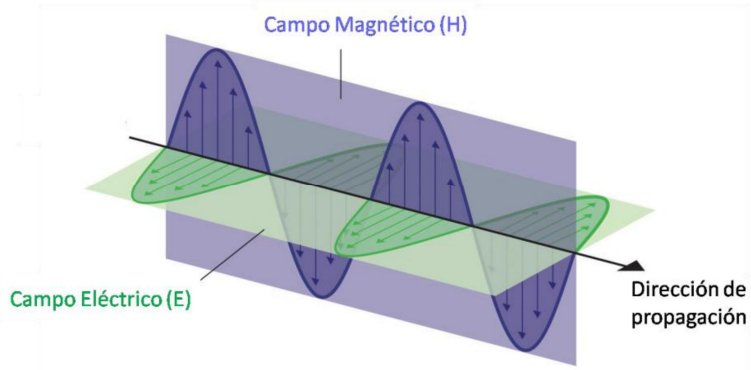

Figura 3.1 Oscilación de los campos eléctrico y magnético en una onda plana.

El fenómeno de la interacción radiación-materia está íntimamente relacionado con la naturaleza dual (ondulatoria y corpuscular) de la radiación electromagnética. Si se considera una onda electromagnética, los campos eléctrico *E* y magnético *H* oscilan perpendiculares entre si y con respecto a la dirección de propagación de la onda, tal y como se muestra en la **Figura 3.1**. Son estos campos ondulatorios los que interaccionan con la materia y permiten la obtención de espectros.

Para describir una onda electromagnética es necesario recurrir a dos parámetros fundamentales: la frecuencia, ν (o número de oscilaciones por segundo), que caracteriza la onda desde el punto de vista temporal, y la longitud de onda, λ, que es la distancia mínima entre dos puntos de la onda que se encuentran en fase (**Figura 3.2**). Ambos parámetros se

encuentran relacionados con la velocidad de propagación de la luz en el vacío *c*.

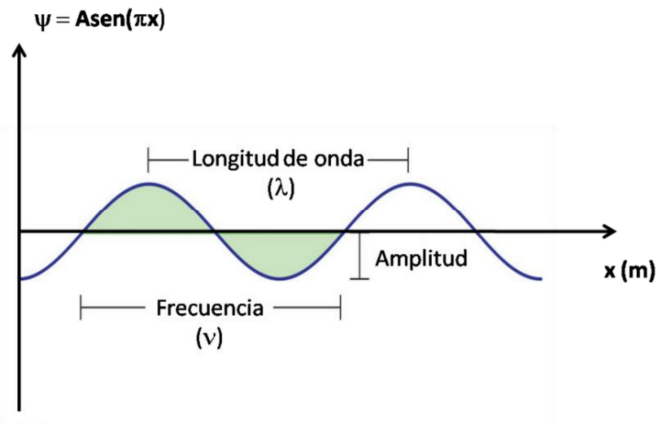

Figura 3.2 Representación de una onda electromagnética con longitud de onda λ.

La naturaleza corpuscular de la radiación electromagnética permite cuantizar la luz en fotones o corpúsculos cuya energía está directamente relacionada con ν a través de la constante de Planck (*h*).

Si se consideran dos estados cuánticos con energías E_1 y E_2, la transferencia de energía máxima entre ellos se produce cuando la energía del haz incidente coincide con $\Delta E=E_2-E_1$. Planck sugirió que la energía absorbida o emitida podía tomar la forma de una radiación electromagnética de frecuencia $\nu=\Delta E/h$. Esto permitiría relacionar la frecuencia de la radiación experimental con la variación de energía entre los niveles (ΔE) a través de la fórmula:

$$(E_{Fotón}=h\nu)_{Experimental} = (\Delta E=E_2-E_1)_{Teórica}$$

La utilidad de las técnicas espectroscópicas para el estudio de propiedades moleculares (geometría y conformación de la molécula,

constantes de fuerza, energías de enlace, etc.) parte de la dependencia de ΔE con la estructura molecular. Esto las ha convertido, a día de hoy, en imprescindibles a la hora de caracterizar materiales moleculares de diversa naturaleza.

Una de las principales ventajas de este tipo de técnicas radica en la posibilidad de acceder a un rango de frecuencias de la radiación incidente muy amplio, que permite analizar procesos de distinta naturaleza (rotaciones, vibraciones, transiciones electrónicas, nucleares, etc.) ya que cada uno de ellos se asocia a una determinada región de la radiación electromagnética (**Figura 3.3**).

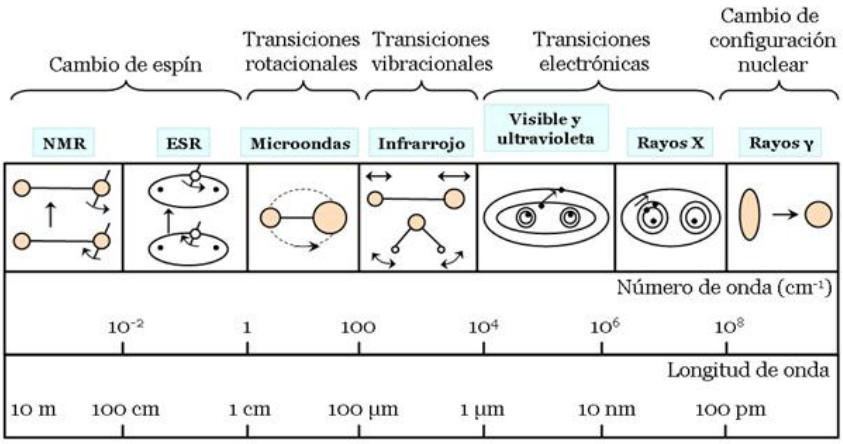

Figura 3.3 Efectos moleculares de la radiación en las distintas regiones del espectro electromagnético.

En el contexto de la investigación en la que se enmarca esta Tesis Doctoral se ha recurrido a una amplia variedad de técnicas espectroscópicas, como espectroscopias de absorción electrónica UV-Vis-NIR, Resonancia Magnética Nuclear (RMN) o Resonancia de Espín Electrónico (ESR). La presente memoria, sin embargo, está enfocada, casi exclusivamente, a la aplicación de la espectroscopia vibracional Raman, e

Infrarroja en menor medida, al estudio de Hidrocarburos Policíclicos Aromáticos (*PAHs*) con carácter birradical.

3.1.2 ESPECTROSCOPIA VIBRACIONAL

Tres cordenadas describen la posición de una partícula aislada en el espacio tridimensional. Ésta presenta tres grados de libertad que representan las tres posibles traslaciones de la misma a lo largo de cada uno de los ejes que describen el sistema de referencia. En el caso de moléculas poliatómicas, éstas deben definirse por la posición de cada uno de los átomos que las integran, o por 3N coordenadas en el espacio cartesiano. De estas 3N coordenadas, tres corresponden a las traslaciones (o desplazamientos del centro de masas) a lo largo de los ejes cartesianos y otras tres corresponden a rotaciones con respecto a los ejes de inercia (en moléculas lineales sólo hay posibilidad de giro sobre dos ejes). El resto de coordenadas corresponden a desplazamientos relativos de los átomos que no conllevan desplazamiento del centro de masas, es decir, 3N-6 vibraciones en moléculas no lineales y 3N-5 en moléculas líneales.

Los espectros vibracionales son más complejos que los espectros electrónicos en cuanto a número de bandas y ofrecen una información más completa acerca de los materiales que se estudian. Se denomina modo normal de vibración a cada uno de los movimientos de vibración de una molécula en los que todos los átomos se mueven con la misma frecuencia.

Aunque a partir de un espectro IR o Raman se puede asignar cada uno de los modos de vibración de la molécula en cuestión, no siempre es necesaria una asignación exhaustiva sino que se puede obtener información valiosa a partir de:

- Comparación de frecuencias en espectros de moléculas parecidas.
- Análisis de los desplazamientos de frecuencias inducidos al variar el patrón de sustitución en las moléculas o el tamaño de las mismas.
- Estudio de los efectos que se produzcan en los espectros al modificar las condiciones de concentración, temperatura, presión o polaridad del medio.

Este tipo de comparaciones serán de gran utilidad para dar respuesta a las múltiples interrogantes que surgen al analizar los resultados experimentales obtenidos para los sistemas objeto de estudio en esta Tesis Doctoral. En base a ellas, en conjunción con las demás técnicas espectroscópicas enumeradas anteriormente, y con ayuda de cálculos químico-cuánticos, se podrá caracterizar de manera inequívoca la configuración electrónica del estado fundamental de los integrantes de cada una de las familias estudiadas y relacionar ésta con los distintos rasgos de la estructura molecular de cada sistema.

Respecto al sistema de detección, las técnicas espectroscópicas vibracionales se pueden dividir en dispersivas e interferométricas. Las técnicas dispersivas fueron las primeras en desarrollarse. En ellas, la radiación policromática procedente de la muestra se dispersa mediante prismas y redes de difracción, permitiendo así que un estrecho rango de frecuencias llegue al detector. Mediante desplazamientos mecánicos de los distintos componentes ópticos del espectrofotómetro se obtiene el espectro completo, al permitir que distintas regiones espectrales lleguen sucesivamente al detector. Este mecanismo, sin embargo, presenta ciertas desventajas, principalmente relacionadas con la lentitud que implica la mínima fracción de luz dispersada por la muestra que llega al detector para cada alineamiento de los elementos ópticos. Esto lleva, inevitablemente, a tiempos de adquisición largos que pueden generar alteraciones significativas en las muestras, sobre todo en las de tipo

orgánico, debido al calentamiento que se puede producir al exponer las muestras durante largo tiempo a una radiación incidente relativamente intensa.

Por su parte, las técnicas interferométricas se basan en el uso de un dispositivo denominado interferómetro, habitualmente de tipo Michelson (**Figura 3.4**).

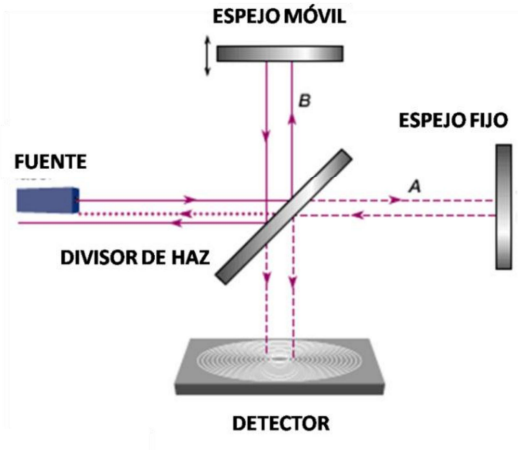

Figura 3.4 Interferómetro de Michelson.

El elemento fundamental del interferómetro es el divisor de haz o *beamsplitter*. Éste es capaz de dividir el haz lumínico procedente de la fuente en dos frentes de onda idénticos que se propagan en direcciones perpendiculares, de forma que una mitad de la radiación se dirige hacia un espejo móvil y la otra hacia un espejo fijo. Tras la reflexión en los correspondientes espejos, ambas radiaciones se recombinan dando lugar a un patrón de interferencias constructivas y destructivas cuya naturaleza depende del desplazamiento del espejo móvil con respecto a su posición de equilibrio. Este nuevo haz recombinado interacciona con la muestra antes de llegar al detector. Finalmente se obtiene el correspondiente interferograma, el cual necesita ser tratado matemáticamente mediante

la transformada de Fourier para presentar la información obtenida de manera útil, es decir, en la forma de un espectro convencional. La espectroscopia interferométrica por transformada de Fourier aventaja a las técnicas dispersivas en términos de tiempo de registro, ya que permite analizar de forma simultánea todo el rango de frecuencias (ventaja *multiplex*). Esta disminución del tiempo de adquisición implica una mejora de la relación señal-ruido y, a su vez, minimiza el riesgo de degradación de las muestras. Por otra parte, se adelgaza el número de elementos móviles y permite una mayor resolución que los sistemas dispersivos.

3.1.2.1 ESPECTROSCOPIA VIBRACIONAL RAMAN

La espectroscopia Raman está basada en el estudio del espectro de la luz dispersada por la materia. En su mayor parte, esta luz dispersada está constituida por radiación de la misma frecuencia que el haz incidente, la conocida como dispersión Rayleigh o elástica. El interés de la espectroscopia Raman tiene que ver, sin embargo, con una pequeña fracción de esa luz que es dispersada a frecuencias diferentes a la de la luz incidente (dispersión inelástica) y que es la que aporta información a nivel molecular.

El fenómeno de dispersión Raman debe su nombre a Chandrasekhara Venkata Raman, que lo descubrió experimentalmente en 1928 [6-8], hallazgo que le haría merecedor del Premio Nobel de Física en 1930.

La radiación electromagnética, en términos de Teoría Cuántica, se puede considerar como un conjunto de fotones de energía *hv*. Éstos pueden interaccionar con las moléculas de forma elástica, dando lugar a la dispersión Rayleigh. Si durante la interacción materia-fotón se inducen movimientos nucleares, se da una transferencia de energía entre ambas entidades. Este proceso inelástico es lo que se conoce como efecto

Raman e implica diferencias de energía de un quanto vibracional entre los fotones incidentes y los fotones dispersados (**Figura 3.5**). Se trata de un fenómeno con una probabilidad muy baja de ocurrir, dado que sólo un fotón de cada 10^6-10^8 es dispersado inelásticamente.

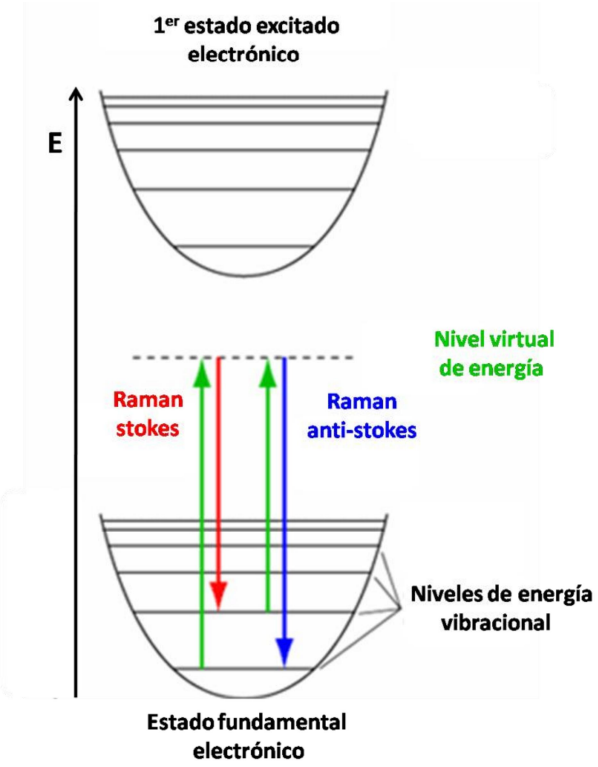

Figura 3.5 Representación de los fenómenos de dispersión Raman Stokes y anti-Stokes.

Si durante la colisión la molécula gana energía vibracional, $\Delta E>0$, la frecuencia de la radiación dispersada es menor que la de la radiación incidente y se denomina Raman Stokes. Sin embargo, puede ocurrir que existan estados vibracionales excitados poblados térmicamente. En este caso, es posible que la molécula transfiera energía al fotón dispersado, dando lugar a la dispersión Raman anti-stokes. Debido a que, según la

distribución de Boltzmann, los estados excitados se encuentran menos poblados que los fundamentales, la radiación Raman Stokes será más intensa que la anti-Stokes en un factor que depende directamente de la temperatura[9]. Es importante destacar que para explicar estos fenómenos de dispersión de luz, se considera que la transición tiene lugar a través de un estado "virtual", el cual no tiene porqué coincidir con un tránsito entre dos estados estacionarios.

En términos clásicos, la actividad Raman de una molécula se relaciona directamente con su polarizabilidad molecular. Cuando una molécula se somete a un campo eléctrico su densidad electrónica se distorsiona o polariza. Esta separación de carga provoca la aparición de un momento dipolar eléctrico inducido. El nuevo vector momento dipolar inducido $\vec{\mu}$ y el vector campo eléctrico $\vec{E}$ están relacionados, en el caso más general, mediante el tensor de polarizabilidad $\bar{\bar{\alpha}}$ según la expresión:

$$\vec{\mu} = \bar{\bar{\alpha}} \cdot \vec{E}$$

Así, $\bar{\bar{\alpha}}$ indica la facilidad con la que se deforma la nube electrónica de la molécula en respuesta al campo eléctrico y se representa gráficamente a través del elipsoide de polarizabilidad.

Asumiendo un comportamiento oscilante del campo eléctrico sin desfase, se obtiene:

$$\mu = \alpha E = \alpha E_0 sen(2\pi\nu \cdot t)$$

La vibración de las moléculas, a su vez, puede provocar cambios en la polarizabilidad y, como consecuencia, en el momento dipolar inducido. Esto puede describirse en los siguientes términos:

$$\alpha = \alpha_0 + \beta sen(2\pi\nu_0 \cdot t)$$

$$\mu = \alpha E = (\alpha_0 + \beta sen(2\pi\nu_0 \cdot t))E_0 sen(2\pi\nu_{vib} \cdot t)$$

$$\mu = \alpha_0 E_0 sen(2\pi\nu \cdot t) + \frac{1}{2}\beta E_0\{cos2\pi(\nu - \nu_{vib})t - cos2\pi(\nu + \nu_{vib})t\}$$

El momento dipolar inducido, por tanto, aporta componentes de frecuencia ν y ν ± ν_{vib}, poniendo de manifiesto la dispersión de la frecuencia incidente en porciones vibracionales, o dispersión Raman vibracional. Se puede decir que la regla de selección para que una vibración sea activa en Raman es que debe cambiar el momento dipolar inducido de la misma durante la vibración molecular, es decir, se debe acusar algún cambio en la magnitud o dirección del elipsoide de polarizabilidad.

Uno de los principales inconvenientes que surgieron en los inicios de la espectroscopia Raman tenía que ver con la debilidad de la señal mencionada con anterioridad. La intensidad de la dispersión Raman vibracional se puede estimar suponiendo una molécula en un estado vibracional *m* la cual interacciona con radiación de frecuencia ν_0 e intensidad I_0. Esta interacción hace que la molécula sea excitada a un nivel vibracional *n* a la vez que se dispersa radiación de frecuencia $\nu_0 + \nu_{mn}$. La intensidad de la luz dispersada, una vez promediadas todas las posibles orientaciones de la molécula, viene expresada de la siguiente forma:

$$I_{mn} = \frac{2^7\pi^5}{3^2c^4} I_0(\nu_0 + \nu_{mn})^4 \sum_{\rho,\sigma} \left|(\sigma_{\rho\sigma})_{mn}\right|^2$$

donde *c* es la velocidad de la luz, *ρ* y *σ* se refieren al sistema de coordenadas centrado en la molécula y $(\alpha_{\rho\sigma})_{mn}$ es la componente m,n del tensor de polarizabilidad para una transición *m*→*n*.

Como puede observarse, la intensidad de la señal Raman es proporcional a la cuarta potencia de la frecuencia de la radiación incidente. Esto implica la necesidad de usar haces altamente energéticos para obtener una señal Raman apreciable, algo que no fue posible hasta la aparición del primer láser en 1960. Este hito, unido al desarrollo de fotomultiplicadores para la detección de la señal, ha permitido el enorme desarrollo alcanzado hasta la fecha por la espectroscopia Raman y técnicas análogas.

Otro de los principales inconvenientes a la hora de registrar espectros Raman tiene que ver con la fluorescencia. Ésta, al ser varios órdenes de magnitud mayor que la señal Raman, es capaz de enmascararla y hacer inviable el estudio de muchos materiales. Una de las soluciones más eficaces para solventar este problema es el uso de un láser de longitud de onda excitatriz correspondiente a zonas de menor energía que la región coloreada o de la región de infrarrojo cercano (NIR). Por ejemplo, el láser de Nd:YAG (*Neodymium doped Ytrium Aluminium Garnet*), 1064 nm, normalmente no es lo suficientemente energético como para causar transiciones electrónicas reales, evitando así fenómenos de fluorescencia.

Una variante muy interesante, y de gran utilidad en el estudio de materiales mediante espectroscopia Raman es el fenómeno de Resonancia Raman. Ésta ocurre cuando la frecuencia de excitación es muy cercana o coincidente con la de una transición electrónica [9, 10]. En estas condiciones tiene lugar una intensificación de la dispersión Raman que puede llegar a ser de hasta seis órdenes de magnitud, lo que permite incrementar los límites de detección (sensibilidad) y disminuir los tiempos de adquisición. Sin embargo, esta condición de cercanía con una transición electrónica puede incrementar la posibilidad de que aparezcan problemas de emisión fluorescente, como se mencionó con anterioridad.

Son múltiples las ventajas prácticas que presenta la espectroscopia Raman ya que se puede aplicar a distintos estados de agregación [4], no es necesaria preparación de muestra, no es destructiva y además permite la detección de muestras en medios acuosos [11].

3.1.2.1.1 ESPECTROSCOPIA VIBRACIONAL RAMAN EN MATERIALES CONJUGADOS

Los materiales conjugados se caracterizan por presentar una nube de electrones π altamente polarizable. La deslocalización π-electrónica que presentan este tipo de sistemas puede evaluarse mediante la longitud de conjugación efectiva, la cual representa la distancia molecular a la que todavía son efectivas las interacciones entre electrones π de las sucesivas unidades que integran la cadena oligomérica. A su vez, este parámetro se puede evaluar cualitativamente a través del desplazamiento de las bandas Raman en una familia de oligómeros conjugados.

El análisis de espectros vibracionales, y más concretamente espectros Raman de sistemas conjugados, implica, necesariamente, considerar un fuerte acoplamiento entre la estructura del esqueleto molecular (geometría nuclear de equilibrio y desplazamiento nuclear vibracional) y la deslocalización π-electrónica. Por este motivo, cualquier modificación de la nube π-electrónica del sistema conlleva una modificación casi instantánea de la geometría molecular y viceversa. En otras palabras, el análisis del espectro Raman de sistemas conjugados ofrece información sobre la geometría molecular y acerca de la estuctura electrónica. Así, la espectroscopia Raman es una herramienta muy útil en términos de, entre otros:

I. Análisis de la efectividad de la π-conjugación a lo largo de una serie homóloga de oligómeros [12-14].

II. Caracterización de defectos conjugacionales introducidos por *doping* químico, fotoexciación, etc [15-17].

III. Estimación del grado de transferencia de carga intramolecular en cromóforos conjugados de tipo *push-pull* (dador-π-aceptor) [18,19].

Posiblemente, una de las aportaciones de mayor impacto en el campo de la espectroscopia Raman de materiales conjugados sea el Modelo de Conjugación Efectiva (ECC, "*Effective Conjugation Coordinate*") propuesto por el grupo del *Prof. Zerbi* del Politécnico de Milán [20-22]. Éste permitía explicar un conjunto de características espectrales observadas en una serie de oligotiofenos aromáticos de longitud de cadena creciente con sustituyentes metilo en las posiciones terminales [23] y que se hacían extensibles a otras familias de oligómeros π-conjugados. De modo muy breve, estas características consistían en una gran simplicidad espectral, en contraste con el elevado número de bandas previsto por las reglas de selección, y en la aparición de bandas intensas en la zona de las vibraciones ν(C=C/C-C), de entre las cuales, las predominantes aumentaban su intensidad y disminuían su frecuencia al aumentar la longitud de cadena. En este contexto, el modelo ECC postula la existencia de un modo de tensión C=C/C-C colectivo a lo largo del cual se produce el acoplamiento electrón-fonón. Esta vibración colectiva describe la evolución de la estructura desde el estado fundamental hasta el estado excitado. En sistemas policonjugados aromáticos o heteroaromáticos esta coordenada ECC colectiva toma la forma de una combinación lineal de tensiones de anillo C=C/C-C que conlleva la evolución del sistema desde una estructura bencenoide (estado fundamental) hacia una quinoide (estado excitado), ocurriendo a la inversa en sistemas con estado fundamental de tipo quinoide.

3.1.2.1.1.1 ESPECTROSCOPIA VIBRACIONAL RAMAN EN BIRRADICALES: DETECCIÓN DE TRIPLETES

Para hablar de la utilidad de la espectroscopia Raman en caracterización de birradicales conjugados es necesario considerar primero una de las técnicas de rutina en caracterización de radicales, la espectroscopia de resonancia de espín electrónico ("*Electron Spin Resonance*", ESR).

De modo genérico, se puede decir que las espectroscopias de resonancia magnética son técnicas en las que un campo magnético oscilante induce transiciones entre niveles de energía de un sistema paramagnético (con electrones desapareados), al desdoblarse éstos por la acción de un campo magnético estático [24]. En particular, la Resonancia de Espín Electrónico (ESR), o Resonancia Paramagnética de Espín, estudia los dipolos magnéticos de origen electrónico (rango de las microondas (10^9-10^{11} Hz), mientras que la Resonancia Magnética Nuclear (RMN) analiza los espines de orígen nuclear [rango de radiofrecuencias (10^6-10^9 Hz)].

En espectroscopia ESR una especie paramagnética es iluminada con radiación de microondas, a una frecuencia constante ν, mientras se somete a un barrido de campo magnético $\vec{H}$. La absorción se produce cuando la diferencia de energía entre los estados asociados al espín desapareado coincide con la energía de la radiación de microondas.

De manera muy simplificada, el funcionamiento de la espectroscopia ESR se puede explicar considerando el caso más sencillo, un sistema con un solo electrón desapareado o monorradical. Este sistema posee un número cuántico de espín de ½ que, en ausencia de campo magnético, existe en dos estados degenerados correspondientes con los números magnéticos de espín: m_S = +1/2 y m_S = -1/2. La aplicación de un campo magnético externo hace que estos niveles se desdoblen,

perdiendo su degeneración y permitiendo inducir transiciones entre ellos si se irradia con la energía adecuada.

Los niveles de energía de las dos orientaciones posibles vienen dados por la ecuación: $E=g\mu_B m_S H$, de forma que la energía de un electrón con $m_S = +1/2$ (α) aumenta y la de un electrón con $m_S = -1/2$ (β) disminuye al aumentar el campo magnético aplicado. La separación de niveles, por tanto, vendrá dada por la expresión: $\Delta E=g\mu_B H$, donde *g* representa el factor de Landé, característico de cada especie, μ_B es el magnetón de Bohr y *H* representa el módulo del campo magnético (**Figura 3.6**).

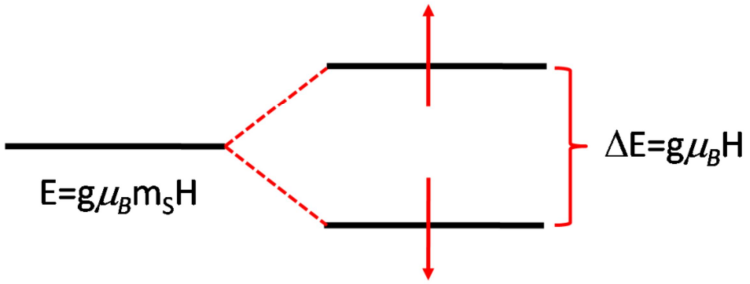

Figura 3.6 Separación de los niveles electrónicos tras aplicar un campo magnético

Esto implica que la especie en cuestión entrará en resonancia para aquellos valores de campo magnético externo en los que la diferencia de energía entre los dos niveles energéticos que difieren en sus momentos angulares de espín sea igual a la energía correspondiente a la frecuencia de irradiación, es decir, cuando se cumpla la relación:

$$\Delta E=h\nu=g\mu_B H$$

La señal de un electrón desapareado puede ser múltiple debido a la interacción del momento magnético de espín electrónico con el momento de espín nuclear (*I*) en átomos con *I* no nulos, como es el caso

de los átomos de nitrógeno, con *I=1*. Esta interacción de espín electrónico y nuclear multiplica las líneas de resonancia debido al desdoblamiento de los niveles energéticos que implica. A estas líneas de resonancia se las denomina acoplamientos hiperfinos (**Figura 3.7**).

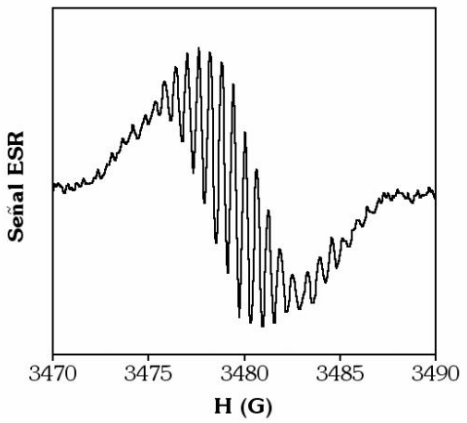

Figura 3.7 Espectro ESR de un anión radical en donde se pueden apreciar acoplamientos hiperfinos.

La existencia de estos acoplamientos es muy útil en el estudio de especies químicas con electrones desapareados ya que permite obtener información relativa a la distribución del electrón en la molécula dependiendo de sus interacciones con los núcleos.

Los parámetros de un espectro ESR a partir de los cuales se puede obtener información relevante sobre la molécula son, principalmente, el factor de Landé [25], el campo magnético de resonancia, la amplitud *h*, y la anchura de la señal ΔH_{pp}, y la constante de acoplamiento *a*, en el caso de existir acoplamientos hiperfinos.

La detección de birradicales suele resultar, a menudo, problemática mediante ESR. En el caso de moléculas conjugadas, la

presencia de tripletes implica *gaps* HOMO-LUMO muy bajos, de modo que el coste energético de desaparear los electrones sea mínimo. Estos sistemas pueden presentar dos comportamientos distintos: (i) en caso de que los dos electrones se encuentren tan alejados que no se sientan entre sí, comportándose en la práctica como un monorradical, (ii) que los dos electrones interaccionen entre sí, manifestando lo que se denomina desdoblamiento a campo cero, como consecuencia del campo magnético que genera cada electrón sobre el otro. En este último caso, aparecen dos estados de distinta energía: uno simétrico (estado triplete, S=1) y otro antisimétrico (estado singlete, S=0) cuyas energías dependen de la integral de canje.

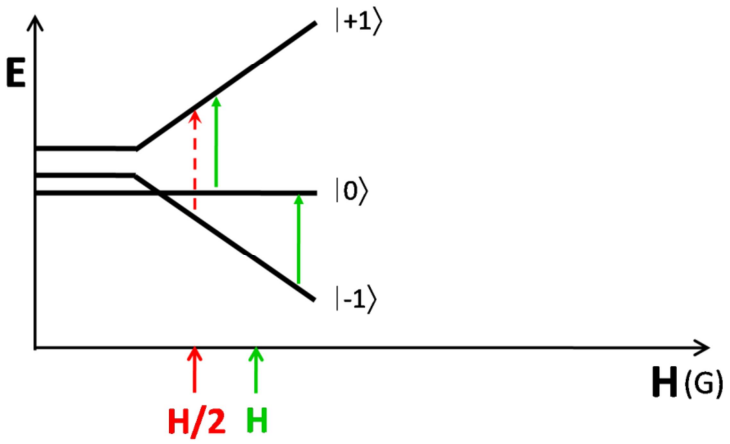

Figura 3.8 Transiciones electrónicas permitidas (en verde) y prohibidas (en rojo) para un sistema con S=1.

En la **Figura 3.8** se puede observar como, por la regla de selección $\Delta M_S = 1$, las transiciones permitidas para un birradical triplete son dos (flechas verdes), las cuales aparecen a distintos valores de campo magnético. Esto se traduce comúnmente en absorciones anchas en el espectro experimental (envolvente de las dos señales) centradas en la

zona de *g*=2, lo que dificulta enormemente discernir entre una señal correspondiente a un monorradical y una que proviene de un birradical. Un indicativo inequívoco de la naturaleza birradicalaria triplete de un determinado sistema es la concocida como prueba del triplete o señal a campo mitad (línea roja en la **Figura 3.8**). Se trata, sin embargo, de una señal muy débil al deberse a una transición prohibida ($\Delta M_S = 2$) y por ello no siempre se puede detectar, lo que constituye uno de los mayores problemas en la identificación de sistemas en estado triplete. Este inconveniente se ve incrementado con la disminución de la diferencia energética singlete-triplete, que implica un ensanchamiento de la señal a campo mitad, algo característico en birradicales orgánicos conjugados como los que se estudian en la presente Tesis Doctoral. Quizá el caso más representivo de esta problemática lo constituya la paradoja de Chichibabin o paradoja del birradical [26], cuya multiplicidad de espín del estado fundamental, tal y como se adelantaba en la introducción ha sido motivo de gran controversia. Esta limitación que comunmente presenta el ESR para la detección de birradicales triplete se puede solventar en muchos casos mediante la aplicación de la espectroscopia Raman.

En 2007, nuestro grupo de investigación consiguió caracterizar el estado fundamental de una serie de oligotiofenos quinoides tetracianosustituidos, cuyos derivados más largos, de cinco y seis unidades, presentaban señales ESR anchas con valores de g=2.0033. El uso de la espectroscopia Raman en condiciones de resonancia y fuera de ellas, y en función de la temperatura, más el apoyo de cálculos químico cuánticos, permitió asignar la señal ESR observada a la presencia de un estado excitado triplete poblado térmicamente a temperatura ambiente. Éste se caracterizaba por una mayor aromaticidad de los anillos centrales con respecto al estado fundamental singlete capa abierta en equilrio con el, cuya existencia quedaba a su vez justificada con la detección de dicho estado excitado triplete [27]. Este trabajo, junto con otro de la misma naturaleza que en 2008 permitió caracterizar el estado fundamental de un

viológeno extendido como birradical triplete [28], sentaron las bases para el estudio que se lleva a cabo en esta Tesis Doctoral y que permite interpretar la evolución del carácter capa abierta y la multiplicidad de espín del estado fundamental en una serie de moléculas policíclicas de base fundamentalmente bencenoide, a partir principalmente de la información que aporta la espectroscopia Raman a nivel de estructura molecular y electrónica.

3.2 BIBLIOGRAFÍA

1. Hollas, J.M., *Modern Spectroscopy*, ed. J.W. Sons. 1992.
2. Colthup, N.B. and Daly, l.H., *Introduction to Infrared and Raman Spectroscopy*. 1975, Academia Press.
3. Banwell, C.N. and McCash, E.M., *Fundaments of Molecular Spectroscopy.* 1994., McGraw-Hill Education
4. Requena, A. and J. Zúñiga, *Espectroscopía*, ed. Pearson. 2004.
5. Harris, D.C. and Bertolucci, M.D., *Symmetry and Spectroscopy. An Introduction to Vibrational and Electronic spectroscopy*. 1989: Docer Publications.
6. Raman, C.V. and K.L. Krishnan, *Nature*, 1928. **121**: p. 501.
7. Raman, C.V., *Indian J. Phys.*, 1928. **2**: p. 387.
8. Raman, C.V. and Krishnan, K.L., *Indian J. Phys.*, 1928. **2**: p. 399.
9. Smith, E. and Dent, G., *Modern Raman Spectroscopy. A Practical Approach*. 2005: Wiley
10. Ball, D.W., Spectroscopy, 2001. **16**: p. 32.
11. Petry, R.; Schmitt, M.; Popp, J., *ChemPhysChem*., 2003. **4**(1): p. 14-30.
12. Hernández, V.; Casado, J.; Ramírez, F. J.; Zotti, G.; Hotta, S.; López Navarrete, Juan T., *J. Chem. Phys.*, 1996. **104**(23): p. 9271-9282.
13. Casado, J.; Hernández, V.; Hotta, S.; López Navarrete, J. T., *J. Chem. Phys.*, 1998. **109**(23): p. 10419-10429.
14. Moreno Castro, C.; Ruiz Delgado, M. C.; Hernández, V.; Hotta, S.; Casado, J.; López Navarrete, J. T., *J. Chem. Phys.*, 2002. **116**(23): p. 10419-10427.
15. Casado, J.; Hernández, V.; Hotta, S.; López Navarrete, Juan T., *Adv. Mater.*, 1998. **10**(17): p. 1458-1461.
16. Casado, J.; Miller, L. L.; Mann, K. R.; Pappenfus, T. M.; Kanemitsu, Y.; Ortí, E.; Viruela, P. M.; Pou-Amérigo, R.; Hernández, V.; López Navarrete, J. T., *J. Phys. Chem. B*, 2002. **106**(15): p. 3872-3881.
17. Casado, J.; Ruiz Delgado, M. C.; Shirota, Y.; Hernández, V.; López Navarrete, J. T., *J. Phys. Chem. B*, 2003. **107**(12): p. 2637-2644.
18. Hernández, V.; Casado, J.; Effenberger, F.; López Navarrete, J. T., *J. Chem. Phys.*, 2000. **112**(11): p. 5105-5112.

19. Casado, J.; Hernández, V.; Kim, O-K.; Lehn, J-M.;López Navarrete, Juan T.; Delgado Ledesma, S.; Ponce Ortiz, R.; Ruiz Delgado, M. C.; Vida, Y.; Pérez-Inestrosa, E., *Chem. Eur. J.*, 2004. **10**(15): p. 3805-3816.
20. Zerbi, G.; Castiglione C.; and Del Zoppo, M., *Electronic Materials: The Oligomeric Approach*. 1998: Wiley-VCH.
21. a) Castiglioni C.; Gussoni, M.; López Navarrete, J. T.; Zerbi, G., Solid State Commun., 1988, **65**, p. 625. b) López Navarrete, J. T. and Zerbi, G., *J. Chem. Phys.*, 1991. **94**(2): p. 957-964.
22. Hernandez, V.; Castiglioni, C.; Del Zoppo, M.; Zerbi, G., *Phys. Rev B*, 1994. **50**(14): p. 9815-9823.
23. Hernández, V.; Casado, J.; Ramírez, F. J.; Zotti, G.: Hotta, S.; López Navarrete, J. T., *J. Chem. Phys.*, 1996. **100**(1): p. 289-293.
24. Wertz, J.R. and Bolton, J.R., *Electron Spin Resonance: Elementary and Practical Applications*. 1972: McGraw-Hill.
25. Zotti, G.; Zecchin, S.; Vercelli, B.; Pasini, M.; Destri, S.; Bertini, F.; Berlin, A., *Chem. Mater.*, 2006. **18**(13): p. 3151-3161.
26. McConnell, H.M., *J. Chem. Phys.*, 1960. **33**(6): p. 1868-1869.
27. Ponce Ortiz, R.; Casado, J.; Hernández, V.; López Navarrete, Juan T.; Viruela, P. M.; Ortí, E.; Takimiya, K-; Otsubo, T., *Angew. Chem. Int. Ed.,* **119**(47): p. 9215-9219.
28. Casado, J.; Patchkovskii, S.; Zgierski, M. Z.; Hermosilla, L.; Sieiro, C.; Moreno Oliva, M.; López Navarrete, Juan T., *Angew. Chem. Int. Ed.*, 2008. **47**(8): p. 1443-1446.

4. Derivados de Perileno bis(dicianometileno)-sustituidos

4. DERIVADOS DE PERILENO BIS(DICIANOMETILENO)

4.1 INFLUENCIA DEL AUMENTO DE LA LONGITUD DE CADENA SOBRE LA GENERACIÓN Y ESTABILIZACIÓN DE ESTADOS BIRRADICALARIOS DE ALTO Y BAJO ESPÍN EN DERIVADOS DE P-QDM BIS(DICIANOMETILENO).

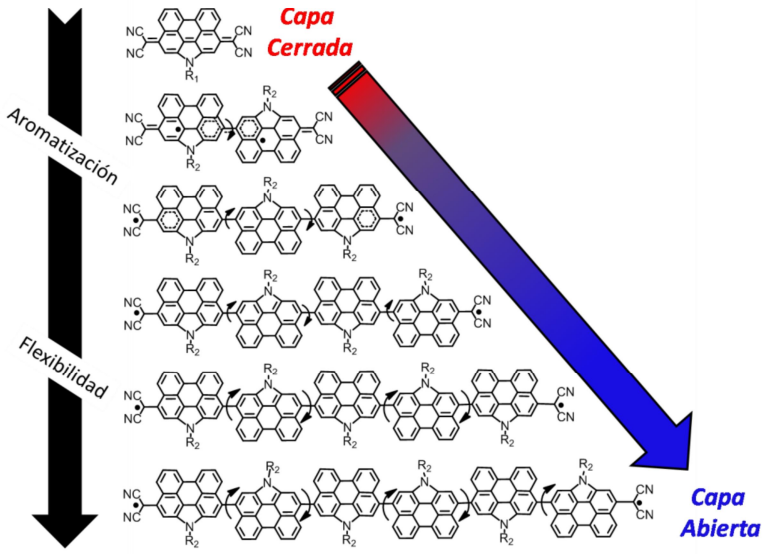

Figura 4.1 Estructuras químicas de las familia de moléculas *nPer-CN* (*n=1-6*), R_1= C_8H_{17} y R_2=$C_{24}H_{49}$.

En este apartado se lleva a cabo el estudio de una serie de oligómeros derivados de perileno con sustituyentes bis(dicianometileno) en los extremos, desde el monómero hasta el hexámero (*nPer-CN, n=1-6*). Se trata de sistemas que permiten estudiar el efecto que la unidad perileno y el aumento de la longitud de cadena tienen sobre la estructura electrónica y molecular, en términos de generación de especies de capa

abierta con carácter birradical [1-3]. Este tipo de estudios se encuentran habitualmente restringidos a sistemas más cortos, debido a la dificultad sintética inherente a los derivados de *para*-quinodimetano (*p-QDM*) al aumentar la longitud de cadena y al aumento de la reactividad química que se produce al disminuir significativamente el *gap HOMO-LUMO*, además de, como se ha mencionado con anterioridad, a problemas de solubilidad propios de sistemas de policíclicos aromáticos de gran tamaño [4, 5].

Estos inconvenientes se solventan con éxito en la presente serie de moléculas a través de diversas estrategias de estabilización habituales en química de hidrocarburos policíclicos aromáticos (*PAHs*) de bajo gap. En el caso de la unidad monomérica *1Per-CN* confluyen factores como la inclusión de la unidad *p-QDM* en un entorno fusionado π-conjugado [6-11], la mejora de la solubilidad gracias a la posibilidad de funcionalizar el átomo de nitrógeno de las posiciones bahía con cadenas alquílicas flexibles [12], o la accesibilidad sintética de las posiciones *peri-* (del perileno), que permite funcionalizarlas selectivamente de cara a obtener oligómeros de mayor tamaño [13]. Además, la inserción de grupos diciano fuertemente electroaceptores en los metilenos terminales supone una contribución adicional a la estabilización de estas moléculas.

Por tanto, la presente familia de compuestos constituye una oportunidad única a la hora de poder caracterizar la estructura electrónica y molecular de sistemas que en química de *PAHs*, y desde una perspectiva *bottom-up*, puedan usarse como modelos extrapolables al estudio de las propiedades físicas del grafeno (nanografenos).

4.1.1 RESUMEN DE LOS RESULTADOS OBTENIDOS.

La información aportada por la espectroscopia RMN de ^{1}H y ^{13}C, caracteriza a la unidad fundamental *1per-CN* como una molécula quinoide de capa cerrada en el estado fundamental, sin embargo, en los sistemas extendidos no se obtiene señal RMN ni tan siquiera a baja temperatura. Este fenómeno se relaciona con la aparición de cierto carácter birradical que empezaría a manifestarse a partir del derivado *2Per-CN.*

Una de las técnicas de rutina en caracterización de birradicales es la espectroscopia ESR, que aporta información muy útil acerca de la multiplicidad de espín del estado fundamental permitiendo incluso estimar magnitudes como la diferencia de energía singlete-triplete ($\Delta E_{S\text{-}T}$).

Como cabe esperar, la molécula *1Per-CN* es ESR inactiva. Sin embargo, los derivados más largos se caracterizan por presentar, tanto en estado sólido como en disolución, señales ESR anchas y sin estructura fina, indicativas de la presencia de especies paramagnéticas [9-11]. El estudio de dichas señales en función de la temperatura permite observar comportamientos opuestos. Mientras que los derivados de longitud intermedia (*2*,*3* y *4Per-CN*) muestran una relación directa de la señal ESR con la temperatura, los sistemas de cinco y seis unidades (*5,6Per-CN*) presentan una relación de tipo inverso, disminuyendo así la señal ESR al aumentar la temperatura. Estos resultados son indicativos de la transición entre un estado fundamental singlete de capa abierta (diamagnético) y un estado birradical triplete (paramagnético) al aumentar la longitud de la cadena. La determinación experimental de los valores de $\Delta E_{S\text{-}T}$ mediante *Superconducting Quantum Interference Device* (SQUID) permitiría además cuantificar, en términos energéticos, la posición relativa de los estados de alto y bajo espín para cada una de las moléculas, todo ello en buena sintonía con las predicciones obtenidas mediante cálculos DFT. Sin embargo, la limitación de estas técnicas a la hora de profundizar en el estudio de la relación estructura molecular-carácter birradical para este

tipo de sistemas, implica recurrir a otros métodos espectroscópicos. Es aquí donde la espectroscopia vibracional Raman emerge como técnica de referencia, única a la hora de evaluar la estructura del estado fundamental en birradicales π-conjugados tipo *Kekulé* y relacionarla con las propiedades que de ella se derivan, en conexión con la evolución de la misma en función del tamaño de la cadena [14-17].

4.1.1.1 Espectroscopia vibracional Raman.

En la **Figura 4.2** se presentan los espectros FT-Raman para todas las moléculas de la serie, registrados en estado sólido y a -170 °C con objeto de minimizar la población térmica de estados excitados o, en otras palabras, para garantizar que ésta sea máxima en el estado fundamental. Se muestran también los correspondientes espectros electrónicos de cada una de ellas para facilitar la visualización de las condiciones de resonancia Raman en las que han sido registrados los espectros vibracionales Raman de cada una de las moléculas.

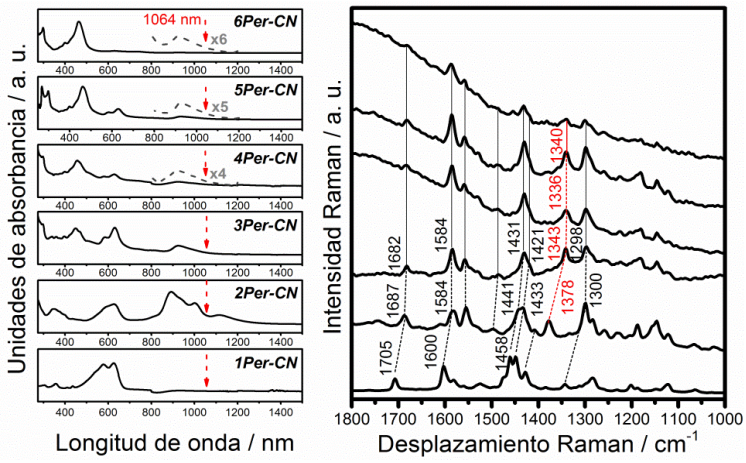

Figura 4.2 Izquierda: espectros de absorción electrónica UV-Vis-NIR registrados en disolución de diclorometano (DCM) para todas las moléculas de la serie**. Derecha:** espectros FT-Raman (1064nm) registrados en estado sólido y a -170 °C para todas las moléculas de la serie, *nPer-CN*.

Para poder interpretar convenientemente la evolución de los espectros al aumentar la longitud de cadena se toma como referencia el espectro Raman de la molécula más corta, *1Per-CN*, cuya asignación de bandas más relevantes se hace en base el espectro Raman teórico calculado a nivel DFT-B3LYP/6-31G** considerando una configuración de capa cerrada, en línea con los datos de H^1-RMN. La buena correspondencia entre éste y el espectro experimental registrado a 1064 nm permite relacionar las señales Raman detectadas en términos de modos normales de vibración, frecuencias teóricas y aspectos de la estructura molecular (**Figura 4.3**).

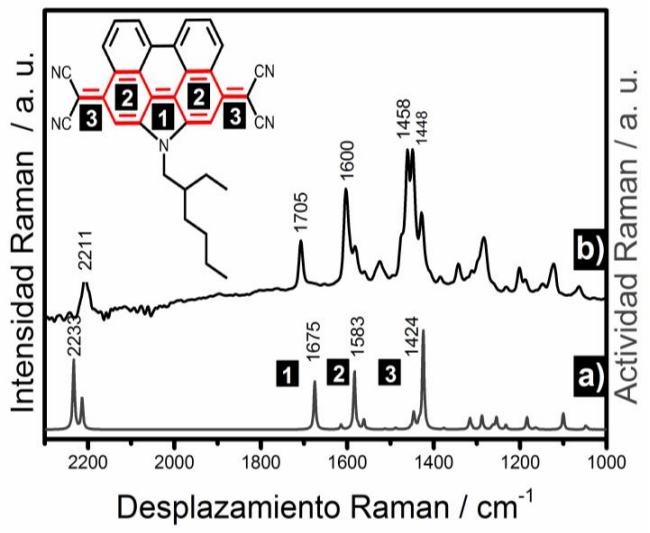

Figura 4.3 a) Espectro Raman teórico calculado a nivel DFT-B3LYP/6-31G** para *1Per-CN* considerando una configuración capa cerrada**. b)** Espectro FT-Raman (1064nm) registrado en estado sólido y a -170 ^{o}C para la molécula *1Per-CN*.

A la vista de los autovectores de cada uno de los modos normales de vibración calculados, se ha llevado a cabo la siguiente asignación de los modos de las bandas Raman del espectro experimental. La banda experimental a 2211 cm^{-1} (calculada a 2233 cm^{-1}) se corresponde con un

modo de vibración de tensión de C≡N ó ν(C≡N) característico de estructuras quinoides de capa cerrada. En el caso de análogos tiofénicos quinoides con grupos bis(dicianometileno), siempre aparece a frecuencias menores que 2200 cm^{-1} cuando se expresa el carácter birradical y por encima de 2200 cm^{-1} para compuestos de capa cerrada tipo *TCNQ*, como es el caso de *1Per-CN*. La banda medida a 1705 cm^{-1} (calculada a 1675 cm^{-1}), por su parte, se asigna a una vibración de tensión de C=C ó ν(C=C) del enlace central que conecta los anillos benzoquinoides y la que aparece a 1600 cm^{-1} (calculada a 1583 cm^{-1}) se asocia con la vibración de tensión ν(C=C) de los dobles enlaces de cada anillo benzoquinoide. Por último, la señal más intensa del espectro experimental, detectada a 1456 cm^{-1} (calculada a 1424 cm^{-1}) se asigna a una vibración de tensión de los enlaces que conectan los grupos diciano con la unidad central conjugada.

Si centramos el análisis en las bandas intensas en la zona entre 1700 cm^{-1} y 1400 cm^{-1} para el monómero (*1Per-CN*), se puede decir que las señales que aparecen a 1705, 1600 y 1458 cm^{-1} corresponden a modos de vibraciones de tensión de enlace C=C, cuyos altos valores de frecuencia caracterizan la estructura como quinoide de capa cerrada.

Al aumentar en una unidad la longitud de cadena (*2Per-CN*), como puede observarse en la **Figura 4.2**, las tres bandas predominantes en el monómero se desplazan a menores frecuencias, apareciendo ahora a valores de 1687, 1584 y 1441 cm^{-1}. Este desplazamiento es indicativo del debilitamiento de los enlaces C=C involucrados en las vibraciones de tensión descritas para la estructura quinoide anterior, fruto de la recuperación parcial de la aromaticidad en las unidades de perileno asociada a la generación de una especie birradical. Además, se detecta una nueva banda a 1378 cm^{-1} que corresponde a la tensión del nuevo enlace C-C existente entre las dos unidades de perileno. La aparición de este modo Raman a una frecuencia tan baja es indicativa de un marcado carácter de enlace simple, lo que constituye una evidencia más que

apunta hacia la transición entre una especie de capa cerrada y una especie birradical de capa abierta al pasar de *1Per-CN* a *2Per-CN*.

La inserción de una nueva unidad de perileno (*3Per-CN*) implica un aumento de la estabilización aromática. Esto se traduce en el consiguiente desplazamiento a menor frecuencia de las bandas Raman características, en consonancia con el aumento del carácter birradical con la longitud de la cadena al pasar de *2Per-CN* a *3Per-CN*. Cabe destacar aquí como el modo asociado a la vibración de tensión del enlace C-C/C=C *interperileno* es la huella más notable de la evolución hacia una estructura más aromática en la unidad de perileno, en consonancia con una estructura de capa abierta que constituye el estado fundamental en el trímero. Esta banda Raman es, con diferencia, la señal que mayor desplazamiento sufre al pasar de *2Per-CN* a *3Per-CN*. Sin embargo, para explicar la magnitud de dicho desplazamiento se hace necesario traer a colación el concepto de flexibilidad estructural, el cual toma sentido en el contexto de un estado fundamental de capa abierta en el que la estabilización aromática conlleva un debilitamiento de los enlaces *interperileno* que, a su vez, unido al impedimento estérico entre unidades de perileno, posibilita la rotación relativa de una respecto a otra. Así, la conjunción de estabilización aromática y distorsión del esqueleto molecular vendrían a dar cuenta del desplazamiento de hasta 35 cm^{-1} que sufre el modo asociado a la vibración de tensión del enlace C-C/C=C *interperileno*. La evolución del espectro al pasar de *3Per-CN* a *4Per-CN* se mantiene en la misma línea de ruptura de la conjugación tipo quinoide inicial o incremento de la aromaticidad en los anillos de benceno del perileno, como muestra de nuevo la adicional disminución de la frecuencia a la que aparece la tensión del enlace C-C *interperileno* al pasar al análogo con cuatro unidades de perileno. A partir del derivado *4Per-CN*, el perfil espectral se mantiene prácticamente inalterado al aumentar la longitud de cadena. Esto se puede explicar en términos de saturación de la flexibilidad conformacional, la cual se alcanzaría en este punto y daría

lugar a una relajación máxima de la rotación *interperileno* que no se vería incrementada en los derivados de cinco y seis unidades.

Si nos centramos en los derivados del *2Per-CN* al *6Per-CN*, se pueden establecer dos comportamientos bien diferenciados en términos de evolución del grado de conjugación/aromaticidad de la unidad de perileno. Mientras que para los derivados más cortos la conjugación disminuye con la longitud de la cadena al favorecerse la estabilización aromática de especies capa abierta y aumentar la flexibilidad estructural, a partir del *4Per-CN* la flexibilidad es máxima, lo cual se podría relacionar con una saturación de la conjugación, responsable de la invariabilidad del espectro Raman al pasar a *5 y 6Per-CN*. Esta información molecular es tremendamente útil a la hora de interpretar la estabilización de estados fundamentales de capa abierta singlete o triplete en términos del mecanismo DSP. En el caso de los derivados cortos, una vez estabilizada la especie capa abierta a través del aumento de la aromaticidad en la unidad de perileno, las variaciones del espectro Raman se pueden explicar a través de la fuerte conjugación de los electrones despareados con el puente π-conjugado, que daría lugar a la estabilización del estado fundamental birradical singlete gracias a la activación del mecanismo DSP. Sin embargo, en el caso de los derivados *5 y 6Per-CN*, el confinamiento de la conjugación en la unidad central hace que haya un desfase entre longitud de conjugación y longitud molecular, lo que implica la desconexión de los centros radicales, como consecuencia el mecanismo DSP queda desactivado y se estabiliza la configuración electrónica birradical triplete, pasando ésta a describir el estado fundamental para los sistemas *5 y 6Per-CN* **(Figura 4.4)**.

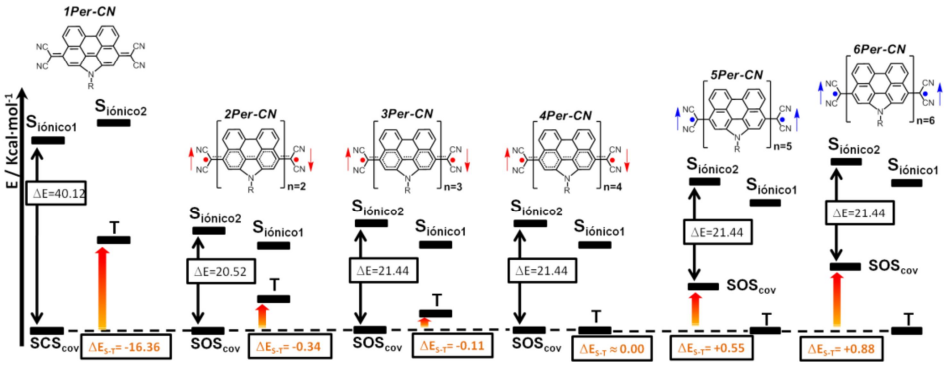

Figura 4.4 Modelo de cuatro estados para los derivados *nPer-CN* (*n=1-6*)**.** Los valores de $\Delta E_{S\text{-}T}$ se obtienen a partir de cálculos químico cuánticos a nivel nivel B3LYP/6-31G** para el sistema capa cerrada (*1Per-CN)*, y a partir de los datos de SQUID para los sistemas capa abierta (*2-6Per-CN*).

Con objeto de intentar obtener evidencias espectroscópicas de la evolución del $\Delta E_{S\text{-}T}$ en función de la longitud de la cadena, se llevó a cabo el estudio Raman en función de la temperatura para cada derivado, cuyos resultados se muestran en la **Figura 4.5**.

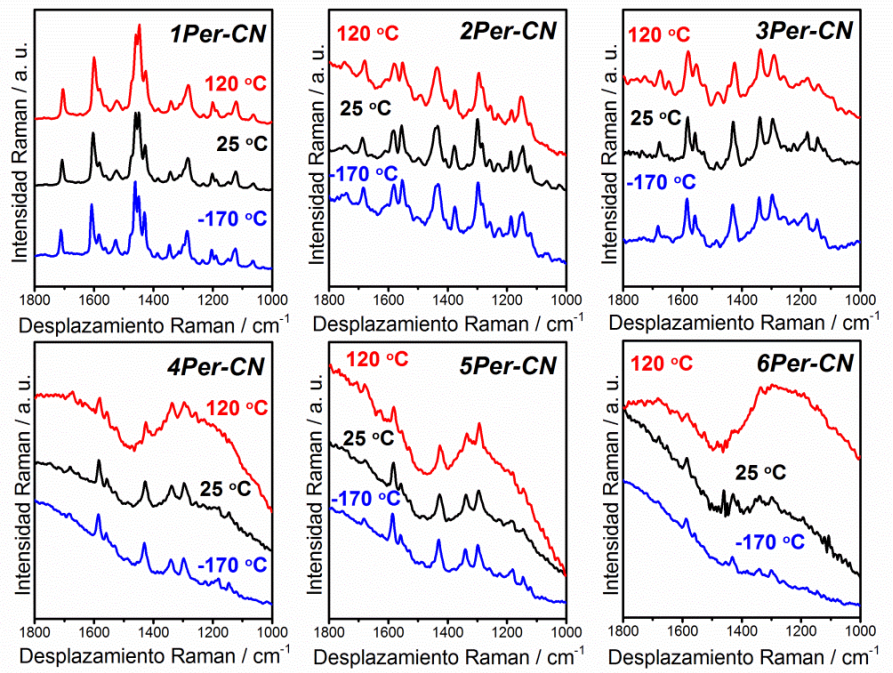

Figura 4.5 Espectros FT-Raman (1064nm) registrados en función de la temperatura y en estado sólido para todas las moléculas de la serie, *nPer-CN*.

A la hora de interpretar los resultados obtenidos en función de la temperatura, llama la atención la prácticamente total invariabilidad del perfil espectral en términos de intensidades relativas y frecuencias para todas las moléculas. La invariabilidad del perfil espectral con la temperatura, para *1Per-CN*, es coherente con la estructura quinoide de capa cerrada propuesta. Ésta implicaría un estado excitado triplete muy alto en energía (**Figura 4.4**) cuya población térmica no sería viable, no observándose por tanto ninguna variación del espectro atribuible a la presencia de la especie triplete. En el caso de los sistemas de longitud intermedia, *2Per-CN*, *3Per-CN* y *4Per-CN*, la constancia del perfil espectral con la temperatura, sin embargo, podría relacionarse con una quasi-degeneración de los estados birradical singlete y triplete, como apuntan las diferencias de energía obtenidas mediante SQUID (**Figura 4.4**). Esto

podría explicar la imposibilidad de observar una interconversión de población neta térmicamente inducida entre estados, ya que ambos se encontrarían significativamente poblados a temperatura ambiente. Además, dada la similitud de las energías relativas de ambas especies en todos los sistemas, cabría esperar espectros muy similares para las configuraciónes singlete capa abierta y birradical triplete, con lo cual, de darse un cruce intersistémico significativo entre los estados singlete y triplete, los espectros resultantes serían prácticamente indistinguibles.

4.1.2 BIBLIOGRAFÍA

1. Montgomery, L. K.; Huffman, J. C. ;Jurczak, E. A.; Grendze, M. P., *J. Am. Chem. Soc*, 1986. **108**(19): p. 6004-6011.
2. Thiele, J. and Balhorn, H., *Ber. Chem.*, 1904. **37**(2): p. 1463-1470.
3. Tschitschibabin, A.E., *Ber. Chem.*, 1907. **40**(2): p. 1810-1819.
4. Maxfield, M., Bloch, A.N.; Cowan, D.O., *J. Org. Chem.*, 1985. **50**(11): p. 1789-1796.
5. Acker, D.S. and Hertler, W.R., *J. Am. Chem. Soc.*, 1962. **84**(17): p. 3370-3374.
6. Chase, D. T.; Rose, B. D.; McClintock, S. P.; Zakharov, L. N.; Haley, M. M., *Angew. Chem. Int. Ed.,*2011. **50**(5): p. 1127-1130.
7. Chase, D. T.; Fix, A. G.; Kang, S. J. Rose, B. D.; Weber, C. D.; Zhong, Y.; Zakharov, L. N.Lonergan, M. C.; Nuckolls, C.; Haley, M. M., *J. Am. Chem. Soc.*, 2012. **134**(25): p. 10349-10352.
8. Ohashi, K.; Kubo, T.; Masui, T.; Yamamoto, K.; Nakasuji, K.; Takui, T.; Kai, Y.; Murata, I., *J. Am. Chem. Soc.*, 1998. **120**(9): p. 2018-2027.
9. Shimizu, A.; Kubo, T.; Uruichi, M.; Yakushi, K.; Nakano, M.; Shiomi, D.; Sato, K.; Takui, T.; Hirao, Y.; Matsumoto, K.; Kurata, H.; Morita, Y.; Nakasuji, K., *J. Am. Chem. Soc.*, 2010. **132**(41): p. 14421-14428.
10. Shimizu, A.; Uruichi, M.; Yakushi, K.; Matsuzaki, H.; Okamoto, H.; Nakano, M.; Hirao, Y.; Matsumoto, K.; Kurata, H.; Kubo, T., *Angew. Chem. Int. Ed.*, 2009. **121**(30): p. 5590-5594.
11. Kubo, T.; Shimizu, A.; Sakamoto, M.; Uruichi, M.; Yakushi, K.; Nakano, M.; Shiomi, D.; Sato, K.; Takui, T.; Morita, Y.; Nakasuji, K., *Angew. Chem. Int. Ed.*, 2005. **117**(40): p. 6722-6726.
12. Jiao, C.; Huang, K-W.; Luo, J.; Zhang, K.; Chi, C.; Wu, J., *Org. Lett.*, 2009. **11**(20): p. 4508-4511.
13. Li, Y. and Wang, Z., *Org. Lett.*, 2009. **11**(6): p. 1385-1387.
14. Ponce Ortiz, R.; Casado, J.; Hernández, V.; López Navarrete, Juan T.; Viruela, P. M.; Ortí, E.; Takimiya, K-; Otsubo, T., *Angew. Chem. Int. Ed.,* **119**(47): p. 9215-9219.
15. Li, Y.; Heng, W-K.; Lee, B. S.; Aratani, N.; Zafra, J. L.; Bao, N.; Lee, R,; Sung, Y. M.; Sun, Z.; Huang, K-W.; Webster, R. D.; López

Navarrete, J. T.; Kim, D.; Osuka, A,; Casado, J.; Ding, J.; Wu, J., *J. Am. Chem. Soc.*, 2012. **134**(36): p. 14913-14922.

16. Zeng, Z.; Sung, Y. M.; Bao, N.; Tan, D.; Lee, R.; Zafra, J. L.; Lee, B. S.; Ishida, M.; Ding, J.; López Navarrete, J. T.Li, Y.; Zeng, W.; Kim, D.; Huang, K-W.; Webster, R. D.; Casado, J.; Wu, J., *J. Am. Chem. Soc.*, 2012. **134**(35): p. 14513-14525.
17. Casado, J.; Patchkovskii, S.; Zgierski, M. Z.; Hermosilla, L.; Sieiro, C.; Moreno Oliva, M.; López Navarrete, Juan T., *Angew. Chem. Int. Ed.*, 2008. **47**(8): p. 1443-1446.

4.2 Efecto de la rigidez estructural sobre la generación de birradicales de capa abierta en los derivados de p-QDM bis(dicianometileno) QR-CN y HR-CN.

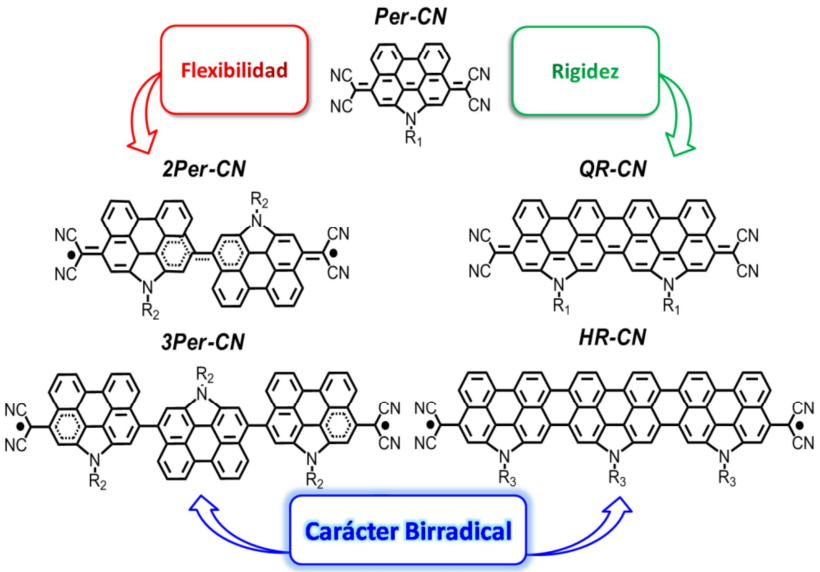

Figura 4.6 Estructuras químicas de las moléculas objeto de estudio(R_1= C_8H_{17}, R_2= $C_{24}H_{49}$ y R_3= $C_{52}H_{103}O_2$) .

En este apartado se presenta el estudio comparativo de los derivados *1-3Per-CN* y sus análogos rigidificados bis(dicianometilen) quater- y hexarrileno, *QR-CN* y *HR-CN*. Este conjunto de moléculas nos permite avanzar en dos direcciones hacia la comprensión de los rasgos que, en términos de estructura molecular, favorecen la estabilización de especies birradicalarias. Por un lado, nos permite estudiar la influencia que sobre la estabilización de especies birradicales tiene la extensión de la longitud de cadena en sistemas planos y libres de efectos conformacionales [1, 2], por otro, nos da la oportunidad de profundizar en

el entendimiento del efecto que la DSP tiene en relación con la mayor conjugación de los electrones desapareados con el esqueleto conjugado y, por tanto, en la separación entre singlete y triplete birradicalarios [3], como se describía en el apartado 4.1.

4.2.1 RESUMEN DE LOS RESULTADOS OBTENIDOS.

Para una misma longitud molecular, la ausencia de señal ESR observada en *QR-CN* esboza un escenario que difiere del observado para su análogo *2Per-CN*, quedando el primero caracterizado como un sistema posiblemente quinoide de capa cerrada o, en cualquier caso, con un mayor carácter de capa cerrada o menor carácter birradical que su análogo sin fusionar, cuyo estado electrónico fundamental quedaba descrito por una configuración singlete de capa abierta. [3].

La molécula *HR-CN*, sin embargo, presenta una señal ESR ancha que sugiere la existencia de especies de capa abierta. Esta asunción queda soportada por el comportamiento de la susceptibilidad magnética en función de la temperatura que describen las medidas de SQUID, las cuales apuntan hacia un estado fundamental singlete de capa abierta, como en el caso de *3-PerCN* [3]. Sin embargo, aunque ambos derivados presentan configuraciones electrónicas del estado fundamental similares, el carácter birradical de ambas moléculas difiere, como demuestran los valores de 4.21 $Kcal \cdot mol^{-1}$ y 0.107 $Kcal \cdot mol^{-1}$ obtenidos para el ΔE_{S-T} de *HR-CN* y *3Per-CN*, respectivamente.

4.2.1.1 ESPECTROSCOPIA VIBRACIONAL RAMAN.

En la **Figura 4.7** se muestran los espectros Raman en condiciones de resonancia Raman para los sistemas *1Per-CN*, *QR-CN* y *HR-CN* obtenidos adecuando las líneas excitatrices a las transiciones más intensas del espectro de absorción UV-Vis-NIR de cada una de ellas, los cuales también se presentan en la figura.

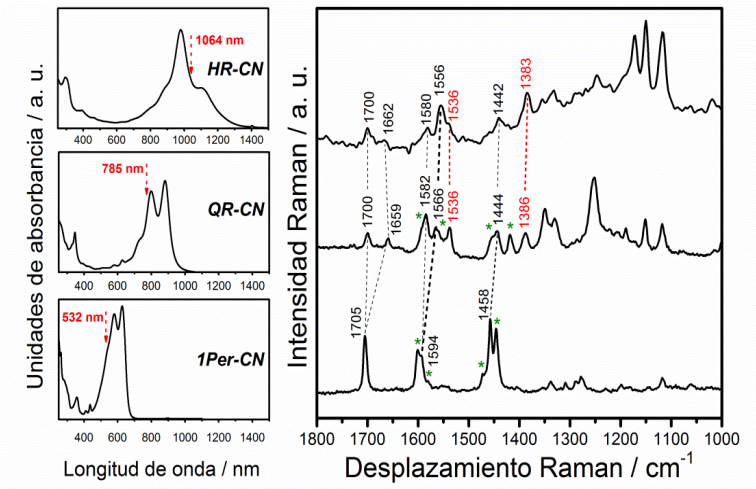

Figura 4.7 **Izquierda:** espectros de absorción de *1Per-CN*, *QR-CN* y *HR-CN* en DCM. **Derecha:** espectros Raman resonantes obtenidos en estado sólido con las líneas excitatrices de 532, 785 y 1064 nm para *1Per-CN*, *QR-CN* y *HR-CN* respectivamente.

Algunas de las bandas que caracterizaban la unidad monomérica *1Per-CN* como quinoide de capa cerrada (1705, 1594 y 1458 cm^{-1}) aparecen a menores frecuencias en *QR-CN*, conviertiéndose a su vez en dobletes. Como puede observarse, los modos de vibración de tensión C=C/C-C a 1705 y 1594 cm^{-1} evolucionan hacia los pares 1700/1659 cm^{-1} y 1582/1566 cm^{-1}, respectivamente. Además, aparecen dos nuevas señales a 1536 y 1386 cm^{-1} que se asocian a modos de vibración en enlaces químicos nuevos, que estarían planarizando las unidades de perileno.

La disminución de frecuencia de estos modos de tensión C=C puede tener que ver con dos efectos:

I. La relajación de la alternancia C-C/C=C debida al aumento de la conjugación que se produce como consecuencia del mayor número de electrones π en el esqueleto molecular [4].

II. La aromatización de los anillos benzoquinoides que se generaría en caso de un aumento del carácter birradical y que, además, iría en detrimento de la fortaleza de los enlaces *interperileno* [5].

El espectro obtenido para la molécula *HR-CN* muestra dos bandas predominantes. La más intensa a 1556 cm^{-1} aparece a menor energía que las correspondientes señales para *QR-CN* y *1Per-CN* (1566 y 1594 cm^{-1}, respectivamente) mientras que la banda a 1383 cm^{-1} aparece 3 cm^{-1} por debajo de su análoga en *QR-CN*. Este último rasgo espectroscópico puede asociarse al debilitamiento del enlace que conecta las unidades de perileno al pasar de *QR-CN* a *HR-CN*, y queda justificado mediante cálculos teóricos, tal y como se muestra en la **Figura 4.8** [4, 6].

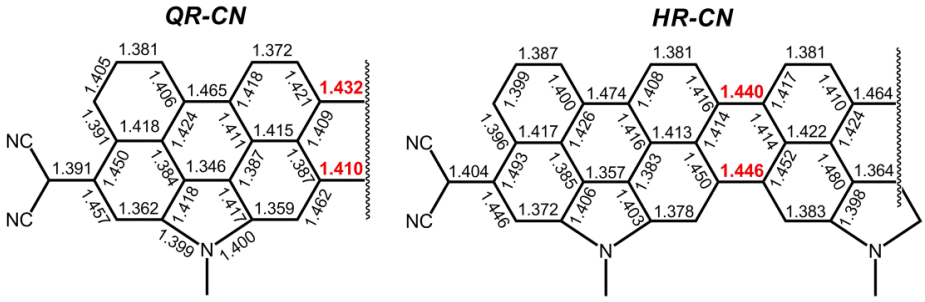

Figura 4.8 Distancias de enlace calculadas a nivel (U)CAM-B3LYP/6-31G** para *QR-CN* en la configuración de capa cerrada y para *HR-CN* en la configuración singlete capa abierta.

En el apartado anterior, se establecía la relación entre los modos vibracionales de tensión de los enlaces C-C *interperileno* y el carácter de capa abierta en derivados *nPer-CN* flexibles. En concreto, para *2Per-CN* y *3Per-CN*, las bandas a 1378 y 1343 cm^{-1} (**Figura 4.2**) se asociaban, respectivamente, a un carácter intermedio a fuerte para el birradical singlete de capa abierta [3]. El análisis de las frecuencias asociadas a los modos normales de vibración de los enlaces *interperileno* en análogos fusionados de igual longitud molecular podrá, por tanto, aportar información directa acerca de la influencia que la rigidez estructural ejerce sobre el carácter birradical. En este contexto, si se establecen las comparaciones *2Per-CN* → *QR-CN* y *3Per-CN* → *HR-CN*, la evolución de las bandas de 1378 →1386 cm^{-1} y de 1343 →1383 cm^{-1} es indicativa del menor carácter birradical singlete de *QR-CN* con respecto a *2Per-CN* y de *HR-CN* con respecto a *3Per-CN*. Esto permite, además, clasificar los sistemas en función del peso que la configuración de capa abierta tiene en el estado fundamental: *QR-CN < 2PerCN, HR-CN < 3Per-CN*, con *HR-CN* $\leq$ *2PerCN*. En pocas palabras, se puede decir que el carácter singlete de capa abierta de *HR-CN* es mayor que el de *QR-CN*, aunque sigue siendo moderado en comparación con el de su análogo no fusionado *3Per-CN*.

Los resultados obtenidos se pueden explicar de manera sencilla recurriendo de nuevo a un modelo de cuatro estados en el contexto de un mecanismo DSP como indica la **Figura 4.9**.

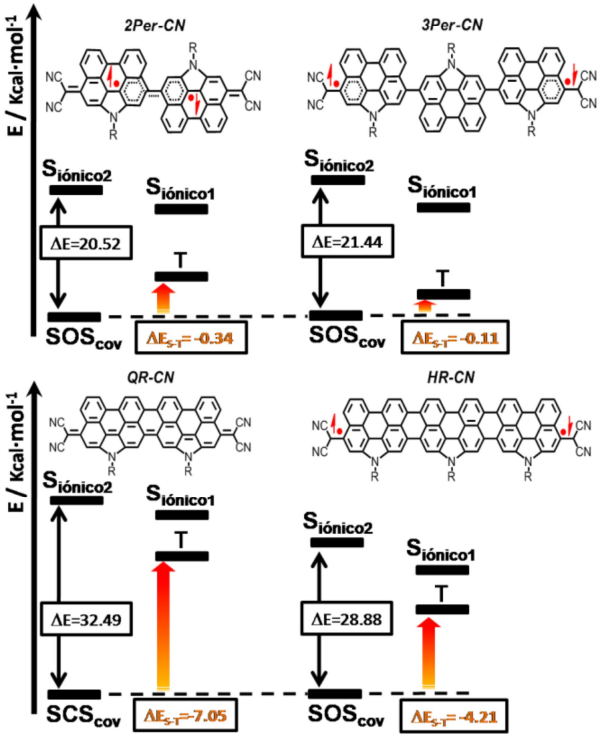

Figura 4.9 Modelo de cuatro estados para los derivados *2,3Per-CN*, *QR-CN* y *HR-CN*. Los valores de $\Delta E_{S\text{-}T}$ se obtienen a partir de cálculos químico cuánticos a nivel CAM-B3LYP/6-31G** para el sistema capa cerrada (*QR-CN)*, y a partir de los datos de SQUID para los sistemas capa abierta (*2,3Per-CN y HR-CN*).

En el caso de los derivados fusionados, con respecto a los que no lo son, al presentar una estructura menos distorsionada que favorece la conjugación, el mecanismo DSP actúa con mayor eficiencia, desestabilizándose el triplete frente al estado fundamental singlete de capa abierta o, en otras palabras, aumentando el $\Delta E_{S\text{-}T}$ y disminuyendo el carácter birradical del estado fundamental. Sin embargo, en el caso de los derivados no fusionados, al disminuir la conjugación y la eficiencia del mecanismo DSP debido al impedimento estérico, se produce una disminución del $\Delta E_{S\text{-}T}$ y se generan especies con mayor carácter birradical. Se pone de manifiesto, por tanto, como la eficiencia con la que se dé el

fenómeno DSP va a determinar, en gran medida, la configuración electrónica del estado fundamental en estos sistemas. Así, para una misma longitud de cadena, mientras que en *QR-CN* la rigidez estructural lo convierte en un sistema capa cerrada frente a la configuración birradical singlete de capa abierta que describía el estado fundamental en *2-Per-CN*, en el caso de *HR-CN* y *3Per-CN* la DSP vendría a explicar el menor carácter birradical mostrado por el primero, en consonancia con el mayor ΔE_{S-T} que éste presenta (**Figura 4.9**).

En la **Figura 4.10** se muestran los espectros Raman en función de la temperatura para los derivados *QR-CN* y *HR-CN*, donde se observa que el perfil espectral se mantiene constante al variar la temperatura, al igual que ocurría en los análogos no fusionados. Para *QR-CN* este resultado es algo esperable en base a su menor carácter birradical y al consecuente alto ΔE_{S-T} calculado (**Figura 4.9**). En el caso de *HR-CN*, sin embargo, este fenómeno podría tener su orígen en la elevada capacidad de los centros radicales para conjugar con el puente π-conjugado. Esto estabilizaría el singlete capa abierta frente al birradical triplete, haciendo significativa la diferencia de energía entre ambos estados (**Figura 4.9)** y dificultando la población térmica entre los mismos, lo que explicaría la no alteración del espectro con la temperatura.

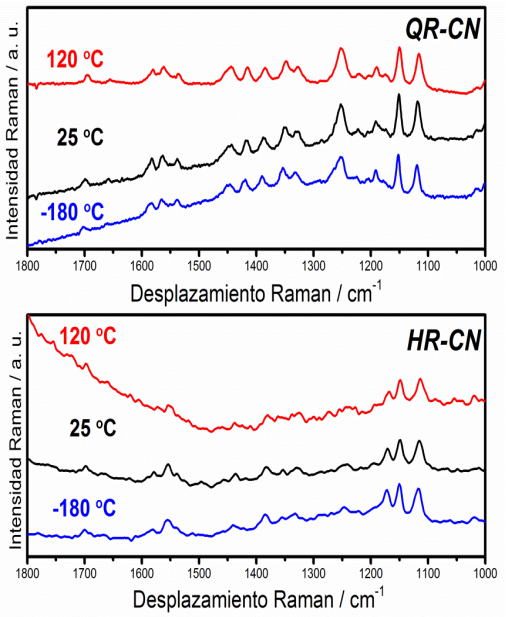

Figura 4.10 Espectros Raman de los derivados *QR-CN* y *HR.CN* registrados en estado sólido con las líneas excitatrices de 785 nm y 1064 nm, respectivamente, en función de la temperatura.

4.2.2 BIBLIOGRAFÍA

1. Weil, T.; Vosch, T.; Hofkens, J.; Peneva, K.; Müllen, K., *Angew. Chem. Int. Ed.*, 2010. **49**(48): p. 9068-9093.
2. Pschirer, N. G.; Kohl, C. Nolde, F. Qu, J. Müllen, K., *Angew. Chem. Int. Ed.*, 2006. **45**(9): p. 1401-1404.
3. Zeng, Z.; Ishida, M.; Zafra, J. L.; Zhu, X.; Sung, Y. M.; Bao, N.; Webster, R. D.; Lee, B. S.; Li, R-W.; Zeng, W.; Li, Y.; Chi, C.; López Navarrete, J.T.;Ding, J.; Casado, J.; Kim, D.; Wu, J., *J. Am. Chem. Soc.*, 2013. **135**(16): p. 6363-6371.
4. Ponce Ortiz, R.; Casado, J.; Hernández, V.; López Navarrete, J. T.; Viruela, P. M.; Ortí, E.; Takimiya, K-; Otsubo, T., *Angew. Chem. Int. Ed.,* **119**(47): p. 9215-9219.
5. Casado, J.; Patchkovskii, S.; Zgierski, M. Z.; Hermosilla, L.; Sieiro, C.; Moreno Oliva, M.; López Navarrete, Juan T., *Angew. Chem. Int. Ed.*, 2008. **47**(8): p. 1443-1446.
6. González, S. R.; Ie, Y.; Aso, Y.; López Navarrete, J. T.; Casado, J., *J. Am. Chem. Soc.*, 2011. **133**(41): p. 16350-16353.

4.3 Estudio de la activación del carácter birradical en 1Per-CN y QR-CN mediante incorporación de anillos adicionales de tiofeno.

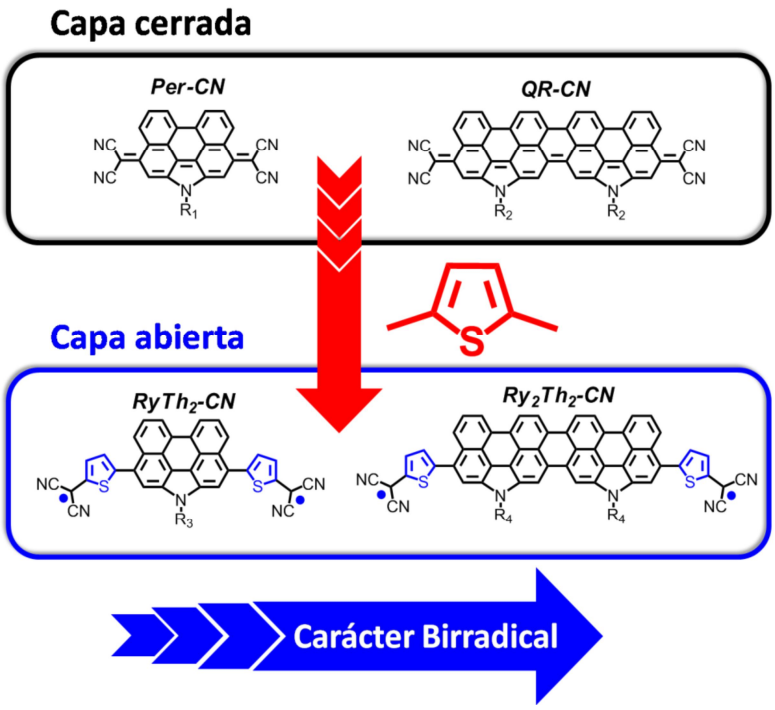

Figura 4.11 Estructuras de las moléculas objeto de estudio (R_1=C_8H_{17}, R_2=$C_{52}H_{103}O_2$, R_3= $C_{16}H_{33}$ y R_4= $C_{24}H_{49}$).

En los apartados 4.1 y 4.2 se ha demostrado como una modificación estructural puede afectar drásticamente a la configuración electrónica del estado fundamental en sistemas pro-aromáticos π-conjugados derivados de *p-QDM* [1,2]. En concreto, resulta muy interesante la transición de un sistema de capa cerrada a uno de capa abierta como consecuencia de la mayor flexibilidad conformacional al pasar del

monómero *1Per-CN* al dímero *2Per-CN* y, a su vez, destaca también la conversión de éste en un sistema con menor carácter birradical en *QR-CN*.

En el presente apartado, con la intención de profundizar en la comprensión de la relación estructura-carácter birradical-propiedad para este tipo de sistemas, se trata de dar respuesta a dos cuestiones nuevas:

i) ¿Cómo activar el mecanismo de expresión del carácter birradical vía inclusión de otras unidades pro-aromáticas?
ii) ¿Cuáles son las diferencias estructurales que caracterizan a los birradicales de carácter mixto tiofeno-perileno?

Para ello se estudian los derivados *$RyTh_2$-CN* y *Ry_2Th_2-CN* resultantes de intercalar anillos de tiofeno entre las unidades de *1Per-CN* y *QR-CN* y los grupos dicianometileno de sus extremos. El motivo de la inclusión de anillos de tiofeno tiene que ver con el previsible aumento del carácter birradical que éstos pueden proporcionar a través de su aromatización [3], a lo que hay que añadir que el anillo de tiofeno se caracteriza por ser más fácilmente funcionalizable que los anillos de benceno del perileno base [4], lo que mejora la accesibilidad sintética a nuevos derivados.

4.3.1 RESUMEN DE LOS RESULTADOS OBTENIDOS.

Las medidas ESR en estado sólido, tanto para *$RyTh_2$-CN* como para *Ry_2Th_2-CN* muestran señales anchas a temperatura ambiente, de mayor intensidad para *Ry_2Th_2-CN*. Al aumentar la temperatura, se observa un incremento de la señal ESR para ambas moléculas, hecho indicativo de configuraciones electrónicas de capa abierta en el estado fundamental, de tipo singlete. Por su parte, el espectro H^1-RMN para *Ry_2Th_2-CN* no muestra señales resueltas ni siquiera a baja temperatura. En el caso de *$RyTh_2$-CN* el comportamiento de éstas en función de la temperatura es de

mayor complejidad, presentando un espectro ancho, de baja resolución a temperaturas altas pero que se estructura progresivamente al disminuir la temperatura.

Estos resultados, por tanto, llevan a pensar en una situación con ambas moléculas en una configuración singlete capa abierta en el estado fundamental, siendo el carácter birradical mayor en el caso del derivado más largo (*Ry_2Th_2-CN*). Esto implicaría una elevada población de especies triplete que podría estar en el origen de la exclusiva detección de señales H^1-RMN anchas, incluso a baja temperatura. Por el contrario, *$RyTh_2$-CN*, presentaría menor carácter birradical, mayor ΔE_{S-T} y, como consecuencia, una menor población de estados triplete que permitiría la detección de señales H^1-RMN bien resueltas, características del estado fundamental birradical singlete. Esta predicción cualitativa de la distribución energética de los estados de alto y bajo espín coincide con los valores obtenidos mediante SQUID, siendo el ΔE_{S-T}, aproximadamente, de -0.16 Kcal·mol^{-1} para *Ry_2Th_2-CN* y alrededor de -4.71 Kcal·mol^{-1} para *$RyTh_2$-CN*.

Se recurre, a continuación, a la espectroscopia Raman para tener acceso a una descripción molecular más exacta y detallada de los estados singlete y triplete [5-7].

4.3.1.1 ESPECTROSCOPIA VIBRACIONAL RAMAN.

En la **Figura 4.12** se muestran los espectros Raman en estado sólido y condiciones de resonancia para las moléculas *1Per-CN*, *$RyTh_2$-CN*, *QR-CN* y *Ry_2Th_2-CN* junto con sus correspondientes espectros de absorción electrónica UV-Vis-NIR [2]. Al pasar de *1Per-CN* a *$RyTh_2$-CN*, se produce un debilitamiento de las intensidades de las bandas características de la estructura quinoide de capa cerrada (1705, 1594 y 1458 cm^{-1} en *1Per-CN*) acompañado de un desplazamiento a menor

frecuencia de las mismas, que las lleva a aparecer a 1678, 1581 y 1398 cm $^{-1}$ en *RyTh$_2$-CN*. En concreto, la evolución de la banda Raman asociada al modo ν(C=C) de los enlaces que conectan los grupos diciano con los tiofenos, al pasar de 1458 a 1398 cm^{-1}, es indicativa del debilitamiento del carácter de doble enlace al pasar de *1Per-CN* a *RyTh$_2$-CN*. Por otra parte, aparece una nueva banda a 1493 cm^{-1} en *RyTh$_2$-CN* que se puede asociar con la vibración de tensión de C=C de los tiofenos ó ν(C=C) de los enlaces dobles en los dos anillos de tiofeno y relacionable con la frecuencia a la que se detecta este modo en un dimetil bitiofeno aromático (1492 cm^{-1}) [8]. Estas evidencias espectroscópicas concordarían, por tanto, con la asunción de un estado fundamental birradical singlete, cuya estabilización sería la resultante del efecto adicional de la aromatización de los tiofenos.

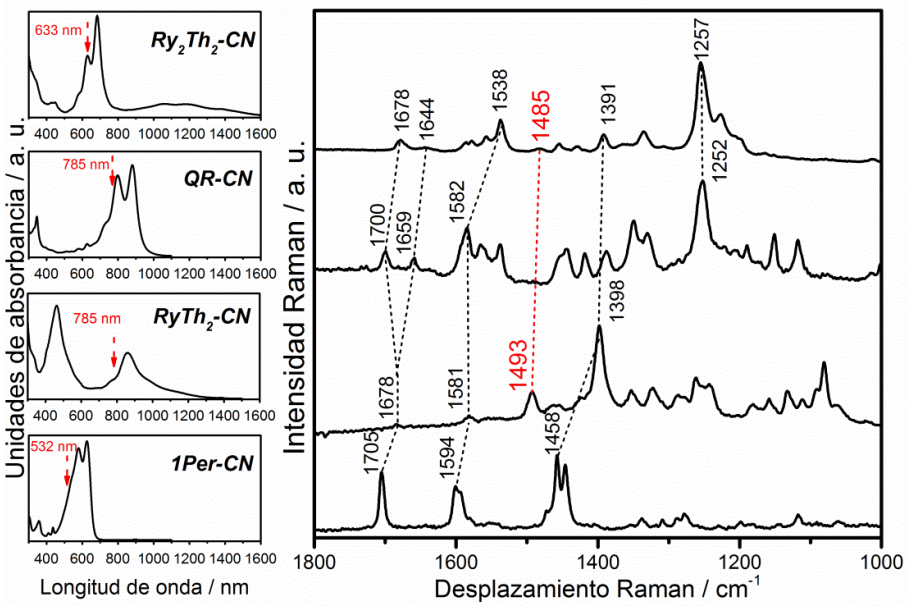

Figura 4.12 **Izquierda:** espectros de absorción de *1Per-CN*, *RyTh$_2$-CN*, *QR-CN* y *Ry$_2$Th$_2$-CN* registrados en disolución de DCM. **Derecha:** espectros Raman resonantes obtenidos en estado sólido a -170 ^{o}C con las líneas excitatrices de 633, 785 y 532 nm para *Ry$_2$Th$_2$-CN*, *QR-CN*, *RyTh$_2$-CN* y *1Per-CN*, respectivamente.

La banda intensa a 1257 cm^{-1} en el espectro de *Ry_2Th_2-CN*, y ausente en el de *$RyTh_2$-CN*, es característica del segmento tetrabenzofusionado central pseudo-aromatizado, típico de nanografenos, como demuestra su presencia en el espectro de *QR-CN* a similar frecuencia y también con gran intensidad. Siguiendo con la asignación de las señales relevantes en *Ry_2Th_2-CN*, las bandas a 1485 y 1391 cm^{-1} se pueden correlacionar con las que aparecían a 1493 y 1398 cm^{-1} y se asignaban a ν(C=C) de los anillos de tiofeno con un marcado carácter pseudoaromático en *$RyTh_2$-CN*.

A nivel molecular, asumida la naturaleza aromática de los fragmentos entre grupos diciano para los derivados tioféncios *$RyTh_2$-CN* y *Ry_2Th_2-CN* como consecuencia de la formación de un birradical, los desplazamientos Raman se pueden relacionar con la DSP y el ΔE_{S-T}. Al pasar de *$RyTh_2$-CN* a *Ry_2Th_2-CN* se produce un desplazamiento a menor frecuencia de las bandas Raman importante, incluidas las del tiofeno, pero que no suponen desplazamientos mayores de 7-8 cm^{-1}. Esto da cuenta de una ligera menor conjugación de los tiofenos con el *core* en *Ry_2Th_2-CN* debido, probablemente, a la mayor distorsión de los tiofenos con respecto al núcleo fusionado en comparación con *$RyTh_2$-CN*. Se bloquearía así el efecto DSP, dando lugar a estados singlete-triplete prácticamente degenerados en *Ry_2Th_2-CN.*

Si se compara el espectro Raman de *$RyTh_2$-CN* registrado con la línea de 785 nm en estado sólido y en disolución de diclorometano mostrados en la **Figura 4.13 (izquierda)** se puede comprobar como el modo ν(C=C) correspondiente a los tiofenos aromáticos aparece en los dos casos a 1493 cm^{-1}, indicando la importante distorsión molecular que afecta a la unión entre el tiofeno y el *core* de rileno. Esta banda a 1493 cm^{-1} es debida a una vibración ν(C=C) de los dos tiofenos, pese a estar separados.

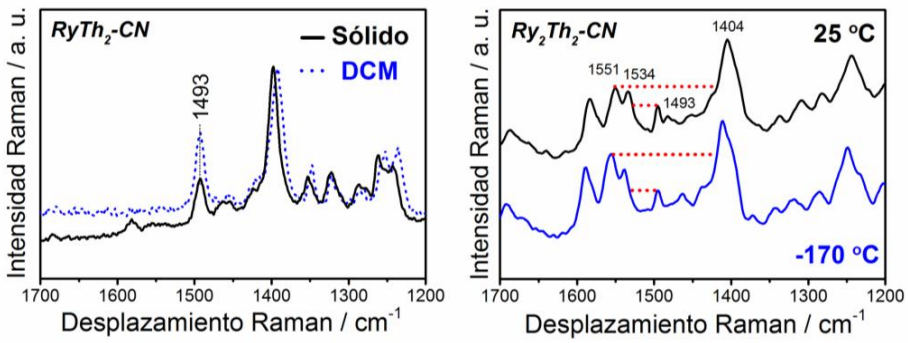

Figura 4.13 **Izquierda:** espectros Raman en disolución de DCM y estado sólido registrados con la línea de 785nm para *$RyTh_2$-CN*. **Derecha:** espectros FT-Raman (1064 nm) registrados en estado sólido a 25 ^{o}C y -170 ^{o}C para *Ry_2Th_2-CN*.

La **Figura 4.13 (derecha)** muestra los espectros FT-Raman registrados en estado sólido y en función de la temperatura para *Ry_2Th_2-CN*. El espectro FT-Raman de *Ry_2Th_2-CN* registrado a -170 ^{o}C compara con el correspondiente espectro a temperatura ambiente. Como puede observarse, se da una disminución de la intensidad relativa de las bandas tiofénicas a 1493 y 1404 cm^{-1} con respecto a las bandas en torno a 1550 cm^{-1}, resultado indicativo del posible aumento de la población de estados singlete de capa abierta a expensas del estado birradical triplete al bajar la temperatura. Todas estas evidencias espectroscópicas soportan, tanto la descripción de un estado fundamental birradical singlete de capa abierta para *Ry_2Th_2-CN*, como la existencia de un estado excitado birradical triplete cercano en energía.

En el contexto de la distribución de los niveles energéticos en el modelo de cuatro estados, en ambos casos, tal y como muestra la **Figura 4.14**, la introducción de los anillos de tiofeno favorece la estabilización de un estado fundamental de capa abierta debido a su aromatización en la forma resonante birradical. Una vez estabilizada la forma birradical, el mecanismo DSP determina la multiplicidad singlete en el estado fundamental para ambos casos. Sin embargo, el carácter birradical difiere,

como consecuencia de la flexibilidad estructural que introducen los propios tiofenos. Éstos, al aumentar su desviación con respecto al plano de la unidad fusionada central al pasar de *RyTh$_2$-CN* a *Ry$_2$Th$_2$-CN*, favorecen el aumento del carácter birradical, fenómeno que se asocia con una disminución del $\Delta E_{S\text{-}T}$ de tal calibre que es capaz de convertir en prácticamente isoenergéticas las configuraciones electrónicas de alto y bajo espín para *Ry$_2$Th$_2$-CN*.

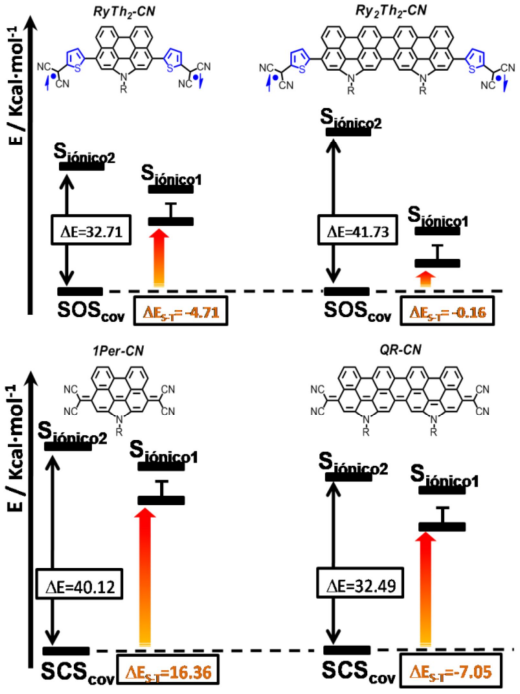

Figura 4.14 Modelo de cuatro estados para los derivados *1Per-CN, QR-CN, RyTh$_2$-CN* y *Ry$_2$Th$_2$-CN*. Los valores de $\Delta E_{S\text{-}T}$ se obtienen a partir de cálculos químico cuánticos a nivel CAM-B3LYP/6-31G** para los sistemas capa cerrada (*1Per-CN y QR-CN)*, y a partir de los datos de SQUID para los sistemas capa abierta (*RyTh2-CN* y *Ry2Th2-CN*).

4.3.2 BIBLIOGRAFÍA

1. Zeng, Z.; Sung, Y. M.; Bao, N.; Tan, D.; Lee, R.; Zafra, J. L.; Lee, B. S.; Ishida, M.; Ding, J.; López Navarrete, J. T.Li, Y.; Zeng, W.; Kim, D.; Huang, K-W.; Webster, R. D.; Casado, J.; Wu, J., *J. Am. Chem. Soc.*, 2012. **134**(35): p. 14513-14525.
2. Zeng, Z.; Lee, S.; Zafra, J. L.;Ishida, M.; Zhu, X.; Sun, Z.; Ni, Y.; Webster, R. D.; Li, R-W.; López Navarrete, J. T.; Chi, C.; Ding, J.; Casado, J.; Kim, D.; Wu, J., *Angew. Chem. Int. Ed.*, 2013. **125**(33): p. 8723-8727.
3. Ponce Ortiz, R.; Casado, J.; Hernández, V.; López Navarrete, Juan T.; Viruela, P. M.; Ortí, E.; Takimiya, K-; Otsubo, T., *Angew. Chem. Int. Ed.,* **119**(47): p. 9215-9219.
4. Takahashi, T.; Matsuoka, K-I.: Takimiya, K.; Otsubo, T.; Aso, Y., *J. Am. Chem. Soc.*, 2005. **127**(25): p. 8928-8929.
5. Li, Y.; Heng, W-K.; Lee, B. S.; Aratani, N.; Zafra, J. L.; Bao, N.; Lee, R,; Sung, Y. M.; Sun, Z.; Huang, K-W.; Webster, R. D.; López Navarrete, J. T.; Kim, D.; Osuka, A,; Casado, J.; Ding, J.; Wu, J., *J. Am. Chem. Soc.*, 2012. **134**(36): p. 14913-14922.
6. Casado, J.; Patchkovskii, S.; Zgierski, M. Z.; Hermosilla, L.; Sieiro, C.; Moreno Oliva, M.; López Navarrete, Juan T., *Angew. Chem. Int. Ed.*, 2008. **47**(8): p. 1443-1446.
7. González, S. R.; Ie, Y.; Aso, Y.; López Navarrete, J. T.; Casado, J., *J. Am. Chem. Soc.*, 2011. **133**(41): p. 16350-16353.
8. Casado, J.; Hicks, R. G.; Hernández, V.; Myles, D. J. T.; Ruiz Delgado, M. C.; López Navarrete, J. T., *J. Chem. Phys.*, 2003. **118**(4): p. 1912-1920.

5. Derivados Cetrénicos

5. Derivados Cetrénicos

5.1 Determinación de la configuración electrónica del estado fundamental en derivados cetrénicos: ¿capa abierta o cerrada?

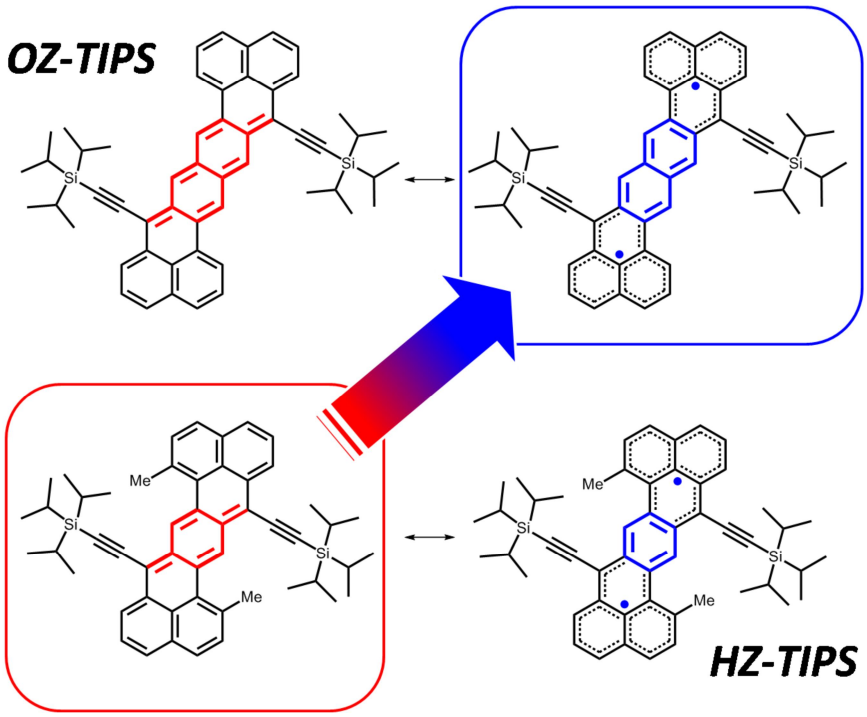

Figura 5.1. Estructuras químicas de las moléculas objeto de estudio.

También conocidos como dibenzoacenos, los cetrenos son un tipo de PAH con forma de zeta para el que se predice un significativo carácter birradical [1]. Ya para el derivado de menor tamaño, que posee seis anillos de benceno y da nombre a la familia, se espera cierto carácter birradical

[2], siendo éste mayor en derivados más largos como el heptacetreno o el octacetreno. Sin embargo, hasta la caracterización del primer derivado cetrénico con siete anillos de benceno, sintetizado por el grupo del Prof *J. Wu* [3], como un sistema singlete de capa abierta, todos los cetrenos y sus derivados presentaban estados fundamentales de capa cerrada con carácter birradical despreciable [4-6].

La pareja de moléculas cuyo estudio se detalla a continuación está constituida por derivados extendidos del cetreno, o heptacetreno, *HZ-TIPS* y su correspondiente análogo de ocho unidades, *OZ-TIPS*. *HZ-TIPS* constituye el segundo ejemplo de derivado cetrénico de siete unidades, tras el heptacetreno diimida del Prof. *J. Wu* mencionado anteriormente. *OZ-TIPS*, por su parte, es el primer derivado con ocho anillos de benceno obtenido hasta la fecha. La intrínseca alta reactividad de los derivados acénicos mayores de seis unidades está relacionada con la predicción de un elevado carácter birradical y es lo que los convierte en objetivos sintéticos difíciles de alcanzar [7]. Este obstáculo se solventa en *HZ-TIPS* y *OZ-TIPS* a través de su estabilización cinética mediante el uso de grupos voluminosos triisopropilsililacetileno (TIPS) para bloquear las posiciones de antemano más reactivas.

El estudio de los sistemas moleculares *HZ-TIPS* y *OZ-TIPS* que se lleva a cabo en el presente capítulo adquiere una especial relevancia en el contexto de la síntesis de *PAHs*, ya que la caracterización de su configuración electrónica en el estado fundamental, así como la comprensión de los orígenes de la misma en conexión con parámetros espectroscópicos, pueden ser de gran ayuda para establecer nuevas relaciones estructura-propiedad.

5.1.1 RESUMEN DE LOS RESULTADOS OBTENIDOS.

La caracterización de *HZ-TIPS* como estructura quinoide de capa cerrada es directa a partir de las señales ^{1}H-NMR, las cuales se obtienen perfectamente resueltas incluso a temperaturas de hasta 100 ^{o}C. Por el contrario, para *OZ-TIPS* se obtienen bandas anchas a temperatura ambiente, rasgo que se acentúa al aumentar la temperatura. El espectro ESR para *OZ-TIPS*, por su parte, presenta una señal ancha para el sólido a temperatura ambiente y una disminución de la absorbancia de la misma con el descenso de la temperatura. Esta evolución de la señal ESR con la temperatura es característica de singletes capa abierta con un estado excitado triplete cercano en energía [8], algo que confirma el valor de -3.87 Kcal· mol^{-1} obtenido para el ΔE_{S-T} mediante SQUID.

Las evidencias experimentales que aportan las medidas magnéticas acerca del estado fundamental de *OZ-TIPS* apuntan hacia una configuración electrónica singlete de capa abierta con un estado excitado triplete. En este contexto, la espectroscopia Raman juega el papel de proporcionar información sobre la estructura molecular de singlete y triplete, así como sobre los mecanismos que intervienen en la estabilización de estados fundamentales de capa abierta. En este caso, el estudio combinado de la evolución de los espectros de *HZ-TIPS* y *OZ-TIPS* con la temperatura permitirá confirmar la existencia del estado excitado birradical triplete en *OZ-TIPS*, aspecto elusivo en el caso de los ejemplos anteriores.

5.1.1.1 ESPECTROSCOPIA VIBRACIONAL RAMAN.

Contrariamente a los casos del capítulo anterior, en este apartado los anillos bencénicos relevantes se encuentran fusionados además de planarizados, sin flexibilidad conformacional posible. Se puede decir, por tanto, que el deplazamiento Raman de los modos característicos del benceno variará exclusivamente en función de la capacidad de conjugación de los radicales. Esta característica es básica a la hora de aplicar la espectroscopia Raman ya que en función de donde aparezcan y como evolucionen los modos vibracionales de tensión ν(C=C) característicos de las estructuras tipo aceno, será posible diferenciar el mayor o menor grado de aromaticidad del puente molecular [9]. Así, se puede considerar que los modos Raman asociados a frecuencias por encima de 1600 cm^{-1} corresponden a estructuras predominantemente bencenoides mientras que los modos quinoides aparecen a menores frecuencias, como consecuencia del debilitamiento neto de los enlaces CC del anillo que ocurre a raíz de la pérdida de aromaticidad en el mismo.

En la **Figura 5.2** se muestran los espectros FT-Raman registrados en estado sólido y con la línea láser de 1064 nm. A primera vista, llama la atención el debilitamiento de las bandas en la zona de las ν(C=C) del benceno al pasar de *HZ-TIPS* a *OZ-TIPS*. Si se centra el análisis en esa zona del espectro, la banda predominante aparece a 1590 cm^{-1} en *HZ-TIPS* y se desplaza a 1602 cm^{-1} para *OZ-TIPS*. Este desplazamiento se puede explicar a través de la evolución de una unidad central tipo *p-QDM* quinoide en *HZ-TIPS* a una estructura tipo naftaleno pseudoaromático en *OZ-TIPS*, en línea con la transición entre un sistema de capa cerrada para *HZ-TIPS* y uno de capa abierta para OZ-TIPS.

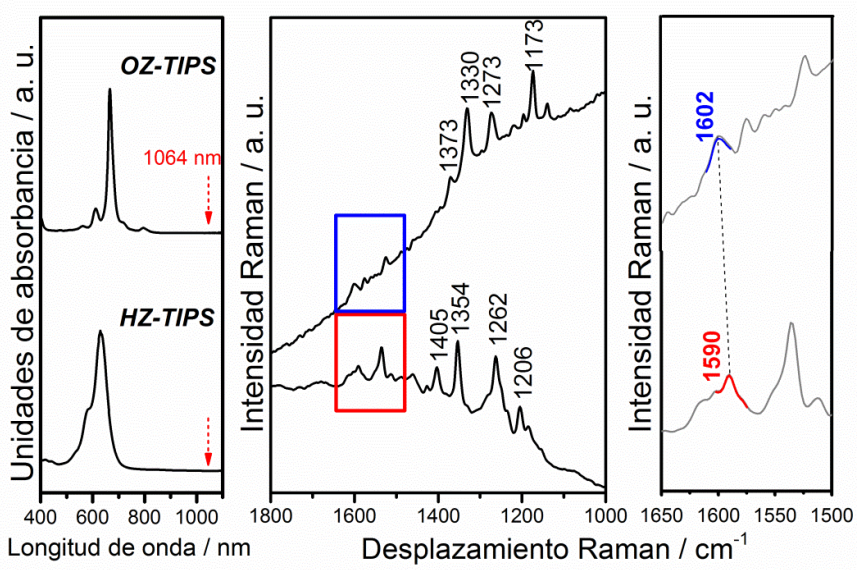

Figura 5.2. Izquierda: espectros de absorción electrónica UV-Vis-NIR registrados para *HZ-TIPS* y *OZ-TIPS* en disolución de DCM. **Centro:** espectros FT-Raman (1064 nm) registrados en estado sólido y a temperatura ambiente para las moléculas *HZ-TIPS* y *OZ-TIPS*. **Derecha:** Ampliación de la zona de 1600 cm^{-1} de los espectros FT-Raman.

El estudio de la zona de interés en ambos sistemas mediante termoespectroscopia Raman plantea dos escenarios diferentes. Mientras que no se observan cambios significativos para *HZ-TIPS*, en el caso de *OZ-TIPS* la evolución del espectro con la temperatura aporta cambios relevantes, como puede verse en la **Figura 5.3.** Esto justifica el análisis pormenorizado de la influencia que la variación de la temperatura ejerce sobre la estructura electrónica y molecular de *OZ-TIPS*.

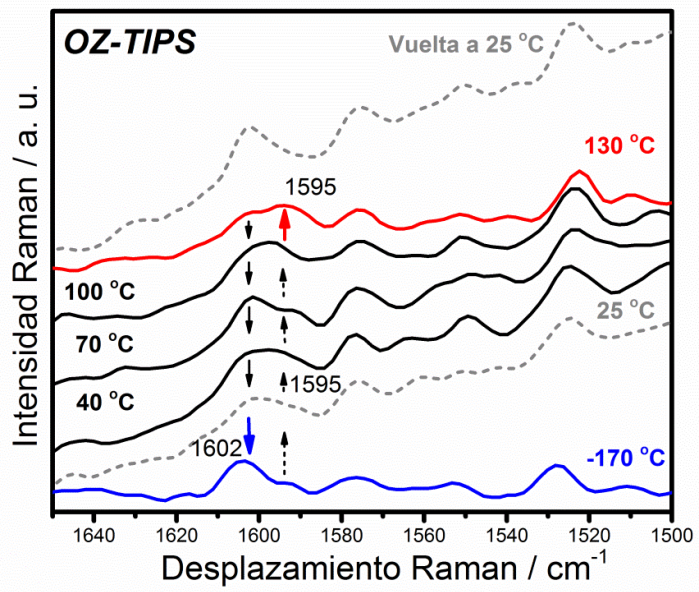

Figura 5.3 Espectros FT-Raman (1064 nm) registrados en estado sólido y en función de la temperatura para las molécula *OZ-TIPS*.

El espectro a 25 °C muestra una banda predominante a 1602 cm^{-1} acompañada por una componente más débil a 1595 cm^{-1}. Si analizamos la evolución de ambas bandas al aumentar la temperatura, se observa claramente una inversión de sus intensidades. La señal intensa de 1602 cm^{-1} en el espectro a -170 °C presenta una debilísima componente en torno a 1590-1595 cm^{-1} cuya intensidad va en progresivo aumento con la temperatura hasta convertirse en la banda más intensa del espectro a 130 °C, siendo esta evolución completamente reversible. Así, la banda a 1602 cm^{-1} que domina el espectro a baja temperatura correspondería con el estado fundamental birradical singlete, mientras que la banda intensa a alta temperatura, que aperece sobre 1595 cm^{-1}, se asigna al primer estado excitado birradical triplete.

En espectros complejos como los que se estudian en el presente apartado, los cálculos químico-cuánticos resultan de gran utilidad a la hora de realizar la asignación de las bandas Raman de manera fiable.

En el caso que nos ocupa, se recurre a cálculos químico-cuánticos basados en la Teoría del Funcional de la Densidad (DFT). Concretamente, se hace uso del funcional CAM-B3LYP [13] y la base 6-31G* para obtener los espectros Raman teóricos de las especies relevantes singlete y triplete de *HZ-TIPS* y *OZ-TIPS* (**Figura 5.4. (Izquierda)**). Para *HZ-TIPS*, las bandas intensas del espectro teórico se calculan a 1581 y 1520 cm^{-1} y corresponden razonablemente bien con las bandas experimentales medidas a 1590 y 1534 cm^{-1}, en base a la similar separación en frecuencias que presenta cada pareja. El análisis del autovector asociado al modo vibracional calculado a 1581 cm^{-1} permite asignar éste a una vibración de tensión de los enlaces CC paralelos de la estructura quinoide del anillo de benceno central. Al pasar a *OZ-TIPS*, esta banda a 1581 cm^{-1} se divide en dos componentes que se calculan a 1592 y 1580 cm^{-1} y que, en base al desplazamiento Raman que las separa, se pueden relacionar con las bandas experimentales a 1602 y 1591 cm^{-1}. El autovector de la banda teórica a 1592 cm^{-1} corresponde con un modo vibracional de tensión de enlaces CC localizado en la unidad central constituida por dos bencenos fusionados y, a diferencia del modo a 1581 cm^{-1} en *HZ-TIPS*, describe un tipo de vibración de carácter aromático en el que los seis enlaces CC de cada benceno central vibran con una amplitud significativa.

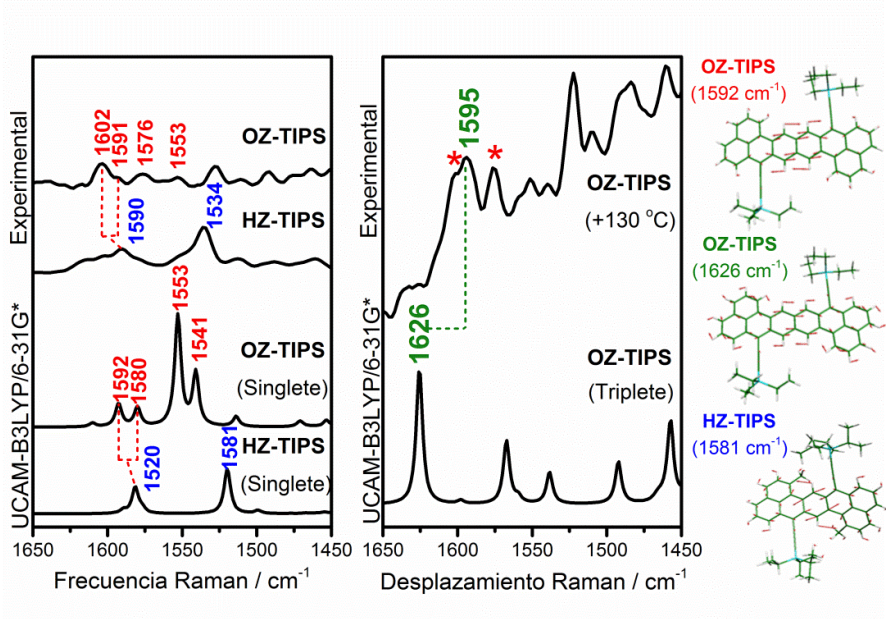

Figura 5.4. Izquierda: espectros Raman teóricos calculados a nivel (U)CAM-B3LYP/6-31G* y espectros experimentales registrados para *HZ-TIPS* y *OZ-TIPS* (-170 °C). **Centro:** espectro Raman teórico calculado para el primer estado excitado triplete de *OZ-TIPS* y espectro experimental registrado a 130 °C para la misma molécula. **Derecha:** autovectores de los modos vibracionales relevantes para cada una de las tres especies discutidas.

En la **Figura 5.4 (centro)** se presenta la comparación entre el espectro experimental obtenido para *OZ-TIPS* a 130 °C y el espectro calculado para su especie triplete. Es interesante constatar como el espectro teórico predice una única banda intensa en la zona de 1600 cm^{-1}, concretamente a 1626 cm^{-1}. Esta señal se puede correlacionar, por tanto, con la única banda que incrementa su intensidad al calentar y que se convierte en la más intensa en el espectro de alta temperatura, la banda a 1595 cm^{-1}.

En base a estos resultados quedan justificadas teóricamente tanto la asignación de las bandas a 1602 y 1591 cm^{-1} (-170 °C) a un estado fundamental singlete de capa abierta, como la de la banda que aparece a

1595 cm^{-1} .y que se intensifica selectivamente con la temperatura, a una especie birradical triplete poblada térmicamente.

Se puede decir, por tanto, que en términos energéticos, la ganancia de un anillo aromático en *HZ-TIPS* no compensa la ruptura de un enlace necesaria para la aparición de la especie birradical, presentando este sistema una configuración electrónica de tipo capa cerrada para el estado fundamental. La inclusión de un nuevo anillo de benceno en el puente molecular para dar lugar a *OZ-TIPS* lleva a la estabilización de la especie de capa abierta debido a que, ahora sí, la energía que aporta la aromatización de la unidad de naftaleno es suficiente como para compensar la ruptura de un enlace. Una vez generada la especie de capa abierta, el mecanismo DSP determina que la multiplicidad de espín del estado fundamental sea singlete, al verse favorecido por la efectiva conjugación de los electrones desapareados con el puente molecular fusionado. En la **Figura 5.5** se muestran los correspondientes diagramas de energía para los estados relevantes en cada situación:

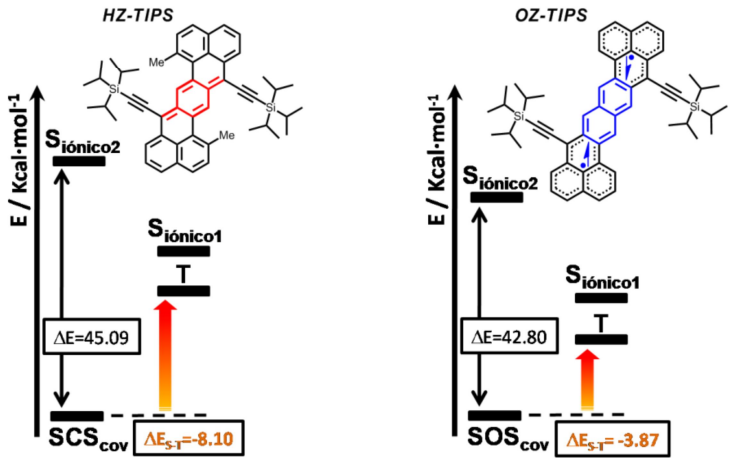

Figura 5.5. Modelo de cuatro estados para los derivados *HZ-TIPS* y *OZ-TIPS*. Los valores de $\Delta E_{S\text{-}T}$ se obtienen a partir de cálculos químico cuánticos a nivel CAM-B3LYP/6-31G* para el sistema capa cerrada (*HZ-TIPS*), y a partir de los datos de SQUID para el sistema capa abierta (*OZ-TIPS*).

El mecanismo DSP puede, además, dar cuenta de la posición relativa a la que se detectan las bandas de singlete y triplete en *OZ-TIP*S. Contrariamente a lo que ocurría en el capítulo anterior, donde sólo cabía representar los sistemas mediante dos estructuras resonantes capa cerrada y capa abierta, en los *OZ-TIPS*, los radicales se pueden localizar en diversas posiciones, hacia el centro de naftaleno y hacia las unidades exteriores de fenalenilo, dando lugar a más de una estructura resonante capa abierta, como muestra la **Figura 5.6**. Es esta propiedad la que determina que la banda Raman característica del birradical singlete aparezca a mayor frecuencia que la correspondiente al triplete.

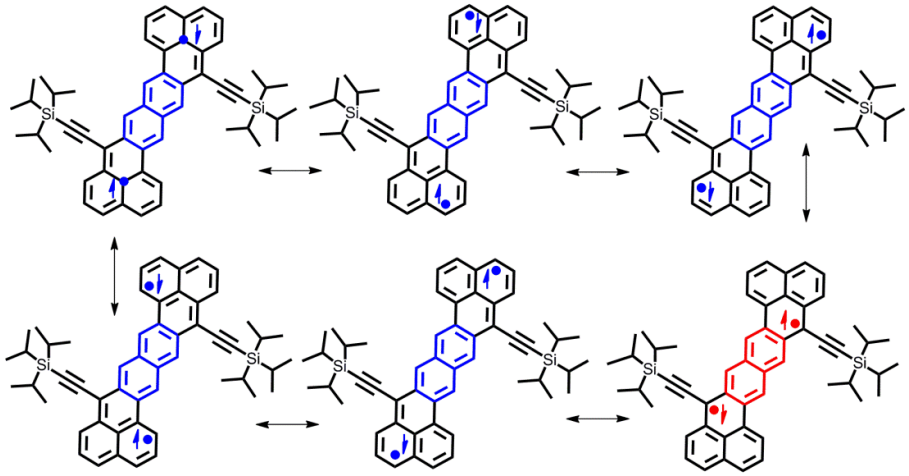

Figura 5.6. Ejemplo de algunas de las estructuras resonantes posibles para *OZ-TIPS*.

5.1.2 BIBLIOGRAFÍA

1. Marković, S.; Radenković, S.; Marković, Z.; Gutman, I., *Russian Journal of Physical Chemistry A*, 2011. **85**(13): p. 2368-2372.
2. Clar, E.; Lang, K.F.; Schulz-Kiesow, H., Chem. Ber., 1955. **88**(10): p. 1520-1527.
3. Sun, Z.; Huang, K.-W.; Wu, J., *J. Am. Chem. Soc.*, 2011. **133**(31): p. 11896-11899.
4. Umeda, R.; Hibi, D.; Miki, K.; Tobe, Y., *Org. Lett.*, 2009. **11**(18): p. 4104-4106.
5. Wu, T-C.; Chen, C-H.; Hibi, D.; Shimizu, A.; Tobe, Y.; Wu, Y-T., Angew. Chem. Int. Ed., 2010. **49**(39): p. 7059-7062.
6. Sun, Z.; Huang, K.-W.; Wu, J. *Org. Lett*., 2010. **12**(20): p. 4690-4693.
7. Clar, E.; Macpherson, I.A., *Tetrahedron*, 1962. **18**(12): p. 1411-1416.
8. Konishi, A.; Hirao, Y.; Nakano, M.; Shimizu, A.; Botek, E.; Champagne, B.; Shiomi, D.; Sato, K.; Takui, T.; Matsumoto, K.; Kurata, H.; Kubo, T., *J. Am. Chem. Soc.*, 2010. **132**(32): p. 11021-11023.
9. Casado, J.; Patchkovskii, S.; Zgierski, M. Z.; Hermosilla, L.; Sieiro, C.; Moreno Oliva, M.; López Navarrete, Juan T., *Angew. Chem. Int. Ed.*, 2008. **47**(8): p. 1443-1446.
10. Yanai, T.; Tew, D.P.; Handy, N.C., *Chem. Phys. Lett.*, 2004. **393**(1–3): p. 51-57.

5.2 Expresión de la pro-aromaticidad en el estado fundamental de derivados cetrénicos. Influencia sobre la estabilización de especies cargadas.

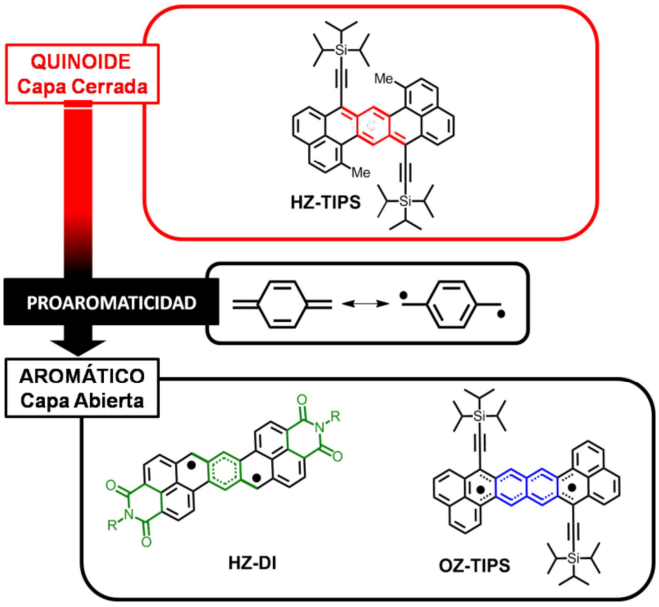

Figura 5.7 Estructuras químicas de las moléculas objeto de estudio (R=$C_{11}H_{23}$).

En este apartado se pretende estudiar la influencia que el carácter pro-aromático de la unidad central de *p-QDM* de los compuestos derivados de cetreno tiene sobre la estructura electrónica y molecular de especies cargadas [1-3]. En concreto, se estudia el conjunto de moléculas formado por *HZ-TIPS* y *OZ-TIPS* [4], al que se añade un nuevo heptacetreno funcionalizado con grupos diimida, *HZ-DI*. Así, se puede abordar el estudio de las mismas desde dos aproximaciones: por una parte, en función de la longitud de cadena en *HZ-TIPS* y *OZ-TIPS* y, por otra, en conexión con el efecto de la inclusión de grupos electroaceptores diimida en *HZ-DI* [5-8]. En particular, esta última presenta un estado electrónico fundamental

singlete capa abierta, en consonancia con el efecto estabilizador de birradicales que ejercen los grupos aceptores de electrones ya descrito en el capítulo cuatro.

5.2.1 RESUMEN DE LOS RESULTADOS OBTENIDOS

El estudio de la evolución del ΔE_{S-T} mediante cálculos químico-cuánticos DFT a nivel (U)CAM-B3LYP/3-21G** [9] mostrado en la **Figura 5.8** describe cómo afectan a la estabilización de especies capa abierta las modificaciones estructurales siguientes: cetrenos, heptacetrenos y octacetrenos sin sustituir (**Figura 5.8 Derecha**), sustituidos con grupos TIPS y sustituidos con grupos diimida. Se observan notables diferencias en la estabilización de un tipo de especie u otra en función del grado de sustitución.

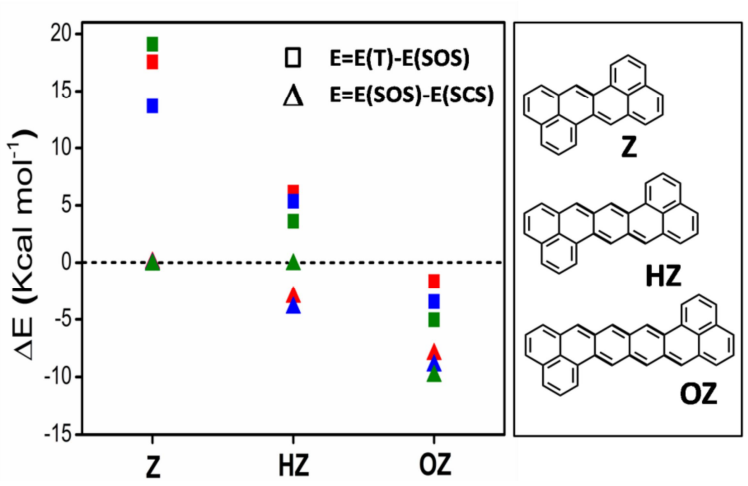

Figura 5.8 Diferencias de energía entre los estados singlete capa abierta (SOS), triplete (T) y singlete de capa cerrada (SCS) calculadas a nivel (U)CAM-B3LYP/3-21G** en función de la longitud de cadena para los derivados sin sustituir (rojo), sustituidos con grupos Diimida (azul) y sustituidos con grupos TIPS (verde).

En los derivados no sustituidos el birradical singlete se estabiliza a partir del heptacetreno, viéndose favorecida esta configuración aún más con la inclusión de grupos diimida, gracias a la participación de éstos en la π-conjugación. La influencia de los grupos aceptores en la generación de birradicales ha sido previamente descrita por nuestro grupo de investigación en términos de una disminución del *BLA* o de la alternancia de enlaces simples y dobles en el esqueleto conjugado. En *HZ-TIPS*, por el contrario, se favorece la estabilización de la estructura de capa cerrada, al bloquear la π-conjugación los grupos TIPS (conjugación cruzada) [4]. En línea con lo establecido en apartados anteriores, el aumento de la longitud de cadena conduce a la progresiva estabilización de especies capa abierta gracias al incremento del número de anillos que recuperan aromaticidad en la forma birradical, siendo ésta la configuración energéticamente más favorable para el octacetreno en todas sus variantes.

En este tipo de birradicales *kekulé*, la estabilización de especies de bajo espín, independientemente de la longitud de cadena y sustitución, se puede interpretar en términos de un mecanismo DSP, que viene a dar cuenta de la conjugación o deslocalización de los radicales en el puente molecular en la estructura singlete de capa abierta, a diferencia del triplete. [10-13].

La **Figura 5.9** muestra las geometrías optimizadas para el estado fundamental (S_0) para *HZ*, *HZ-TIPS* y *HZ-DI*, además de la del primer estado excitado triplete (T_1) para esta última. En *HZ-TIPS* se observa un claro patrón de estructura quinoide en el benceno central, en línea con su configuración de capa cerrada y, a su vez, en claro contraste con la aromatización parcial que muestra el derivado *HZ-DI* en esa misma unidad que evidencia el carácter birradical de su estado fundamental. Cabe destacar como el carácter aromático del benceno central se acentúa en el primer estado excitado triplete de *HZ-DI*.

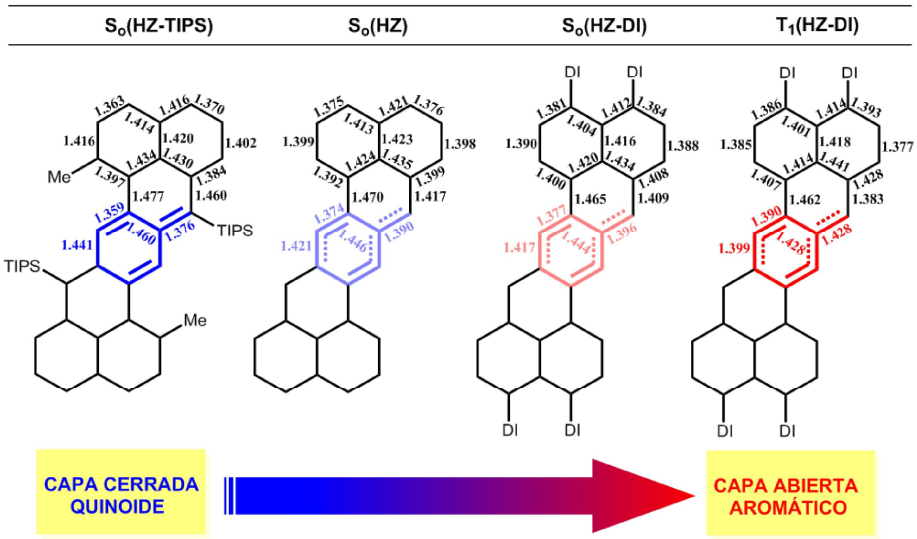

Figura 5.9 Geometrías optimizadas a nivel (U)CAM-B3LYP/3-21G** para el estado fundamental singlete (S_o) de *HZ-TIPS*, *HZ* y *HZ-DI*, junto con el primer estado excitado triplete (T_1) de este último.

5.2.1.1 ESPECTROSCOPIA VIBRACIONAL RAMAN DE ESPECIES NEUTRAS.

Con carácter general, cabe destacar que, de entre todos los anillos de benceno que poseen los cetrenos, aquellos en los que la π-conjugación se hace máxima presentan modos de tensión CC más intensificados [14-16]. Esto sirve de diagnóstico inicial a la hora de caracterizar la multiplicidad de espín del estado fundamental en este tipo de derivados dado que, como se estudió en el apartado anterior para el caso de los derivados *HZ-TIPS* y *OZ-TIPS* [4, 6], permite detectar directamente los modos vibracionales Raman de los enlaces CC correspondientes a los anillos de benceno del puente molecular entre fenalenos, a través de los cuales la π-conjugación es máxima. Por tanto, mediante el análisis de la región de 1600 cm^{-1}, donde aparecen estas señales, se puede obtener información directa de la relación estructura-propiedad para nuestros sistemas en los siguientes términos:

i) En unidades bencénicas con estructura aromática las bandas Raman se detectarán a valores alrededor de 1600 cm^{-1} o superiores.

ii) Cuando la estructura de los anillos de benceno presente un cierto carácter quinoide, las bandas Raman de registrarán a menores frecuencias, apareciendo en torno a 1580-1570 cm^{-1} para estructuras totalmente quinoides.

En la **Figura 5.10** se presentan los espectros FT-Raman registrados en estado sólido y con la línea láser de 1064 nm para las tres moléculas objeto de estudio junto con sus correspondientes espectros de absorción electrónica UV-Vis-NIR en disolución de DCM.

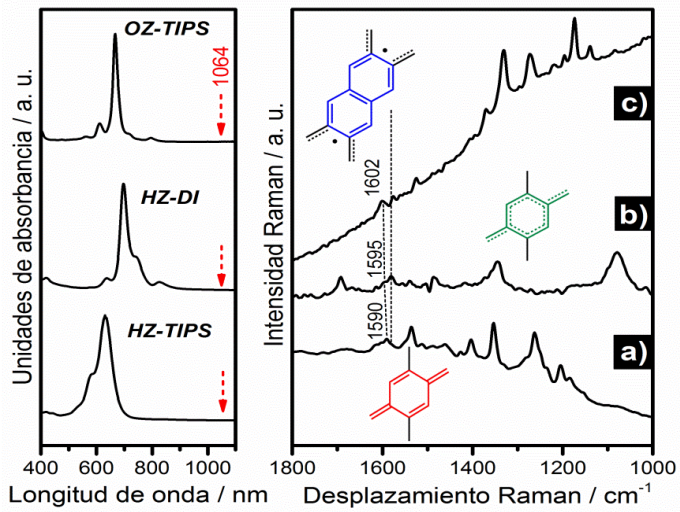

Figura 5.10 **Izquierda:** espectro de absorción electrónica UV-Vis-NIR registrado en disolución de DCM para *HZ-DI, HZ-TIPS y OZ-TIPS*. **Derecha:** espectros FT-Raman registrados en estado sólido y a temperatura ambiente para las moléculas *HZ-TIPS* (a), *HZ-DI* (b) y *OZ-TIPS* (c).

Si se analizan las bandas intensas en la región de 1600 cm^{-1} asociadas a las vibraciones de las unidades centrales en cada una de las moléculas, para *HZ-DI*, la banda a 1595 cm^{-1} se puede relacionar con una transición entre estructuras quinoides y aromáticas en la unidad *p-QDM* central, lo que vendría a confirmar la predicción teórica de un estado fundamental birradical singlete responsable de la aromatización parcial del *p-QDM* central en *HZ-DI*. Resulta evidente, por tanto, que *HZ-DI* se encontraría a medio camino entre la estructura benzoquinoide de *HZ-TIPS,* caracterizada por la banda intensa a 1590 cm^{-1}, y la estructura benzoaromática del naftaleno central en *OZ-TIPS* a la que responde la señal Raman detectada a 1602 cm^{-1}.

5.2.1.2 ESPECTROSCOPIA VIBRACIONAL RAMAN DE ESPECIES CARGADAS.

La pro-aromaticidad de las estructuras quinoides no sólo es relevante para la formación de especies birradicales neutras [17,18], sino que también es un factor [19] clave para la estabilización de especies cargadas. Con objeto de profundizar en este aspecto, se caracterizan los diversos procesos redox mediante técnicas espectroelectroquímicas de absorción electrónica en el UV-Vis NIR y se estudia la estructura molecular de las especies oxidadas mediante espectroscopia Raman, todo ello soportado por cálculos químico-cuánticos DFT.

La **Figura 5.11a** muestra los espectros de absorción para el proceso de reducción electroquímica de *HZ-TIPS* a potenciales que nunca superan las primeras ondas de oxidación o reducción monoelectrónicas obtenidas en la CV. Se observa la aparición de cuatro nuevas bandas (dos significativamente intensas) en la región Vis-NIR cuyo patrón es el característico de un anión radical, al presentar dobles bandas en la región del NIR. El proceso de oxidación electroquímica (**Figura 5.11b**), por su parte, genera el catión radical correspondiente, que se caracteriza por presentar un perfil espectral similar al del anión. Estos rasgos espectrales constituyen nuevas evidencias de la estructura quinoide de *HZ-TIPS* y de su carácter pro-aromático, lo que lleva a la molécula a aromatizarse para acomodar el exceso de carga, ya sea negativo o positivo, como muestra la **Figura 5.11c**, en donde se representan, cualitativamente, los resultados obtenidos para las geometrías optimizadas de anión y catión a nivel (U)CAM-B3LYP/6-31G*.

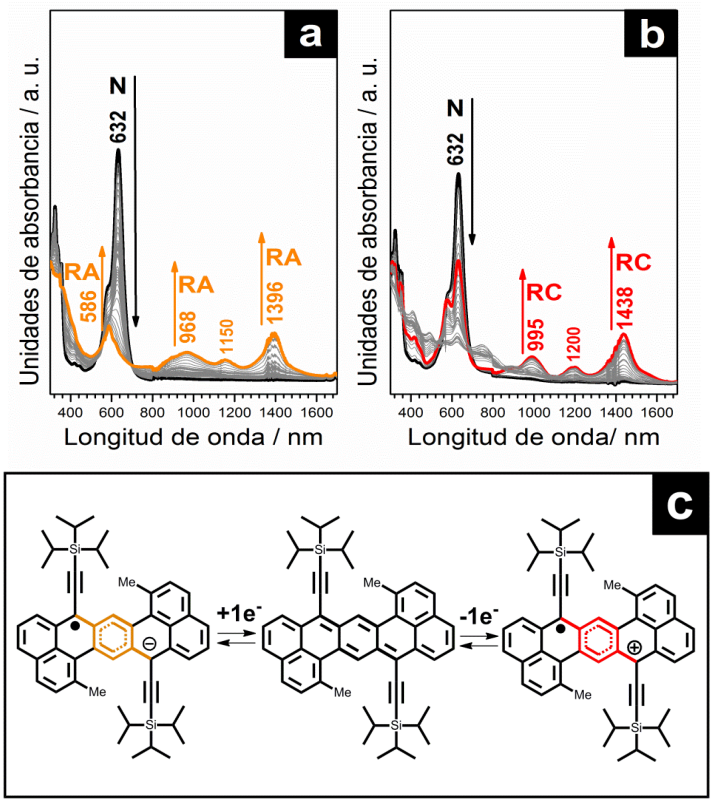

Figura 5.11 Espectros de absorción electrónica UV-Vis-NIR de los procesos redox obtenidos electroquímicamente registrados *in situ* para *HZ-TIPS*: **a)** Reducción monoelectrónica, **b)** Oxidación monoelectrónica (N: Neutro, RA: radical anión, RC: Radical Catión), **c)** Estructuras cualitativas deducidas mediante cálculos teóricos a nivel (U)CAM-B3LYP/6-31G** para las especies cargadas.

La **Figura 5.12** muestra los espectros de absorción electrónica UV-Vis-NIR para los procesos de reducción electroquímica de *HZ-DI* y *OZ-TIPS*. Llama la atención que, aunque similares entre sí, los procesos de reducción de estos derivados presentan diferencias evidentes con respecto a lo descrito para *HZ-TIPS*. Como puede verse, se caracterizan por la aparición de una banda en el espectro de absorción a menores longitudes de onda que la del neutro, algo típico de la formación directa de especies dianiónicas. En *OZ-TIPS*, la generación directa de la especie

dianiónica se favorece por la aromatización del naftaleno central, ya parcialmente aromatizado en la forma neutral birradicalaria. En el caso de *HZ-DI*, son dos los factores que influyen en la estabilización directa del dianión: la completa aromatización del anillo de benceno central y el efecto electroaceptor de las unidades diimida. De nuevo, las geometrías optimizadas a nivel (U)CAM-B3LYP/6-31G** confirman los resultados experimentales (**Figura 5.12c**).

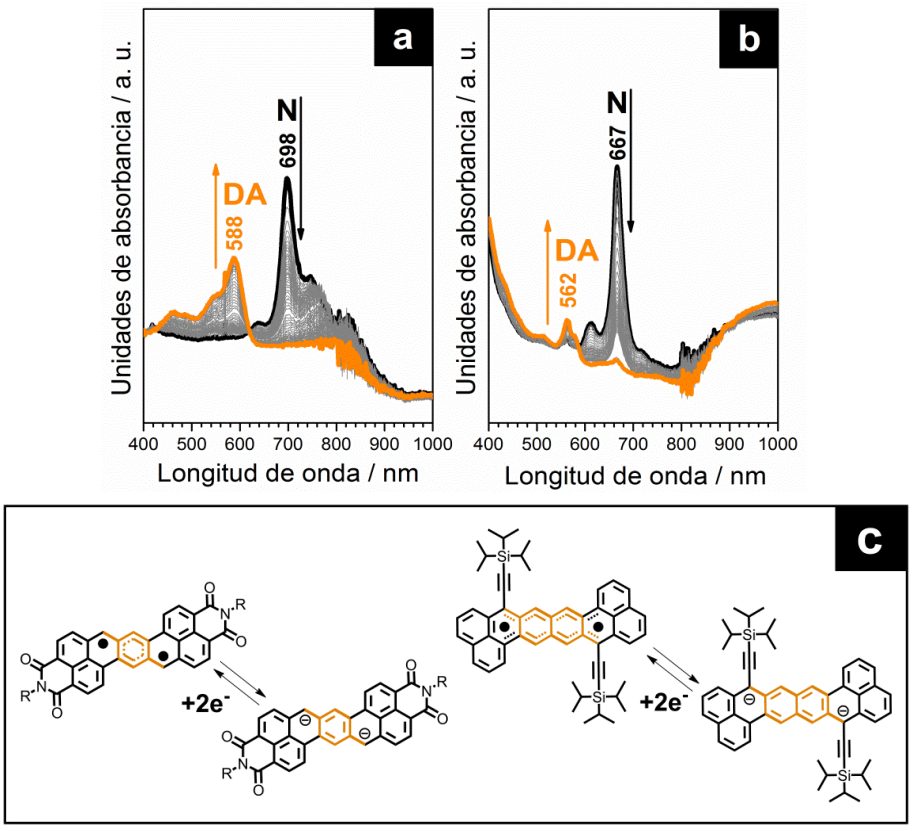

Figura 5.12. Espectros de absorción electrónica UV-Vis-NIR de las reducciones electroquímicas registrados *in situ* para **a)** *HZ-DI* y **b)** *OZ-TIPS* (N: Neutro, DA: Dianión). **c)** Estructuras cualitativas deducidas mediante cálculos teóricos a nivel (U)CAM-B3LYP/6-31G** para el proceso de reducción bielectrónico para las dos moléculas.

La posibilidad de llevar a cabo la oxidación de las tres moléculas permite obtener los espectros Raman de los tres cationes radicales por vía espectroquímica (en condiciones de resonancia o pre-resonancia). En la **Figura 5.13** se presentan los espectros FT-Raman para las especies catiónicas de *HZ-TIPS*, *OZ-TIPS* y *HZ-DI* obtenidas en disolución de DCM usando $FeCl_3$ como oxidante, junto con los correspondientes espectros de absorción electrónica UV-Vis-NIR de cada especie.

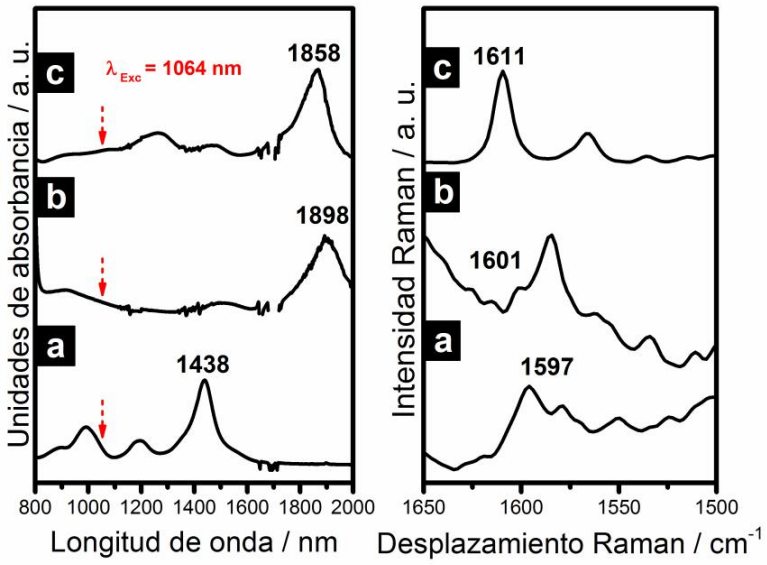

Figura 5.13 **Izquierda:** espectros de absorción electrónica UV-Vis-NIR del catión radical obtenido con $FeCl_3$ en DCM para: **a)** *HZ-TIPS*, **b)** *HZ-DI y* **c)** *OZ-TIPS*. **Derecha:** espectros FT-Raman (1064 nm) de los mismos cationes radicales.

Las bandas que aparecen a 1597 cm^{-1} en *HZ-TI*PS, 1601 cm^{-1} en *HZ-DI* y 1611 cm^{-1} en *OZ-TIPS* se asignan a los modos de tensión CC relevantes de la unidad central benceno/naftaleno. El desplazamiento a mayores valores que sufren estas bandas con respecto a las frecuencias de 1590, 1595 y 1602 cm^{-1} en las correspondientes especies neutras, da cuenta de

un aumento en la aromaticidad de estas estructuras a raíz de la extracción de un electrón. Es interesante observar como, en el caso del catión de *HZ-DI*, debido a la influencia del grupo aceptor diimida, el defecto de carga se encuentra confinado en el centro de la molécula en mayor medida que en *HZ-TIPS*, lo que provoca una mayor aromatización del benceno central en el primero. En el caso del catión radical de *OZ-TIPS*, la aromatización del naftaleno central conduce a la aparición de su banda Raman a la frecuencia más elevada de las tres.

5.2.2 BIBLIOGRAFÍA

1. Clar, E.; Lang, K.F.; Schulz-Kiesow, H., *Chem. Ber.*, 1955. **88**(10): p. 1520-1527.
2. Umeda, R.; Hibi, D.; Miki, K.; Tobe, Y., *Org. Lett.*, 2009. **11**(18): p. 4104-4106.
3. Wu, T-C.; Chen, C-H.; Hibi, D.; Shimizu, A.; Tobe, Y.; Wu, Y-T., Angew. Chem. Int. Ed., 2010. **49**(39): p. 7059-7062.
4. Li, Y.; Heng, W-K.; Lee, B. S.; Aratani, N.; Zafra, J. L.; Bao, N.; Lee, R,; Sung, Y. M.; Sun, Z.; Huang, K-W.; Webster, R. D.; López Navarrete, J. T.; Kim, D.; Osuka, A,; Casado, J.; Ding, J.; Wu, J., *J. Am. Chem. Soc.*, 2012. **134**(36): p. 14913-14922.
5. Ponce Ortiz, R.; Casado, J.; Hernández, V.; López Navarrete, J. T.; Viruela, P. M.; Ortí, E.; Takimiya, K-; Otsubo, T., *Angew. Chem. Int. Ed.,* **119**(47): p. 9215-9219.
6. Casado, J.; Patchkovskii, S.; Zgierski, M. Z.; Hermosilla, L.; Sieiro, C.; Moreno Oliva, M.; López Navarrete, Juan T., *Angew. Chem. Int. Ed.*, 2008. **47**(8): p. 1443-1446.
7. Casado, J.; Ponce Ortiz, R.; Lopez Navarrete, J.T.. *Chem. Soc. Rev.*, 2012. **41**(17): p. 5672-5686.
8. González, S. R.; Ie, Y.; Aso, Y.; López Navarrete, J. T.; Casado, J., *J. Am. Chem. Soc.*, 2011. **133**(41): p. 16350-16353.
9. Yanai, T.; Tew, D.P.; Handy, N.C., *Chem. Phys. Lett.*, 2004. **393**(1–3): p. 51-57.
10. Borden, W.T., *Diradicals*, ed. W. Interscience. Vol. 1. 1982, New York.
11. Berson, J.A., *Acc. Chem. Res.*, 1997. **30**(6): p. 238-244.
12. Karafiloglou, P., *J. Chem. Ed.*, 1989. **66**(10): p. 816.
13. Karafiloglou, P., *J. Chem. Phys.*, 1985. **82**(8): p. 3728-3740.
14. Zerbi, G.; Castiglione C.; and Del Zoppo, M., *Electronic Materials: The Oligomeric Approach*. 1998: Wiley-VCH.
15. a) Castiglioni C.; Gussoni, M.; López Navarrete, J. T.; Zerbi, G., Solid State Commun., 1988, **65**, p. 625. b) López Navarrete, J. T. and Zerbi, G., *J. Chem. Phys.*, 1991. **94**(2): p. 957-964.
16. Hernandez, V.; Castiglioni, C.; Del Zoppo, M.; Zerbi, G., *Phys. Rev B*, 1994. **50**(14): p. 9815-9823.

17. Sun, Z.; Huang, K.-W.; Wu, J., *J. Am. Chem. Soc.*, 2011. **133**(31): p. 11896-11899.
18. Sun, Z.; Huang, K.-W.; Wu, J., *Org. Lett.*, 2010. **12**(20): p. 4690-4693.
19. Casado, J.; Miller, L. L.; Mann, K. R.; Pappenfus, T. M.; Higuchi, H.; Ortí, E.; Milián, B.; Pou-Amérigo, R.; Hernández, V.; López Navarrete, J. T., *J. Am. Chem. Soc.*, **2002**, *124* (41), pp 12380–12388.

6. Derivados tetrabenzo-chichibabin

6. DERIVADOS TETRABENZO-CHICHIBABIN

6.1 ESTABILIZACIÓN DE ESTADOS NEUTROS CAPA ABIERTA Y ESPECIES OXIDADAS EN NUEVOS DERIVADOS ESTABLES DE LA MOLÉCULA DE CHICHIBABIN. CARACTERIZACIÓN RAMAN DEL ESTADO FUNDAMENTAL.

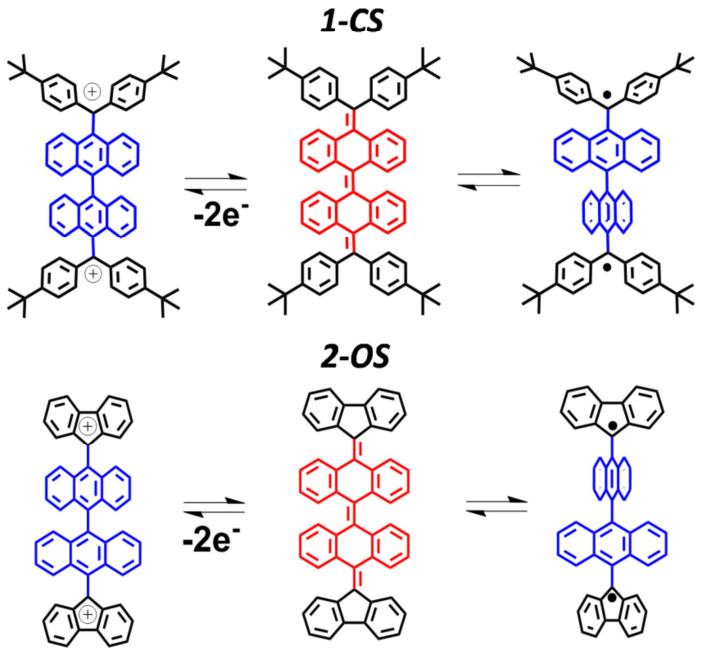

Figura 6.1 Estructuras químicas de las moléculas objeto de estudio.

Como se mencionó en la introducción, la molécula de Chichibabin presenta un elevado carácter birradical en el estado electrónico fundamental [1-3]. Esto le confiere una gran inestabilidad y complica tanto su caracterización como sus aplicaciones prácticas. En el presente apartado, en línea con el interés que durante décadas ha tenido la

búsqueda de nuevos *PAHs* estables tipo Chichibabin [3-7], se presenta el estudio de las moléculas *1-CS* y *2-OS*, ambos derivados tetrabenzofusionados, que pueden representarse mediante estructuras resonantes quinoide de capa cerrada y birradical de capa abierta **(Figura 6.1)**. La alta estabilidad que muestran estos sistemas con respecto a la molécula de Chichibabin original proviene de la estabilización termodinámica que inducen las unidades tipo fluoreno y antraceno.

El rasgo que diferencia a los dos sistemas objeto de estudio se encuentra en las unidades que presentan a ambos extremos del bifenilo central. La molécula *1-CS* se caracteriza por presentar cuatro grupos fenilo de los extremos. La molécula *2-OS*, por su parte, presenta unidades de fluorenilo. Estas unidades muestran una gran capacidad de estabilizar centros radicales al permitir la deslocalización de los mismos en su esqueleto π-conjugado [8], lo que, en principio, debiera favorecer la estabilización de especies de capa abierta. La pareja de moléculas *1-CS/2-OS* constituye, por tanto, una magnífica oportunidad para estudiar el estado fundamental de nuevos derivados tipo Chichibabin.

6.1.1 RESUMEN DE LOS RESULTADOS OBTENIDOS.

Para el derivado *1-CS*, los datos de ^{1}H-RMN a temperatura variable y absorción electrónica UV-Vis-NIR apuntan hacia una configuración quinoide de capa cerrada. Los resultados obtenidos por difracción de Rayos X, además, revelan ese carácter quinoide de la parte central, con una estructura molecular de tipo mariposa. Esta distorsión de la estructura molecular difiere de la planaridad que caracteriza a la molécula de Chichibabin. El motivo de la estabilización de *1-CS* en su forma de capa cerrada se puede racionalizar en términos de una menor aromaticidad del anillo central del antraceno y por la desviación del plano central de los bencenos exteriores.

A la hora de caracterizar el estado fundamental del derivado *2-OS*, las medidas magnéticas describen una configuración de capa abierta. Los resultados de ^{1}H-RMN a temperatura variable y ESR indican una notable presencia de especies paramagnéticas, mientras que las medidas de SQUID en función de la temperatura permiten calcular un $\Delta E_{S\text{-}T}$ de 0.33 Kcal·mol^{-1} con un estado fundamental birradical triplete. Asumiendo esta configuración electrónica, cabe destacar el efecto estabilizante que sobre dicha especie de capa abierta introducen los grupos fluorenilo y las unidades de antraceno respectivamente.

6.1.1.1 ESPECTROSCOPIA VIBRACIONAL RAMAN DE ESPECIES NEUTRAS.

La **Figura 6.2** muestra los espectros FT-Raman registrados en estado sólido y con la línea láser de 1064 nm, junto con sus correspondientes espectros de absorción UV-Vis-NIR registrados en DCM. Si se centra el análisis del espectro Raman en la zona de 1600 cm^{-1} donde aparecen las ν(CC) de los anillos de benceno/antraceno, se observan diferencias significativas.

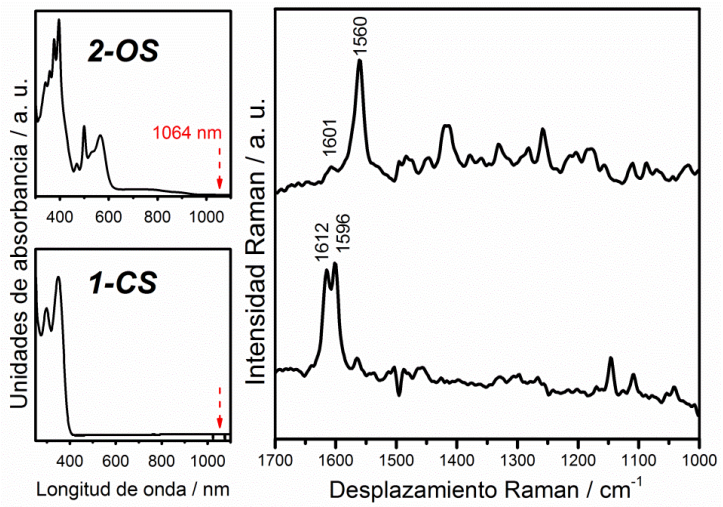

Figura 6.2 **Izquierda:** espectros de absorción electrónica UV-Vis-NIR para las moléculas *1-CS* y *2-OS* en disolución de DCM. **Derecha:** espectros FT-Raman (1064 nm) registrados en estado sólido para las mismas especies.

El sistema *1-CS* presenta una banda a 1596 cm^{-1} claramente indicativa de la presencia de anillos benzoquinoides [9] junto con otra que aparece a 1612 cm^{-1}, frecuencia cercana a la zona característica de las tensiones de enlaces C=C oligoénicos conjugados (doble enlaces externos). Ambas señales indican una configuración quinoide de capa cerrada. En *2-OS*, sin embargo, el perfil espectral en la zona de 1600 cm^{-1}

es diferente, siendo la banda más intensa la que aparece a 1560 cm^{-1}. Ésta se puede asignar a una estructura de tipo antraceno que se habría generado como consecuencia de la formación de especies de capa abierta, o birradicales [10].

La **Figura 6.3** muestra los espectros FT-Raman en función de la temperatura para los dos sistemas. Para *2-OS* el perfil espectral apenas cambia, resultado que demuestra la robustez térmica del estado fundamental triplete. Como ΔE_{S-T} es pequeño, los estados de alto y bajo espín han de ser prácticamente isoenergéticos, implicando poblaciones parecidas del estado fundamental triplete y el primer estado excitado singlete que impedirían observar por espectroscopia Raman un trasvase de población de un estado a otro. Además, ambos estados tendrán espectros parecidos, por lo que no se observarían diferencias significativas. Por su parte, la invariabilidad del espectro FT-Raman en *1-CS* con la temperatura da cuenta de la robustez térmica de la configuración quinoide de capa cerrada y de un alto ΔE_{S-T}.

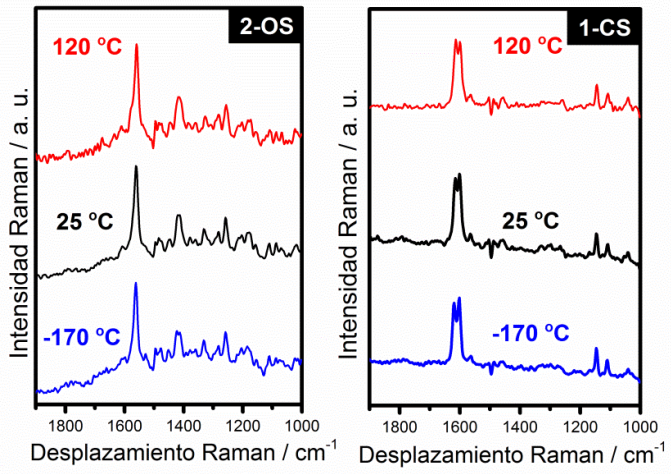

Figura 6.3 Izquierda: espectros FT-Raman registrados en estado sólido y con la línea de 1064 nm para *2-OS* en función de la temperatura. **Derecha:** espectros FT-Raman registrados en estado sólido y con la línea de 1064 nm para *1-CS* en función de la temperatura.

En términos de estabilización de especies capa cerrada o capa abierta, queda claro el importante papel que juega el grupo fluorenilo. Su presencia en *2-OS* favorece esta última configuración, gracias a que permite la deslocalización de los centros radicales en su entorno conjugado. En el caso de *1-CS* la imposibilidad de deslocalizar los electrones desapareados en la unidad de fluorenilo, convierte en más estable la configuración de capa cerrada. Por su parte, la estabilización del estado fundamental de alto espín en *2-OS*, una vez generada la especie de capa abierta, tiene que ver con el impedimento estérico entre unidades de antraceno, ya que, al disponerse éstas perpendicularmente, rompen la conjugación y eliminan la conexión entre los centros radicales. Esta característica estructural niega la posibilidad de que intervenga el mecanismo DSP, y por tanto, se estabiliza el estado birradical triplete sobre el singlete de capa abierta, como muestra el valor de $\Delta E_{S\text{-}T}$ obtenido mediante SQUID (**Figura 6.4**).

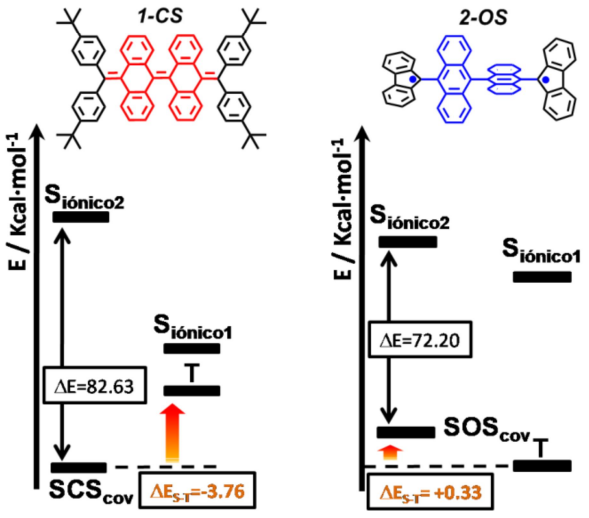

Figura 6.4 Diagrama de cuatro estados para las moléculas *1-CS* y *2-OS*. Los valores de $\Delta E_{S\text{-}T}$ se obtienen a partir de cálculos químico-cuánticos a nivel CAM-B3LYP/6-31G* para el sistema capa cerrada (*1-CS)*, y a partir de los datos de SQUID para el sistema capa abierta (2-*OS*).

6.1.1.2 ESPECTROSCOPIA VIBRACIONAL RAMAN DE ESPECIES OXIDADAS.

Las propiedades redox de ambos sistemas permiten obtener directamente los correspondientes dicationes mediante oxidación de las especies neutras con $FeCl_3$. En *1-CS*, las bandas de absorción electrónica del dicatión se detectan a 500 y 832 nm, mientras que para *2-OS*, éstas aparecen como una doble banda a 475 y 528 nm seguida de una banda ancha en torno a 1130 nm. En ambos casos la aparición de bandas anchas desplazadas al NIR va a ser de gran importancia, ya que permitirán recurrir a condiciones de resonancia con la línea excitatriz Raman de 1064 nm y, por tanto, dará la oportunidad de realizar un estudio comparativo entre especies cargadas y neutras.

En la **Figura 6.5** se muestran los espectros de absorción de las especies neutras y dicatiónicas para los dos sistemas, junto con sus correspondientes espectros FT-Raman en la zona de 1600 cm^{-1}.

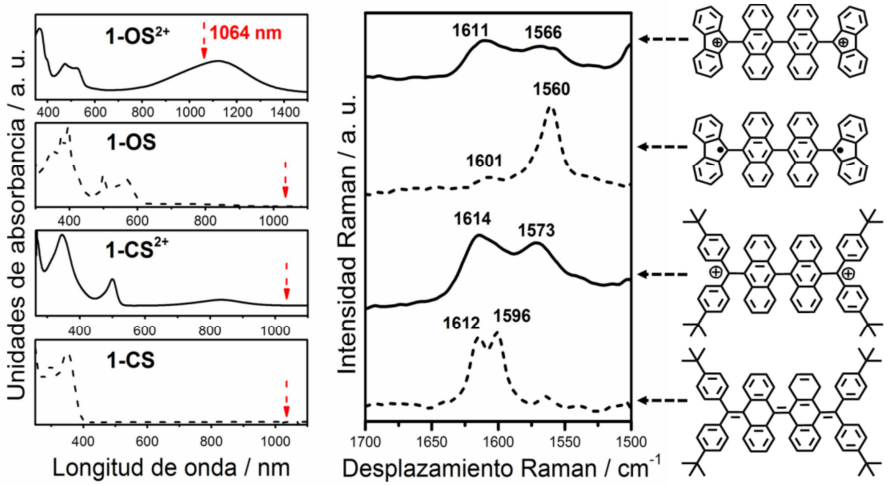

Figura 6.5 Izquierda: espectros de absorción electrónica UV-Vis-NIR registrados en DCM para las especies neutras y doblemente oxidadas de *1-CS* y *2-OS*. **Derecha:** espectros FT-Raman (1064 nm) registrados en disolución de DCM para las mismas especies. Neutros (----) y Dicationes (——).

Si se comparan los espectros de las especies cargadas entre sí, se puede observar como, al contrario de lo que ocurre en las especies neutras, los perfiles espectrales son muy parecidos. Esto sugiere que ambos sistemas comparten geometrías moleculares similares en el estado fundamental en sus especies doblemente oxidadas. La aparición de una señal en torno a 1570 cm^{-1} en ambos casos se puede asignar a una estructura de tipo antracenoide para la unidad central de la molécula, de acuerdo con la formación de los correspondientes carbocationes en las unidades de fluorenilo y de difenilmetileno en *2-OS* y *1-CS,* respectivamente. Además, la comparación de estas bandas con la componente que aparece a 1560 cm^{-1} en la especie neutra *2-OS* y que prácticamente no se detecta en *1-CS*, constituye una evidencia más de la estructura antracenoide del núcleo central de la molécula con fluorenilos descrita como rasgo estructural de la configuración de capa abierta para el mismo.

6.1.2 BIBLIOGRAFÍA

1. Tschitschibabin, A.E., *Ber. Chem.*, 1907. **40**(2): p. 1810-1819.
2. Montgomery, L. K.; Huffman, J. C. ;Jurczak, E. A.; Grendze, M. P., *J. Am. Chem. Soc*, 1986. **108**(19): p. 6004-6011.
3. Porter, W.W.; Vaid, T.P.; Rheingold, A.L., *J. Am. Chem. Soc.*, 2005. **127**(47): p. 16559-16566.
4. Sloan, G.J. and Vaughan, W.R., *J. Org. Chem.*, 1957. **22**(7): p. 750-761.
5. Morozova, D. and Dyatkina, E.M., *Russian Chemical Reviews*, 1968. **37**: p. 377.
6. Ballester, M.; Pascual, I.; Carreras, C.; Vidal-Gancedo, J., *J. Am. Chem. Soc.*, 1994. **116**(10): p. 4205-4210.
7. Sartorius, R. and Brauer, H. D., *Angew. Chem. Int. Ed.*, 1972. **11**(6): p. 531-532.
8. Theilacker, W; Schulz, H.; Baumgarte, U.; Drössler, H. G.; Rohde, W.; Thater, F.; Uffmann, H., *Angew. Chem. Int. Ed.*, 1957. **69**(10): p. 322-333.
9. Berezin, K.V.; Krivokhizhina, T.V.; Nechaev, V. V., *Optics and Spectroscopy*, 2004, **97**(4): p. 530-536.
10. Shinohara, H.; Yamakita, Y.; Ohno, K., *Journal of Molecular Structure*, 1998, **44**: p. 221-234.

7. Derivados de Naftoditiofeno

7. DERIVADOS DE NAFTODITIOFENO

7.1 COMPETENCIA ENTRE ESTRUCTURAS π-CONJUGADAS QUINOIDES Y AROMÁTICAS EN LA σ-DIMERIZACIÓN DE NUEVOS DERIVADOS DE NAFTODITIOFENO. ROL DEL CARÁCTER BIRRADICAL EN LA DOBLE FORMACIÓN DE ENLACES σ INTERMOLECULARES.

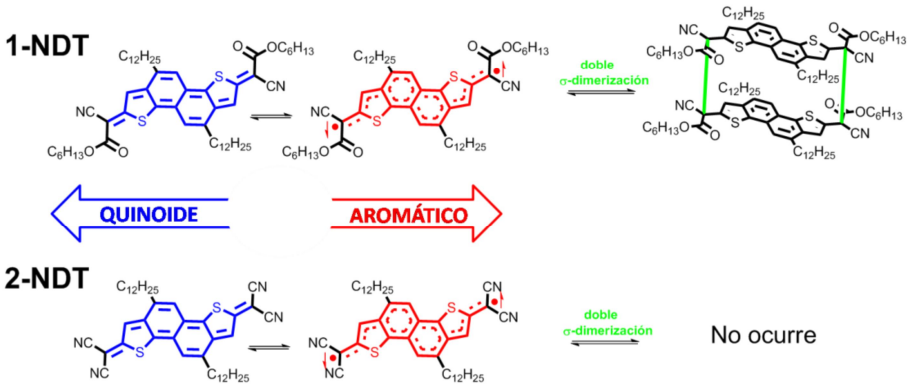

Figura 7.1 Estructuras químicas de las moléculas objeto de estudio, *1-NDT* y *2-NDT*.

En este último apartado se lleva a cabo un estudio espectroscópico de las implicaciones que la expresión del carácter birradical en sistemas pro-aromáticos puede llegar a tener sobre la capacidad de éstos para generar interacciones intermoleculares de largo alcance (o enlaces débiles). En este contexto, se presenta el estudio de dos nuevos derivados de naftoditiofeno, *1-NDT* y *2-NDT*. Ambas moléculas comparten la unidad central *NDT* y constan de grupos electro-aceptores en los extremos del esqueleto fusionado π-conjugado, introducidos con objeto de dotar a éste

de carácter quinoide, o pro-aromático [1,2]. Concretamente, *1-NDT* consta de unidades ciano-acil metileno mientras que *2-NDT* está funcionalizado con grupos diciano metileno en ambos extremos (**Figura 7.1**).

Como se muestra en la **Figura 7.1**, ambos sistemas se pueden representar a través de sus estructuras resonantes de capa cerrada y capa abierta, lo que abre la puerta a la estabilización aromática de especies birradicales singlete. Además, atendiendo a su estructura plana (como en los rilenos), y dado el bajo número de unidades pro-aromáticas que presentan, es de esperar que el carácter birradical de estos sistemas sea pequeño.

7.1.1 RESUMEN DE LOS RESULTADOS OBTENIDOS.

Atendiendo a los espectros de absorción electrónica UV-Vis en disolución de DCM que muestra la **Figura 7.2a,** los diferentes patrones de sustitución en *1-* y *2-NDT* no parecen afectar significativamente al perfil espectral, ya que ambas muestran espectros típicos de estructuras quinoides de la misma longitud de conjugación, de acuerdo con el bajo carácter birradical esperado [1]. Sin embargo, al depositar los sistemas sobre vidrio, el *film* que se genera se vuelve incoloro en el caso de *1-NDT*, siendo capaz de recuperar su color al ser redisuelto, y pudiéndose repetir el proceso un número indefinido de ciclos. Este fenómeno no se da en *2-NDT*, donde se mantiene el color azul en todo momento, tanto en sólido como en disolución (**Figura 7.2b**).

En base a la hipótesis de participación del carácter birradical en el estado fundamental de ambas moléculas, causante del cromismo observado, existen descritos en bibliografía casos de procesos de dimerización en sistemas con electrones desapareados, de tipo monoradical y de birradicales [3-9]. Así, se plantea la posibilidad de un

proceso de doble σ-dimerización intramolecular asistido por una especie birradical (**Figura 1.7b** de la Introducción), que se daría en *1-NDT* pero no en *2-NDT*.

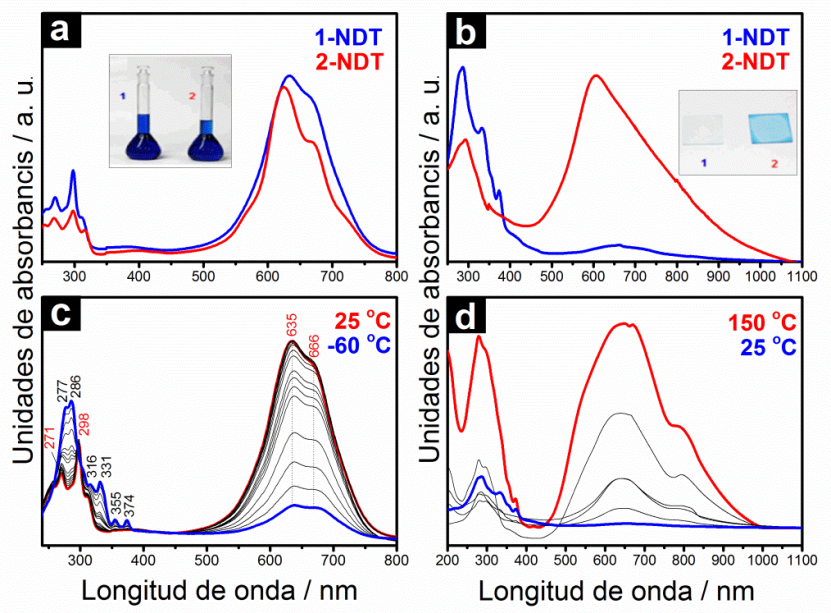

Figura 7.2 a) Espectros de absorción electrónica UV-Vis en disolución de DCM para *1-NDT y 2-NDT*. **b)** Espectros de absorción electrónica UV-Vis en estado sólido para *1-NDT y 2-NDT*. **c)** Espectros de absorción electrónica UV-Vis en disolución de DCM para *1-NDT* en función de la temperatura. **d)** Espectros de absorción electrónica UV-Vis para *1-NDT* en *film* en función de la temperatura.

En la **Figura 7.2c** se muestran los espectros de absorción electrónica UV-Vis en función de la temperatura para *1-NDT* en disolución de DCM. Al enfriar se observa la desaparición de la banda a 635 nm característica del monómero, acompañada de la aparición de una nueva banda con máximos a 286 y 331 nm. El proceso de calentamiento/enfriamiento mantiene la reversibilidad en disolución, y transcurre a través de un claro punto isosbéstico alrededor de 450 nm. Esto permite calcular los parámetros termodinámicos asociados a la interconversión de las bandas con la temperatura [10,11]. Asumiendo un

equilibrio de dimerización y a través de una representación de *Van't Hoff* (**Figura 7.3**), se obtiene un valor de -14.81 Kcal·mol^{-1} para la variación de entalpía estándar del proceso (ΔH^o), a partir del cual, y a través del cálculo de la energía libre de Gibbs, se obtiene un valor de variación de entropía estándar de dimerización (ΔS^o) de -224.20 J·K^{-1}·mol^{-1} a -40 °C.

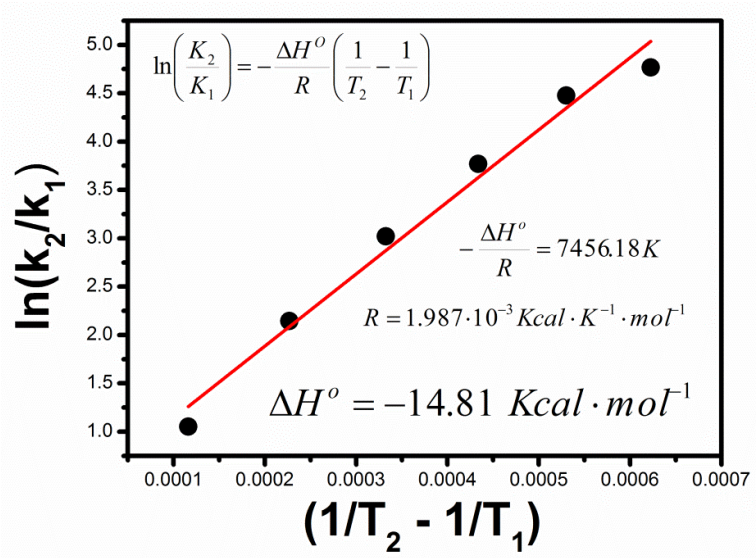

Figura 7.3 Representación de Van't Hoff para el proceso de dimerización de *1-NDT*.

Se realizó una serie de cálculos químico cuánticos a nivel de cálculo (U)M06/6-31G* para distintas disposiciones relativas de *1-NDT* formando dímeros. En todos los casos las estructuras responden a acoplamientos cofaciales que dan lugar a dos tipos de dímeros, π- y σ-, resultando los acoplamientos σ-dobles los más estables en todos los casos y de entre éstos, el que presenta una configuración con los azufres en disposición *syn*-, al que se ha denominado *syn*-σ-dímero. La energía de formación para este dímero es -10.38 Kcal·mol^{-1} y similar a la ΔH^o obtenida experimentalmente.

La **Figura 7.2d** también muestra los espectros de absorción electrónica UV-Vis del compuesto *1-NDT* partiendo del *film* a 25 ^{o}C y aumentando la temperatura hasta 150 ^{o}C. Se observa la progresiva desaparición de las bandas en torno a 250-300 nm atribuidas a la especie dimerizada y la aparición de una banda ancha en torno a 650-700 nm debido a la recuperación de la especie monomérica de *1-NDT*. Este cambio se observa a simple vista a través de la progresiva aparición del color azulado en el *film* al calentar.

En estado sólido, la formación del *film* por evaporación rápida del disolvente da lugar a estructuras que tras analizarse por ICP-MS, han demostrado pertenecer a unidades oligoméricas superiores al dímero, o poliméricas (en disposición tipo escalera), aunque formadas a través de similares enlaces σ. Comoquiera que estos oligómeros han de presentar una disposición de los grupos acilo y ciano fuera del plano del *core* conjugado *NDT*, como veremos a continuación, desde un punto de vista de la estructura electrónica y vibracional, se asemejan al doble σ-dímero en disolución, por lo que sus espectros electrónicos y vibracionales son correlacionables y semejantes como veremos. Es por esto que a continuación se recurre a la espectroscopia vibracional infrarroja y Raman para estudiar los cambios que a nivel de estructura molecular tienen lugar durante el proceso, recurriendo a los correspondientes espectros teóricos del dímero para guiar la asignación e interpretación de los espectros experimentales tanto los de disolución como los obtenidos en estado sólido.

7.1.1.1 Espectroscopia vibracional.

La espectroscopia vibracional en sus variantes Raman e infrarroja aporta información a nivel molecular de las estructuras formadas durante el proceso de dimerización/oligomerización/polimerización. En concreto, la espectroscopia Raman ha sido utilizada para estudiar este tipo de procesos en multitud de casos previamente [12]. Comoquiera que el fenómeno crómico descrito es exclusivo del compuesto *1-NDT*, se realiza también un estudio paralelo y comparativo con el sistema *2-NDT*.

7.1.1.1.1 Espectroscopia vibracional Infrarroja.

En la **Figura 7.4** se muestran los espectros FT-IR en función de la temperatura para el *film* obtenido mediante *spin coating* de una disolución de *1-NDT* en DCM junto con los espectros teóricos obtenidos mediante cálculos DFT a nivel B3LYP/6-31G** sobre las geometrías (U)M06/6-31G* para el monómero, *syn*-σ-dímero más estable y también para el *anti*-π-dímero, que es el siguiente más estable y que se incluye para establecer una comparación más clara. La región que se muestra es aquella en la que aparecen las bandas más intensas en IR. En nuestro caso, éstas serán las asociadas a los modos vibracionales de tensión de los grupos ciano y carbonilo, ν(C≡N) y ν(C=O) respectivamente.

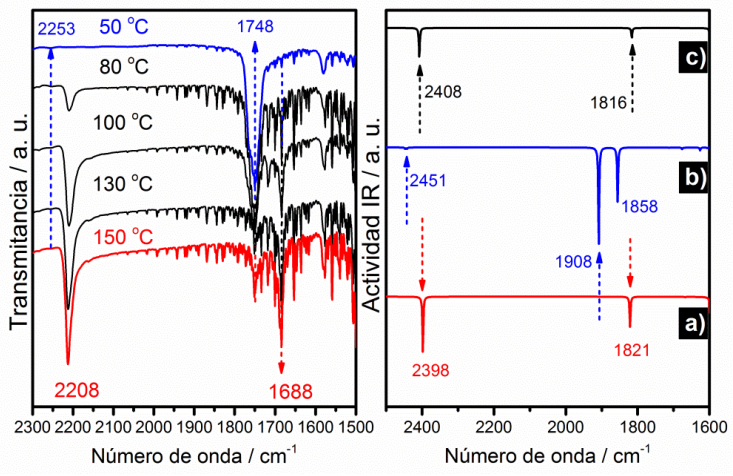

Figura 7.4 **Izquierda:** espectros FT-IR para el *film* de *1-NDT* en función de la temperatura. **Derecha:** espectros teóricos calculados a nivel B3LYP/6-31G** para: **a)** monómero, **b)** *syn*-σ-dímero y **c)** *anti*-π-dímero.

Resulta evidente la correspondencia entre el espectro experimental del *film* a 150 °C y el espectro teórico calculado para el monómero, presentando dos bandas predominantes a 2208 y 1688 cm^{-1} que se asocian a las calculadas a 2398 y 1821 cm^{-1}. Estas señales corresponden a los modos ν(C≡N) y ν(C=O), respectivamente, como ya se ha mencionado. La frecuencia a 2208 cm^{-1} es llamativamente inferior a los valores típicos de estructuras en las que los grupos ciano se encuentran electrónicamente aislados, como el acetonitrilo, en el cual la ν(C≡N) se detecta en torno a 2250 cm^{-1} [13]. Esto permite interpretar la banda a 2208 cm^{-1} como característica de una estructura principalmente quinoide. En ella, los grupos C≡N se encontrarían conjugados con la unidad central *NDT*. El desplazamiento a menor frecuencia observado con respecto a los 2250 cm^{-1} en el acetonitrilo es consecuencia de la polarización intramolecular que se da en el estado fundamental como consecuencia del carácter electro-dador y electro-aceptor del puente conjugado y los grupos ciano, respectivamente. La aparición del modo ν(C=O) a 1688 cm^{-1}, por su parte, se puede relacionar con una situación en la que el grupo

C=O estaría conjugando fuertemente, más allá de en una estructura tipo α-β insaturada que daría una banda típica alrededor de 1700-1720 cm^{-1} (**Figura 7.5b**). Por tanto, el grupo C=O se encontraría en una situación intermedia entre α-β insaturado y aislado **(Figura 7.5c)** [14], lo que está de acuerdo con la posibilidad de que el C=O se encuentre conjugando con un orbital p_z radicalario o con un electrón desapareado (**Figura 7.5a**).

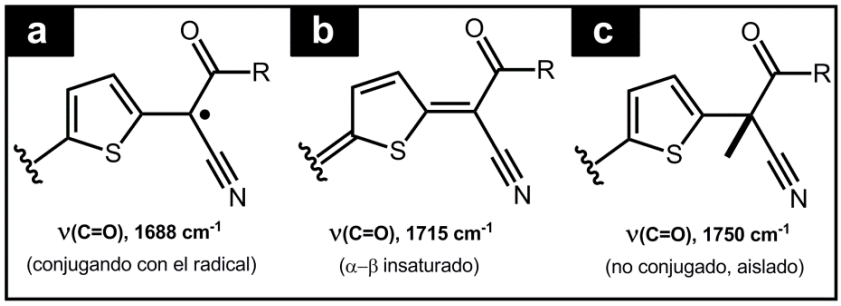

Figura 7.5 Frecuencias típicas del modo ν(C=O) en IR para grupos carbonilo: **a)** En conjugación con un centro radical, **b)** α-β insaturados y **c)** Sin conjugación o electrónicamente aislados.

Por su parte en el espectro infrarrojo del *film* recién formado (incoloro) a 25 °C se observa como la banda ν(C=O) aparece ahora con una elevada intensidad a 1749 cm^{-1}. Esto indica la transición hacia un grupo carbonilo aislado de la conjugación del *core* central (**Figura 7.5c**). Simultáneamente, se observa como la banda de ν(C≡N) a 2208 cm^{-1}, que aparecía como la más intensa en el espectro 150 °C, ahora se detecta con una intensidad muy débil a una frecuencia de 2253 cm^{-1} (como en el acetonitrilo). En la **Figura 7.4** se puede ver cómo este espectro corresponde razonablemente bien con el espectro teórico del *syn*-σ-dímero, que presenta una banda muy débil a 2451 cm^{-1} y otra intensa a 1908 cm^{-1}, a la vista de la similares diferencias de frecuencias observadas, para los valores experimentales y teóricos, 504 cm^{-1} y 543 cm^{-1}, respectivamente. Por tanto, los datos obtenidos sugieren una prácticamente completa desconexión de los grupos ciano y carbonilo de

la unidad central conjugada *NDT* al fomarse el oligómero/polímero. Ésta desactivaría la transferencia de carga intramolecular responsable de la banda intensa de absorción electrónica a 634 nm del monómero y daría lugar a las bandas en torno a 260-300 nm (típicas de compuestos aromáticos de esta naturaleza). La **Figura 7.4** muestra igualmente el espectro teórico del *anti*-π-dímero, con bandas importantes a 2408 cm^{-1} y 1816 cm^{-1}. En ningún caso los espectros experimentales son correlacionables con este espectro teórico.

7.1.1.1.2 ESPECTROSCOPIA VIBRACIONAL RAMAN.

La **Figura 7.6** presenta los espectros Raman para el *film* de *1-NDT* registrados con la línea de 532 nm en distintas condiciones junto con los correspondientes espectros teóricos obtenidos para monómero, *syn*-σ-dímero y *anti*-π-dímero en el intervalo de frecuencias donde aparecen las bandas Raman más intensas, en la región de las vibraciones de tensión C=C/C-C del esqueleto conjugado central. Es decir, la espectroscopia Raman, al asociarse sus señales a la unidad conjugada *NDT* de la molécula, permite complementar la información obtenida mediante espectroscopia FT-IR, que hacía referencia a los cambios estructurales que afectan a los grupos ciano y carbonilo situados en la periferia de la molécula.

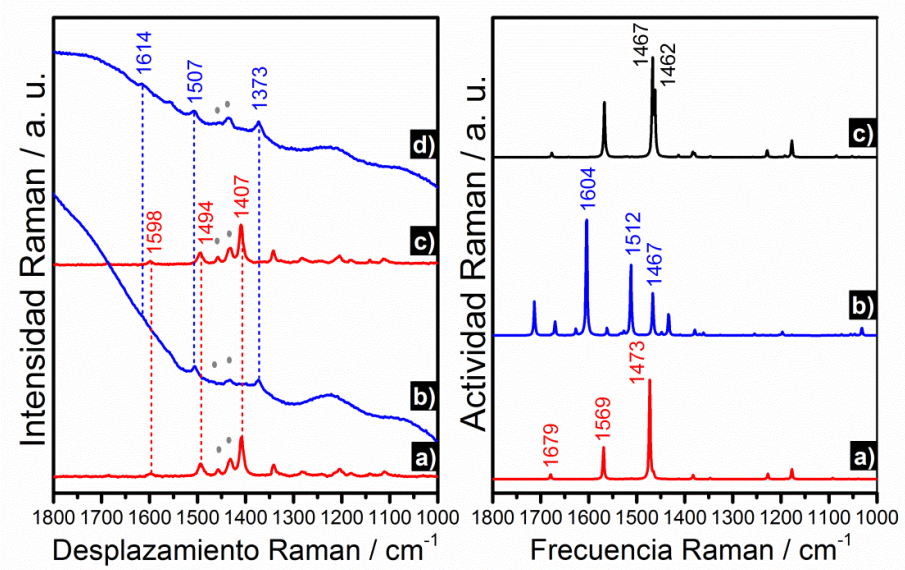

Figure 7.6 Izquierda: espectros registrados para *1-NDT* en estado sólido y con la línea láser de 532 nm para: **a)** *bulk* (sólido azul), **b)** *film* incoloro a temperature ambiente, **c)** después de calentar a 150 ºC el *film* generado en b) y **d)** tras redisolver el *film* formado en c) y volver a generarlo por *spin coating*. **Derecha:** espectros Raman calculados a nivel B3LYP/6-31G** para **a)** monómero, **b)** *syn*-σ-dímero y **c)** *anti*- π-dímero.

Como puede verse, la correlación entre el espectro experimental del *bulk* y el calculado para la unidad monomérica es adecuada. El espectro calculado para el monómero está dominado por dos bandas que aparecen a 1473 y 1569 cm^{-1}, las cuales se asignan a las medidas a 1407 y 1494 cm^{-1} en el espectro experimental. La primera de ellas se corresponde con una vibración de tensión CC principalmente localizada en los tiofenos, la cual es típica de estructuras más o menos quinoides [15]. La banda a 1494 cm^{-1} también proviene de una tensión similar de los anillos de tiofeno pero que se encuentra acoplada con la unidad de naftaleno en un modo de tensión colectivo deslocalizado por toda la molécula. Por su parte, el espectro calculado para el *syn*-σ dímero predice tres bandas a 1604, 1512, 1467 cm^{-1}, que se asignan a las bandas experimentales observadas a 1614, 1507 y 1373 cm^{-1} para el *film* incoloro

a 25 ^{o}C. Esto constituye una nueva evidencia de la formación del oligómero/polímero en el *film* generado por *spin-coating* a 25 ^{o}C. El desplazamiento a mayores frecuencias que se produce, tanto en los espectros experimentales como en los teóricos, al pasar del *bulk* al el *film*, se puede interpretar en términos de la transición de una estructura de tipo quinoide a una de tipo aromático en la unidad central *NDT*. Si se describe brevemente el espectro teórico calculado para el *anti*-π-dímero, éste es tremendamente similar al del monómero, en concordancia con una afectación mínima del esqueleto conjugado tras la formación de este dímero. Por último, y como experimento de control, el mismo procedimiento de generación del film, calentamiento del mismo y re-disolución se llevó a cabo para la molécula *2-NDT* sin encontrar cambios significativos en ninguno de los casos.

Resultados de espectros Raman similares a los obtenidos en estado sólido por espectroscopia Raman para *1-NDT* han sido reproducidos en disolución de DCM y MCH al bajar la temperatura, lo que correlaciona el fenómeno de dimerización observado en disolución al enfriar con la estructura generada en estado sólido (*film*).

Desde el punto de vista de su estructura molecular, los datos espectroscópicos señalan que en la formación del *syn*-σ-dímero se parte de una especie monomérica inicial. Ésta, que presenta una estructura quinoide con cierto carácter birradical, evolucionaría a través de la aromatización de la unidad *NDT,* dando lugar a la conversión de los cuatro centros radicales situados en los carbonos exometilénicos en dos enlaces σ, generando una estructura tipo *syn*-σ-dímero. Así, la formación del σ-dímero se vería favorecida por la estabilización energética del núcleo central al aromatizarse y ésta implicaría la ruptura de la conjugación de la unidad *NDT* con los grupos externos, dando lugar al balance e interconversión de estructuras observado.

La detección del proceso de dimerización/polimerización en función de estímulos relativamente suaves que se ha venido describiendo a lo largo del presente apartado da pie a pensar en la posibilidad de inducir este fenómeno mecánicamente. Para esto se lleva a cabo el estudio del espectro Raman en función de la presión aplicada a *1* y *2-NDT* en el *bulk*. Como se puede ver en la **Figura 7.6**, el incremento progresivo de la presión sobre *1-NDT* da lugar a un espectro que, a 6 GPa, se caracteriza por la presencia de una banda ancha en torno a 1627 cm^{-1} y un doblete a 1512 y 1528 cm^{-1}, junto con otra banda a 1470 cm^{-1} y una última a 1434 cm^{-1}.

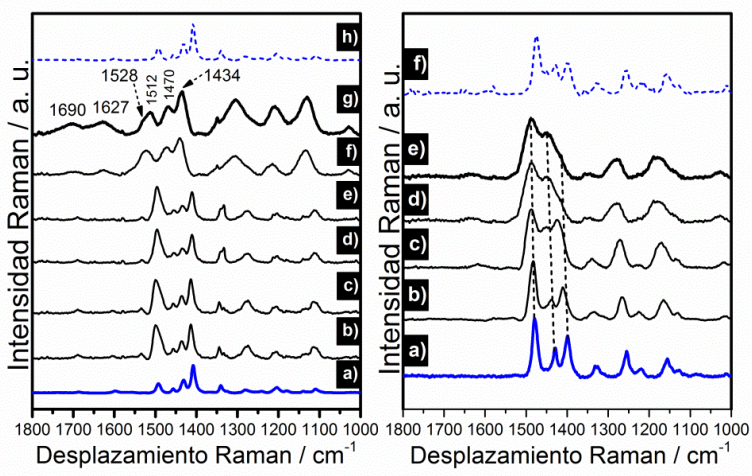

Figura 7.6. Izquierda: espectros Raman de *1-NDT* registrados en el *bulk* con la línea láser de 532 nm: **a)** sin aplicar presión (línea azul sólida), **b)** P1, **c)** P2, **d)** P3, **e)** P4, **f)** P5, **g)** P6 y **h)** espectro recuperado. **Derecha:** espectros Raman de *2-NDT* registrados en el *bulk* con la línea láser de 532 nm: **a)** sin aplicar presión (línea azul sólida), **b)** P1, **c)** P2, **d)** P3, **e)** P4 y **f)** espectro recuperado.

De estas señales, las bandas medidas a 1627, 1528 y 1434 cm^{-1} podrían corresponder a aquellas a 1614, 1513 y 1373 cm^{-1} características del dímero u oligómero, pero desplazadas a mayores frecuencias por un mero efecto de presión. Las señales que aparecen a 1512 y 1470 cm^{-1}

también podrían estar relacionadas con las bandas del monómero que persiste, de nuevo desplazadas a mayor frecuencia como consecuencia del aumento del estrés mecánico. En el caso de *2-NDT*, el efecto de la presión sobre el espectro es significativamente distinto, mostrando éste un ensanchamiento y desplazamiento a mayor frecuencia de las bandas pero manteniendo una buena correspondencia con el perfil espectral registrado sin presión. En ambos casos, al retirar el efecto de la presión se recuperan los perfiles espectrales característicos de *1* y *2-NDT* en el *bulk*.

La evolución de los espectros en *2-NDT* indica la ausencia de procesos químicos apreciables inducidos por presión, sin embargo, éstos llegan a ser muy significativos en el caso de *1-NDT*, como puede extraerse de la similitud entre el espectro a 6 GPa y el del *syn*-σ-dímero.

La combinación de espectroscopias vibracionales Raman e Infrarroja ha permitido caracterizar, en diferentes condiciones y bajo distintos estímulos, las estructuras moleculares del dímero formado por el acoplamiento intramolecular de cuatro electrones desapareados existentes inicialmente como dos birradicales singlete en *1-NDT* para el proceso en disolución, y para el oligómero/polímero que se genera en estado sólido. La información aportada por los espectros infrarrojos da cuenta de la desconexión de la conjugación entre los grupos aceptores y el puente molecular *NDT* que acompaña a la formación del doble σ-dímero. Así, se puede describir el proceso en términos de rehibridación de los carbonos donde se localiza la mayor densidad de espín en los birradicales originales, los cuales pasarían de sp^2 a sp^3 al formarse los nuevos enlaces. Esta densidad de espín, pasaría a desaparecer tras la formación de los enlaces intermoleculares, dando cuenta de una estructura de tipo capa cerrada para la especie dimerizada u oligómero. La espectroscopia Raman, por su parte, aporta información complementaria sobre la estructura de la unidad central *NDT*, que pasaría de quinoide con un débil carácter birradical a aromática y capa cerrada tras la formación de la entidad supramolecular.

El balance energético entre estructuras quinoides (conjugadas) y aromáticas es el responsable de desplazar el equilibrio del proceso hacia la formación del σ-dímero en *1-NDT* y hacia el monómero en *2-NDT*. En éste último, la conjugación entre los grupos diciano y la unidad *NDT* es mayor que la de los grupos ciano-acilo en *1-NDT*, lo que explica la estabilización preferencial del monómero. Esto pone de manifiesto la importancia que el grado de carácter birradical de los monómeros tiene sobre la evolución del proceso de dimerización/oligomerización. En *1-NDT*, el menor poder electro-aceptor de las unidades ciano-acilo con respecto a los grupos tetraciano de *2-NDT* implicaría una mayor disponibilidad de los radicales del birradical para formar los débiles enlaces intermoleculares que dan lugar al σ-dímero.

La caracterización de este fenómeno de doble σ-dimerización asistida por especies birradicales, cuyo origen se halla en el balance entre configuraciones quinoides y aromáticas de un mismo sistema, es especialmente interesante si se tiene en cuenta la reversibilidad y la magnitud de la variación de color resultante. La conjunción de estas dos características en un mismo sistema es algo bastante inusual, dado que cambios tan acusados en la respuesta a un determinado estímulo externo suelen venir acompañados de modificaciones profundas e irreversibles de la estructura química del sistema en cuestión. Es por esto que la interconversión reversible de las estructuras quinoide y aromática de *1-NDT* hace de este sistema una prometedora plataforma molecular de cara al desarrollo de nuevos materiales multifuncionales orgánicos.

7.1.2 BIBLIOGRAFÍA

1. Suzuki, Y.; Miyazaki, E.; Takimiya, K., *J. Am. Chem. Soc.*, 2010. **132**(30): p. 10453-10466.
2. Li, J.; Qiao, X.; Xiong, Y.; Li, H.; Zhu, D., *Chem. Mater.*, 2014. **26**(19): p. 5782-5788.
3. Kikuchi, A.; Iwahori, F.; Abe, J., *J. Am. Chem. Soc.*, 2004. **126**(21): p. 6526-6527.
4. Shimizu, A.; Hirao, Y.; Matsumoto, K.; Kurata, H.; Kubo, T.; Uruichi, M.; Yakushi, K., *Chem. Comm.*, 2012. **48**(45): p. 5629-5631.
5. Cui, Z.-H.; Lischka, H. Beneberu, H. Z.; Kertesz, M., *J. Am. Chem. Soc.*, 2014. **136**(15): p. 5539-5542.
6. Nakasuji, K.; Yoshida, K.: Murata, I., *J. Am. Chem. Soc.*, 1982. **104**(5): p. 1432-1433.
7. Morita, Y.; Suzuki, S.; Sato, K.; Takui, T., *Nat Chem*, 2011. **3**(3): p. 197-204.
8. Kolb, B.; Kertesz, M.; Thonhauser, T., *J. Phys. Chem. A*, 2013. **117**(17): p. 3642-3649.
9. Liao, P.; Itkis, M. E.; Oakley, R. T.;Tham, F. S.; Haddon, R. C., et al., *J. Am. Chem. Soc.*, 2004. **126**(43): p. 14297-14302.
10. Zaitsev, V.; Rosokha, S. V.; Head-Gordon, M.; Kochi, J. K., *J. Org. Chem.*, 2005. **71**(2): p. 520-526.
11. Lambert, C., *Angew. Chem. Int. Ed.*, 2011. **50**(8): p. 1756-1758.
12. Casado, J.; Takimiya, K.; Otsubo, T.; Ramírez, F. J.; Quirante, J. J.; Ponce Ortiz, R. P.; González, S. R.; Moreno Oliva, M.; López Navarrete, J. T., *J. Am. Chem. Soc.*, 2008. **130**(43): p. 14028-14029.
13. Givan, A. and Loewenschuss, A., *Journal of Molecular Structure*, 1983. **98**(3–4): p. 231-238.
14. Dillon, R.T. and Dickinson, R.G., *PNAS*, 1929, **15**(9): p. 699-702.
15. Ponce Ortiz,R.; Casado, J.; Rodríguez González, S.; Hernández, V.; López Navarrete, J. T.; Viruela, P. M.; Ortí, E.; Takimiya, K.; Otsubo, T., *Chem. Eur. J.*, 2010, **16**(2): p. 470-484.

8. Summary and Conclusions

8. SUMMARY AND CONCLUSIONS

The present Ph.D. Thesis is divided in the following sections: introduction, aim of the research, main results and discussions of each chapter or family of compounds and general conclusions.

8.1 INTRODUCTION.

Atomic or molecular systems in which the electrons are not completely assigned to orbitals in pairs are known as open-shell systems. For molecules, it signifies that there are unpaired electrons and, in terms of Molecular Orbital Theory, this leads to molecular orbitals that are singly occupied, in contrast to closed-shell configurations which are characterized by having the molecular orbitals doubly occupied or empty [1].

Since the end of the last century, the development of the chemistry of open-shell molecules has increased significantly, focused mainly in the achievement of longer lifetimes for these species [2-4]. One of the most interesting properties of these kind of systems is the intrinsic biradical character, responsible for the unconventional electronic, optical and magnetic properties that make them potential candidates for applications in the field of organic electronics, mainly related to Non-Linear Optics, Organic Photovoltaics or Spintronics [2, 5, 6]. However, the biradical character is, at the same time, a big drawback for these systems, due to the high reactivity straightforward related with the presence of unpaired electrons [7-10].

In the context of the present Ph.D. Thesis we will use the term biradical for every system bearing two unpaired electrons. In particular,

we will focus the study on a class of organic biradicals known as *Kekulé* biradicals. These are systems that can be depicted by closed-shell and open-shell resonant structures.

The very first examples of *Kekulé* biradicals were those synthesized by *Thiele* in 1904 [4] and *Tschitschibabin* in 1907 [3]. The Chichibabin molecule has attracted broad attention since then, due to the unconventional electronic configuration expected for its ground electronic state. Nevertheless, the high reactivity of this derivative has made elusive the determination of its ground electronic state spin multiplicity [11] and many attempts have been made to synthesize new derivatives that could help to clarify the electronic configuration of the Chichibabin biradical [12].

Determination of the spin state in *Kekulé* biradicals is an interesting topic nowadays due to the fact that most of them, in contrast with the expectation of Hund's Rule, have been theoretically predicted and experimentally confirmed, to display open-shell singlet ground electronic states [9, 13]. This behavior can be explained in terms of the spatial distribution of the non bonding molecular orbitals where the two unpaired electrons are located [8, 14, 15]: If there is no overlapping between them and the dipole-dipole coulombic interaction is small, then, the mechanism of Double Spin Polarization can occur [8, 9, 16, 17], which will lead to the stabilization of the open-shell singlet over the triplet biradical.

The unconventional energy distribution of the ground state and low-lying excited states of open-shell singlet biradicals could make them promising candidates for applications related to singlet exciton fission, two photon absorption and magnetic switching [18-22].

A common feature in several *Kekulé* biradicals with open-shell singlet ground electronic states is the presence of the p-quinodimethane (*p-QDM*) unit as a fundamental building block [5, 6, 23]. The *p-QDM* unit is a *Kekulé* biradical itself, and it can be depicted by quinoidal closed-shell and

biradical open-shell resonant structures. The stabilization of the biradical structure is achieved as a consecuence of the gain of an aromatic ring in the open-shell resonant structure. As a result, the stability of open shell singlet biradicals based on *p-QDM* can be connected to its pro-aromaticity.

8.2 AIM OF THE RESEARCH.

We have studied four families (six subfamilies) of molecules with the aim of characterizing their ground states. Basically, we tried to elucidate the electronic configuration of the ground electronic states, in terms of closed-shell or open-shell character, and also the spin multiplicity of the latter. At the same time, we have established connections between this information and the different structural motifs introduced in each of the families, in order to obtain relationships between the molecular structure and the stabilization of open-shell species with biradical character that can lead synthetic chemists to tune the chemical design of new organic biradicals with potential applications in organic electronics. To this end, the experimental technique that will be mainly used is Raman spectroscopy [24-29], which is well know as a unique tool for characterization of π-conjugated molecules in general [12, 30]. This Ph.D. Thesis is one of the few studies of the application of Raman spectroscopy to the study of π-conjugates biradicals.

The families studied can be classified as follows:

- ✓ Bis(dicyanomethylene)-substituted Perylene derivatives *nPer-CN* (*n=1-6*), bis(dicyanomethylene)-substituted Rylenes (*QR-CN*, *HR-CN*) and bis(dicyanomethylene)-substituted Rylene thiophenes ($RyTh_2$-CN, Ry_2Th_2-CN).

With this set of molecules, we will study the effect that the increase of the number of perylene units, the rigidification of the conjugated backbone, and the insertion of thiophene units at both ends of the conjugated framework have on the stabilization of open-shell species and on the ground electronic state spin multiplicity.

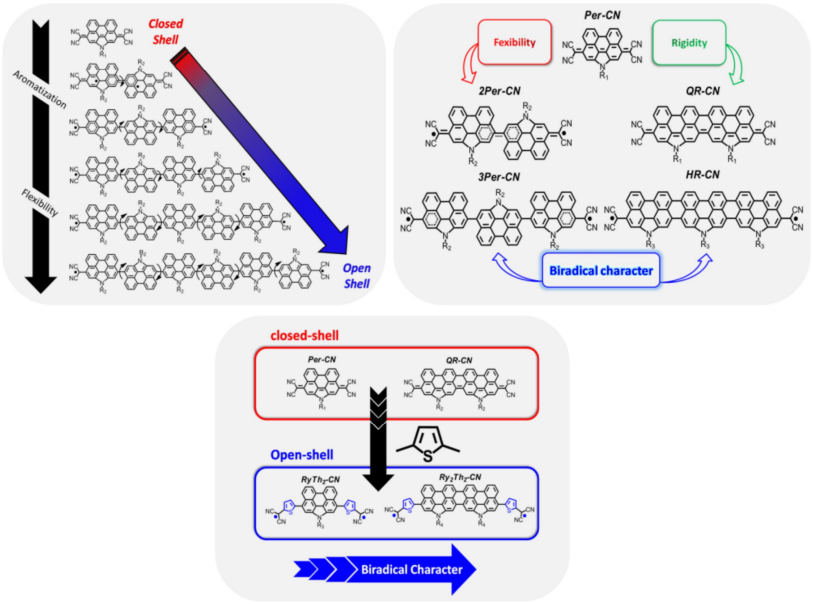

Figure 8.1 Families of molecules studied in sections 4.1 (top-left), 4.2 (top-right) and 4.3 (bottom).

✓ Zethrene derivatives, *HZ-TIPS*, *OZ-TIPS* and *HZ-DI*.

In this chapter, three new large zethrene derivatives are characterized in terms of the influence that the increase in the length of the conjugated bridge between phenalyls and the insertion of electron withdrawal diimide groups at both ends of the molecules have on the generation and stabilization of neutral open-shell systems and charged species.

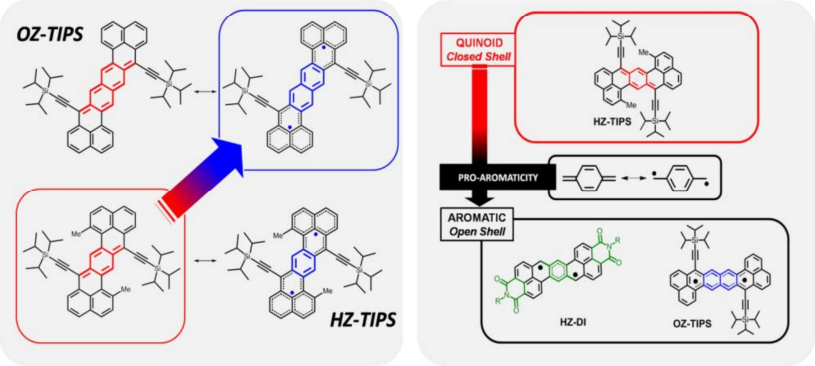

Figure 8.2 Families of molecules studied in sections 5.1 (left) and 5.2 (right).

✓ Tetrabenzo-chichibabin derivatives, *1-CS* and *2-OS*.

This couple of molecules allows us to study how the inclusion of spin-delocalizing fluorenyl units at both ends of the central unit can affect the stabilization of neutral open-shell and charged species. At the same, we can address the implications that structural flexibility can have on the preference for high or low spin multiplicities in the ground electronic state.

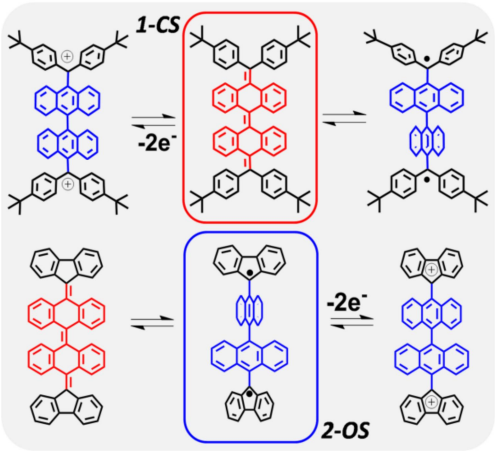

Figure 8.3 Family of molecules studied in chapter 6.

✓ Bis(dicyanomethylene) and bis(cyanoacylmethylene) naphtodithiophene derivatives, *1-NDT* and *2-NDT*.

In this last section, the objective is to analyze the influence that the potential biradical character of these naphtodithiophene derivatives has on the formation of σ weak intermolecular bonds, and the spectroscopic characterization of the evolution of the electronic and molecular structure on the monomer display upon formation of the supramolecular dimer.

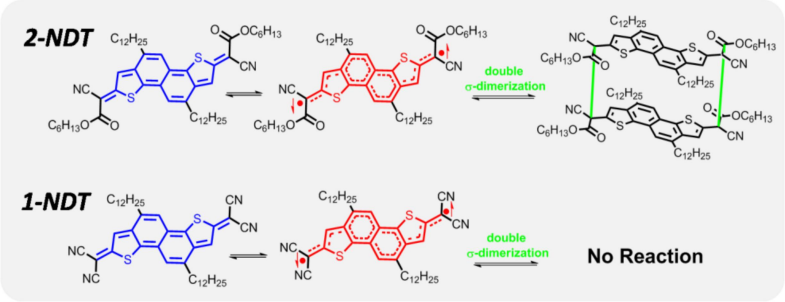

Figure 8.4 Family of molecules studied in chapter 7.

As a transversal aim of this Thesis, we will try to rationalize the experimental evidences in terms of a Double Spin Polarization or Dynamic Polarization Mechanism. Thus, we will be able to understand the effect that the different structural modifications introduced have on the ground electronic states of these interesting biradicaloid molecular systems.

8.3 Results and Discussions.

8.3.1 Influence of increasing the chain length on the generation and stabilization of high and low spin biradicals on bis(dicyanomethylene)-substituted perylene derivatives.

Here we first study a serie of *nPer-CN* derivatives from the monomer to the hexamer. These are interesting molecules because studies of the stabilization of birradical species with different spin multiplicity have been usually limited to shorter systems, and in this family, the longer molecule presents twelve *p-QDM* units.

The main results obtained can be summarized as follow:

1. In terms of ground state electronic configuration, the monomer *1-Per-CN* is characterized by a quinoidal conjugated backbone consistent with a closed-shell ground state. Interestingly, by adding a new perylene unit, the dimer, in line with magnetic measurements, displays a biradical character which is progressively increased in the longer oligomers. These results lead to consider that the systems *2-6Per-CN* could be characterized as open-shell birradical species. Moreover, ESR measurements as a function of temperature give evidences of a transition from diamagnetic ground electronic state (singlet biradical) species in *2-4Per-CN* to a paramagnetic one (triplet biradical) in *5,6Per-CN*.

2. In line with the results outlined above and by means of Raman spectroscopy, we were able to assign the three main Raman signals pf 1*Per-CN* around 1600 cm^{-1} to stretching C=C characteristic of a quinoidal closed-shell structure. The downshift of these bands in *2Per-CN*, is indicative of a weaker quinoidal structure due to the partial recovery of aromaticity on the perylene units. Moreover, the detection of the new interperylene band at 1378 cm^{-1} in 2*Per-CN* indicates that the two units are connected by a bond with a marked single character. These two findings are consistent with the generation of an open-shell birradical on going from the monomer to the dimer. This aromatic stability is further evidenced in *3Per-CN*, where the three aforementioned bands are again downshifted. If we analize the evolution of the Raman bands associated with the normal mode of the interperylene C-C bonds, we observe that this is the one that displais a more pronounced downshift. We adscribe this shift to the weakening of the bond provoked by the structural flexibility. Thus, the aromatic stabilization would weak the interpeylene C-C bond and this weakening together with the steric hindrance between the anthracene units would explain the downshift of 35 cm^{-1} of the interperylene C-C normal mode. The relevant bands are, again, slightly downshifted in *4Per-CN* with respect to *3Per-CN* and are almost unaltered in *5* and *6 Per-CN*, something that could be due to the saturation of conjugation.

3. For molecules *2-6Per-CN* two different behaviors can be identified in terms of evolution of the conjugation. In the shorter oligomers the conjugation length progressively decreases with the extension of the chain length, due to the aromatic stabilization of the open-shell species and also to the increased structural flexibility. This conformational flexibility would be rather significant in *4Per-CN*

and thus, the conjugation is confined. This molecular information is very useful for the interpretation of the evolution of the spin states as a function of the chain length in terms of a Double Spin Polarization Mechanism (*DSP*). In the shorter oligomers, the evolution of the conjugation (and Raman frequencies) is due to the *DSP* mechanism, which leads to a violation of Hund's Rule and to the stabilization of open-shell singlets over triplet biradicals. On the contrary, for the longer oligomers, *5,6Per-CN*, a high spin configuration of the ground state is preferred, because flexibility is already relaxed and deactivates DSP.

8.3.2 Effect of the structural rigidity on the generation of open-shell biradicals in bis(dicyanomethylene)-substituted Rylene derivatives (QR-CN and HR-CN).

Here we perform a comparative Raman study on "flexible" *2-3Per-CN* derivatives and their corresponding rigidified parents *QR-CN* and *HR-CN*.

The main results can be summarized as follow:

1. For the same length of the central core, magnetic measurements indicate that the dimers, *2Per-CN* and *QR-CN* display different electronic ground states, being the latter characterized as a closed-shell quinoidal structure. The same measurements show that both trimers, *3Per-CN* and *HR-CN*, would share the same open-shell singlet electronic configuration for the ground state.

2. Resonant Raman spectroscopy results very helpful to understand how the rigidification of the structure affects to the relative

stability of open-shell species. If we follow the evolution of the three characteristic bands of *1Per-CN*, in the case of *QR-CN* they split and downshift, which may be related with a relaxation of the *C=C/C-C* pattern as a consecuence of the increased number of π electrons, and also with the recovery of aromaticity. In the case of *HR-CN*, from the spectra we can observe a weakening of the interperylene bonds with respect to *QR-CN*, in line with a larger biradical character. Comparing the frecuencies of the Raman bands associated with the interperylene C-C normal modes we can establish the following classification in terms of open-shell character of the ground state: *QR-CN* < *2Per-CN*, *HR-CN* < *3Per-CN*, with *HR-CN* ≤ *2Per-CN.*

3. It can be concluded that the planarity of the fused systems improves the conjugation, leading to a more efficient *DSP* mechanism which would imply the destabilization of the triplet over the open-shell singlet with respect to flexible *nPer-CN* systems. In other words, the rigidity of the system would decrease the biradical character. In the case of the longer molecules, the *DSP* mechanism would explain the smaller biradical character of *HR-CN* compaired to *3Per-CN*.

8.3.3 STUDY OF THE BIRADICAL STATE ACTIVATION IN 1PER-CN AND QR-CN BY THE INCORPORATION OF THIOPHENE RINGS IN THE CONJUGATED BACKBONE.

In connection with the results obtained in sections 4.3.1 and 4.3.2, we now work on different structural modifications to activate the biradical character in the shorter systems *1Per-CN* and *QR-CN*. To this end, we studied the *RyTh$_2$-CN* and *Ry$_2$Th$_2$-CN* parent molecules, which are

characterized by the insertion of thiophene rings in between the conjugated core and the dicyanomethylene units.

The main results of this research can be summarized as follow:

1. The magnetic measurements reveal a singlet open-shell configuration for both *RyTh$_2$-CN* and *Ry$_2$Th$_2$-CN* but with a different biradical character.

2. To obtain valuable information at the molecular level, Raman spectroscopy working in on/off resonant conditions, and Raman thermospectroscopy can be used to detect the low-lyng birradical singlet and the triplet excited state. Careful inspection of the resonant Raman spectra the downshift of a Raman band associated with the CC stretching of the bond connecting the dicyano groups and the thiophene rings on *RyTh$_2$-CN* regarding *1Per-CN*, and also a new band appears that correspond with a C=C stretching of pseudoaromatic thiophene rings, in line with an aromatic stabilization of the thiophene rings.

3. Based on the particular structure, one could expect some steric hindrance between the thiophene rings and the fused cores, thus, it makes sense to campare *RyTh$_2$-CN* with the fused *QR-CN* derivative. They both have four pro-aromatic rings but different electronic configuration of the ground state. This comparison leads us to consider that the stabilization of the open-shell configuration in *RyTh$_2$-CN* is fueled by the rotation of thiophene and perylene units. This rotation is confirmed by the comparison of the 785 nm Raman spectrum of *RyTh$_2$-CN* on both solid state and solution.

4. We take advantage also of the possibility to obtain Raman spectra as a function of temperature to probe the existence of a low-lying triplet excited state in *Ry_2Th_2-CN* by comparison of its solid state FT-Raman spectra at 25 ^{o}C and at -170 ^{o}C. This was unsuccessful since the similar energy of the both states.

5. In the context of the distribution of energetic levels we can assume that the aromatization of the thiophene rings in the open-shell resonant structure is the driving force for the estabilization of the biradical, whose spin multiplicity is determined by an efficient DSP mechanism in both cases. However, the biradical character extension is mainly due to the structural flexibility of the thiophene rings, which decrease the singlet-triplet gap, leading to high and low spin states close in energy.

8.3.4 DETERMINATION OF THE GROUND ELECTRONIC STATE CONFIGURATION IN ZETHRENE DERIVATIVES: CLOSED OR OPEN SHELL MOLECULAR SYSTEMS?

Also known as dibenzoacenes, zethrenes derivatives are a Z-shaped class of *PAHs* that, unsubstituted, have been theoretically predicted to display a significant biradical character, even for the shorter members. Therefore, the synthesis of longer oligomers is difficult and not many derivatives with open-shell nature have been successfully obtained. Here we addressed the study of three new zethrene derivatives, heptazethrene and octazethrene, whose intrinsic instability is avoided by kinetic blocking of the reactive sites with bulky TIPS groups, and heptazethrene with diimide groups.

The most relevant results can be summarized as follows:

1. Magnetic measurements indicate that the nature of the ground electronic state of the shorter oligomer is characterized by a closed-shell quinoidal structure. For the *OZ-TIPS*, however, the evolution of the ESR and NMR as a function of temperature, and SQUID data revealed a singlet open-shell character.

2. The study of the FT-Raman spectrum of *HZ-TIPS* and *OZ-TIPS* in the region of 1600 cm^{-1} is very informative in terms of the interconversion between benzoquinoidal and benzoaromatic structures as a function of the chain length. Thus, in this region, we assign the main band of the *HZ-TIPS* spectrum at 1592 cm^{-1} to a closed-shell quinoidal structure of the central benzene, and that at 1602 cm^{-1} for the *OZ-TIPS*, to a more benzenoid character of the central naphthalene, in line with an open-shell ground state for the latter, due to aromatic stabilization. Thermospectroscopic Raman analysis was carried out for the two molecules, and the behavior was completely different: the spectrum of *HZ-TIPS* remained almost unaltered due to the robustness of the closed-shell configuration but, in the case of the *OZ-TIPS*, there is an intensity inversion of the main band at 1602 cm^{-1} and the weak one at 1595 cm^{-1}, becoming the latter the most intense at high temperatures. This result can be interpreted in terms of a thermally induced interconversion of low into high spin states, being the singlet open-shell the ground electronic state.

3. In the case of *HZ-TIPS* one could expect the aromatic stabilization of the open-shell specie but this does not happen because the gain of aromaticity is not enough to compensate the breaking of a double bond. However, in the case of the *OZ-TIPS*, the biradical resonant form shows two aromatic rings whose stabilization is

strong enough to compensate the aforementioned double bond breaking. In the case of *HZ-DI*, the diimide acceptor units decrease the BLA with respect to the *HZ-TIPS*, making easier the breaking of a double bond and stabilizing the open-shell specie. This trend is well reproduced by the corresponding FT-Raman spectra of the three derivatives in the 1600 cm^{-1} region, displaying a more quinoidal structure for the central benzene in *HZ-TIPS,* a pseudo-aromatic structure in *HZ-DI* for the same unit, and a more aromatic naphthalene unit in *OZ-TIPS*. Once the open-shell biradicals are formed in *OZ-TIPS* and *HZ-DI*, the planar and conjugated bridge allows the efficient Double Spin Polarization mechanism responsible for the stabilization of the low spin ground state. For OZ-TIPS, the $\Delta E_{S\text{-}T}$ is suitable to observe thermally induced intersystem crossing between the singlet and the triplet. The unconventional location of singlet and triplet Raman bands in terms of frequency for OZ-TIPS can be explained by the possibility of the singlet to delocalize over the phenalenyl units in a greater extent than the triplet.

8.3.5 EXPRESION OF THE PRO-AROMATICITY IN THE GROUND STATE OF ZETHRENE DERIVATIVES. INFLUENCE ON THE STABILITY OF CHARGED SPECIES.

In this section we study the influence of the pro-aromatic character of the central *p-QDM* unit on the electronic and molecular structure of the three zethrene derivatives in their charged states. This set of molecules is interesting because it allows us to get deep insights on the relationship between the pro-aromaticity concept and the stabilization of the charged species of *kekulé* biradicals.

The main results can be summarized as follow:

1. The characterization of the different redox processes was carried out by means of UV-Vis-NIR absorption spectroscopy and resonant Raman spectroscopy. For *HZ-TIPS* the electronic spectra of the cationic and anionic have similar pattern of bands in the Uv-Vis-NIR. Due to its pro-aromaticity the central *p-QDM* unit would tend to further aromatize in order to accommodate the charge excess, either positive or negative. In the case of the open-shell derivatives the scenario is different: only the dianionic species were obtained electrochemically. For *OZ-TIPS* the driving force for the stabilization of the dianion can be adscribed to the further aromatization of the central naphthalene unit, already pseudoaromatic in the neutral biradical form. Finally, for *HZ-DI*, the dianion is stabilized by means of two different effects: the complete aromatization of the central benzene unit and the electron-withdrawing effect of the diimide units. These experimental findings are in accordance with theoretical calculations.

2. The molecular structures of the three cationic species, chemically obtained, were conveniently characterized by means of resonant Raman spectroscopy. The most remarkable feature is the upshift of the relevant CC stetching modes of the central bencenoid units with respect to the neutral species, a clear evidence of further aromatization of the central rings with oxidation/reduction. It is quite interesting that, for *HZ-DI*, the confinement of the charge defect at the center of the molecule is larger than in the case of *HZ-TIPS*, in line with a larger aromatization for the diimide derivative, while the aromatization of the naphthalene unit in the *OZ-TIPS* cation explains the appearance of the Raman band at the highest frequency of the three.

3. We can conclude that pro-aromaticity, or tendency to aromatization of the quinoidal bridge, favours the stabilization of *Kekulé* neutral biradicals and its corresponding charged species. Furthermore, for the same number of benzenoid units, the electron-withdrawing effect of the diimide groups is able to change the ground state electronic configuration from a closed-shell structure in *HZ-TIPS* to an open-shell one in *HZ-DI*. In the latter, as we described for OZ-TIPS, the effective DSP mechanism stabilizes the singlet biradical over the triplet.

8.3.6 Stabilization of neutral open-shell states and oxidized species in new tetrabenzo-chichibabin derivatives. Raman characterization of the ground state.

As stated in the introduction, the high instability of Chichibabin's biradical leads to difficulties for characterizing its ground electronic state. In this section, we studied two tetrabenzo-chichibabin derivatives that can be depicted by closed-shell and biradical resonant structures *1-CS/1-OS* and *2-CS/2-OS*, and whose high stability emerges from the application of thermodynamic and kinetic concepts. Both systems differ by the groups attached to the ends of the biphenyl core. While molecule *1-CS* is characterized by having four outermost phenyl rings with tert-butyl groups kinetically blocking the *para*- positions, molecule *2-OS* has fluorenyl units attached to the exomethylene groups, which are well known spin-delocalizing units. This set of molecules gives us the opportunity to understand, at the molecular level, the origin of the preference for a closed-shell structure in *1-CS* and for an open-shell triplet biradical in the case of *2-OS*.

The most relevant results of this research are the following:

1. For molecule *1-CS*, TV-H^1-NMR studies reveal a closed-shell quinoid structure. X-Ray diffraction data are in line with these results, disclosing a quinoidal central unit and a highly distorted butterfly-like structure for *1-CS*, whose structural distorsion could arise from the steric hindrance between anthracene units. Derivative *2-OS* is characterized by magnetic measurements as an open-shell structure, revealing a large population of paramagnetic species in the ground state, and pointing out towards a triplet ground state.

2. Careful analysis of the FT-Raman spectra focused on the band placed at the central biphenyl unit confirms the quinoidal pattern in *1-CS*. However, the spectrum of *2-OS* is better assigned to an antracenoid structure, resulting from the stabilization of the open-shell species. This transition between open and closed-shell structures would be connected to the possibility of the radical centers to delocalize over the planar cyclopentadienyl motif in the fluorenyl unit.

3. For *2-OS*, the small SQUID value of $\Delta E_{S\text{-}T}$ is in accordance with the invariance of the FT-Raman spectrum as a function of temperature. This result is another evidence of the thermal robustness of the triplet biradical ground state of *2-OS* but is also in accordance with the small $\Delta E_{S\text{-}T}$ since the quasi-degeneracy of energy levels of both singlet and triplet biradical states hampers the Raman detection of a net flux of population between the states.

4. The dicationic species for both samples were characterized by UV-Vis-NIR absorption spectroscopy and we took advantage of the NIR

bands to record the resonant Raman spectrum of both dications. A direct comparison of the oxidized species reveals similar geometries characterized by an antracenoid structure as a result of the formation of the corresponding carbocations on the fluorenyl and diphenylmethylene units. This is in clear contrast with the neutral species of *1-CS*.

5. In terms of molecular structure and *DSP* mechanism, the high spin preference of *2-OS* is related to the steric hindrance between anthracene units, whose orthogonal relative disposition breaks the conjugation, eliminating the connection between radical centers. This structural feature denies any chance of *DSP* to take place and, as a consequence, the triplet biradical is the most favourable electronic configuration.

8.3.7 AROMATIC-TO-QUINOIDAL Π-CONJUGATED STRUCTURES INTERPLAY ON THE σ-DIMERIZATION OF NEW NAPHTODITHIOPHENE DERIVATIVES. ROLE OF THE BIRADICAL CHARACTER ON THE DOUBLE σ-INTERMOLECULAR BONDING.

In this last section we carried out a detailed spectroscopic study about how the biradical character of pro-aromatic systems affects their ability to originate long intermolecular interactions. To this end we studied two molecules, *1-NDT* and *2-NDT*. Both share the naphtodithiophene central core (*NDT*) but differ in the electron-withdrawing groups attached to the outermost positions of the π-conjugated fused backbone, *1-NDT* having cyano-acyl-methylene groups, while *2-NDT* is substituted with dicyano-methylene units. These two systems are weak *Kekulé* biradicals with an open-shell singlet configuration.

The main results can be summarized as follows:

1. The Uv-Vis-NIR electronic absorption spectra of both samples are very similar, indicating that the different substitution pattern does not affect the electronic structure of the ground state in a significative way. However, the spin-coated films are quite different, being the *1-NDT* film colourless while the corresponding *2-NDT* film remains blue. Interestingly, the colourless film recovered the blue colour after thermal annealing, coming back to the colourless form if redissolved.

2. The same process was observed by temperature dependant UV-Vis-NIR electronic absorption spectroscopy for *1-NDT* in solution, where a progressive and reversible decreaseing of the monomer band together with the appearance of a new band around 280/300 nm was found, the latter being coincident with the absorption band recorded for the colourless film.

3. Assumig a dimerization process for *1-NDT* on cooling, the thermodynamic parameters were also experimentally obtained, by means of a Van't Hoff's plot, and values of -14.81 $Kcal \cdot mol^{-1}$ and -224.20 $J \cdot K^{-1} \cdot mol^{-1}$ where found for the standard enthalpy and entropy of the process. These results were well reproduced by theoretical calculations for the σ-dimer in a syn configuration with respect to the sulphur atoms and justify the exothermicity of the dimerization reaction.

4. By means of infrared spectroscopy and theoretical calculations we carried out a complete study of the dimerization process in *1-NDT* from a molecular structure point of view. The infrared spectra of the film as a function of temperature indicate the electronic

connection/disconnection of the π-conjugated central unit (*NDT*) with the perypheral electron-withdrawing groups. The spectrum recorded at 150 ^{o}C would correspond to the momomer with a quinoidal estructure, where the cyano-acyl groups are conjugated with the molecular bridge. The spectrum of the evaporated film, corresponds to a colorless form similar to the dimer, and evidences the disconnection between the electron-withdrawing groups and the π-conjugated *NDT* central unit upon formation of the dimer.

5. The outlined above IR study is complemented by the Raman characterization, which is very informative about the structural modifications occurring within the conjugated *NDT* core during dimerization in solution and polymerization in solid state. The 532 nm Raman spectrum of the bulk, together with the theoretical calculations, confirm a benzoquinoidal structure for the *NDT* unit in the momomer. However, the spectral profile changes in the evaporated film, revealing a more aromatic structure of the central units, result that is well correlated with the theoretical spectrum calculated for the σ-syn-dimer although in solid state, what we obtain is a structurally similar polymer. From a structural point of view, the dimerization/polymerization process would start from a quinoidal monomer with weak biradical character that evolves through the aromatization of the *NDT* induced by the formation of the two intermolecular σ bonds between radical centers. Thus, one can say that the cyano-acyl groups would be responsible for the quinoidal shape of the monomeric form and the aromatic one would be located on a sandwich-like σ-dimer/stair-chain polymer.

6. We also recorded the Raman spectra of both samples, as a function of the pressure applied. We observed that, for *2-NDT* no

significant chemical alterations were observed by increasing the pressure, being the monomer the only molecular entity present in all the experimental conditions. However, in the case of *1-NDT* the evolution of the spectrum leads to one spectrum, at 6 GPa, that correlates well with the one of the dimer/polymer.

8.4 CONCLUSIONS.

From the research carried out in this Ph.D we conclude:

- We have established a clear dependency of the ground state structures with the chain length for a new perylene derivatives (*nPer-CN, n=1-6*), going from a closed-shell *Per-CN* in *1Per-CN* to a singlet open-shell configuration in *2,3Per-CN* and, finally to a triplet biradical configuration in *5,6Per-CN*.

- A clear structure-property relationship between the gaining of aromaticity, biradical character and steric hindrance between neighboring perylene units was stablished by compairing fused rylene derivatives *QR-CN* and *HR-CN* with their corresponding "flexible" analogs, *2,3Per-CN.*

- We have demonstrated how the biradical state of closed-shell 1*Per-CN* and *QR-CN* can be turned on by the insertion of thiophene rings (*RyTh$_2$-CN, Ry$_2$Th$_2$-CN*), whose aromaticty and steric hindrance contributes to the stabilization of singlet open-shell ground states.

- We have characterized the ground state of the first stable octazethrene derivative, *OZ-TIPS*, as a singlet biradical. At the same time we have studied the influence of the pro-aromatic unit *p-QDM* on the stabilization of open-shell systems and charged species for *OZ-TIPS*, *HZ-TIPS* and *HZ-DI*.

- The ground state structure of two new and stable tetrabenzo-chichibabin derivatives has been characterized. The *2-OS* triplet biradical ground state preference is related to the steric repulsion between anthracene units and the thermodynamic stabilization induced by the fluorenyl spin delocalizing unit, while *1-CS* exhibits a closed-shell quinoidal structure in the ground state and a butterfly-like geometry.

- Finally, we have characterized the reversible double σ-dimerization (in solution) and the formation of stair-chain polymers (in solid state) of a new naphtodithiophene derivative (*1-NDT*) and established the importance of the role that the weak biradical character of the *1-NDT* monomer has on the formation of the corresponding four-center weak intermolecular bond formed.

With this research we have been able to establish relationships between the molecular structure and stabilization of open-shell systems in a wide variety of molecular platforms. In terms of stabilization of low spin biradicals, the set of molecules studied have allowed us to undertand how the Double Spin Polarization Mechanism works at the molecular level, information that can be very useful for the synthesis of new and stable singlet open-shell biradicals.

8.5 REFERENCES.

1. *IUPAC Compendium of Chemical Terminology*. release 2.3.2 ed. 2012. 168.
2. Abe, M., *Chem.Rev.*, 2013. **113**(9): p. 7011-7088.
3. Tschitschibabin, A.E., *Ber. Chem.*, 1907. **40**(2): p. 1810-1819.
4. Thiele, J. and Balhorn, H., *Ber. Chem.*, 1904. **37**(2): p. 1463-1470.
5. Sun, Z.; Ye, Q.; Chi, C.: Wu, J., *Chem Soc. Rev.*, 2012. **41**(23): p. 7857-7889.
6. Sun, Z.; Zeng, Z.; Wu, J., *Acc. Chem. Res.*, 2014. **47**(8): p. 2582-2591.
7. *IUPAC Compendium of Chemical Terminology*. release 2.3.2 ed. 2012. 427.
8. Borden, W.T., *Diradicals*, ed. W. Interscience. Vol. 1. 1982, New York.
9. Borden, W.T.; Iwamura, H.; Berson, J.A., *Acc. Chem. Res.*, 1994. **27**(4): p. 109-116.
10. Matsuda, K. and Iwamura, H., *J. Am. Chem. Soc.*, 1997. **119**(31): p. 7412-7413.
11. Montgomery, L. K.; Huffman, J. C. ;Jurczak, E. A.; Grendze, M. P., *J. Am. Chem. Soc*, 1986. **108**(19): p. 6004-6011.
12. Porter, W.W.; Vaid, T.P.; Rheingold, A.L., *J. Am. Chem. Soc.*, 2005. **127**(47): p. 16559-16566.
13. Sun, Z.; Huang, K.-W.; Wu, J., *J. Am. Chem. Soc.*, 2011. **133**(31): p. 11896-11899.
14. Borden, W.T., *J. Am. Chem. Soc.*, 1975. **97**(21): p. 5968-5970.
15. Borden, W.T. and Davidson, E.R., *J. Am. Chem. Soc.*y, 1977. **99**(14): p. 4587-4594.
16. Karafiloglou, P., *J. Chem. Ed.*, 1989. **66**(10): p. 816.
17. Breslow, R., *Acc. Chem. Res.*, 1973. **6**(12): p. 393-398.
18. Coronado, E. and Epstein, A.J., *J. Mater. Chem.*, 2009. **19**(12): p. 1670-1671.
19. Lee, J.; Jadhav, P.; Reusswig, P. D.; Yost, S. R.; Thompson, N. J.; Congreve, D. N.; Hontz, E.; Van Voorhis, T.; Baldo, M. A., *Acc. Chem. Res.*, 2013. **46**(6): p. 1300-1311.
20. Smith, M.B. and Michl, J. *Chem. Rev.* 2010. **110**(11): p. 6891-6936.

21. Wilson, M.; W. B. Rao, A.; Ehrler, B.; Friend, R. H., *Acc. Chem. Res.*, 2013. **46**(6): p. 1330-1338.
22. Zimmerman, P. M.; Musgrave, C. B.; Head-Gordon, M., *Acc. Chem. Res.*, 2013. **46**(6): p. 1339-1347.
23. Konishi, A.; Hirao, Y.; Nakano, M.; Shimizu, A.; Botek, E.; Champagne, B.; Shiomi, D.; Sato, K.; Takui, T.; Matsumoto, K.; Kurata, H.; Kubo, T., *J. Am. Chem. Soc.*, 2010. **132**(32): p. 11021-11023.
24. Banwell, C.N. and McCash, E.M. *Fundaments of Molecular Spectroscopy.* 1994.
25. Hollas, J.M., *Modern Spectroscopy*, ed. J.W. Sons. 1992.
26. Requena, A. and J. Zúñiga, *Espectroscopía*, ed. Pearson. 2004.
27. Raman, C.V., *Indian J. Phys*., 1928. **2**: p. 387.
28. Raman, C.V. and Krishnan, K.L.,*Nature*, 1928. **121**: p. 501.
29. Raman, C.V. and Krishnan, K.L., *Indian J. Phys*., 1928. **2**: p. 399.
30. Ponce Ortiz, R.; Casado, J.; Hernández, V.; López Navarrete, J. T.; Viruela, P. M.; Ortí, E.; Takimiya, K-; Otsubo, T., *Angew. Chem. Int. Ed.,* **119**(47): p. 9215-9219.

Apéndices

APÉNDICE A: ÍNDICE DE SIGLAS MÁS FRECUENTES

ψ: Función de Onda

$\vec{\mu}$: Momento dipolar inducido

B3LYP: Becke, three-parameter, Lee-Yang-Parr

CAM: Coulomb Attenuating Method

CS: Closed Shell

DCM: Dichloromethane

DFT: Density Functional Theory

DI: Diimide

DSP: Double Spin Polarization

E: Campo Eléctrico

ECC: Effective Conjugation Coordinate

ESR: Electron Spin Resonance

FT: Fourier Transform

H: Campo Magnético

HOMO: Highest Occupied Molecular Orbital

IC: Interacción de Configuraciones

ICP-MS: Inductively Coupled Plasma Mass Spectrometry

IDPL: Indacenodifenaleno

IR: Infrared

j_{ii}: Integral de Coulomb para un único centro

j_{ij}: Integral de Coulomb para dos centros

k: Integral de Canje

LCAO: Linear Combination of Atomic Orbitals

LUMO: Lowest Unoccupied Molecular Orbital

MO: Molecular Orbital

NBMO: Non Bondig Molecular Orbital

Nd:YAG: Neodymium doped Ytrium Aluminium Garnet

NDT: Naphtodithiophene

NIR: Near Infrared

OFET: Organic Field Effect Transistor

OS: Open Shell

PAHs: Hidrocarburos Policíclicos Aromáticos

p-QDM: para-quinodimetano

RMN: Resonancia Magnética Nuclear

S: Singlete

SOMO: Singly Occupied Molecular Orbital

SP: Spin Polarization

SQUID: Superconducting Quantum Interference Device

T: Triplete

THF: Tetrahydrofuran

TIPS: Triisopropylsilyl

TME: Trimetilenetano

TMM: Trimetilenmetano

U: Unrestricted

α: Tensor de polarizabilidad

ΔE_{S-T}: Singlet-triplet gap

APÉNDICE B: LISTA DE ARTÍCULOS

El trabajo de investigación desarrollado en la presente Tesis Doctoral ha dado lugar a las siguientes publicaciones:

Capítulo 4: Derivados de Perileno bis(dicianometileno)-sustituidos:

- ***Pushing Extended p-Quinodimethanes to the Limit: Stable Tetracyano-oligo(N-annulated perylene)quinodimethanes with Tunable Ground States***

  Zeng, Z.; Ishida, M.; Zafra, J. L.; Zhu, X.; Mo Sung, Y.; Bao, N.; Webster, R. D.; Lee, B. S.; Li, R-W.; Zeng, W.; Li, Y.; Chi, C.; López Navarrete, J. T.; Ding, J.; Casado, J.; Kim, D. and Wu, J.

  J. Am. Chem. Soc., ***2013***, *135 (16), pp 6363–6371*

- ***Tetracyanoquaterrylene and Tetracyanohexarylenequinodimethanes with TunableGround states and Strong Near-Infrared Absorption***

  Dr. Zebing Zeng, Sangsu Lee, José L. Zafra, Dr. Masatoshi Ishida, Xiaojian Zhu, Zhe Sun, Yong Ni, Prof. Richard D. Webster, Prof. Run-Wei Li, Prof. Juan T. López Navarrete, Prof. Chunyan Chi, Prof. Jun Ding, Prof. Juan Casado,Prof. Dongho Kim and Prof. Jishan Wu

  Angew. Chem. Int. Ed, ***2013***, *52 , pp 8561–8565*

- ***Turning on the biradical state of tetracyano-perylene and quaterrylenequinodimethanes by incorporation of additional thiophene rings***

  Zebing Zeng, Sangsu Lee, José L. Zafra, Masatoshi Ishida, Nina Bao, Richard D. Webster, Juan T. López Navarrete, Jun Ding, Juan Casado, Dongho Kim and Jishan Wu

  Chem. Sci. ***2014***, *5, pp 3072-3080*

Capítulo 5: Derivados Cetrénicos:

- ***Kinetically Blocked Stable Heptazethrene and Octazethrene: Closed-Shell or Open-Shell in the Ground State?***

  Yuan Li, Wee-Kuan Heng, Byung Sun Lee,Naoki Aratani, José L. Zafra, Nina Bao,Richmond Lee, Young Mo Sung, Zhe Sun, Kuo-Wei Huang, Richard D. Webster, Juan T. López Navarrete, Dongho Kim, Atsuhiro Osuka, Juan Casado, Jun Ding, and Jishan Wu

  J. Am. Chem. Soc., ***2013****, 134 (36), pp 14913–14922*

- ***Zethrene biradicals: How pro-aromaticity is expressed in the ground electronic state and in the lowest energy singlet, triplet, and ionic states***

  José Luis Zafra, Rafael C. González Cano, M. Carmen Ruiz Delgado, Zhe Sun, Yuan Li, Juan T. López Navarrete, Jishan Wu and Juan Casado

  J. Chem. Phys. ***140****, 054706 (2014)*

Capítulo 6: Derivados tetrabenzo-chichibabin

- ***Stable Tetrabenzo-Chichibabin's Hydrocarbons: Tunable Ground State and Unusual Transition between Their Closed-Shell and Open-Shell Resonance Forms***

  Zebing Zeng, Young Mo Sung, Nina Bao, Davin Tan, Richmond Lee, José L. Zafra, Byung Sun Lee, Masatoshi Ishida, Jun Ding, Juan T. López Navarrete, Yuan Li, Wangdong Zeng, Dongho Kim, Kuo-Wei Huang, Richard D. Webster, Juan Casado, and Jishan Wu

  J. Am. Chem. Soc., ***2013****, 134 (35), pp 14513–14525*

Capítulo 7: Derivados de Naftoditiofeno

- ***Giant and Reversible Chromism by Double σ-Bond Dimerization of a New Janus-Type σ-Diradical with Quinoidal-Aromatic Antagonistic Faces***

  José L. Zafra, Naoyuki Yanai, Takamich Mori, Itaru Osaka, Lili Qiu, Miklos Kertesz, Juan T. López Navarrete, Kazuo Takimiya, Juan Casado

  Submitted

- ***Vibrational Infrared and Raman Fingerprints of the Double σ-Bond with A π-geometry. On the Key Role of the Diradicaloid Precursor***

  José L. Zafra, Rafael C. González Cano, Naoyuki Yanai, Takamich Mori, Itaru Osaka, Lili Qiu, Miklos Kertesz, Juan T. López Navarrete, Kazuo Takimiya, Juan Casado

  Submitted

JACS
JOURNAL OF THE AMERICAN CHEMICAL SOCIETY
Article
pubs.acs.org/JACS

Pushing Extended *p*-Quinodimethanes to the Limit: Stable Tetracyano-oligo(*N*-annulated perylene)quinodimethanes with Tunable Ground States

Zebing Zeng,[†] Masatoshi Ishida,[‡] José L. Zafra,[§] Xiaojian Zhu,[∥] Young Mo Sung,[‡] Nina Bao,[⊥] Richard D. Webster,[#] Byung Sun Lee,[‡] Run-Wei Li,[∥] Wangdong Zeng,[†] Yuan Li,[†] Chunyan Chi,[†] Juan T. López Navarrete,[§] Jun Ding,*[,⊥] Juan Casado,*[,§] Dongho Kim,*[,‡] and Jishan Wu*[,†,▽]

[†]Department of Chemistry, National University of Singapore, 3 Science Drive 3, 117543, Singapore

[‡]Spectroscopy Laboratory for Functional π-Electronic Systems and Department of Chemistry, Yonsei University, Seoul 120-749, Korea

[§]Department of Physical Chemistry, University of Malaga, Campus de Teatinos s/n, 229071 Malaga, Spain

[∥]Key Laboratory of Magnetic Materials and Devices, Ningbo Institute of Materials Technology and Engineering, Chinese Academy of Sciences, Ningbo 315201, People's Republic of China

[⊥]Department of Materials Science & Engineering, National University of Singapore, 119260, Singapore

[#]Division of Chemistry & Biological Chemistry, School of Physical & Mathematical Sciences, Nanyang Technological University, 21 Nanyang Link, 637371, Singapore

[▽]Institute of Materials Research and Engineering, A*STAR, 3 Research Link, 117602, Singapore

Supporting Information

ABSTRACT: *p*-Quinodimethane (*p*-QDM) is a fundamental building block for the design of π-conjugated systems with low band gap and open-shell biradical character. However, synthesis of extended *p*-QDMs has usually suffered from their intrinsic high reactivity and poor solubility. In this work, benzannulation together with terminal cyano-substitution was demonstrated to be an efficient approach for the synthesis of a series of soluble and stable tetracyano-oligo(*N*-annulated perylene)-quinodimethanes ***n*Per-CN** (n = 1−6), with the longest molecule having 12 *para*-linked benzenoid rings! The geometry and electronic structures of these oligomers were investigated by steady-state and transient absorption spectroscopy, nuclear magnetic resonance, electron spin resonance, superconducting quantum interference device, and FT Raman spectroscopy assisted by density functional theory calculations. They showed tunable ground states, varying from a closed-shell quinoidal structure for monomer, to a singlet biradical for dimer, trimer, and tetramer, and to a triplet biradical for pentamer and hexamer. Large two-photon absorption cross-section values were observed in the near-infrared range, which also exhibited a clear chain-length dependence.

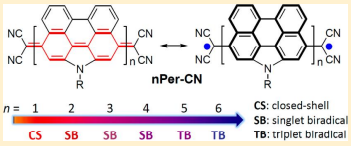

I. INTRODUCTION

p-Quinodimethane (*p*-QDM) (Figure 1) and its biradical form were originally proposed as products in the pyrolysis of *p*-xylene.[1] It has a large biradical character in the ground state due to recovery of the aromaticity of the central benzenoid ring, and thus it is highly reactive. Great efforts have been made to prepare stable *p*-QDM derivatives and its extended analogues. For example, substitution of the terminal methylene sites in *p*-QDM and *p*-dibenzoquinodimethane by four phenyl groups resulted in relatively stable Thiele's hydrocarbon[2] and highly reactive but still characterizable Tschitschibabin's hydrocarbon,[3] respectively. Terminal substitution by cyano group turned out to be another efficient approach, and several stable *p*-QDM derivatives such as 7,7,8,8-tetracyanoquinodimethane (TCNQ),[4] 13,13,14,14-tetracyano-4,5,9,l0-tetrahydro-2,7-pyrenoquinodimethane (TCNTP),[5] and 13,13,14,14-tetracyano-2,7-pyrenoquinodimethane (TCNP)[5] have been successfully prepared (Figure 1). The tetracyanodiphenoquinodimethane (TCNDQ) without any substitution on the diphenoquinoid moiety (Figure 1), however, could not be isolated as it tended to simultaneously polymerize.[6] The further extension of TCNTP and TCNP frameworks is problematic because of their poor solubility and limited functionalization sites. An alternative approach to extend quinoidimethanes is to replace the benzenoid ring by other heterocycles such as thiophene and thiazole, and some soluble and stable tetracyano-heteroquinoids[7] have been prepared and used as acceptors in charge-transfer conductors[8] and as semiconductors for *n*-channel or ambipolar field-effect transistors.[9] Among them, a series of

Received: March 9, 2013
Published: April 5, 2013

   dx.doi.org/10.1021/ja402467y | J. Am. Chem. Soc. 2013, 135, 6363−6371

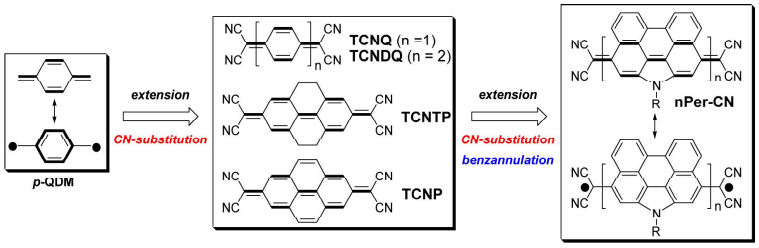

Figure 1. Structural evolution of extended *p*-QDMs.

Scheme 1. Synthesis of *n*Per-CN[a]

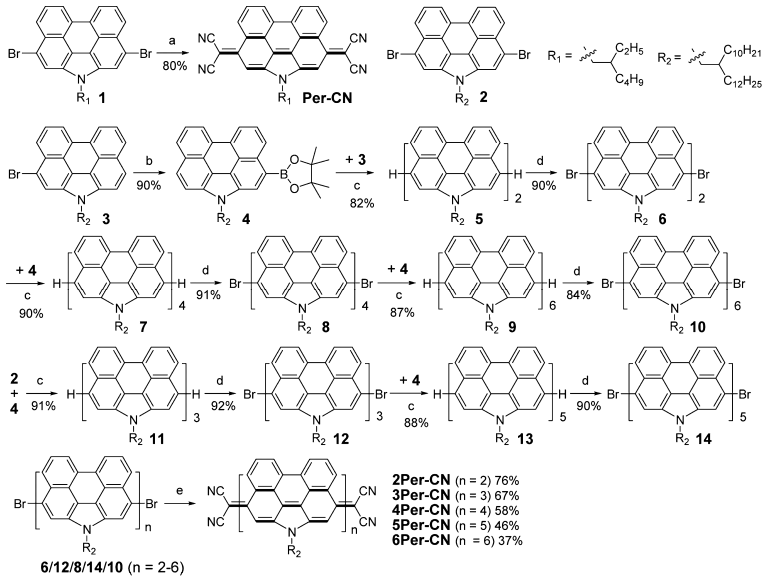

[a]Reagents and conditions: (a) (i) malononitrile, NaH, $Pd(PPh_3)_2Cl_2$, reflux, 48 h; (ii) HCl (2M), air; (b) pinacolborane, $PdCl_2(PPh_3)_2$, 1,2-dichloroethane/Et_3N, 90 °C, 24 h; (c) $Pd(PPh_3)_4$, Cs_2CO_3, toluene/DMF, 90 °C, 24 h; (d) NBS (2 equiv), DCM/DMF, 0−25 °C, overnight; (e) (i) malononitrile, NaH, $Pd(PPh_3)_2Cl_2$, reflux, 48 h; (ii) HCl (2M); (iii) *p*-chloranil, $CHCl_3$, room temperature.

quinoidal oligothiophenes up to hexamer displayed interesting chain-length dependence of their ground-state electronic structures, with the pentamer and hexamer showing significant singlet biradical character.[10] Incorporation of a *p*-QDM moiety and its analogues such as 2,6-naphthoquinodimthane[11] and 2,6-anthraquinodimethane[12] into a fused π-conjugated framework has proved to be an efficient way to generate polycyclic hydrocarbons with potential open-shell biradical ground states, and typical examples include indenofluorenes,[13] bis-(phenalenyls),[14] and zethrenes.[15] These polycyclic hydrocarbons exhibit unique optical, electronic, and magnetic properties and have promising applications in nonlinear optics,[16] organic electronics,[17] organic spintronics,[18] and energy storage devices.[19]

Although many useful materials based on *p*-QDM have been prepared and well investigated in recent years, how to make largely extended *p*-QDMs is still a big challenge due to their intrinsic high reactivity arising from their increasing biradical character with extension of their chain length. Solubility of course is another critical concern. Recently, we demonstrated that benzannulation is an efficient approach to stabilize the highly reactive Tschitschibabin's hydrocarbon.[20] Inspired by

this success, in this research we demonstrate that by using a *N*-annulated perylene (NP) as a building block, we are able to prepare a series of soluble and stable oligo(*N*-annulated perylene)quinodimethanes ***n*Per-CN** (n = 1−6), with the longest molecule having 12 *para*-linked benzenoid rings (Figure 1). The NP was chosen on the basis of the following considerations: (1) the quinoidal NP can be regarded as a structure where the *p*-diphenoquinoid is annulated by two aromatic benzene rings, and thus stability will be improved; (2) flexible alkyl chain can be easily attached to the N-site and thus resolve the solubility problem; and (3) selective functionalization can be easily conducted at the *peri*-edges of NP and allows us to prepare higher order oligomers.[21] In addition, the electron-withdrawing cyano-groups at the terminal methylene sites will further stabilize the systems. The ground-state geometry and electronic structure of these oligomers were systematically investigated by steady-state absorption and transient absorption (TA), variable-temperature (VT) nuclear magnetic resonance (NMR), electron spin resonance (ESR), superconducting quantum interference device (SQUID) measurements, and FT Raman spectroscopy assisted by density functional theory (DFT) calculations. Our research disclosed interesting chain-length dependence of their ground states and optical, electrochemical, and magnetic properties.

II. RESULTS AND DISCUSSION

Synthesis. As shown in Scheme 1, all of the target compounds ***n*Per-CN** (n = 1−6) were prepared by Takahashi coupling[22] from the corresponding dibromo-oligo(*N*-annulated perylenes), followed by oxidative dehydrogenation. For the monomer **Per-CN**, short alkyl substituent (2-ethylhexyl) can provide sufficient solubility. However, for higher oligomers ***n*Per-CN** (n = 2−6), a long branched dove-tailed chain (2-decyltetradecyl) has to be employed to ensure sufficient solubility for the intermediates and final products. The dibromo-NPs **1** and **2** and the monobromo-NP **3** were first synthesized by controlled bromination with *N*-bromosuccinimide (NBS) according to previous reports.[21] Pd-catalyzed Takahashi coupling of **1** with malononitrile in the presence of sodium hydride in anhydrous THF worked smoothly and afforded the **Per-CN** as a deep blue solid in 80% yield after acidification and simultaneous oxidation in air. The higher order oligomers were synthesized by repetitive Suzuki coupling/bromination reactions. The NP monoboronic ester **4** as a key intermediate was prepared by Miyaura borylation reaction from **3**. Suzuki coupling between **3** and **4** gave the NP dimer **5**, which was brominated with NBS to afford the dibromo-NP dimer **6**. Suzuki coupling between **6** and **4** generated NP tetramer **7**, and subsequent bromination provided the dibromo-NP tetramer **8**. Similar Suzuki coupling/bromination protocol from **8** gave the dibromo-NP hexamer **10**. The dibromo- NP trimer **12** was prepared by Suzuki coupling between **2** and **4**, followed by bromination with NBS. Subsequent Suzuki coupling with **4** and bromination afforded the dibromo-NP pentamer **14**. The quinoidal oligomers ***n*Per-CN** (n = 2−6) were then prepared in tens of milligram scale by similar Takahashi coupling reaction from the corresponding dibromo-NP oligomers (**6**, **12**, **8**, **14**, and **10**) followed by oxidation with *p*-chloranil in chloroform in 76−37% yields. In these cases, oxygen in air can only oxidize the dihydro-intermediates very slowly; thus a stronger oxidant such as *p*-chloranil has to be used to ensure a complete dehydrogenation. All of the target molecules ***n*Per-CN** are soluble in common organic solvents such as chloroform, toluene, and THF. The compounds were stable enough to be readily obtained as analytically pure products in both solid and solution except that the hexamer **6Per-CN** in solution was moderately sensitive to light and it partially decomposed on silica gel column, which prevented us from separating even longer oligomers. All of the intermediates were well characterized by ^{1}H and ^{13}C NMR and mass spectrometry (MS), and the purity of the final products was confirmed by high-resolution MS and by high performance liquid chromatography (HPLC) (see the Supporting Information).

Magnetic Properties. The ^{1}H and ^{13}C NMR spectrum of the smallest derivative, **Per-CN**, in $CDCl_3$ at 298 K exhibits well-resolved resonance signals, indicating that **Per-CN** has a closed-shell quinoidal structure in the ground state. In contrast, the higher ***n*Per-CN** (n = 2−6) showed NMR silence even at low temperature (−100 °C in CD_2Cl_2), indicating that these extended quinodimethanes derivatives have a large biradical character in the ground state (vide infra). Accordingly, ESR measurements of all samples except **Per-CN** displayed featureless broad signals in both solid state and solution centered with g_e = 2.0031 (Figure S1 in the Supporting Information). The signal broadening and absence of $\Delta M_s = \pm 2$ forbidden transitions would be due to the long-distance spin−spin dipole interaction within the molecules and the extended spin-delocalization.[14,15e,f] The VT ESR measurements for the powders of ***n*Per-CN** (n = 2−6) disclosed the significant temperature dependency of the signal intensities; the intensity decreased with decreasing temperature for **2Per-CN**−**4Per-CN**, indicating that they all have a singlet biradical ground state, which is in equilibrium with a higher energy triplet biradical state. The change however became rather slight for **4Per-CN** as compared to that of **2Per-CN**. The trend reversed in case of **5Per-CN** and **6Per-CN**; that is, the ESR intensity increased when lowering the temperature. This infers that the biradicals in the higher oligomers behave more like two individual radicals, presumably due to the very weak coupling through a long distance between two unpaired electrons.

The singlet−triplet energy gap ΔE_{S-T} (i.e., $-2J/k_B$) was estimated by SQUID measurements on the powder form of ***n*Per-CN** (n = 2−6) at 5−300 K by means of careful fitting of the curves by the Bleaney−Bowers equation[23] (Figure 2 and

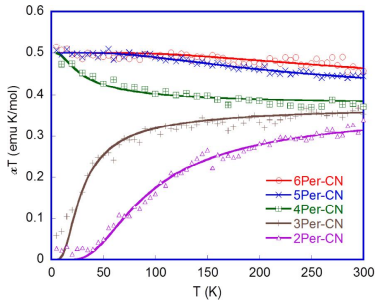

Figure 2. $\chi T-T$ curves in the SQUID measurements for the powder of ***n*Per-CN** (n = 2−6). The solid lines are the fitting curves according to Bleaney−Bowers equation; *g*-factor was taken to be 2.

dx.doi.org/10.1021/ja402467y | J. Am. Chem. Soc. 2013, 135, 6363−6371

Table 1. Photophysical and Electrochemical Data of *n*Per-CN[a]

compd	λ_{abs} (nm)	ε_{max} (M^{-1} cm^{-1})	τ (ps)	$\sigma^{(2)}_{max}$ (GM)	$E^{1}_{1/2(ox)}$ (V)	$E^{1}_{1/2(red)}$ (V)	HOMO (eV)	LUMO (eV)	E_g^{EC} (eV)	E_g^{opt} (eV)	ΔE_{S-T} (kcal/mol)
Per-CN	579	61 400	17.2	1300[b]		−0.54		−4.26		1.74	
	626	66 000				−0.78					
						−1.5					
2Per-CN	351	20 230	8.6	1060[c]	0.36	−0.45	−5.11	−4.50	0.61	0.89	0.342
	620	28 300			0.54						
	901	54 700									
3Per-CN	451	34 800	3.5	770[c]	0.35	−0.41	−5.05	−4.52	0.53	0.93	0.107
	635	67 600			1.0						
	930	22 600									
4Per-CN	460	72 200	3.1	710[c]	0.31	−0.44	−5.05	−4.53	0.52	0.93	−0.064
	635	70 800			0.80						
	930	21 400									
5Per-CN	466	84 900	2.9	730[c]	0.30	−0.45	−5.04	−4.47	0.57	0.93	−0.556
	635	59 600			0.89						
	929	17 300									
6Per-CN	469	10 4400	2.7	710[c]	0.30	−0.43	−5.03	−4.50	0.53	0.93	−0.883
	634	45 400			0.84						
	927	13 000									

[a] λ_{abs}: absorption maximum measured in THF. ε_{max}: molar extinction coefficient at the absorption maximum in the unit of M^{-1} cm^{-1}. τ is singlet excited lifetime obtained from TA. $E_{1/2}^{ox}$ and $E_{1/2}^{red}$ are half-wave potentials of the oxidative and reductive waves, respectively, with potentials vs Fc/Fc^{+} couple. HOMO and LUMO energy levels were calculated according to equations: HOMO = $-(4.8 + E_{ox}^{onset})$ and LUMO = $-(4.8 + E_{red}^{onset})$, where E_{ox}^{onset} and E_{red}^{onset} are the onset potentials of the first oxidative and reductive redox wave, respectively. E_g^{EC}: electrochemical energy gap derived from LUMO−HOMO. E_g^{opt}: optical energy gap derived from lowest energy absorption onset in the absorption spectra. ΔE_{S-T}: singlet−triplet energy gap estimated from SQUID measurements. [b] $\sigma^{(2)}_{max}$ is the maximum TPA cross section at the wavelength of 1200 nm. [c] $\sigma^{(2)}_{max}$ is the maximum TPA cross section at the wavelength of 1700 nm.

Table 1). The ΔE_{S-T} values were estimated as 0.342 and 0.107 kcal/mol for **2Per-CN** and **3Per-CN**, respectively, further confirming that both compounds have a singlet biradical ground state, with the two unpaired electrons weakly coupled. Such small ΔE_{S-T} values allow the facile thermal excitation to the higher energy triplet biradical state. A very small ΔE_{S-T} (−0.064 kcal/mol) was estimated for **4Per-CN**, indicating very weak coupling between the two radicals. Given the unavoidable error during the data fitting for this borderline molecule, the ground state of **4Per-CN** is better described as a singlet biradical with very large biradical character based on the VT ESR measurements, which is also in agreement with DFT calculations to be discussed later. In passing from **4Per-CN** to **5Per-CN** and **6Per-CN**, the ΔE_{S-T} became −0.56 and −0.88 kcal/mol, respectively, implying a triplet biradical ground state. However, considering the long distance between the two radicals, these two compounds may be better described as two individual radicals.

Raman Characterizations. Raman spectroscopy is a unique tool to evaluate the electronic ground state of conjugated biradicals and to understand macroscopic magnetic and optical data with molecular level information.[10b,15f,20,24] To warrant a maximum population of the ground electronic state, either singlet or triplet, the FT-Raman spectra of the ***n*Per-CN** samples were recorded at −180 °C (Figure 3). For **Per-CN**, the Raman bands at 1705, 1600, and 1458 cm^{-1} are clearly associated with the quinoidal structure (C═C stretching modes) between the two dicyano groups corroborating its singlet closed-shell nature. In **2Per-CN**, the Raman spectrum experiences a frequency down-shift of the above three important bands toward 1687, 1584, and 1441 cm^{-1}, respectively. This spectroscopic feature reflects the weakening of the C═C bond strength of the quinoidal path due to the recovery of aromatic-like rings for the perylene units. This

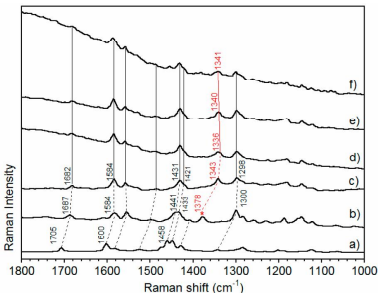

Figure 3. FT-Raman spectra of the ***n*Per-CN** at −180 °C in the solid state: (a) **Per-CN**; (b) **2Per-CN**; (c) **3Per-CN**; (d) **4Per-CN**; (e) **5Per-CN**; and (f) **6Per-CN**.

quinoid-to-aromatic tuning of the molecular backbone is the molecular confirmation of the formation of biradical species in **2Per-CN**. From **Per-CN** to **2Per-CN**, a new band appeared at 1378 cm^{-1} due to the creation of the CC interperylene stretching mode with a predominant single C−C character further affirming its biradicaloid state. From **2Per-CN** to **3Per-CN**, the characteristic FT-Raman bands were further down-shifted because of increased aromatic stabilization by the incorporation of an additional perylene unit, which reveals a more remarkable biradical character of the molecular framework. The frequency down-shift of the interperylene (C−C) modes (by 35 cm^{-1}) is particularly noticeable because it overexpresses the aromatic character of the open-shell structure of the ground electronic state of **3Per-CN**. However, this large

dx.doi.org/10.1021/ja402467y | J. Am. Chem. Soc. 2013, 135, 6363−6371

biradical aromatization incorporates backbone flexibility (constrained in quinoidals structures), which produces interperylene dihedral rotations easily fuelled by steric crowing. Acting together, the planar distortions and the strong perylene aromatization clearly account for the large −35 cm^{-1} displacement. In going from **3-PerCN** to **4-PerCN**, the interperylene C−C stretch down-shifts by 7 cm^{-1}, indicating that the distortive effect increased and conjugation (aromatization) decreased (increased). From **4-PerCN** to **5Per-CN** and **6Per-CN**, the spectra remained unchanged in frequencies, and their spectral profiles were essentially identical. This might indicate that molecular conjugation is already saturated in **4-PerCN** and interperylene rotations are fully relaxed. This molecular spectroscopic information is relevant because saturation of conjugation confines its effect to the molecular center (equivalent to ∼4 NP units) of **5Per-CN** and **6Per-CN** decoupling the two radical centers and deactivating the double spin polarization effect that produces the stabilization of the triplet state in the two largest molecules. In other words, conjugation length (CL) in **5Per-CN** and **6Per-CN** is smaller than the molecular length (ML) supposing a transition from a singlet biradical ground electronic state (CL ≈ ML in **2Per-CN**, **3Per-CN**, and **4Per-CN**) to a triplet ground electronic state (CL < ML in **5Per-CN** and **6Per-CN**).

From a viewpoint of molecular structures, quinoidal ***n*Per-CN** may exist as cis/trans isomers. For example, the two NP units in quinoidal **2Per-CN** could adopt a *trans*- or a *cis*-configuration through the ethylene linkage (Figure 4a). However, its corresponding biradical resonance form may interconvert them by rotating along the single C−C bond. To identify cis/trans isomerization, IR and Raman spectroscopies can be used invoking the mutual exclusion principle, which is verified in molecules that contain an inversion center among the operations of symmetry, for example, in *trans*-**2Per-CN** (i.e., C_{2h}). The Raman spectra excited at 785 nm and the infrared spectra of **2Per-CN** are clearly complementary (Figure 4b), meaning that those bands especially active in infrared are weakly active or inactive in Raman, and vice versa. This suggests that **2Per-CN** in its ground electronic state is mostly in the *trans*-form between its two NP units. However, by exciting with the 532/1064 nm Raman lasers, the corresponding spectra did not strictly follow the IR/Raman complementary rule (Figure 4b), which suggests that there could exist in **2Per-CN** a certain quantity of *cis*-isomer (C_{2v} molecular symmetry). Thus, the infrared signal averages all possible isomers, while the Raman spectrum, with different excitation wavelengths, can selectively probe one or the other isomer even in minority. The presence of a significant fraction of *cis*-isomer in **2Per-CN** might result from the high energy barrier required to overcome the perpendicular transition state imposed by the medium biradical character. In this regard, for the larger molecules, the progressive interperylene C−C bonds weakening will decrease the cis−trans energy barrier facilitating the dominance of the all-*trans* conformer, which is the disposition that better mitigates steric repulsions.

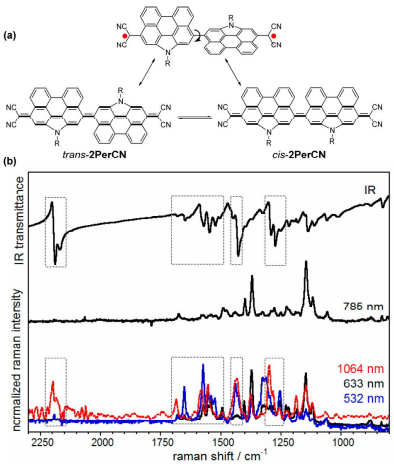

Figure 4. (a) An equilibrium between *cis*- and *trans*-**2Per-CN** via a biradical transition state; and (b) FT infrared and Raman spectra of **2Per-CN** in the solid state at different excitation wavelengths (532, 633, 785, and 1064 nm).

Optical Properties. This series of ***n*Per-CN** used in this study exhibit different one-photon absorption (OPA) spectral features as the number of rylene core increased (Figure 5 and Table 1). The monomer **Per-CN** displayed an intense absorption band with maximum at 626 nm (log ε = 4.82; ε: molar extinction coefficient in M^{-1} cm^{-1}), along with a shoulder at 579 nm, which is relatively similar to that of TCNP (λ_{max} = 557 nm, log ε = 4.12).[5] In contrast, the absorption spectrum of **2Per-CN** consisted of three major absorption bands appearing with absorption maxima at 351, 620, and 901 nm, respectively. The characteristic structured long-wavelength absorption bands were observed in the near IR region extending up to 1400 nm, with a very small optical energy gap of 0.89 eV. Such remarkable red-shift of the lowest excitation band and the band shape change as compared to **Per-CN** imply a transformation of their electronic ground state. The trimer **3Per-CN** also showed a very broad near IR band extending to 1400 nm as observed in **2Per-CN** and relatively intense band with λ_{max} of 635 nm in the visible region. This optical feature is entirely seen in further higher ***n*Per-CN** (n = 4−6). Notably, it was found that the wavelengths of lowest transition band are not further extended despite the extension of chain length, and the relative intensity of higher energy bands emerged around 450−470 nm are remarkably enhanced upon the number of rylene core increases in ***n*Per-CN**. This characteristic band around 450−470 nm may originate from the absorption of aromatic NP cores,[25] which indicates the recovery of the aromatic-like rylene cores by means of perturbation of the quinoidal electronic structures of higher ***n*Per-CN** associated with terminal spin localization.

Femtosecond TA measurements were carried out to explore the excited-state dynamics of ***n*Per-CN** (Figure 6, Table 1, and Figure S2 in the Supporting Information). The TA spectrum of **Per-CN** exhibited a ground-state bleaching (GSB) signal around 628 nm, as well as a small excited-state absorption (ESA) band in the 450−510 nm spectral region. The decay profiles probed at 628 nm were fitted by two exponential functions of 2.7 and 17.2 ps. This short singlet excited state lifetime of **Per-CN** is well in agreement with the nonfluorescent properties. In the case of open-shell derivative, **2Per-CN**, one

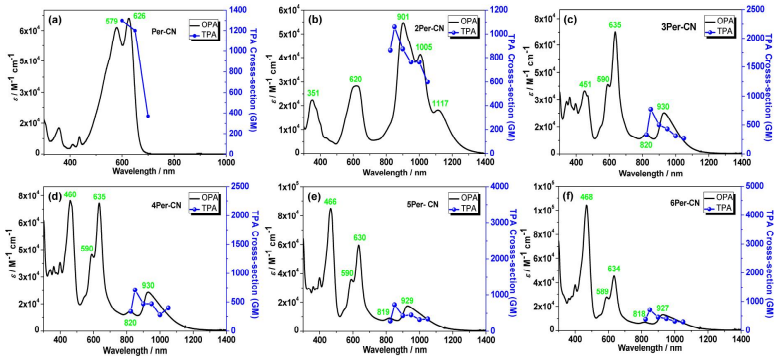

Figure 5. One-photon and two-photon absorption spectra of ***n*Per-CN**. The spectra were recorded in chloroform and THF, respectively: (a) **Per-CN**; (b) **2Per-CN**; (c) **3Per-CN**; (d) **4Per-CN**; (e) **5Per-CN**; and (f) **6Per-CN**.

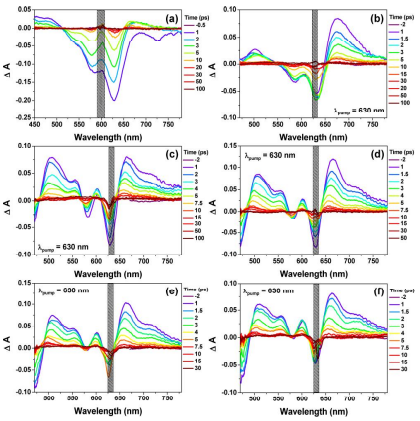

Figure 6. Femtosecond transient absorption spectra of ***n*Per-CN** measured in tetrahydrofuran at room temperature (296 K): (a) **Per-CN**; (b) **2Per-CN**; (c) **3Per-CN**; (d) **4Per-CN**; (e) **5Per-CN**; and (f) **6Per-CN**.

distinct GSB signals around 550−650 nm and two relative higher intensity ESA bands in spectral regions similar to those of **Per-CN** were observed, with a shorter excited-state lifetime of 8.6 ps. This fast decay kinetic profile of **2Per-CN** is considered to reflect an acceleration of the nonradiative internal conversion rates arising from the smaller energy gap between the lowest excited state and the open-shell ground state. The TA spectra of further higher ***n*Per-CN** (n = 3−6) demonstrated similar spectral features; two major ESA bands in the 480−570 and 645−780 nm regions were observed with shorter singlet excited lifetimes of 2.7−3.5 ps. Considering the similar optical energy gaps among these derivatives estimated in steady-state absorption spectra, this kinetic trend of fast decay of the excited state could be due to the molecular flexibility with the larger rylene arrays.

As it is known that an open-shell (singlet) biradical character can enhance the two-photon absorption activity,[1Sf,16,20] TPA measurements were conducted for ***n*Per-CN** by using the open-aperture Z-scan method to clarify the structure−TPA relationship (Figure 5, Table 1, and Figure S3 in the Supporting Information). The excitation wavelength was scanned in the near IR region from 1200 to 2100 nm where one-photon absorption contribution is negligible. Large TPA cross sections were observed for the closed-shell **Per-CN** with the maximum value of $\sigma^{(2)}$ = 1300 GM at 1200 nm, which could be due to that the quinoidal molecular structures bearing fluctuated atomic bonds may have larger hyperpolarizabilities.[26] As expected, open-shell higher ***n*Per-CN** also exhibited strong TPA response in the region of 1650−2100 nm, with the maximum TPA cross-section values of $\sigma^{(2)}$ = 1060, 770, 710, 730, and 710 GM, respectively, observed at 1700 nm. In comparison with typical hydrocarbon chromophores, relatively larger cross sections in NIR region were obtained. This trend of $\sigma^{(2)}$ may be correlated to the resonance enhancement of the transitions observed in OPA spectra and the degree of their biradical characters, because the intermediate biradical indices have proved to enhance the second hyperpolarizability (γ), which is the origin of the third-order nonlinear optical (NLO) properties.[27] This result demonstrates the important insights into the correlation between a biradical character index and structural backbones to enhance the TPA property.

Electrochemical Properties. Cyclic voltammetry and differential pulse voltammetry measurements were performed to investigate the electrochemical properties of these oligomers (Figure 7, Table 1, and Figure S4 in the Supporting Information). Most of the compounds displayed multiple chemically reversible reductive and/or oxidative electron transfer processes, indicating that the reduced/oxidized states survived fully or partially on the voltammetric time scale (which is for at least a few seconds). **Per-CN** in dichloromethane exhibited two chemically reversible reductive processes with half-wave potentials $E^{r}_{1/2}$ = −0.54 V and $E^{r}_{1/2}$ = −0.78 V. The $E^{r}_{1/2}$-values were determined from the midpoint of the anodic (E_p^{ox}) and cathodic (E_p^{red}) peak potentials [$E^{r}_{1/2}$ = (E_p^{ox} +

dx.doi.org/10.1021/ja402467y | J. Am. Chem. Soc. 2013, 135, 6363−6371

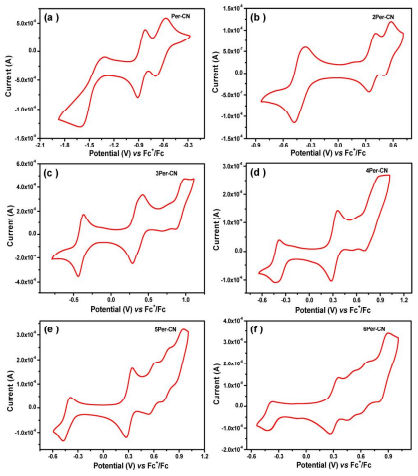

Figure 7. Cyclic voltammograms of (a) **Per-CN**; (b) **2Per-CN**; (c) **3Per-CN**; (d) **4Per-CN**; (e) **5Per-CN**; and (f) **6Per-CN** in dry dichloromethane with 0.1 M Bu_4NPF_6 as supporting electrolyte, Ag/AgCl as reference electrode, Au disk as working electrode, Pt wire as counter electrode, and scan rates at 100, 20, 20, 20, 20, and 20 mV/s, respectively.

$E_p^{red})/2]$ when the anodic (i_p^{ox}) to cathodic (i_p^{red}) peak current ratios were equal to unity ($i_p^{ox}/i_p^{red} = 1$). **Per-CN** showed another reduction process at more negative potentials ($E^r_{1/2} \approx -1.5$ V vs Fc/Fc^+) where the i_p^{ox}/i_p^{red}-ratio was <1 (at a scan rate of 100 mV s^{-1}), indicating that the highly reduced state was relatively short-lived. The i_p^{red}-value for the most negative reduction process of **Per-CN** was much greater than the two less negative processes, indicating that more electrons were transferred. No oxidative wave was observed for neutral **Per-CN**. All of the other compounds (**2Per-CN** to **6Per-CN**) could be reduced in one chemically reversible process (or partly chemically reversible process) at negative potentials and oxidized in at least two processes at positive potentials, but with the oxidation processes displaying varying degrees of chemical reversibility. **2Per-CN** was electrochemically oxidized in two chemically reversible processes at $E^r_{1/2} = 0.36$ V and $E^r_{1/2} = 0.54$ V vs Fc/Fc^+, together with one chemically reversible reduction process at $E^r_{1/2} = -0.45$ V vs Fc/Fc^+, with the reduction process showing twice the peak current of each oxidation process (indicating the transfer of a higher number of electrons). **3Per-CN** exhibited a chemically reversible oxidative process at $E^r_{1/2} = 0.35$ V vs Fc/Fc^+ (consisting of two closely overlapping peaks) and another oxidation process at $E^r_{1/2} \approx 1.0$ V vs Fc/Fc^+ (where the i_p^{ox}/i_p^{red}-ratio >1), together with one chemically reversible reductive process at $E^r_{1/2} = -0.41$ V vs Fc/Fc^+. A similar CV profile was observed for **4Per-CN**, with one chemically reversible oxidation process at $E^r_{1/2} = 0.31$ V vs Fc/Fc^+, one oxidation process at ~0.80 V vs Fc/Fc^+, and one reduction process at $E^r_{1/2} = -0.44$ V vs Fc/Fc^+. For **5Per-CN** and **6Per-CN**, two major oxidation processes and one reduction process were detected, at potentials similar to those observed for **3Per-CN** and **4Per-CN**. However, two additional oxidation processes with much smaller peak currents (indicating the transfer of lesser numbers of electrons) were also detected at potentials between the two major oxidation processes. A summary of the half-wave potentials is provided in Table 1. In situations where the i_p^{ox}/i_p^{red}-ratios were different from unity, the reversible half-wave potentials are difficult to determine accurately, and thus the reported $E^r_{1/2}$-values are only approximate. Rather low electrochemical energy gaps were estimated for ***n*Per-CN** ($n = 2-6$) as 0.61, 0.53, 0.52, 0.57, and 0.53 eV, respectively. Such chain-length dependence of electrochemical behavior must be correlated to the change of π-conjugation and electronic structure in these extensive homologues.

Theoretical Calculations. DFT (B3LYP) and 6-31G(d,p) basis set calculations were carried out to establish a better understanding of the spectral and magnetic findings obtained in a series of ***n*Per-CN** (see details in the Supporting Information). Limited by the computation capacity, the calculation was performed for only shorter derivatives, **Per-CN** up to tetramer **4Per-CN**. For the shortest oligomer **Per-CN**, a closed-shell structure was predicted as the ground state, agreeing with all experimental results (Figure S5 in the Supporting Information). The energy of the triplet state (TB) is higher by +16.36 kcal/mol than that of the singlet (closed shell (CS)/biradical (SB)) solutions. As it is expected, the open-shell SB states of **2Per-CN** obtained by using an unrestricted broken-symmetry wave function method (BS-UB3LYP/6-31G(d,p)) turned out to have the lowest energy than those of the corresponding CS and TB one, and the singlet−triplet energy gaps (ΔE_{SB-TB}) were estimated to be 0.755 kcal/mol, which is close to the experimental values (e.g., 0.342 kcal/mol for **2Per-CN**) (Figure S6 in the Supporting Information). From the structural point of views in **2Per-CN**, the energy of *trans*-isomer can be possibly considered as an energetic minimum geometry in the ground state. The small energy difference (0.377 kcal/mol) between the *trans*- and *cis*-forms leads us to consider that each geometry can be easily interconverted through free rotation of C−C bonds, which is consistent with the vibrational Raman observations (Figure S7 in the Supporting Information). Thus, the higher oligomeric ***n*Per-CN** ($n = 3-4$) were calculated as all *trans*-forms, which supported the ground-state singlet biradical structures with further smaller ΔE_{SB-TB} of 0.042 and 0.002 kcal/mol, respectively (Figures S8 and S9 in the Supporting Information). With decreasing distinct singlet−triplet energy gaps, it is noteworthy that the singlet biradical character (y) of ***n*Per-CN** ($n = 2-4$) estimated by the CASSCF(2,2)/6-31G calculation[28] gave larger LUMO occupation numbers of 0.85, 0.99, and 0.99, respectively. These larger (almost saturated: $0 < y < 1$) biradical characters for higher series are well consistent with the experimental observations of distinct magnetic susceptibility behaviors.

As in the investigation of the molecular geometries and the frontier molecular orbitals, a typical disjointed feature in the singly occupied molecular orbital (SOMO) profiles of the biradical species was found; the unpaired electrons (α and β) were mainly delocalized at the backbone of terminal rylene units bearing malononitrile groups (Figures S10−S12 in the Supporting Information). Accordingly, large spin densities on the terminal malononitrile-substituted rylene units in the ***n*Per-CN** are retained with antiparallel spin electron patterns (Figure 8). The electronic structure of **2Per-CN** in a ground state is

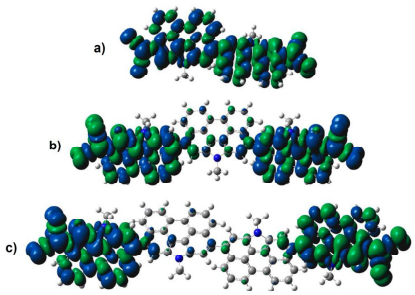

Figure 8. Calculated (UB3LYP) spin density distribution: (a) **2Per-CN**; (b) **3Per-CN**; and (c) **4Per-CN**. Blue and green surfaces represent α and β spin densities, respectively. Isovalue is 0.002.

thus best represented by the resonance of closed-shell Kekulé and biradical canonical forms as shown in Figure 1. Furthermore, this characteristic spin distribution pattern is found to be remarkable in the higher derivatives ($n > 3$), indicating that two terminal spin radicals are less electronic coupled due to the disruption of the effective π-bond character with the twisted orientations of rylene core units.

The fact of the larger singlet biradical character of ***n*Per-CN** would be also manifested by the bond elongations and dihedral angles between each perylene unit in the molecular structures. In comparison to the quinoidal **Per-CN** (Figure S5 in the Supporting Information), the singlet biradical **2Per-CN** and their higher ones showed longer bond lengths for the exo methylene bonds as the weakening of the C═C bonds was observed in vibrational studies. Upon an increase of the index *y*, dihedral angles of the singlet biradical ***n*Per-CN** between the NP cores are getting larger (55−64°) and close to that of the triplet biradical states (Figures S6, S8, S9 in the Supporting Information). Moreover, the determination of nucleus independent chemical shift (NICS) values[29] (e.g., NICS(1) and NICS(1)$_{zz}$) indicates more benzenoid character of the six-membered rings of the NP moieties in the singlet biradical species of ***n*Per-CN** as prolonging the molecular lengths (Figure S13 in the Supporting Information). These geometric findings suggest that the generation of aromaticity of rylene cores arising from biradical electronic structures would be one driving force to push the unpaired electrons out to the terminal edges of the molecules with breaking π bonds. In addition, the large strain arising from streric repulsion between the NP units in the quinoidal form can be partially released in the biradical form, which could be regarded as another importance driving force.

On the basis of the open-shell biradical nature of ***n*Per-CN** (n = 2−6), the characteristic low-lying excited states assigned by the admixing spin-associated (H, H → L, L) double excited electron configurations were identified by time-dependent BS-UB3LYP/6-31G(d,p) level calculations (Figure S14 in the Supporting Information). The lowest energy transitions ($S_0 \rightarrow S_1$) are 0.98 eV (1210 nm, f = 0.0012) for **2Per-CN**, 1.12 eV (1109 nm, f = 0.0028) for **3Per-CN**, and 1.10 eV (1128 nm, f = 0.1863) for **4Per-CN**, respectively. The smaller energy gaps are consistent with the larger biradical character of ***n*Per-CN**, because a HOMO−LUMO gap is closely related to the promotion of electrons from HOMO to LUMO. The other simulated transitions given by this UB3LYP method are consistent with the experimental spectra (Tables S1−S3 in the Supporting Information).

III. CONCLUSION

We have demonstrated an efficient method to prepare a series of soluble and stable extended benzoquinodimethanes oligomers ***n*Per-CN** (n = 1−6) with the conjugated benzoquinoid units longer than any other extended *p*-QDMs reported to date. Their electronic structure and geometry in the ground state were investigated by various experiments assisted by DFT calculations. Our results disclosed a clear chain-length dependence of the photophysical and electrochemical properties as well as magnetic properties. This series of molecules exhibited tunable ground-state structures, with **Per-CN** as a closed-shell hydrocarbon, **2Per-CN**−**4Per-CN** as open-shell singlet biradical species, and the higher order compounds **5Per-CN** and **6Per-CN** as triplet biradicals. Such a difference was caused by steric repulsion between the neighboring perylene units in the oligomers as well as the recovery of aromaticity of the quinoidal NP rings in the biradical forms, with the experimental evidence from Raman spectra and theoretical calculations. The unique nature of these oligomers in the ground state is responsive for the chain-length-dependent optical, electrochemical, and magnetic findings. Theoretical calculations helped to further understand the experimental observations. This series of compounds provide important information to understand the nature of chemical bonding and the fundamental chemical and physical phenomenon of largely extended quinoidal systems. Moreover, they are promising candidates for nonlinear optics, ambipolar field effect transistors, and organic spintronics due to their unique optical, electronic, and magnetic properties.

■ ASSOCIATED CONTENT

Supporting Information

Synthetic procedures and characterization data of all other new compounds. Details for all physical characterizations and theoretical calculations. Additional spectroscopic and computational data. This material is available free of charge via the Internet at http://pubs.acs.org.

■ AUTHOR INFORMATION

Corresponding Author

chmwuj@nus.edu.sg; dongho@yonsei.ac.kr; casado@uma.es; msedingj@nus.edu.sg

Notes

The authors declare no competing financial interest.

■ ACKNOWLEDGMENTS

J.W. acknowledges the financial support from the BMRC grant (10/1/21/19/642), MOE Tier 2 grant (MOE2011-T2-2-130), MINDEF-NUS JPP Program (MINDEF-NUS-JPP-12-02-05), and IMRE Core funding (IMRE/10-1P0509). The work at Yonsei University was supported by WCU (World Class University) programs (R32-2010-10217-0) and an AFSOR/APARD grant (no. FA2386-09-1-4092). The work at the University of Málaga was supported by the Ministerio de Educación y Ciencia (MEC) of Spain and by FEDER funds (project CTQ2009-10098 and to the Junta de Andalucía for the research project PO9-4708).

REFERENCES

(1) (a) Coulson, C. A.; Craig, D. P.; Maccoll, A.; Pullman, A. *Discuss. Faraday Soc.* **1947**, *2*, 36−38. (b) Szwarc, M. *Discuss. Fraraday Soc.* **1947**, *2*, 46−49. (c) Hush, N. S. *J. Polym. Sci.* **1952**, *11*, 289−298.

(2) (a) Thiele, J.; Balhorn, H. *Chem. Ber.* **1904**, *37*, 1463−1470. (b) Flynn, C. R.; Michl, J. *J. Am. Chem. Soc.* **1974**, *96*, 3280−3288.

(3) (a) Tschitschibabin, A. E. *Chem. Ber.* **1907**, *40*, 1810−1819. (b) Sloan, G. J.; Vaughan, W. R. *J. Org. Chem.* **1957**, *22*, 750−761. (c) Morozova, D. I.; Dyatkina, E. M. *Russ. Chem. Rev.* **1968**, *37*, 377−391. (d) Montgomery, L. K.; Huffman, J. C.; Jurczak, E. A.; Grendze, M. P. *J. Am. Chem. Soc.* **1986**, *108*, 6004−6011. (e) Porter, W. W., III; Vaid, T. P.; Rheingold, A. L. *J. Am. Chem. Soc.* **2005**, *127*, 16559−16566.

(4) Acker, D. S.; Hertler, W. R. *J. Am. Chem. Soc.* **1962**, *84*, 3370−3374.

(5) Maxfield, M.; Bloch, A. N.; Cowan, D. O. *J. Org. Chem.* **1985**, *50*, 1789−1796.

(6) (a) Hartzler, H. D. *J. Am. Chem. Soc.* **1964**, *86*, 2174−2175. (b) Addison, A. W.; Dalal, N. S.; Hoyano, Y.; Huizinga, S.; Weiler, L. *Can. J. Chem.* **1977**, *55*, 4191−4199.

(7) Casado, J.; Ortiz, R. P.; López Navarrete, J. T. *Chem. Soc. Rev.* **2012**, *41*, 5672−5686.

(8) (a) Gronowitz, S.; Uppström, B. *Acta Chem. Scand., Ser. B* **1974**, *28*, 981−985. (b) Suzuki, K.; Tomura, M.; Tanakaa, S.; Yamashita, Y. *Tetrahedron Lett.* **2000**, *41*, 8359−8364. (c) Fukushima, T.; Okazeri, N.; Miyashi, T.; Suzuki, K.; Yamashita, Y.; Suzuki, T. *Tetrahedron Lett.* **1999**, *40*, 1175−1178.

(9) (a) Pappenfus, T. M.; Chesterfield, R. J.; Frisbie, C. D.; Mann, K. R.; Casado, J.; Raff, J. D.; Miller, L. L. *J. Am. Chem. Soc.* **2002**, *124*, 4184−4185. (b) Chesterfield, R. J.; Newman, C. R.; Pappenfus, T. M.; Ewbank, P. C.; Haukaas, M. H.; Mann, K. R.; Miller, L. L.; Frisbie, C. D. *Adv. Mater.* **2003**, *15*, 1278−1282.

(10) (a) Takahashi, T.; Matsuoka, K. I.; Takimiya, K.; Otsubo, T.; Aso, Y. *J. Am. Chem. Soc.* **2005**, *127*, 8928−8929. (b) Ortiz, R. P.; Casado, J.; Gonzalez, S. R.; Hernandez, V.; Ortiz, R. P.; Casado, J.; Hernandez, V.; Navarrete, J. T. L.; Viruela, P. M.; Orti, E.; Takimiya, K.; Otsubo, T. *Angew. Chem., Int. Ed.* **2007**, *46*, 9057−9061.

(11) Sandman, D. J.; Garito, A. J. *J. Org. Chem.* **1974**, *39*, 1165−1166.

(12) Yanagimoto, T.; Takimiya, K.; Otsubo, T.; Ogura, F. *J. Chem. Soc., Chem. Commun.* **1993**, *6*, 519−520.

(13) (a) Chase, D. T.; Rose, B. D.; McClintock, S. P.; Zakharov, L. N.; Haley, M. M. *Angew. Chem., Int. Ed.* **2011**, *50*, 1127−1130. (b) Chase, D. T.; Fix, A. G.; Kang, S. J.; Rose, B. D.; Weber, C. D.; Zhong, Y.; Zakharov, L. N.; Lonergan, M. C.; Nuckolls, C.; Haley, M. M. *J. Am. Chem. Soc.* **2012**, *134*, 10349−10352.

(14) (a) Ohashi, K.; Kubo, T.; Masui, T.; Yamamoto, K.; Nakasuji, K.; Takui, T.; Kai, Y.; Murata, I. *J. Am. Chem. Soc.* **1998**, *120*, 2018−2027. (b) Kubo, T.; Sakamoto, M.; Akabane, M.; Fujiwara, Y.; Yamamoto, K.; Akita, M.; Inoue, K.; Takui, T.; Nakasuji, K. *Angew. Chem., Int. Ed.* **2004**, *43*, 7474−6479. (c) Kubo, T.; Shimizu, A.; Sakamoto, M.; Uruichi, M.; Yakushi, K.; Nakano, M.; Shiomi, D.; Sato, K.; Takui, T.; Morita, Y.; Nakasuji, K. *Angew. Chem., Int. Ed.* **2005**, *44*, 6564−6568. (d) Shimizu, A.; Uruichi, M.; Yakushi, K.; Matsuzaki, H.; Okamoto, H.; Nakano, M.; Hirao, Y.; Matsumoto, K.; Kurata, H.; Kubo, T. *Angew. Chem., Int. Ed.* **2009**, *48*, 5482−5486. (e) Shimizu, A.; Kubo, T.; Uruichi, M.; Yakushi, K.; Nakano, M.; Shiomi, D.; Sato, K.; Takui, T.; Hirao, Y.; Matsumoto, K.; Kurata, H.; Morita, Y.; Nakasuji, K. *J. Am. Chem. Soc.* **2010**, *132*, 14421−14428. (f) Shimizu, A.; Hirao, Y.; Matsumoto, K.; Kurata, H.; Kubo, T.; Uruichi, M.; Yakushi, K. *Chem. Commun.* **2012**, *48*, 5629−5631.

(15) (a) Sun, Z.; Ye, Q.; Chi, C.; Wu, J. *Chem. Soc. Rev.* **2012**, *41*, 7857−7889. (b) Umeda, R.; Hibi, D.; Miki, K.; Tobe, Y. *Org. Lett.* **2009**, *11*, 4104−4106. (c) Wu, T. C.; Chen, C. H.; Hibi, D.; Shimizu, A.; Tobe, Y.; Wu, Y. T. *Angew. Chem., Int. Ed.* **2010**, *49*, 7059−7062. (d) Sun, Z.; Huang, K.-W.; Wu, J. *Org. Lett.* **2010**, *12*, 4690−4693. (e) Sun, Z.; Huang, K.; Wu, J. *J. Am. Chem. Soc.* **2011**, *133*, 11896−11899. (f) Li, Y.; Heng, W.-K.; Lee, B. S.; Aratani, N.; Zafra, J. L.; Bao, N.; Lee, R.; Sung, Y. M.; Sun, Z.; Huang, K.-W.; Webster, R. D.; López Navarrete, J. T.; Kim, D.; Osuka, A.; Casada, J.; Ding, J.; Wu, J. *J. Am. Chem. Soc.* **2012**, *134*, 14913−14922.

(16) Kamada, K.; Ohta, K.; Kubo, T.; Shimizu, A.; Morita, Y.; Nakasuji, K.; Kishi, R.; Ohta, S.; Furukawa, S.-I.; Takahashi, H.; Nakano, M. *Angew. Chem., Int. Ed.* **2007**, *46*, 3544−3546.

(17) Chikamatsu, M.; Mikami, T.; Chisaka, J.; Yoshida, Y.; Azumi, R.; Yase, K. *Appl. Phys. Lett.* **2007**, *91*, 043506.

(18) Son, Y. W.; Cohen, M. L.; Louie, S. G. *Phys. Rev. Lett.* **2006**, *97*, 216803.

(19) Morita, Y.; Nishida, S.; Murata, T.; Moriguchi, M.; Ueda, A.; Satoh, M.; Arifuku, K.; Sato, K.; Takui, T. *Nat. Mater.* **2011**, *10*, 947−951.

(20) Zeng, Z.; Sung, Y.-M.; Bao, N.; Tan, D.; Lee, R.; Zafra, J.- L.; Lee, B.-S.; Ishida, M.; Ding, J.; López Navarrete, J.-T.; Li, Y.; Zeng, W.; Kim, D.-H.; Huang, K.-W.; Webster, R. D.; Casado, J.; Wu, J. *J. Am. Chem. Soc.* **2012**, *134*, 14513−14525.

(21) (a) Li, Y.; Wang, Z. *Org. Lett.* **2009**, *11*, 1385−1387. (b) Jiao, C.; Zhang, K.; Chi, C.; Wu, J. *Org. Lett.* **2009**, *11*, 4508−4511. (c) Jiao, C.; Huang, K.-W.; Guan, Z.; Xu, Q.-H.; Wu, J. *Org. Lett.* **2010**, *12*, 4046−4049. (d) Li, Y.; Gao, J.; Motta, S. I.; Negri, F.; Wang, Z. *J. Am. Chem. Soc.* **2010**, *132*, 4208−4213.

(22) Uno, M.; Seto, K.; Masuda, M.; Ueda, W.; Takahashi, S. *Tetrahedron Lett.* **1985**, *26*, 1553−1556.

(23) Bleaney, B.; Bowers, K. D. *Proc. R. Soc. London, Ser. A* **1952**, *214*, 451−465.

(24) (a) Casado, J.; Patchkovskii, S.; Zgierski, M. Z.; Hermosilla, L.; Sieiro, C.; Moreno Oliva, M.; López Navarrete, J. T. *Angew. Chem., Int. Ed.* **2008**, *47*, 1443−1446. (b) González, S. R.; Ie, Y.; Aso, Y.; López Navarrete, J. T.; Casado, J. *J. Am. Chem. Soc.* **2011**, *133*, 16350−16353.

(25) Zhu, L.; Jiao, C.; Xia, D.; Wu, J. *Tetrahedron Lett.* **2011**, *52*, 6411−6414.

(26) Zeng, W. D.; Lee, B. S.; Sung, Y. M.; Huang, K.-W.; Li, Y.; Kim, D.; Wu, J. *Chem. Commun.* **2012**, *48*, 7684−7686.

(27) Nakano, M.; Minami, T.; Yoneda, K.; Muhammad, S.; Kishi, R.; Shigeta, Y.; Kubo, T.; Rougier, L.; Champagne, B.; Kamada, K.; Ohta, K. *J. Phys. Chem. Lett.* **2011**, *2*, 1094−1101.

(28) Döýhnert, D.; Koutecký, J. *J. Am. Chem. Soc.* **1980**, *102*, 1789−1796.

(29) Chen, Z. F.; Wannere, C. S.; Corminboeuf, C.; Puchta, R.; Schleyer, P. V. *Chem. Rev.* **2005**, *105*, 3842−3888.

Biradicaloids

DOI: 10.1002/anie.201305348

Tetracyanoquaterrylene and Tetracyanohexarylenequinodimethanes with Tunable Ground States and Strong Near-Infrared Absorption**

Zebing Zeng, Sangsu Lee, José L. Zafra, Masatoshi Ishida, Xiaojian Zhu, Zhe Sun, Yong Ni, Richard D. Webster, Run-Wei Li, Juan T. López Navarrete, Chunyan Chi,* Jun Ding,* Juan Casado,* Dongho Kim,* and Jishan Wu**

Recently, there has been increasing interest in singlet open-shell polycyclic hydrocarbons,[1] which possess unique optical, electronic, and magnetic properties for potential applications in organic electronics,[2] non-linear optics,[3] spintronics,[4] and energy storage devices.[5] A general design is to embed a quinoidal unit such as *p*-quinodimethane (*p*-QDM), 2,6-naphthoquinodimethane and 2,6-anthraquinodimethane into a polycyclic hydrocarbon framework, and the obtained hydrocarbons can show a singlet biradical nature owing to the recovery of aromaticity of the proaromatic subunit and the spin-polarization at the terminal carbon atoms. With diverse synthetic approaches, numerous examples of this type of hydrocarbons, including bisphenalenyls,[6] indenofluorenes,[7] and zethrenes[8] have been developed as open-shell biradical species. In addition, zigzag-edged nanographenes, such as higher-order acenes,[9] periacenes,[10] and anthenes,[11] can show a singlet biradical ground state owing to the gain of additional aromatic sextet rings in the biradical form. Moreover, quinoidal hydrocarbons embedded with π-extended *p*-QDM structure,[12] quinoidal oligothiophenes,[13] and quinoidal porphyrins and its dimers[14] are intriguing in view of their unique chemical and physical properties.

We recently have synthesized a series of tetracyanooligo(*N*-annulated perylene (NP)) quinodimethanes (Per-CN and *n*Per-CN, $n = 2$–6, Figure 1) as soluble and stable π-extended *p*-QDMs.[15] The smallest member of this series, Per-CN, has a closed-shell quinoidal structure, while the longer oligomers all exhibit a ground-state biradicaloid character. The chain-length dependent physical properties (for example, magnetic, optical, electronic) lead us to prepare new oligomeric quinoidal derivatives containing fully fused NP units for a systematic investigation of the structural effect on the open-shell biradical nature of π-extended quinodimethanes. In this study, the tetracyanoquaterrylenequinodimethane (QR-CN)

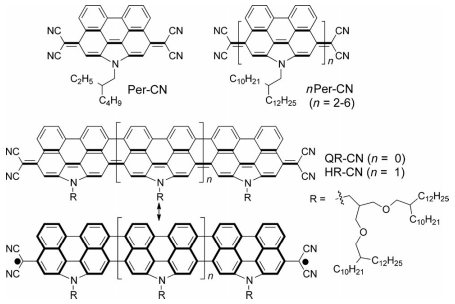

Figure 1. Chemical structures of Per-CN, *n*Per-CN, QR-CN, and the two resonance structures of HR-CN.

[*] Dr. Z. Zeng, Z. Sun, Y. Ni, Prof. C. Chi, Prof. J. Wu
Department of Chemistry, National University of Singapore
3 Science Drive 3, 117543, Singapore (Singapore)
E-mail: chmcc@nus.edu.sg
chmwuj@nus.edu.sg
S. Lee, Dr. M. Ishida, Prof. D. Kim
Department of Chemistry, Yonsei University
Seoul 120-749 (Korea)
E-mail: dongho@yonsei.ac.kr
J. L. Zafra, Prof. J. T. López Navarrete, Prof. J. Casado
Department of Physical Chemistry, University of Malaga
Campus de Teatinos s/n 229071 Malaga (Spain)
E-mail: teodomiro@uma.es
casado@uma.es
X. Zhu, Prof. R.-W. Li
Key Laboratory of Magnetic Materials and Devices
Ningbo Institute of Materials Technology and Engineering
Chinese Academy of Sciences, Ningbo 315201 (China)
Prof. R. D. Webster
Division of Chemistry & Biological Chemistry
School of Physical & Mathematical Sciences
Nanyang Technological University
21 Nanyang Link, 637371, Singapore (Singapore)
Prof. J. Ding
Department of Materials Science & Engineering
National University of Singapore, 119260 (Singapore)
E-mail: msedingj@nus.edu.sg
Prof. J. Wu
Institute of Materials Research and Engineering, A*STAR
3 Research Link, 117602, Singapore (Singapore)

[**] J.W. acknowledges the financial support from MOE Tier 2 grant (MOE2011-T2-2-130) and IMRE Core funding. The work at Yonsei Univ. was supported by WCU programs (R32-2010-10217-0) and an AFSOR/APARD grant (no. FA2386-09-1-4092). The work at Spain was supported by the Ministerio de Educación y Ciencia of Spain and by FEDER funds.

Supporting information for this article is available on the WWW under http://dx.doi.org/10.1002/anie.201305348.

and tetracyanohexarylenequinodimethane (HR-CN), with highly planar fused structures, were synthesized, and their ground-state electronic properties were investigated by various steady-state and time-resolved spectroscopic techniques and magnetic susceptibility measurements (Figure 1). Understanding the electronic structures of QR-CN and HR-CN would be of importance to extract information about the steric effect on the biradical resonance contribution by comparison with with non-fused derivatives (that is, 2Per-CN and 3Per-CN). The dihedral angles between the rylene units in *n*Per-CN were dependent on the distinct biradical character (*y*). Therefore the fully fused quinodimethane cores in QR-CN and HR-CR would be informative derivatives to evaluate the nature of chemical bonding characters. Furthermore, the rylene derivatives belong to an important family of organic dyes,[16] and therefore the largely extended π-conjugation in quinoidal QR-CN and HR-CN would result in a small energy gap, giving a strong electronic absorption in the near-infrared (NIR) region.

Synthesis of π-extended quinoidal rylenes horizontally longer than perylenes is still a challenging subject because of the intrinsic chemical instability. Furthermore, the intramolecular C–C bond formation between adjacent rylene units either by oxidative cyclodehydrogenation[16,17] or by base-mediated Michael addition followed by aromatization in air is a difficult step.[16,18] Our initial attempts of direct intramolecular cyclization of *n*Per-CN by using various oxidants (for example, $FeCl_3$ or DDQ/$Sc(OTf)_3$) or bases all gave complicated mixtures. Therefore, we have changed the strategy by using Takahashi cross-coupling[19] reaction of the pre-constructed *fused* quaterrylene (**9**) and hexarylene (**10**) dibromide precursors with maronontrile (Scheme 1). A highly branched aliphatic ether substituent at the *N*-position (for details of the synthesis, see the Supporting Information) was used to ensure sufficient solubility of both the intermediate compounds (**9** and **10**) and the final products.[20] The dibromo- NP dimer **5** and trimer **6** were prepared by stepwise coupling reactions starting from the monomer **1**. Bromination of **5** and **6** by NBS gave the dibromo- NP dimer **7** and trimer **8**, respectively, in high yields. The key intermediates **9** and **10** were successfully prepared by oxidative cyclodehydrogenation of the corresponding precursors **7** and **8** with DDQ/$Sc(OTf)_3$.[17,18] The absorption spectra of **9** and **10** are similar to those of the previously reported *N*-annulated quaterrylene[18] and hexarylene,[17] respectively (Supporting Information, Figure S1). The longer fused rylenes (for example, dibromooctarylene) were not obtained under the same conditions because of the difficulty in purification of the crude product (containing imcomplete reaction products). Subsequent Takahashi coupling of **9** and **10** with malononitrile followed by simultaneous oxidation in air afforded the desired products QR-CN and HR-CN. These products were carefully purified by column chromatography followed by preparative thin-layer chromatography. The purity of the final products was confirmed by high-resolution MALDI mass spectrometry and high performance liquid chromatography (see the Supporting Information).

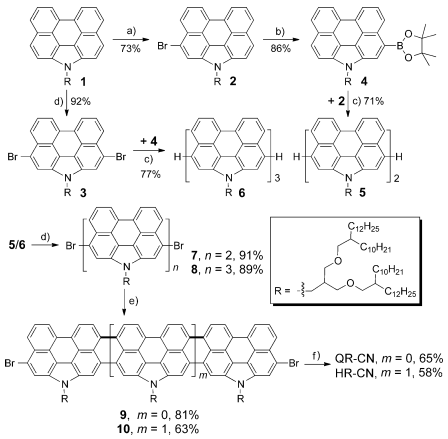

Scheme 1. Reagents and conditions: a) NBS (1 equiv), CH_2Cl_2, 0°C; b) pinacolborane, $[PdCl_2(PPh_3)_2]$, 1,2-dichloroethane/Et_3N, 90°C; c) $[Pd(PPh_3)_4]$, Cs_2CO_3, toluene/DMF, 90°C; d) NBS (2 equiv), CH_2Cl_2/DMF, 0–25°C; e) DDQ/$Sc(OTf)_3$, toluene, reflux; f) i) malononitrile, NaH, $[Pd(PPh_3)_2Cl_2]$, reflux; ii) HCl (2 M), 0–5°C.

The electronic structures of QR-CN and HR-CN were investigated by a combination of electron spin resonance (ESR), a superconducting quantum interference device (SQUID), and Raman spectroscopy as well as the density functional theory (DFT) calculations. The solid-state EPR spectra of QR-CN exhibited no active signals, though no clear ^{1}H NMR spectrum of QR-CN was obtained, which is presumably due to the strong aggregation in solution. This implies a closed-shell ground state structure of QR-CN. In contrast, a broad ESR signal with a *g*-tensor of $g_e = 2.0029$ recorded at 153 K suggested an existence of open-shell species in HR-CN, as seen in the non-fused 3Per-CN (Supporting Information, Figure S2).[15] Accordingly, the temperature-dependent magnetic susceptibility behaviors of HR-CN (5-380 K) obtained by SQUID measurements revealed that HR-CN has a singlet biradical electronic structure in the ground state (Supporting Information, Figure S3). Upon careful fitting of the plots by using the Bleaney–Bowers equation,[21] the exchange interaction, $2J/k_B$ was estimated to be −2120 K. The singlet–triplet energy gap ($\Delta E_{SB\text{-}TB}$) of about 4.21 kcal mol^{-1} was found to be significantly larger than that of 3Per-CN (0.107 kcal mol^{-1}).

To get further insights on the shape of the electronic ground state, resonant Raman spectra[12,13c,15,22] were recorded for Per-CN, QR-CN, and HR-CN (Figure 2 A) with laser excitations at 532, 785, and 1064 nm, respectively, which coincide with their most intense Vis-NIR electronic absorptions in Figure 3. The most intense bands of Per-CN (1705, 1594, and 1458 cm^{-1}) are typical markers for closed-shell quinoidal structure. On passing to QR-CN, some of these Raman bands experience a simultaneous frequency downshift and splitting, that is, the 1705 and 1594 cm^{-1} bands evolved into the 1700/1659 cm^{-1} and 1582/1566 cm^{-1} pairs, respectively. At the same time, two new bands appeared at 1536 and

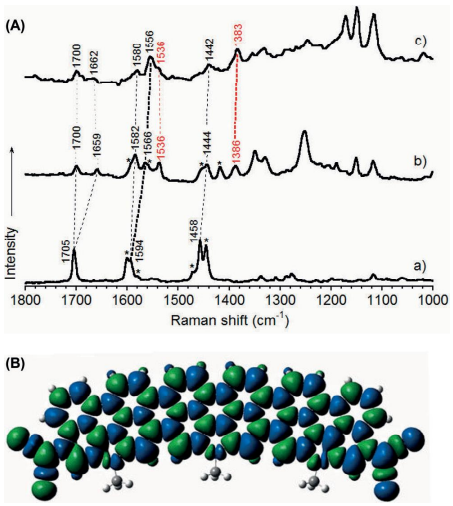

Figure 2. A) Solid-state resonant Raman spectra of a) Per-CN (λ_{exc} = 532 nm), b) QR-CN (λ_{exc} = 785 nm), and c) HR-CN (λ_{exc} = 1064 nm). Asterisks denote bands that do not change within the series. B) Calculated (UCAM-B3LYP/6-31G(d,p)) spin-density distribution of HR-CN (singlet biradical, the methyl group was used for the N-subsitutents); the blue and green surfaces represent α and β spin densities, respectively.

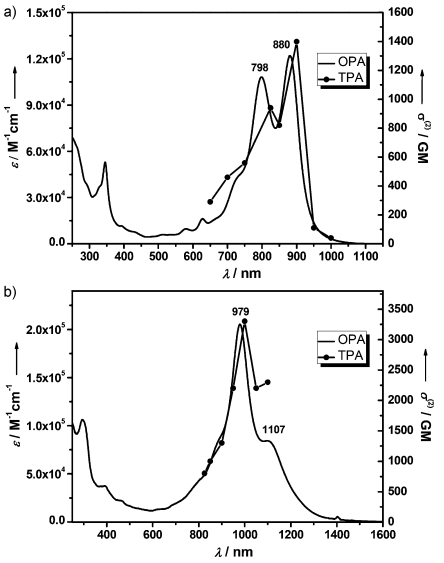

Figure 3. OPA spectra (left vertical axis) and TPA spectra (right vertical axis) of (a) QR-CN and (b) HR-CN in toluene. TPA spectra are plotted at $\lambda_{ex}/2$.

1386 cm^{-1}, which are likely associated with the new bonds planarizing the NP units. The frequency downshift of the ν_s(C=C) modes might result from: 1) increased conjugation that is due to the increment of π-electrons, which relaxes the bond length alternation path; and 2) an aromatization of the quinoidal benzenes owing to the gaining of biradical character which also weakens the inter-rylene CC bonds. On passing to HR-CN, the most intense Raman bands are those at 1556 cm^{-1} (1594 cm^{-1} in Per-CN and 1566 cm^{-1} in QR-CN) and at 1383 cm^{-1} (1386 cm^{-1} in QR-CN), the latter revealing a further weakening of the inter-rylene C–C bonds upon QR-CN→HR-CN. The bands at 1386 cm^{-1} and 1383 cm^{-1} in QR-CN and HR-CN are related with those at 1378 cm^{-1} in 2Per-CN and 1343 cm^{-1} in 3Per-CN. We have interpreted the frequencies of these Raman modes as indicative of a medium open-shell character for 2Per-CN and a large open-shell character for 3Per-CN both with a singlet biradical ground state.[15] This comparison reveals that: 1) QR-CN and HR-CN both have singlet ground electronic states; and 2) the relative weights of the open-shell property are expressed as follows: QR-CN < 2Per-CN, HR-CN < 3Per-CN, and HR-CN ≤ 2Per-CN. Summing up, HR-CN has a higher singlet open-shell character than QR-CN but still moderate and not comparable to that of 3Per-CN. This spectroscopic finding can be interpreted in terms of double-spin polarization, which favors the singlet open-shell form versus the triplet owing to preferred conjugation of the unpaired electrons in the singlet format, which causes an enlargement of the singlet–triplet energy gap. In our case, the planar structure of the oligorylene would certainly favor conjugation, which would enlarge the singlet–triplet gap and reduce the open-shell character. In contrast, for 2Per-CN and 3Per-CN, the large steric repulsion between the NP units drives the molecules into a much more accentuated open-shell biradical state.

On the basis of these experimental findings, unrestricted broken-symmetry DFT (UCAM-B3LYP/6-31G(d,p)) calculations were carried out for a better understanding of the ground state of open-shell HR-CN. The optimized geometry of HR-CN demonstrated the highly planar core with a curved quinoidal backbone restricted by *N*-fusion of five-membered rings (Supporting Information, Figure S4). The molecular orbital profiles of the singlet biradical state of HR-CN exhibit a characteristic disjoint feature as seen in the singlet biradical molecules.[12,13c,15,22] The spin electrons are delocalized over the whole π-framework (Figure 2B; Supporting Information, Figure S5). The theoretically predicted singlet–triplet energy gap ($\Delta E_{SB\text{-}TB}$) is 6.02 kcal mol^{-1}, which is well correlated with the experimentally determined value (see above).[23] The singlet biradical character (y) of HR-CN was determined to be 0.064 by using CASSCF(2.2)/6-31G calculation. Compared to that of non-fused 3Per-CN, the fact that HR-CN has a larger singlet–triplet energy gap and a smaller biradical index indicates the core geometry should be responsible for the degree of biradical nature. The dihedral angle between the rylene cores would be one of the critical factors for fine-

tuning the electronic configuration of quinoidal molecules. The restricted CAM-B3LYP calculation for QR-CN and Per-CN produced the similar planar geometries to that of HR-CN. Analyses on the calculated bond lengths and the nucleus independent chemical shift (NICS) values (for example, NICS(1) and NICS(1)$_{zz}$) reveal that more aromatic benzenoid characters of the six-membered rings of the rylene moieties are seen as prolonging the molecular lengths from Per-CN, QR-CN to HR-CN (Supporting Information, Figures S6 and S7). This feature supports that the recovery of the aromaticity is the major driving force for the increased singlet biradical character.

Along with the different electronic structures, the characteristic optical properties of the fused quinoidal rylenes were realized in the one-photon absorption (OPA) and two-photon absorption (TPA) spectra of QR-CN and HR-CN (Figure 3). QR-CN has a green color in dichromethane solution, and its absorption spectrum revealed quite similar spectral feature to that of Per-CN but showed a remarkable red-shit of the band (approximately 254 nm) with a drastic increase of the extinction coefficient ($\varepsilon = 1.2 \times 10^5\,L\,mol^{-1}\,cm^{-1}$ for QR-CN and $6.6 \times 10^4\,L\,mol^{-1}\,cm^{-1}$ for Per-CN). This supports the notion that QR-CN has a closed-shell quinoidal structure in the ground state, the same as Per-CN. The time-dependent (TD) DFT stick spectra of closed shell QR-CN and Per-CN are consistent with this conclusion (Supporting Information, Figure S8). In a sharp contrast, the OPA spectrum of HR-CN displays characteristic optical features; the intense band at 979 nm ($\varepsilon = 2.1 \times 10^5\,L\,mol^{-1}\,cm^{-1}$) together with a shoulder at longer wavelength (1107 nm) was observed. The narrower optical HOMO–LUMO gap was estimated to be 0.97 eV, and the lowest energy absorption band structures were identified by TD-DFT calculation approach as admixing the doubly excited electronic configuration $^1\Phi_{H,H\rightarrow L,L}$ into the ground state (Supporting Information, Figure S8).[24] This result is consistent with that HR-CN is a ground singlet biradical species. It is also worthy to note that due to negligible absorption in the visible region (400–700 nm), HR-CN is almost colorless in solution, thus it represents a rare organic dye with very strong NIR absorption but transparent in visible spectral window. This finding would meet up with the technological applications, such as for security printing.

The excited electronic properties of fused quinoids, QR-CN and HR-CN, were analyzed by time-resolved optical spectroscopy. Interestingly, the singlet excited lifetimes of the series of quinoids were found to increase upon extension of the rylene cores (Per-CN (17 ps)[15] < QR-CN (24 ps) < HR-CN (29 ps)) by femtosecond transient absorption measurement, albeit their larger molecular sizes (Supporting Information, Figure S9). This is an opposite trend to those of Per-CN species, which may imply that the recovery of the aromatic rylene cores especially in HR-CN would contribute to their excited state dynamics.

The intermediate singlet biradical character ($0 < y < 1$) is known as a diagnostic parameter that enhances nonlinear optical responses in open-shell biradical molecules.[3] The two-photon absorption (TPA) measurements for Per-CN, QR-CN, and HR-CN were conducted in toluene in the NIR region from 1300 to 2200 nm where one-photon absorption contribution is negligible (Figure 3; Supporting Information, Figure S10). QR-CN exhibited a $\sigma^{(2)}{}_{max} = 1400$ GM at 1800 nm which is slightly larger than Per-CN ($\sigma^{(2)}{}_{max} = 1300$ GM at 1200 nm). In particular, the significantly larger value of $\sigma^{(2)}{}_{max} = 3300$ GM excited at 2000 nm for HR-CN was observed compared to that of 3Per-CN ($\sigma^{(2)}{}_{max} = 770$ GM)[15] despite smaller singlet indices of 0.06 for HR-CN (vs 0.99 for 3Per-CN). This could be due to the extended conjugation induced by increased rigidity of HR-CN, which greatly enhances the second hyperpolarizability and improves the third-order optical nonlinearity including the TPA performance.[25]

QR-CN showed amphoteric redox behavior with three oxidation processes at $E_{1/2}{}^{ox} = 0.18$, 0.36, 0.84 V and four reduction waves at $E_{1/2}{}^{red} = -0.87$, −0.97, −1.50, −2.15 V (*vs* Fc/Fc^+, Fc = ferrocene) in cyclic voltammetry and differential pulse voltammetry experiments (Supporting Information, Figure S11). In contrast, Per-CN does not show any detectable oxidation waves,[15] indicating that the larger extended π system in QR-CN can stabilize multiple positive/negative charges. The HOMO and LUMO energy levels were determined to be −4.83 and −4.03 eV, respectively, from the onset potentials of the first oxidation and reduction waves. Unfortunately, HR-CN did not exhibit the well-resolved redox waves possibly due to intrinsically strong π–π stacking between the highly planar hexarylene cores.

In summary, two new soluble and stable quinoidal rylene molecules QR-CN and HR-CN were successfully prepared. With extension of the rylene core size, the ground state electronic structures of these quinoidal derivatives are changed from a closed-shell singlet for Per-CN and QR-CN to an open-shell singlet biradical for HR-CN. As being different from the non-fused oligomeric rylenes (that is, 2Per-CN and 3Per-CN), QR-CN and HR-CN showed very strong OPA and TPA response in the NIR range owing to the extended π-conjugation as well as the appropriate singlet biradical character. Our research demonstrated that stable, highly extended quinoidal polycyclic hydrocarbons can be achieved by rational design and appropriate synthetic strategy, which leads to new opportunities to develop new NIR chromophores and semiconductors for photonics, electronics and spintronics.

Received: June 21, 2013
Published online: July 23, 2013

Keywords: biradicaloids · hexarylene · near-infrared dyes · polycyclic hydrocarbons · quaterrylene

[1] a) C. Lambert, *Angew. Chem.* **2011**, *123*, 1794 – 1796; *Angew. Chem. Int. Ed.* **2011**, *50*, 1756 – 1758; b) Y. Morita, K. Suzuki, S. Sato, T. Takui, *Nat. Chem.* **2011**, *3*, 197 – 204; c) Z. Sun, Q. Ye, C. Chi, J. Wu, *Chem. Soc. Rev.* **2012**, *41*, 7857 – 7889; d) A. Shimizu, Y. Hirao, T. Kubo, M. Nakano, E. Botek, B. Champagne, *AIP Conf. Proc.* **2012**, *1504*, 399 – 405.

[2] a) M. Chikamatsu, T. Mikami, J. Chisaka, Y. Yoshida, R. Azumi, K. Yase, *Appl. Phys. Lett.* **2007**, *91*, 043506; b) D. T. Chase, A. G. Fix, S. J. Kang, B. D. Rose, C. D. Weber, Y. Zhong, L. N.

Zakharov, M. C. Lonergan, C. Nuckolls, M. M. Haley, *J. Am. Chem. Soc.* **2012**, *134*, 10349 – 10352.
[3] K. Kamada, K. Ohta, T. Kubo, A. Shimizu, Y. Morita, K. Nakasuji, R. Kishi, S. Ohta, S. I. Furukawa, H. Takahashi, M. Nakano, *Angew. Chem.* **2007**, *119*, 3614 – 3616; *Angew. Chem. Int. Ed.* **2007**, *46*, 3544 – 3546.
[4] Y. W. Son, M. L. Cohen, S. G. Louie, *Phys. Rev. Lett.* **2006**, *97*, 216803.
[5] Y. Morita, S. Nishida, T. Murata, M. Moriguchi, A. Ueda, M. Satoh, K. Arifuku, K. Sato, T. Takui, *Nat. Mater.* **2011**, *10*, 947 – 951.
[6] a) K. Ohashi, T. Kubo, T. Masui, K. Yamamoto, K. Nakasuji, T. Takui, Y. Kai, I. Murata, *J. Am. Chem. Soc.* **1998**, *120*, 2018 – 2027; b) T. Kubo, M. Sakamoto, M. Akabane, Y. Fujiwara, K. Yamamoto, M. Akita, K. Inoue, T. Takui, K. Nakasuji, *Angew. Chem.* **2004**, *116*, 6636 – 6641; *Angew. Chem. Int. Ed.* **2004**, *43*, 6474 – 6479; c) A. Shimizu, T. Kubo, M. Uruichi, K. Yakushi, M. Nakano, D. Shiomi, K. Sato, T. Takui, Y. Hirao, K. Matsumoto, H. Kurata, Y. Morita, K. Nakasuji, *J. Am. Chem. Soc.* **2010**, *132*, 14421 – 14428; d) A. Shimizu, Y. Hirao, K. Matsumoto, H. Kurata, T. Kubo, M. Uruichi, K. Yakushi, *Chem. Commun.* **2012**, *48*, 5629 – 5631.
[7] a) D. T. Chase, B. D. Rose, S. P. McClintock, L. N. Zakharov, M. M. Haley, *Angew. Chem.* **2011**, *123*, 1159 – 1162; *Angew. Chem. Int. Ed.* **2011**, *50*, 1127 – 1130; b) A. Shimizu, R. Kishi, M. Nakano, D. Shiomi, K. Sato, T. Takui, I. Hisaki, M. Miyata, Y. Tobe, *Angew. Chem.* **2013**, *125*, 6192 – 6195; *Angew. Chem. Int. Ed.* **2013**, *52*, 6076 – 6079.
[8] a) R. Umeda, D. Hibi, K. Miki, Y. Tobe, *Org. Lett.* **2009**, *11*, 4104 – 4106; b) T. C. Wu, C. H. Chen, D. Hibi, A. Shimizu, Y. Tobe, Y. T. Wu, *Angew. Chem.* **2010**, *122*, 7213 – 7216; *Angew. Chem. Int. Ed.* **2010**, *49*, 7059 – 7062; c) Z. Sun, K.-W. Huang, J. Wu, *Org. Lett.* **2010**, *12*, 4690 – 4693; d) Z. Sun, K.-W. Huang, J. Wu, *J. Am. Chem. Soc.* **2011**, *133*, 11896 – 11899; e) Y. Li, W.-K. Heng, B. S. Lee, N. Aratani, J. L. Zafra, N. Bao, R. Lee, Y. M. Sung, Z. Sun, K.-W. Huang, R. D. Webster, J. T. López Navarrete, D. Kim, A. Osuka, J. Casada, J. Ding, J. Wu, *J. Am. Chem. Soc.* **2012**, *134*, 14913 – 14922.
[9] M. Bendikov, H. M. Duong, K. Starkey, K. N. Houk, E. A. Carter, F. Wudl, *J. Am. Chem. Soc.* **2004**, *126*, 7416 – 7417.
[10] D. E. Jiang, B. G. Sumpter, S. Dai, *J. Chem. Phys.* **2007**, *127*, 124703.
[11] a) A. Konishi, Y. Hirao, M. Nakano, A. Shimizu, E. Botek, B. Champagne, D. Shiomi, K. Sato, T. Takui, K. Matsumoto, H. Kurata, T. Kubo, *J. Am. Chem. Soc.* **2010**, *132*, 11021 – 11023; b) A. Konishi, Y. Hirao, K. Matsumoto, H. Kurata, R. Kishi, Y. Shigeta, M. Nakano, K. Tokunaga, K. Kamada, T. Kubo, *J. Am. Chem. Soc.* **2013**, *135*, 1430 – 1437.
[12] a) Z. Zeng, Y. M. Sung, N. Bao, D. Tan, R. Lee, J. L. Zafra, B. S. Lee, M. Ishida, J. Ding, J. T. López Navarrete, Y. Li, W. Zeng, D. Kim, K.-W. Huang, R. D. Webster, J. Casado, J. Wu, *J. Am. Chem. Soc.* **2012**, *134*, 14513 – 14525; b) X. Zhu, H. Tsuji, K. Nakabayashi, S. Ohkoshi, E. Nakamura, *J. Am. Chem. Soc.* **2011**, *133*, 16342 – 16345.
[13] a) J. Casado, R. P. Ortiz, J. T. López Navarrete, *Chem. Soc. Rev.* **2012**, *41*, 5672 – 5686; b) T. Takahashi, K. I. Matsuoka, K. Takimiya, T. Otsubo, Y. Aso, *J. Am. Chem. Soc.* **2005**, *127*, 8928 – 8929; c) R. P. Ortiz, J. Casado, V. Hernandez, J. T. López Navarrete, P. M. Viruela, E. Orti, K. Takimiya, T. Otsubo, *Angew. Chem.* **2007**, *119*, 9215 – 9219; *Angew. Chem. Int. Ed.* **2007**, *46*, 9057 – 9061.
[14] a) I. M. Blake, H. L. Anderson, D. Beljonne, J. L. Brédas, W. Clegg, *J. Am. Chem. Soc.* **1998**, *120*, 10764 – 10765; b) I. M. Blake, A. Krivokapic, M. Katterle, H. L. Anderson, *Chem. Commun.* **2002**, 1662 – 1663; c) W. D. Zeng, B. S. Lee, Y. M. Sung, K.-W. Huang, Y. Li, D. Kim, J. Wu, *Chem. Commun.* **2012**, *48*, 7684 – 7686.
[15] Z. Zeng, M. Ishida, J. L. Zafra, X. Zhu, Y. M. Sung, N. Bao, R. D. Webster, B. S. Lee, R.-W. Li, W. Zeng, Y. Li, C. Chi, J. T. López Navarrete, J. Ding, J. Casado, D. Kim, J. Wu, *J. Am. Chem. Soc.* **2013**, *135*, 6363 – 6371.
[16] a) T. Weil, T. Vosch, J. Hofkens, K. Peneva, K. Müllen, *Angew. Chem.* **2010**, *122*, 9252 – 9278; *Angew. Chem. Int. Ed.* **2010**, *49*, 9068 – 9093; b) N. G. Pschirer, C. Kohl, F. Nolde, J. Qu, K. Müllen, *Angew. Chem.* **2006**, *118*, 1429 – 1432; *Angew. Chem. Int. Ed.* **2006**, *45*, 1401 – 1404.
[17] Y. Li, J. Gao, S. D. Motta, F. Negri, Z. Wang, *J. Am. Chem. Soc.* **2010**, *132*, 4208 – 4213.
[18] C. Jiao, K.-W. Huang, J. Luo, J. Wu, *Org. Lett.* **2009**, *11*, 4508 – 4511.
[19] M. Uno, K. Seto, M. Masuda, W. Ueda, S. Takahashi, *Tetrahedron Lett.* **1985**, *26*, 1553 – 1556.
[20] An analogue of **9** with the *N*-2-decyltetradecyl substitution (same as the *n*Per-CN) showed much less solubility, which hampered the subsequent Takahashi coupling reaction.
[21] B. Bleaney, K. D. Bowers, *Proc. R. Soc. London Ser. A* **1952**, *214*, 451 – 465.
[22] a) J. Casado, S. Patchkovskii, M. Z. Zgierski, L. Hermosilla, C. Sieiro, M. M. Oliva, J. T. López Navarrete, *Angew. Chem.* **2008**, *120*, 1465 – 1468; b) *Angew. Chem. Int. Ed.* **2008**, *47*, 1443 – 1446; S. R. González, Y. Ie, Y. Aso, J. T. López Navarrete, J. Casado, *J. Am. Chem. Soc.* **2011**, *133*, 16350 – 16353.
[23] The relatively larger energy difference (ca. 2 kcal mol^{-1}) between the calculation and experimental values can be ascribed to the wavefunctional contribution by the overestimation for a larger π-conjugated open-shell system as well as the technical fitting errors resulting from the smaller magnetic susceptibility signal in the SQUID measurement.
[24] S. Di Motta, F. Negri, D. Fazzi, C. Castiglioni, E. V. Canesi, *J. Phys. Chem. Lett.* **2010**, *1*, 3334 – 3339.
[25] K. S. Kim, J. M. Lim, A. Osuka, D. Kim, *J. Photochem. Photobiol. C* **2008**, *9*, 13 – 28.

Chemical Science

EDGE ARTICLE

View Article Online
View Journal

Turning on the biradical state of tetracyano-perylene and quaterrylenequinodimethanes by incorporation of additional thiophene rings†

Cite this: DOI: 10.1039/c4sc00659c

Zebing Zeng,[a] Sangsu Lee,[b] José L. Zafra,[c] Masatoshi Ishida,[b] Nina Bao,[d] Richard D. Webster,[e] Juan T. López Navarrete,*[c] Jun Ding,*[d] Juan Casado,*[c] Dongho Kim*[b] and Jishan Wu*[af]

Received 3rd March 2014
Accepted 5th April 2014

DOI: 10.1039/c4sc00659c

www.rsc.org/chemicalscience

Polycyclic hydrocarbon with a singlet biradical ground state has recently become a hot topic among various studies on π-conjugated systems and it is of importance to understand the fundamental structure–biradical character–physical properties relationship. In this work, we found that after incorporation of two additional thiophene rings into the closed-shell tetracyano-perylene (**Per-CN**) and quaterrylenequinodimethanes (**QR-CN**), the obtained new quinoidal compounds **QDTP** and **QDTQ** became a singlet biradical in the ground state due to the recovery of aromaticity of the thiophene rings in the biradical form and additional steric repulsion between the thiophene rings and the rylene unit. The ground state geometries and electronic structures of **QDTP** and **QDTQ** were systematically studied by variable-temperature nuclear magnetic resonance, electron spin resonance, superconducting quantum interference device measurements and FT Raman spectroscopy, assisted by density functional theory calculations. Both compounds were found to be a singlet biradical in the ground state with a small singlet–triplet energy gap and the biradical character was enlarged by elongation of the π-conjugation length. Strong one-photon absorption and large two-photon absorption cross-sections were observed for both compounds in the near-infrared region. Our studies demonstrated that a slight structural modification could significantly change the ground state and the electronic, optical and magnetic properties of a pro-aromatic π-conjugated system, and finally lead to new materials with unique properties.

Introduction

Recently, polycyclic hydrocarbons (PHs) with a singlet biradical ground state[1] have attracted much attention due to their unique optical, electronic and magnetic properties and promising applications for non-linear optics,[2] molecular electronics,[3] organic photovoltaics,[4] organic spintronics[5] and energy storage devices.[6] A fundamental reason for the appearance of a singlet biradical ground state can be ascribed to the gain of additional aromatic sextet rings in the biradical form in comparison to the closed-shell form. Good examples are Kubo's teranthene and quarteranthene molecules in which three and four additional aromatic sextet rings are obtained in the respective biradical forms, which can compensate the energy required to break an sp^2–sp^2 double bond.[7] Other examples are quinoidal hydrocarbons including indenofluorenes,[8] bis(phenalenyls)[9] and zethrenes,[10] in which a pro-aromatic quinodimethane unit such as *p*-quinoidimethane (*p*-QDM), 2,6-naphthoquinodimethane and 2,6-anthraquinodimethane is embedded into an aromatic framework. In addition, extended *p*-QDMs[11] and their thiophene analogs[12] with chain-length dependent ground states were recently reported. For example, our group has synthesized a series of tetracyano-oligo(*N*-annulated perylene (NP))quinodimethanes (**Per-CN** and ***n*Per-CN**, n = 2–6, Fig. 1).[11a] It was found that the monomer **Per-CN** has a closed-shell ground state while all of the higher oligomers ***n*Per-CN**s have a biradical ground state, and the steric repulsion between the NP units serves as the major driving force to rupture the quinoidal structure into a biradical configuration. When the two NP units in **2Per-CN** are fused together, the obtained

[a]Department of Chemistry, National University of Singapore, Science Drive 3, 117543, Singapore. E-mail: chmwuj@nus.edu.sg; Fax: +65-67791691; Tel: +65-65162677
[b]Spectroscopy Laboratory for Functional π-Electronic Systems and Department of Chemistry, Yonsei University, Seoul 120-749, Korea. E-mail: dongho@yonsei.ac.kr
[c]Department of Physical Chemistry, University of Malaga, Campus de Teatinos s/n, 229071 Malaga, Spain. E-mail: casado@uma.es; teodomiro@uma.es
[d]Department of Materials Science & Engineering, National University of Singapore, 119260, Singapore. E-mail: msedingj@nus.edu.sg
[e]Division of Chemistry & Biological Chemistry, School of Physical & Mathematical Sciences, Nanyang Technological University, 21 Nanyang Link, 637371, Singapore
[f]Institute of Materials Research and Engineering, A*STAR, 3 Research Link, 117602, Singapore

† Electronic supplementary information (ESI) available: Synthetic procedures and characterization data of all other new compounds. Details for all physical characterizations and theoretical calculations. Additional spectroscopic and computational data. See DOI: 10.1039/c4sc00659c

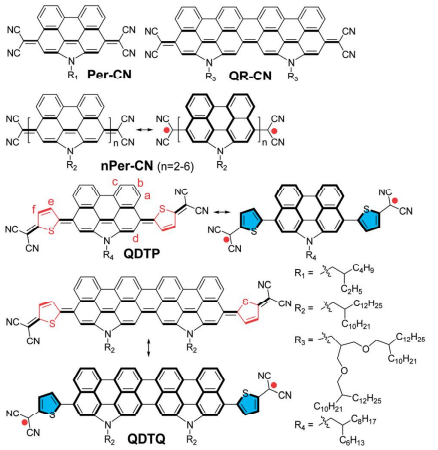

Fig. 1 Chemical and resonance structures of Per-CN, *n*Per-CNs, QR-CN, QDTP and QDTQ.

tetracyano-quaterrylenequinodimethane **QR-CN** (Fig. 1) becomes a closed-shell quinoid in the ground state due to the efficient double spin polarization through a planarized quaterrylene framework.[11b]

In principle, the closed-shell **Per-CN** and **QR-CN** can be also drawn in an open-shell biradical form similar to ***n*Per-CNs**, and then the particular questions arise: (1) how to turn on their biradical state, and (2) what are the differences between their physical properties under different ground states? Answers to these questions will help us to understand the fundamental *structure–biradical character–physical properties* relationship and thereby enable a tailored design. We expected that incorporation of a thiophene ring between the dicyanomethane moiety and the NP unit may significantly increase the biradical character of the molecules due to the recovery of the aromaticity of the quinoidal thiophene in the biradical form (Fig. 1). The thiophene ring was chosen rather than the benzene ring due to the synthetic feasibility for the former (*vide infra*). To validate this assumption, quinoidal perylene **QDTP** and quaterrylene **QDTQ** containing two thiophene units were designed and synthesized (Fig. 1). Their geometries and electronic structures in the ground state were systematically investigated by variable-temperature nuclear magnetic resonance (VT-NMR), electron spin resonance (ESR), superconducting quantum interference device (SQUID) measurements and FT Raman spectroscopy, assisted by density functional theory (DFT) calculations. Their physical properties were studied by steady-state and transient absorption (TA) spectroscopy, two-photon absorption (TPA) and cyclic voltammetry. Our studies revealed that both **QDTP** and **QDTQ** showed a singlet biradical ground state with very different physical properties from those of **Per-CN** and **QR-CN**.

Results and discussion

Synthesis

As shown in Scheme 1, the target compounds **QDTP** and **QDTQ** were prepared by Takahashi coupling[13] from the corresponding dibromo-dithienoperylene **3** and dibromo-dithienoquaterrylene **7**, followed by oxidative dehydrogenation. Firstly, two thiophene units were attached to the active *peri*-position of NP by a two-fold Stille coupling reaction between the dibromo-NP **1** and tributyl-(thiophen-2-yl)stannane to give the dithienoperylene **2** in 75% yield (Scheme 1). Compared to the simple monomer **Per-CN**, longer branched aliphatic chain (R_4, 2-hexyldecyl) was introduced to surmount the solubility problem for the subsequent synthetic steps. Bromination of compound **2** with two equiv. *N*-bromosuccinimide (NBS) afforded the key intermediate **3** in 87% yield. Takahashi coupling reaction of **3** with malononitrile gave the crude precursor, which was partially dehydrogenated in the air. Subsequent oxidation of the crude product by a catalytic amount of *p*-chloranil in acetonitrile resulted in immediate precipitation of the target compound **QDTP** from the mixture, which was further carefully purified by silica gel column chromatography.

The synthesis of the more extended dithienoquaterrylenequinodimethane **QDTQ** is challenging because a fused quaterrylene framework has to be built up first. Our previous attempts to conduct direct intramolecular oxidative cyclodehydrogenation of the dibromo-NP dimer **4** carrying two 2-decyltetradecyl substituents (R_2 in Fig. 1) gave an insoluble mixture due to the strong π–π stacking of the obtained quaterrylene molecules, which hampered the subsequent coupling reactions.[11b] Therefore, a highly branched alkyl ether group (R_3, Fig. 1) has to be used. In this study, we fortunately found that the dibromo-dithieno-NP dimer **6** with the 2-decyltetradecyl chains can be successfully cyclodehydrogenated by using 2,3-dichloro-5,6-dicyano-1,4-benzoquinone (DDQ) and $Sc(OTf)_3$ and afforded the key intermediate **7**, which is soluble in common organic solvents and possesses an absorption spectrum similar to the previously reported bis-*N*-annulated quaterrylene[14] (Fig. S1 in the ESI†). The good solubility of **7** can be explained by the existence of large torsional angle between the thiophene ring and the quaterrylene unit which partially suppresses the π–π stacking and thus there is no need to introduce the synthetically demanding R_3 substituents. The intermediate **6** was prepared by a similar Stille coupling-followed-by-bromination sequence starting from the dibromo-NP dimer **4**.[11a] Compound **7** was then converted into the target compound **QDTQ** by similar Takahashi coupling followed by spontaneous oxidation in air without the need to use additional oxidants such as *p*-chloranil. Both **QDTP** and **QDTQ** are soluble in common solvents such as chloroform, toluene and THF. These deeply coloured products are stable in both solid state and in solution, except that **QDTQ** partially decomposed on a silica gel column, which prevented us from separating even longer homologs. The high-resolution mass spectra (MALDI-TOF) agreed well with their corresponding molecular weight, and the purity of the final products was further confirmed by high performance liquid chromatography and elemental analysis (see ESI†).

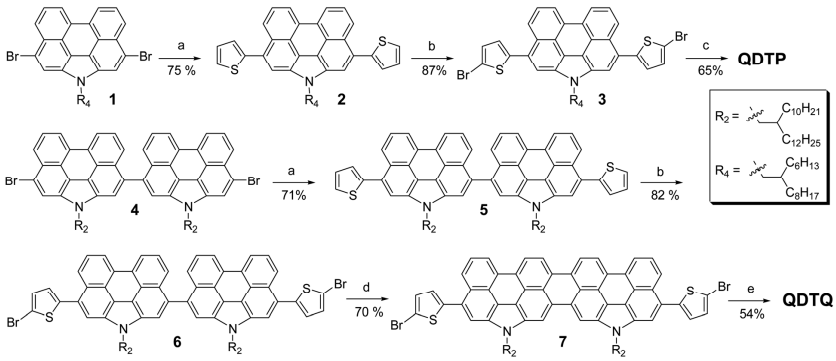

Scheme 1 Synthesis of **QDTP** and **QDTQ**. *Reagents and conditions*: (a) tributyl-(thiophen-2-yl)stannane, $Ph(PPh_3)_4$, toluene–DMF, 80 °C, 24 h; (b) NBS (2 equiv.), DCM/DMF, 0–25 °C, 4 h; (c) (i) malononitrile, NaH, $Pd(PPh_3)_2Cl_2$, reflux, 48 h; (ii) HCl (2 M); (iii) *p*-chloranil, CH_3CN, r.t.; (d) DDQ, $Sc(OTf)_3$, toluene, reflux, 24 h; (e) (i) malononitrile, NaH, $Pd(PPh_3)_2Cl_2$, reflux, 60 h; (ii) HCl (2 M), air.

Magnetic properties

ESR measurements of the solids of both **QDTP** and **QDTQ** displayed intense one-line signals at $g_e = 2.0030$ and the intensity decreases when the temperature is lowered (Fig. S2 in ESI†). While **QDTQ** in various solvents showed strong ESR signals, a solution of **QDTP** only exhibited a weak ESR signal under the same condition probably due to smaller spin concentration. The VT ^{1}H NMR spectra of **QDTP** recorded in THF-d_8 are shown in Fig. 2a. Sharp resonance signals well-assigned to proton "a", "b" and "c" of the central NP unit were observed upon cooling from 298 to 220 K. In contrast, the resonance for proton "d" showed obvious changes with temperature, which was significantly broadened at 298 K but became sharper as the temperature decreased. Nevertheless, no clear peaks were detected for protons "e" and "f" on the thiophene rings at room temperature but the resonances appeared at low temperatures. These findings indicate that **QDTP** exists as a singlet biradical in the ground state, which is in equilibrium with a thermally excited triplet biradical. From a view point of molecular structures, the quinoidal **QDTP** may exist as three conformers with different configurations through the ethylene linkage (Fig. 2b). DFT calculations predicted a small energy difference (*ca.* 1 kcal mol^{-1}) between the different conformers and the energy barrier from the highest-energy conformer **3** to the middle-energy conformer **2** and then to the lowest-energy conformer **1** is also small (*ca.* 3.8 kcal mol^{-1}) (Fig. 2b), which allow a fast interconversion between different conformers at the room temperature. The large biradical character may weaken the double bond character between the thiophenes and the rylene unit and lead to a small rotation energy barrier. In fact, calculations also predicted that the bond length between the thiophene rings and the rylene unit is 1.43 Å (see ESI†) in the ground state, indicating a large single bond character. Such a small energy barrier isomerization process can explain the observed complicated NMR spectra at low temperatures (*e.g.*, 200 K), that is to say, inter-conversion is slower than the NMR time scale when the temperature is below a certain point. On the other hand, compound **QDTQ** showed NMR silence even at very low temperature (−100 °C in CD_2Cl_2), indicating that this extended derivative has a larger biradical character and a very small singlet–triplet energy gap (ΔE_{S-T}), resulting in a large population of triplet species.

SQUID measurements were conducted for the powders of **QDTP** and **QDTQ** at 5–380 K and the temperature dependent magnetic signal changes indicated that both compounds have a singlet biradical ground state (Fig. 3). The singlet–triplet energy gap ΔE_{S-T} (*i.e.*, $2J/k_B$) were estimated to be −4.71 kcal mol^{-1} (−2368 K) for **QDTP** and −0.16 kcal mol^{-1} (−80.8 K) for **QDTQ** by careful fitting of the data with Bleaney–Bowers equation.[15] The small singlet–triplet gaps allow facile thermal excitation to the higher energy triplet biradical state and lead to NMR signal broadening. In particular, the **QDTQ** has a very small singlet–triplet gap and the triplet biradical species become dominant at room temperature and thus it is NMR silent.

Raman characterizations

Raman spectroscopy is a unique tool to evaluate the electronic ground state of conjugated biradicals and to understand macroscopic magnetic and optical data with molecular level information.[10e,11a–c,16] To provide new insights into the correlation between their structures and properties, resonance Raman experiments on **QDTP** and **QDTQ** were conducted at laser wavelengths of 785 and 633 nm respectively (Fig. 4), which are in resonance with their strongest electronic absorptions (*vide infra*) due to their singlet ground electronic states. We compare in Fig. 4 these spectra with those of the non-thiophenic homologues with the same rylene core, **Per-CN** ($\lambda_{exc} = 532$ nm) and **QR-CN** ($\lambda_{exc} = 785$ nm).[11b]

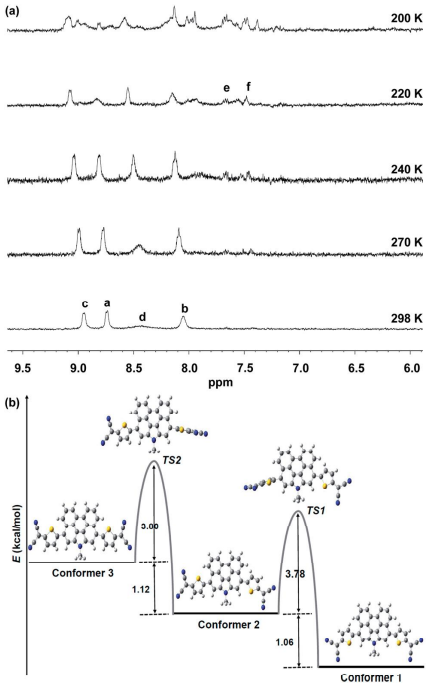

Fig. 2 (a) Variable temperature ^{1}H NMR spectra (aromatic region) of **QDTP** in THF-d_8. The resonance assignment referred to the structure shown in Fig. 1. (b) Energy diagram of three conformers of **QDTP** and their inter-conversion transition states.

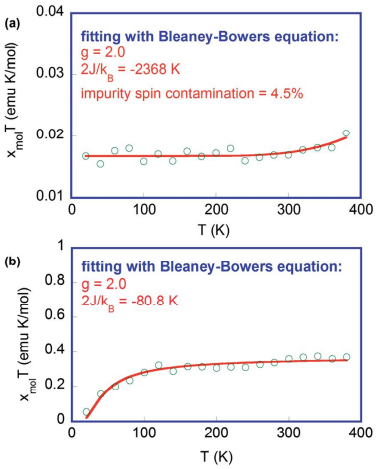

Fig. 3 χT–T curves in the SQUID measurements for the powder of (a) **QDTP** and (b) **QDTQ**. The solid lines are the fitting curves according to Bleaney–Bowers equation; g-factor was taken to be 2.

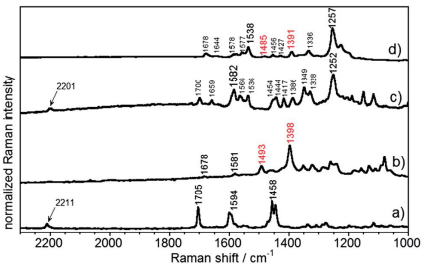

Fig. 4 Solid-state resonant Raman spectra of (a) **Per-CN** (λ_{exc} = 532 nm); (b) **QDTP** (λ_{exc} = 785 nm), (c) **QR-CN** (λ_{exc} = 785 nm); and (d) **QDTQ** (λ_{exc} = 633 nm).

The intense quinoidal bands of **Per-CN** at 1705, 1594, and 1458 cm^{-1} (Fig. 4a) became weaker and frequency down-shifted in **QDTP** at 1678 and 1581 and 1398 cm^{-1} respectively (Fig. 4b). In particular, the ν (C=C) modes of the bonds attaching the dicyano groups to the thiophene cores change from 1458 cm^{-1} in full quinoidal **Per-CN** to 1398 cm^{-1} in **QDTP**, revealing the evolution from a C=C character towards a weaker C–C feature. The new band at 1493 cm^{-1} could be assigned to a C=C stretching mode of the two thiophene rings as a similar strong Raman band with frequency at 1492 cm^{-1} was reported for aromatic dimethyl-bithiophene.[17] As a result, the most stable configuration of **QDTP** in the ground state can be ascribed to a singlet biradical promoted by the aromatization of the thiophene and NP moieties. As for the ν (C≡N) bands around 2200 cm^{-1}, these are clearly observed as medium intensity Raman bands for closed-shell structures and experience a strong weakening, turning undetectable, in open-shell biradical species.[12b,16] This is the case of **Per-CN** and **QR-CN** with the well-resolved bands at 2211 and 2201 cm^{-1} (this latter is borderline between closed-shell and open-shell) respectively, while no bands are observed within the same signal-to-noise ratio in **QDTP** and **QDTQ** revealing their biradical shapes. For the non-thiophenic derivatives, the Raman spectrum experienced a splitting and the appearance of new bands due to the existence of new bonds on **Per-CN** → **QR-CN** (Fig. 4c). Several medium-weak bands around 1600 cm^{-1} in **QDTQ** could be attributed to modes of the central benzenoid moieties due to their aromatic shapes. The most intense Raman band was at 1257 cm^{-1} in **QDTQ** and was absent in **QDTP** and hence ascribable to the tetrabenzo fused innermost group. Such intense Raman bands at the frequencies between 1250 and

1300 cm^{-1} have been reported in fused benzenoid polycyclic hydrocarbons.[18] The bands at 1485 and 1391 cm^{-1} in **QDTQ** can be related with the thiophenic bands at 1493 and 1398 cm^{-1} in **QDTP** bearing a pseudo-aromatic character for the bithiophene moiety. Assuming the biradical character for **QDTP** and **QDTQ**, the larger separation between the two electrons in the radical centers of the latter benefits charge repulsion and produces a decrease of the singlet–triplet energy gap, in concordance with the SQUID measurements. The singlet–triplet gaps in the non-thiophenic compounds are expected to be significantly larger due to their closed-shell ground state forms. Comparing **QDTP** and **QR-CN**, both with four pro-aromatic rings, the expression of biradical character in the former is related with the possibility of rotation around the thiophene–rylene single bond in the biradical state which has been described as the driving force for the closed-shell rupture in the ***n*Per-CN** compounds. In line with this argument, Fig. S3 (ESI†) compares the 785 nm Raman spectra of **QDTP** in solid state and in dichloromethane (DCM) solution. Both spectra display the 1493 cm^{-1} intra-ring thiophene aromatic band at the same value, while that at 1398 cm^{-1} in solid displaces to 1391 cm^{-1} in DCM revealing the distortion of the dicyanomethylene groups relative to the thiophenes as a result of the greater flexibility in the biradical state.

Given the small singlet–triplet energy gap, −0.16 kcal mol^{-1} in **QDTQ**, the first excited triplet might be significantly populated at room temperature by thermally activated intersystem crossing from the singlet ground electronic state. In contrast with the NMR data, the existence of triplets in ambient conditions allows us to obtain their spectra by tuning the laser Raman excitation along the Vis-NIR spectrum. The Raman spectra of **QDTQ** obtained with the 532 and 1064 nm are shown in Fig. 5 together with that of at 785 nm due to its ground state singlet. For **QDTQ**, the spectrum with 532 nm excitation was almost identical to that at 633 nm corresponding to the singlet open-shell species (Fig. 5b and c). However, when excited with the 1064 nm laser, the spectrum is in resonance with the broad weak absorption extending from 1000 to 1300 nm which is a distinctive property of **QDTQ** regarding **QDTP** (see below). This 1064 nm spectrum significantly changes and up to four new bands (marked with circles in Fig. 5) were in co-existence with those of the singlet. The most noticeable aspect was the strong band at 1404 cm^{-1} together with that at 1490 cm^{-1} which are due to the thiophene moieties. The enhancement of these two bands upon resonance with this NIR band could indicate the preferred reorganization of the electronic structure around the terminal thiophenes in the new species. This is in accordance with this species being the biradical triplet since the wave-function of the molecular orbitals with the unpaired electrons in the triplet configuration must display zero overlap which is achieved by localizing them further apart in the thiophenes. Due to the small singlet–triplet gap, we could expect some changes in the relative intensity of the singlet and triplet as a function of the temperature. Fig. 5 also shows the spectra at room temperature together with that at −170 °C. Upon cooling we observed that the intensity of the 1490/1404 cm^{-1} bands seemingly decrease regarding those at 1550 cm^{-1} or, in other words, the population of the triplet decreases regarding that of the singlet upon lowering the temperature. This is in agreement with: (i) the singlet being the ground electronic state, and (ii) the triplet being very close in energy to the singlet. Interestingly by exciting **QDTP** with the 532 nm laser we obtained a Raman spectrum with new features regarding that at 785 nm which are similar to those described for the triplet species of **QDTQ**. The detection of the triplet in the Raman experiment of **QDTP**, in despite of being 4.71 kcal mol^{-1} higher, is a consequence of the selective outstanding resonant intensity enhancement with the 532 nm excitation.

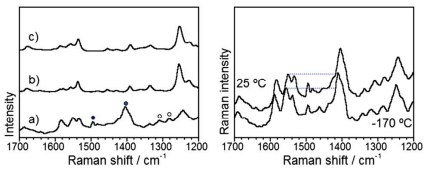

Fig. 5 (Left) Raman spectra of **QDTQ** at different excitation wavelengths: (a) 1064 nm, (b) 633 nm, (c) 532 nm. (Right) 1064 nm FT-Raman spectra of **QDTQ** in solid state at different temperatures.

Optical properties

Compounds **QDTP** and **QDTQ** exhibited very different one-photon absorption (OPA) spectra in DCM compared to their corresponding closed-shell counterparts **Per-CN** and **QR-CN**, respectively.[11a,11b] While the characteristic band at 626 nm together with a shoulder absorption at 579 nm was assigned to the typical quinoidal structure of **Per-CN**,[11a] one intense absorption band with maximum at 874 nm ($\log \varepsilon = 4.56$), along with two unresolved shoulders at 765 and 1005 nm in the NIR region, was observed for **QDTP** (Fig. 6a). Remarkably, the longest absorption tail reached the wavelength region of ~1400 nm, leading to a very small optical energy gap (0.94 eV). This big difference in the absorption band structure indicates that **QDTP** has a different ground-state electronic structure from the quinoidal **Per-CN**. **QR-CN** has a very similar band structure to **Per-CN**, with an intense absorption band at 880 nm and a shoulder at 798 nm.[11b] On passing to **QDTQ**, a band maximum at 685 nm ($\log \varepsilon = 4.34$) with one shoulder at 626 nm was detected (Fig. 6b). This intense band experienced an obvious blue-shift in comparison with **QDTP** (approximately 189 nm), resulting in an absorption spectrum quite similar to that of the fused bis-*N*-annulated quaterrylene.[14] The most outstanding character is the existence of three overlapping bands in the infrared region with the absorption maxima at 1052, 1103 and 1384 nm, respectively. This spectral evolution is comparable to the band structure change from quinoidal **Per-CN** to the biradicals of higher series (***n*Per-CNs**, $n > 2$),[11a] and ascribable to the significant population of triplets in ambient conditions. An optical energy gap of 0.75 eV was determined for **QDTQ**. All these compounds showed no fluorescence due to their open-shell character.

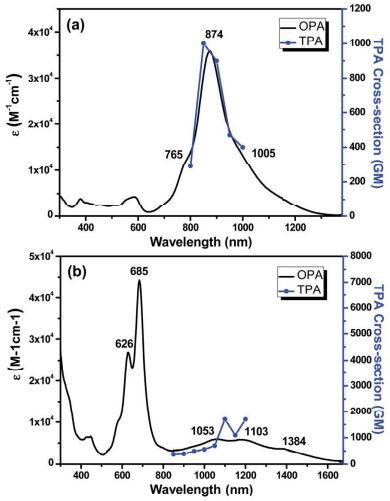

Fig. 6 OPA spectra (solid line and left vertical axis) and TPA spectra (blue symbols and right vertical axis) of (a) **QDTP** and (b) **QDTQ** recorded in DCM. TPA spectra are plotted at $\lambda_{ex}/2$.

Femtosecond transient absorption measurements were performed to explore the excited-state dynamics of **QDTP** and **QDTQ** (Fig. S4 in ESI†). Compound **QDTP** has a short singlet excited lifetime ($\tau = 1.6$ ps), which is much shorter than that of **Per-CN** ($\tau = 17.2$ ps).[11a] This fast decay indicates an acceleration of the non-radiative internal conversion arising from the shorter energy gap between the lowest excited state and the open-shell ground state. The decay profiles of **QDTQ** probed at 700 nm were fitted by a biexponential function with $\tau_1 = 0.4$ ps and $\tau_2 = 11$ ps (Fig. S4 in ESI†), which are also faster than that for **QR-CN** ($\tau = 24$ ps). The short excited-state lifetimes of **QDTP** and **QDTQ** are in good agreement with their non-fluorescent properties. Two-photon absorption measurements were carried out for **QDTP** and **QDTQ** in DCM by the *Z*-scan technique in the NIR region from 1600 to 2400 nm where one-photon absorption contribution is negligible (Fig. 6 and S5 in ESI,† the TPA spectra are plotted at $\lambda_{ex}/2$ for comparison with the OPA spectrum). Large TPA cross sections ($\sigma^{(2)}$) were observed for both quinoidal chromophores, with $\sigma^{(2)}_{max} = 1000$ GM at 1700 nm for **QDTP**, and $\sigma^{(2)}_{max} = 1700$ GM at 2400 nm for **QDTQ**, which are comparable to the case of the biradicals ***n*Per-CNs** ($n = 2$–5).[11a]

Electrochemical properties

Cyclic voltammetry and differential pulse voltammetry were used to investigate the electrochemical properties of **QDTP** and **QDTQ** (Fig. 7 and S6 in ESI†). In contrast to the **Per-CN** without obvious oxidative waves,[11a] **QDTP** demonstrated amphoteric redox behaviour with two chemically reversible oxidative processes with half-wave potential ($E^{ox}_{1/2}$) at −0.37 and 0.48 V, two chemically irreversible oxidation waves with $E^{ox}_{1/2}$ −0.03 and −0.69 V, and one reductive process with half-wave potential ($E^{red}_{1/2}$) at −1.37 V (*vs.* Fc/Fc^+, Fc: ferrocene). The HOMO and LUMO energy levels were determined to be −4.40 and −3.57 eV, respectively, from the onset potentials of the first oxidation and reduction wave. On passing to **QDTQ**, five closely overlapping oxidative processes with $E^{ox}_{1/2}$ at −0.49, −0.21, −0.04, 0.37, 0.70 V were observed, together with four overlapping chemically irreversible reductive processes with $E^{red}_{1/2}$ at −1.50, −1.35, −1.09, −0.98 V. Accordingly, the HOMO and LUMO energy levels of **QDTQ** were estimated to be −4.23 and −3.86 eV, respectively. Rather low electrochemical energy gaps of 0.83 and 0.37 eV were determined for **QDTP** and **QDTQ**, respectively.

Theoretical calculations

Broken-symmetry DFT (BS-UB3LYP/6-31G**) calculations were carried out to provide further understanding of the electronic structures and spectral findings in **QDTP** and **QDTQ**. The calculations revealed that both compounds have a singlet biradical ground state, agreeing with all experimental results. The singlet–triplet energy gap ΔE_{S-T} for **QDTP** and **QDTQ** was estimated to be −1.45 and −1.35 kcal mol^{-1}, respectively, and both show a relatively large deviation from the SQUID data, indicating the challenges to calculate a large open-shell system. However, the trend of increasing the conjugated length leading to a smaller singlet–triplet energy gap is in good agreement with

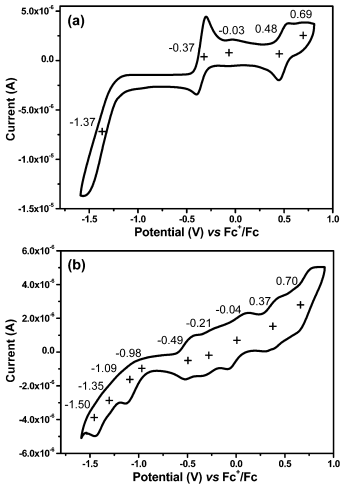

Fig. 7 Cyclic voltammograms of (a) **QDTP** and (b) **QDTQ** in dry DCM with 0.1 M Bu_4NPF_6 as supporting electrolyte, Ag/AgCl as reference electrode, Au disk as working electrode, Pt wire as counter electrode, and scan rate at 50 and 20 mV s^{-1}, respectively.

observations for other polycyclic hydrocarbons.[19] The singlet biradical characters (y) of **QDTP** and **QDTQ** were estimated to be 0.81 and 0.93 by the CASSCF(2,2)/6-31G calculations.[20] The larger biradical character for **QDTQ** is consistent with the observed stronger ESR signal and larger magnetic susceptibility in SQUID experiments in comparison to **QDTP**. The molecular orbital profiles of **QDTP** and **QDTQ** exhibit a characteristic disjoint feature for the singly occupied molecular orbital (Fig. S7 and S8 in ESI†), which is a requisite to display small singlet–triplet gaps as seen in many singlet biradicals. The spin densities in these biradical species were distributed throughout the whole molecular framework and largely delocalized at the backbone of terminal malononitrile-substituted thiophene units (Fig. 8). This can further explain the more significant NMR signal broadening for the thiophene ring protons than those of NP units as shown in Fig. 2a.

Theoretical calculations also demonstrated an optimized geometry for the singlet biradical of **QDTP** with a moderate dihedral angle (34.3) between the thiophene and NP unit (Fig. S9 in ESI†) in agreement with the flexibility property described above. On passing to **QDTQ**, the dihedral angle of the singlet biradical becomes slightly smaller (33.0°) (Fig. S9 in ESI†). This dihedral angles resulting from twisting the C=C bonds of the backbones play roles in generation of the biradical contribution. In comparison to the quinoidal **Per-CN**,[11a] these singlet biradicals showed longer bond lengths for the *exo* methylene bonds as the weakening of the C=C bonds was observed in the vibrational studies. It is also noteworthy that the C=C bonds between thiophene and rylene rings displayed a longer length in all states (closed-shell, singlet biradical and triplet) compared to the other double bonds along the π-extended quinodimethane chain (Fig. S9 in ESI†), indicating that the thiophene rings have a large aromatic character. On the basis of calculated nucleus independent chemical shift (NICS) values[21] (NICS(1) and NICS(1)$_{zz}$), both singlet biradicals of **QDTP** and **QDTQ** exhibited more benzenoid character for the NP moieties and aromatic characteristic for the thiophene units (Fig. S10 in ESI†), which are consistent with the Raman spectral findings. It also suggests that the recovery of aromaticity of the central rylene core and the side thiophene rings would be a driving force for the formation of singlet biradical in the ground state together with the conformational effect between the thiophenes and rylene.

Time-dependent DFT calculations were conducted to predict the electronic absorption spectra of **QDTP** and **QDTQ** (Fig. S11 in ESI†). The characteristic low-lying excited states assigned by the admixing spin-associated (H, H → L, L) double excited electron configurations[22] were well identified in these biradical species and the lowest energy transitions ($S_0 \rightarrow S_1$) are predicted to be 1.02 eV (1200 nm, $f = 0.0137$) for **QDTP** and 0.78 eV (1574 nm, $f = 0.0199$) for **QDTQ**, respectively. Such smaller energy gaps are favourable to promote electrons from HOMO to LUMO and lead to an open-shell singlet biradical ground state. The other calculated transitions are close to the experimental observations (Tables S1 and S2 in ESI†).

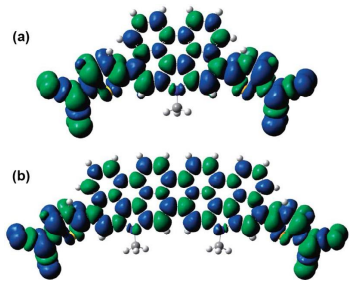

Fig. 8 Calculated (UB3LYP) spin density distribution of (a) **QDTP** and (b) **QDTQ**. Blue and green surfaces represent α and β spin densities, respectively. Isovalue is 0.002. The long branched *N*-alkyl chains are replaced by methyl groups during the calculations.

Conclusions

In conclusion, two new soluble and stable tetracyano-dithienoperylene and dithienoquaterrylenequinodimethanes (**QDTP** and **QDTQ**) were successfully prepared and their electronic structures and geometries in the ground state were systematically investigated by various experimental methods and DFT calculations. Both of them have a singlet biradical ground state and such an evolution from closed-shell quinoids (**Per-CN**/**QR-CN**) to singlet biradicals (**QDTP**/**QDTQ**) can be explained by the recovery of two additional aromatic thiophene rings in the biradical resonance forms together with the conformational flexibility around the thiophene–rylene connections. With extension of the conjugation length, the biradical character y increases from **QDTP** to **QDTQ** due to the decreased energy gap. Both chromophores showed very strong one-photon absorption and large two-photon absorption response in the near infrared region. Our studies demonstrated that the ground state of a closed-shell polycyclic hydrocarbon can be converted into a singlet biradical state by accurate tuning of its structure and aromaticity. In response to the change of ground state, the optical, electronic and magnetic properties of the open-shell species are significantly different from the closed-shell species. The obtained materials also possess potential applications for non-linear optics, ambipolar field effect transistors and organic spintronics and these studies are underway in our laboratories.

Acknowledgements

J.W. acknowledges the financial support from MOE Tier 2 grant (MOE2011-T2-2-130), MINDEF-NUS-JPP (12/02/05) grant and IMRE Core funding (IMRE/13-1C0205). The work at Yonsei University was supported by Mid-career Researcher Program (2010-0029668) and Global Research Laboratory (2013K1A1A2A02050183) through the National Research Foundation of Korea (NRF) funded by the Ministry of Science, ICT (Information and Communication Technologies) and Future Planning. The work at the University of Málaga was supported

by the Ministerio de Educación y Ciencia (MEC) of Spain (project CTQ2012-33733) and to the Junta de Andalucía (project PO9-4708). J.L.Z. is grateful to MINECO for a personal grant.

Notes and references

1 (*a*) C. Lambert, *Angew. Chem., Int. Ed.*, 2011, **50**, 1756–1758; (*b*) Y. Morita, K. Suzuki, S. Sato and T. Takui, *Nat. Chem.*, 2011, **3**, 197–204; (*c*) Z. Sun and J. Wu, *J. Mater. Chem.*, 2012, **22**, 4151–4160; (*d*) Z. Sun, Q. Ye, C. Chi and J. Wu, *Chem. Soc. Rev.*, 2012, **41**, 7857–7889; (*e*) A. Shimizu, Y. Hirao, T. Kubo, M. Nakano, E. Botek and B. Champagne, *AIP Conf. Proc.*, 2012, **1504**, 399–405; (*f*) Z. Sun, Z. Zeng and J. Wu, *Chem. - Asian J.*, 2013, **8**, 2894–2904; (*g*) M. Abe, *Chem. Rev.*, 2013, **113**, 7011–7088.

2 K. Kamada, K. Ohta, T. Kubo, A. Shimizu, Y. Morita, K. Nakasuji, R. Kishi, S. Ohta, S.-I. Furukawa, H. Takahashi and M. Nakano, *Angew. Chem., Int. Ed.*, 2007, **46**, 3544–3546.

3 (*a*) M. Chikamatsu, T. Mikami, J. Chisaka, Y. Yoshida, R. Azumi and K. Yase, *Appl. Phys. Lett.*, 2007, **91**, 043506; (*b*) D. T. Chase, A. G. Fix, S. J. Kang, B. D. Rose, C. D. Weber, Y. Zhong, L. N. Zakharov, M. C. Lonergan, C. Nuckolls and M. M. Haley, *J. Am. Chem. Soc.*, 2012, **134**, 10349–10352.

4 J. Lee, P. Jadhav, P. D. Reusswig, S. R. Yost, N. J. Thompson, D. N. Congreve, E. Hontz, T. Van Voorhis and M. A. Baldo, *Acc. Chem. Res.*, 2013, **46**, 1300–1311.

5 Y. W. Son, M. L. Cohen and S. G. Louie, *Phys. Rev. Lett.*, 2006, **97**, 216803.

6 Y. Morita, S. Nishida, T. Murata, M. Moriguchi, A. Ueda, M. Satoh, K. Arifuku, K. Sato and T. Takui, *Nat. Mater.*, 2011, **10**, 947–951.

7 (*a*) A. Konishi, Y. Hirao, M. Nakano, A. Shimizu, E. Botek, B. Champagne, D. Shiomi, K. Sato, T. Takui, K. Matsumoto, H. Kurata and T. Kubo, *J. Am. Chem. Soc.*, 2010, **132**, 11021–11023; (*b*) A. Konishi, Y. Hirao, K. Matsumoto, H. Kurata, R. Kishi, Y. Shigeta, M. Nakano, K. Tokunaga, K. Kamada and T. Kubo, *J. Am. Chem. Soc.*, 2013, **135**, 1430–1437.

8 (*a*) D. T. Chase, B. D. Rose, S. P. McClintock, L. N. Zakharov and M. M. Haley, *Angew. Chem., Int. Ed.*, 2011, **50**, 1127–1130; (*b*) A. Shimizu and Y. Tobe, *Angew. Chem., Int. Ed.*, 2011, **50**, 6906–6910; (*c*) A. Shimizu, R. Kishi, M. Nakano, D. Shiomi, K. Sato, T. Takui, I. Hisaki, M. Miyata and Y. Tobe, *Angew. Chem., Int. Ed.*, 2013, **52**, 6076–6079.

9 (*a*) K. Ohashi, T. Kubo, T. Masui, K. Yamamoto, K. Nakasuji, T. Takui, Y. Kai and I. Murata, *J. Am. Chem. Soc.*, 1998, **120**, 2018–2027; (*b*) T. Kubo, M. Sakamoto, M. Akabane, Y. Fujiwara, K. Yamamoto, M. Akita, K. Inoue, T. Takui and K. Nakasuji, *Angew. Chem., Int. Ed.*, 2004, **43**, 6474–6479; (*c*) T. Kubo, A. Shimizu, M. Sakamoto, M. Uruichi, K. Yakushi, M. Nakano, D. Shiomi, K. Sato, T. Takui, Y. Morita and K. Nakasuji, *Angew. Chem., Int. Ed.*, 2005, **44**, 6564–6568; (*d*) A. Shimizu, M. Uruichi, K. Yakushi, H. Matsuzaki, H. Okamoto, M. Nakano, Y. Hirao, K. Matsumoto, H. Kurata and T. Kubo, *Angew. Chem., Int. Ed.*, 2009, **48**, 5482–5486; (*e*) A. Shimizu, T. Kubo, M. Uruichi, K. Yakushi, M. Nakano, D. Shiomi, K. Sato, T. Takui, Y. Hirao, K. Matsumoto, H. Kurata, Y. Morita and K. Nakasuji, *J. Am. Chem. Soc.*, 2010, **132**, 14421–14428; (*f*) A. Shimizu, Y. Hirao, K. Matsumoto, H. Kurata, T. Kubo, M. Uruichi and K. Yakushi, *Chem. Commun.*, 2012, **48**, 5629–5631.

10 (*a*) R. Umeda, D. Hibi, K. Miki and Y. Tobe, *Org. Lett.*, 2009, **11**, 4104–4106; (*b*) T. C. Wu, C. H. Chen, D. Hibi, A. Shimizu, Y. Tobe and Y. T. Wu, *Angew. Chem., Int. Ed.*, 2010, **49**, 7059–7062; (*c*) Z. Sun, K.-W. Huang and J. Wu, *Org. Lett.*, 2010, **12**, 4690–4693; (*d*) Z. Sun, K.-W. Huang and J. Wu, *J. Am. Chem. Soc.*, 2011, **133**, 11896–11899; (*e*) Y. Li, W.-K. Heng, B. S. Lee, N. Aratani, J. L. Zafra, N. Bao, R. Lee, Y. M. Sung, Z. Sun, K.-W. Huang, R. D. Webster, J. T. López Navarrete, D. Kim, A. Osuka, J. Casado, J. Ding and J. Wu, *J. Am. Chem. Soc.*, 2012, **134**, 14913–14922; (*f*) Z. Sun and J. Wu, *J. Org. Chem.*, 2013, **78**, 9032–9040; (*g*) W. Zeng, M. Ishida, S. Lee, Y. M. Sung, Z. Zeng, Y. Ni, C. Chi, D.-H. Kim and J. Wu, *Chem. - Eur. J.*, 2013, **19**, 16814–16824; (*h*) L. Shan, Z.-X. Liang, X.-M. Xu, Q. Tang and Q. Miao, *Chem. Sci.*, 2013, **4**, 3294–3297; (*i*) Z. Sun, S. Lee, K. Park, X. Zhu, W. Zhang, B. Zheng, P. Hu, Z. Zeng, S. Das, Y. Li, C. Chi, R. Li, K.-W. Huang, J. Ding, D.-H. Kim and J. Wu, *J. Am. Chem. Soc.*, 2013, **135**, 18229–18236.

11 (*a*) Z. Zeng, M. Ishida, J. L. Zafra, X. Zhu, Y. M. Sung, N. Bao, R. D. Webster, B. S. Lee, R.-W. Li, W. Zeng, Y. Li, C. Chi, J. T. López Navarrete, J. Ding, J. Casado, D.-H. Kim and J. Wu, *J. Am. Chem. Soc.*, 2013, **135**, 6363–6371; (*b*) Z. Zeng, S. Lee, J. L. Zafra, M. Ishida, X. Zhu, Z. Sun, Y. Ni, R. D. Webster, R.-W. Li, J. T. López Navarrete, C. Chi, J. Ding, J. Casado, D.-H. Kim and J. Wu, *Angew. Chem., Int. Ed.*, 2013, **52**, 8561–8565; (*c*) Z. Zeng, Y. M. Sung, N. Bao, D. Tan, R. Lee, J. L. Zafra, B. S. Lee, M. Ishida, J. Ding, J. T. López Navarrete, Y. Li, W. Zeng, D.-H. Kim, K.-W. Huang, R. D. Webster, J. Casado and J. Wu, *J. Am. Chem. Soc.*, 2012, **134**, 14513–14525; (*d*) L. K. Montgomery, J. C. Huffman, E. A. Jurczak and M. P. Grendze, *J. Am. Chem. Soc.*, 1986, **108**, 6004–6011.

12 (*a*) T. Takahashi, K. I. Matsuoka, K. Takimiya, T. Otsubo and Y. Aso, *J. Am. Chem. Soc.*, 2005, **127**, 8928–8929; (*b*) R. P. Ortiz, J. Casado, S. R. Gonzalez, V. Hernandez, J. Casado, V. Hernandez, J. T. López Navarrete, P. M. Viruela, E. Orti, K. Takimiya and T. Otsubo, *Angew. Chem., Int. Ed.*, 2007, **46**, 9057–9061.

13 M. Uno, K. Seto, M. Masuda, W. Ueda and S. Takahashi, *Tetrahedron Lett.*, 1985, **26**, 1553–1556.

14 (*a*) Y. Li and Z. Wang, *Org. Lett.*, 2009, **11**, 1385–1387; (*b*) C. Jiao, K. Zhang, C. Chi and J. Wu, *Org. Lett.*, 2009, **11**, 4508–4511; (*c*) C. Jiao, K.-W. Huang, Z. Guan, Q.-H. Xu and J. Wu, *Org. Lett.*, 2010, **12**, 4046–4049; (*d*) Y. Li, J. Gao, S. I. Motta, F. Negri and Z. Wang, *J. Am. Chem. Soc.*, 2010, **132**, 4208–4213.

15 B. Bleaney and K. D. Bowers, *Proc. R. Soc. London, Ser. A*, 1952, **214**, 451–465.

16 (*a*) J. Casado, S. Patchkovskii, M. Z. Zgierski, L. Hermosilla, C. Sieiro, M. Moreno Oliva and J. T. López Navarrete, *Angew. Chem., Int. Ed.*, 2008, **47**, 1443–1446; (*b*) S. R. González,

Y. Ie, Y. Aso, J. T. López Navarrete and J. Casado, *J. Am. Chem. Soc.*, 2011, **133**, 16350–16353.
17 J. Casado, R. G. Hicks, V. Hernández, D. J. T. Myles, M. C. R. Delgado and J. T. López Navarretea, *J. Chem. Phys.*, 2003, **118**, 1912–1920.
18 J. Wu, L. Gherghel, M. D. Watson, J. Li, Z. Wang, C. D. Simpson, U. Kolb and K. Müllen, *Macromolecules*, 2003, **36**, 7082–7089.
19 (*a*) S. D. Motta, F. Negri, D. Fazzi, C. Castiglioni and E. V. Canesi, *J. Phys. Chem. Lett.*, 2010, **1**, 3334–3339; (*b*) K. Kamada, K. Ohta, A. Shimizu, T. Kubo, R. Kishi, H. Takahashi, E. Botek, B. Champagne and M. Nakano, *J. Phys. Chem. Lett.*, 2010, **1**, 937–940.
20 D. Döýhnert and J. Koutecký, *J. Am. Chem. Soc.*, 1980, **102**, 1789–1796.
21 Z. F. Chen, C. S. Wannere, C. Corminboeuf, R. Puchta and P. V. Schleyer, *Chem. Rev.*, 2005, **105**, 3842–3888.
22 S. D. Motta, F. Negri, D. Fazzi, C. Castiglioni and E. V. Canesi, *J. Phys. Chem. Lett.*, 2010, **1**, 3334–3339.

JACS
JOURNAL OF THE AMERICAN CHEMICAL SOCIETY

Article

pubs.acs.org/JACS

Kinetically Blocked Stable Heptazethrene and Octazethrene: Closed-Shell or Open-Shell in the Ground State?

Yuan Li,[†] Wee-Kuan Heng,[†] Byung Sun Lee,[‡] Naoki Aratani,[§] José L. Zafra,[∥] Nina Bao,[⊥] Richmond Lee,[#] Young Mo Sung,[‡] Zhe Sun,[†] Kuo-Wei Huang,[#] Richard D. Webster,[¥] Juan T. López Navarrete,[∥] Dongho Kim,*[,‡] Atsuhiro Osuka,*[,§] Juan Casado,*[,∥] Jun Ding,*[,⊥] and Jishan Wu*[,†,▽]

[†]Department of Chemistry, National University of Singapore, 3 Science Drive 3, 117543, Singapore

[‡]Spectroscopy Laboratory for Functional π-Electronic Systems and Department of Chemistry, Yonsei University, Seoul 120-749, Korea

[§]Department of Chemistry, Graduate School of Science, Kyoto University, Sakyo-ku, Kyoto 606-8502, Japan

[∥]Department of Physical Chemistry, University of Malaga, Campus de Teatinos s/n, 229071 Malaga, Spain

[⊥]Department of Materials Science & Engineering, National University of Singapore, 119260, Singapore

[#]Division of Chemical and Life Sciences and Engineering and KAUST Catalysis Center, King Abdullah University of Science and Technology (KAUST), Thuwal 23955-6900, Saudi Arabia

[¥]Division of Chemistry & Biological Chemistry, School of Physical & Mathematical Sciences, Nanyang Technological University, 21 Nanyang Link, 637371, Singapore

[▽]Institute of Materials Research and Engineering, A*Star, 3 Research Link, Singapore, 117602

Supporting Information

ABSTRACT: Polycyclic aromatic hydrocarbons with an open-shell singlet biradical ground state are of fundamental interest and have potential applications in materials science. However, the inherent high reactivity makes their synthesis and characterization very challenging. In this work, a convenient synthetic route was developed to synthesize two kinetically blocked heptazethrene (**HZ-TIPS**) and octazethrene (**OZ-TIPS**) compounds with good stability. Their ground-state electronic structures were systematically investigated by a combination of different experimental methods, including steady-state and transient absorption spectroscopy, variable temperature NMR, electron spin resonance (ESR), superconducting quantum interfering device (SQUID), FT Raman, and X-ray crystallographic analysis, assisted by unrestricted symmetry-broken density functional theory (DFT) calculations. All these demonstrated that the heptazethrene derivative **HZ-TIPS** has a closed-shell ground state while its octazethrene analogue **OZ-TIPS** with a smaller energy gap exists as an open-shell singlet biradical with a large measured biradical character (y = 0.56). Large two-photon absorption (TPA) cross sections ($\sigma^{(2)}$) were determined for **HZ-TIPS** ($\sigma^{(2)}_{max}$ = 920 GM at 1250 nm) and **OZ-TIPS** ($\sigma^{(2)}_{max}$ = 1200 GM at 1250 nm). In addition, **HZ-TIPS** and **OZ-TIPS** show a closely stacked 1D polymer chain in single crystals.

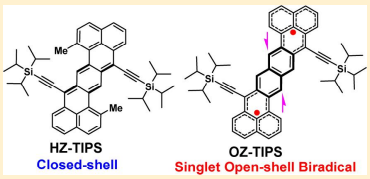

1. INTRODUCTION

Open-shell polycyclic aromatic hydrocarbons (PAHs)[1] are of interest for understanding fundamental chemical and physical phenomenon (e.g., the nature of chemical bonding). In addition, their unique electronic, nonlinear optical (NLO),[2] and magnetic properties make them suitable for functional materials in electronic devices,[3] quantum information processing systems,[4] lithium ion batteries,[5] and organic spintronics.[6] However, the open-shell structure of these molecules renders them vulnerable to degradation reactions; therefore, instability remains a key obstacle for their practical applications. Recent progress in synthetic methods has led to successful synthesis and characterization of several types of stable open-shell PAHs: (1) *p*-quinodimethane[7] and *o*-quinodimethane[8] derivatives, in which the open-shell biradical resonance form contributes largely to the ground-state electronic structure due to the recovery of aromaticity of the quinodimethane unit; (2) phenalenyl[9] and bisphenalenyl[10] derivatives, in which the radicals are thermodynamically stabilized by delocalization throughout the phenalenyl moiety; and (3) low band gap PAHs with Kekulé structure, such as teranthene, in which the breaking of a double bond is compensated by recovery of three Clar's sextet rings.[11] Higher order acenes[12] and periacenes[13] are also predicted to show open-shell character in the ground state, but there is no reported example so far. In most cases, kinetic blocking of the reactive radical sites with bulky groups is necessary to obtain stable materials, even if they are

Received: May 18, 2012
Published: August 21, 2012

   dx.doi.org/10.1021/ja304618v | J. Am. Chem. Soc. 2012, 134, 14913−14922

thermodynamically stabilized by π-electron delocalization or by substitution with electron-withdrawing groups.

Remarkable open-shell biradical character was predicted for the zethrene family, a type of *Z*-shaped PAH which can also be regarded as a dibenzoacene. Theoretical calculations predicted their enhanced static second hyperpolarizability and large two-photon absorption (TPA) cross section.[14] The large biradical character for heptazethrene and octazethrene can be explained by recovery of an aromatic benzene or naphthalene ring in the biradical resonance form, as indicated in Chart 1. Although the smallest member of the zethrene family, i.e. zethrene, was also predicted to have a significant biradical character, so far all reported zethrene and its derivatives[15] have showed a closed-shell ground state. The synthesis of parent heptazethrene[16] was not successful due to its high reactivity. We recently reported the first synthesis of a heptazethrene derivative, the heptazethrene diimide (**HZ-DI**, Chart 1), and demonstrated that it existed as a singlet open-shell biradical in the ground state.[17] **HZ-DI** showed reasonable photostability in solution; however, the material slowly decomposed during storage either in solution or in solid. The higher order octazethrene[18] and its derivatives have never been reported due to their expected extremely high reactivity. In this paper, we report an efficient synthetic route for a new kinetically blocked heptazethrene derivative (**HZ-TIPS**), in which the most reactive sites (indicated by arrows in Chart 1) are substituted by bulky triisopropylsilylacetylene (TIPS) groups (Chart 1). By using a similar concept, the first stable octazethrene derivative (**OZ-TIPS**, Chart 1), which was found to have a singlet open-shell ground state, was also obtained. The ground-state electronic structures of both compounds were systematically studied by various experiments and density functional theory (DFT) calculations. Their NLO properties and solid-state packing were also investigated in detail.

Chart 1. Resonance Structures of Heptazethrene and Octazethrene, and Structures of HZ-TIPS and OZ-TIPS

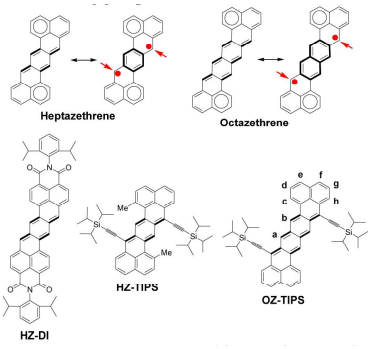

2. RESULTS AND DISCUSSION

Synthesis and Structural Characterization. Our previous synthetic methods for the zethrene diimide[15f] and heptazethrene diimide[17] using intramolecular transannular cyclization afforded the final products in low yields. Herein, the heptazethrene diketone **4** was chosen as a key intermediate for the high-yield synthesis of **HZ-TIPS** (Scheme 1). Suzuki coupling between the diester **1**[19] and 2-methylnaphthalen-1-yl-1-boronic acid[20] followed by acidification of the product **2** gave the diacid **3** in an overall 78% yield. The desired diketone **4** was then obtained from **3** under reflux for 3 h with polyphosphoric acid (PPA). The introduction of a methyl group at the 2-position of the naphthalene moiety prevents the formation of a five-membered ring containing isomers and also improves the solubility of the diketone **4**. Addition of **4** with excessive triisopropylsilylacetylene Grignard reagent followed by reduction with $SnCl_2$ provided **HZ-TIPS** in 87% yield. Using a similar strategy, the octazethrene derivative **OZ-TIPS** was prepared from the corresponding diketone **5**[18] in 35% yield. The structures of **HZ-TIPS** and **OZ-TIPS** were unambiguously identified by 1D ^{1}H (^{13}C) NMR, 2D NOE/COSY/NOESY NMR spectroscopy, high-resolution mass spectrometry (Figure S1−S10 in the Supporting Information (SI)), and single-crystal analysis (vide infra).

Scheme 1[a]

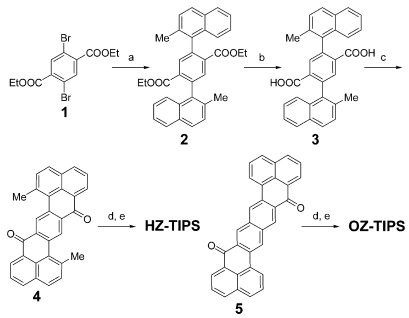

[a]Reagents and conditions: (a) 2-methylnaphthalen-1-yl-1-boronic acid, 3 equiv, $Pd(PPh_3)_4$/ Na_2CO_3, toluene/EtOH, reflux, 82%; (b) NaOH, 8 equiv, THF/MeOH, 70 °C, 95%; (c) PPA, reflux, 93%; (d) *i*-$Pr_3SiC{\equiv}CMgCl$, THF, rt; (e) $SnCl_2$, rt, 2 h; 87% for **HZ-TIPS** and 35% for **OZ-TIPS**, over two steps.

Steady-State and Transient Absorption Spectroscopic Measurements of HZ-TIPS and OZ-TIPS. The solution of **HZ-TIPS** has a blue color and shows a well-resolved one-photon absorption (OPA) spectrum with a *p*-band at 634 nm (Figure 1 and Table 1), which is typical for many closed-shell PAHs, such as rylenes and acenes.[21] **HZ-TIPS** also exhibits a moderate fluorescence quantum yield (16%) with emission maximum at 704 nm (Figure S11 in SI). In addition, **HZ-TIPS** displays a well-resolved ^{1}H NMR spectrum even under elevated temperatures (e.g., 100 °C in $CDCl_2CDCl_2$, Figure S1 in SI). All these indicate that **HZ-TIPS** likely has a closed-shell structure in the ground state, which is in contrast to its analogue **HZ-DI**, which possesses the same heptazethrene chromophore but with a different substituent.[17] For comparison, **HZ-DI** shows a different absorption band characteristic of a biradicaloid species and there is almost no fluorescence.[17] **OZ-TIPS** has a blue-to-green color and the absorption spectrum displays a well-resolved band in the far-red and near-infrared region, with maxima at 795, 719, 668, and 613

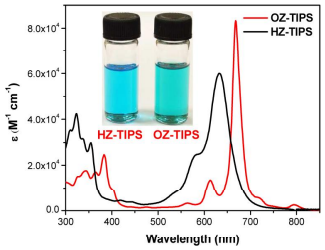

Figure 1. UV−vis−NIR absorption spectra of **HZ-TIPS** and **OZ-TIPS** in chloroform.

nm. The band shape is different from **HZ-TIPS** but is similar to other open-shell PAHs such as teranthene[11] and **HZ-DI**.[17] Moreover, **OZ-TIPS** exhibits a low fluorescence quantum yield of 1.5% with emission maximum at 807 nm (Figure S11 in SI). All these data indicate that **OZ-TIPS** may exist as an open-shell biradical in the ground state, and the lowest energy absorption band likely originates from the presence of a low-lying excited singlet state dominated by a doubly excited electronic configuration (H, H→L, L), as theoretically and experimentally demonstrated by the quinoidal oligothiophene oligomers.[22]

Femtosecond transient absorption (TA) measurements were then carried out to explore the excited-state photophysical properties of **HZ-TIPS** and **OZ-TIPS**. The TA spectra of **HZ-TIPS** and **OZ-TIPS** exhibit ground-state bleach signals around 630 and 670 nm as well as weak excited-state absorption bands in 450−550 and 700−750 nm spectral regions, respectively (Figure 2). The singlet excited-state lifetimes of **HZ-TIPS** and **OZ-TIPS** were estimated to be 3.4 and 1.6 ns, respectively, which are consistent with the fluorescence lifetimes measured by the time-correlated single-photon-counting (TCSPC) technique (Figure S12 in SI). The radiative decay rate constants can be calculated by $k_r = \Phi_f / \tau_f$. Also, because we already know τ_f and k_r, the nonradiative deactivation rate constants can be estimated through $\tau_f = 1/(k_r + k_{nr})$ (Table 1). While the nonradiative decay rate of **OZ-TIPS** was faster than that of **HZ-TIPS**, the radiative decay rate of **OZ-TIPS** was observed much slower than that of **HZ-TIPS**. The difference in the radiative decay rates as well as the nonradiative decay rates between **OZ-TIPS** and **HZ-TIPS** is thought to reflect their respective electronic character.

VT NMR, ESR, and SQUID Measurements. Variable temperature (VT) ^{1}H NMR spectra of **OZ-TIPS** were recorded

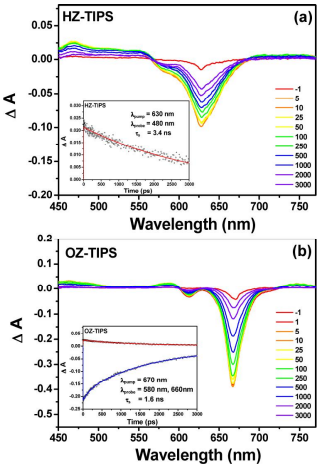

Figure 2. Transient absorption spectra of **HZ-TIPS** (a) and **OZ-TIPS** (b) in chloroform. Insert are the decay curves.

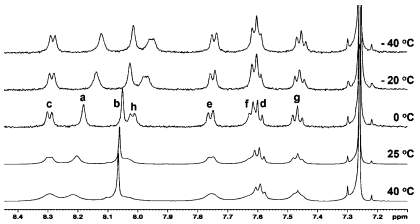

Figure 3. Variable-temperature ^{1}H NMR spectra (aromatic region) of **OZ-TIPS** in $CDCl_3$ and assignment of all aromatic protons. The resonance assignment referred to the structure shown in Chart 1.

in $CDCl_3$ (Figure 3). In contrast to **HZ-TIPS**, the resonances from the octazethrene core in **OZ-TIPS** are significantly broadened at room temperature and further broadened at elevated temperatures. However, these peaks become obviously

Table 1. Photophysical and Electrochemical Data of HZ-DI, HZ-TIPS, and OZ-TIPS[a]

compd	λ_{abs} (nm)	ϵ_{max} (M^{-1} cm^{-1})	PL (nm)	QY (%)	τ_f (ns)	k_r (s^{-1})	k_{nr} (s^{-1})	$E_{ox}^{1/2}$ (V)	$E_{red}^{1/2}$ (V)	HOMO (eV)	LUMO (eV)	E_g^{EC} (eV)	E_g^{Opt} (eV)
HZ-DI	641, 701, 747, 827	24382	–	–	–	–	–	0.62, 0.93	−0.65, −0.69	−5.22	−4.23	0.99	1.16
HZ-TIPS	584, 634	60000	704	16	3.4	4.7×10^7	2.5×10^8	0.17, 0.69	−1.48, −1.86	−4.87	−3.41	1.46	1.82
OZ-TIPS	613, 668, 719, 795	83300	807	1.5	1.6	9.4×10^6	6.2×10^8	0.02, 0.22, 0.61	−1.30, −1.56, −1.82	−4.73	−3.60	1.13	1.50

[a] λ_{abs}: absorption peak wavelength. ϵ_{max}: molar extinction coefficient at the absorption maximum. PL: photoluminescence wavelength. QY: fluorescence quantum yield. τ_f: fluorescence lifetime. k_r: radiative decay rate constant. k_{nr}: nonradiative deactivation rate constant. $E_{ox}^{1/2}$ and $E_{red}^{1/2}$ are half-wave potentials of the oxidative and reductive waves, respectively. HOMO and LUMO are determined from the oxidation and reduction onset, respectively. E_g^{EC}: electrochemical energy gap. E_g^{Opt}: optical energy gap.

dx.doi.org/10.1021/ja304618v | J. Am. Chem. Soc. 2012, 134, 14913−14922

sharper as the temperature decreases to 0 °C. This is a typical phenomenon for other PAHs with a singlet open-shell ground state. The NMR signal broadening results from a thermally excited triplet species, which is slightly higher in energy than the singlet biradical state.[10,11,17] Further decrease of temperature led to signal broadening and upfield shift of the resonances of the octazethrene core, particularly for the protons a, b, and h, which can be explained by enhanced aggregation at lower temperature. The existence of strong intermolecular association in solution is supported by the crystallographic analysis to be discussed later on.

Solution and solid powder of **HZ-TIPS** did not show any electron spin resonance (ESR) signal, even at elevated temperatures (up to 400 K), further supporting its closed-shell structure. The solution of **OZ-TIPS** did not show any ESR signal, too; however, its powder exhibited a ESR signal at g = 2.0026 (Figure 4a), and the intensity decreases with a

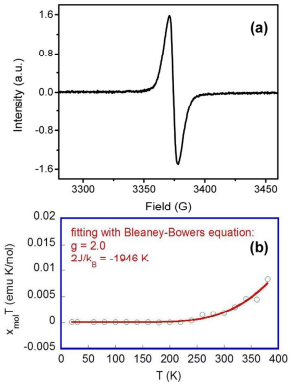

Figure 4. (a) ESR spectrum of **OZ-TIPS** in powder measured at room temperature. (b) $\chi T-T$ plot for the solid **OZ-TIPS**. The measured data was plotted as open circles, and the fitting curve was drawn using the Bleaney–Bowers equation with g = 2.00.

decrease of temperature, presumably due to the lower population of triplet species at lower temperature. However, zero-field splitting and $\Delta m_s = \pm 2$ transition were not observed, probably due to long mean spin–spin separation, and a similar phenomenon was also observed in a *meso*-diketo hexaphyrin biradical.[23] The singlet–triplet energy gap ($\Delta E_{S\text{-}T}$) of **OZ-TIPS** was estimated by superconducting quantum interfering device (SQUID) measurements for a powder sample at 5–380 K. The measurements showed an increasing susceptibility above 220 K (Figure 4b), and careful fitting of the data by using Bleaney–Bowers equation[24] gave a $2J/k_B = -1946$ K (0.168 eV or 3.87 kcal/mol). These measurements prove that **OZ-TIPS** has a singlet open-shell ground state, which can be thermally excited to its triplet excited state at room temperature due to a small singlet–triplet energy gap ($\Delta E_{S\text{-}T} \approx 3.87$ kcal/mol). The percentage of the triplet species at room temperature was thus estimated to be about 0.14%. This also means that there is very low spin concentration in the dilute solution of **OZ-TIPS**, which can explain the ESR silence in solution. However, in the powder form, the increased spin concentration allowed detection of the paramagnetic signal by ESR. SQUID measurement on **HZ-TIPS** only revealed diamagnetism.

FT Raman Spectroscopic Measurements. Raman spectroscopy has proven to be very useful for the characterization of benzene-type aromatic biradicals, either singlets or triplets.[25] This is based on the fact that there exist characteristic benzene vibrational Raman bands around 1600 cm^{-1} that are very sensitive to the electronic configuration within the six-membered benzene ring, either "benzoquinoidal" or "benzoaromatic". Benzoaromatic Raman modes are associated with frequency bands higher than 1600 cm^{-1}, while benzoquinoidal modes always appear at lower frequencies due to the overall CC bond weakening of the benzenoid ring by the loss of aromaticity. Therefore, FT 1064 nm Raman spectroscopy was used to further probe the electronic configuration of the *p*-xylylene and 2,6-naphthodimethane units in **HZ-TIPS** and **OZ-TIPS**.

At room temperature, a diagnostic ν(C=C) band at 1590 cm^{-1} was observed for **HZ-TIPS**, while this band was shifted to 1602 cm^{-1} in **OZ-TIPS** (Figure 5). Such a change could be

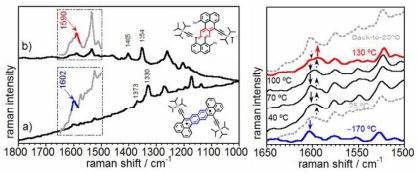

Figure 5. Solid-state 1064 nm FT-Raman spectra of **OZ-TIPS** (a) and **HZ-TIPS** (b) with the regions of interest expanded (left) and variable-temperature Raman spectra of **OZ-TIPS** (right). Arrows highlight the intensity inversion.

explained by the evolution of a *p*-quinodimethane-like structure in the closed-shell **HZ-TIPS** to a pseudoaromatic naphthalene structure in the open-shell **OZ-TIPS** (highlighted in Figure 5).

Variation of temperature did not result in significant change for the Raman spectrum of **HZ-TIPS**. However, for **OZ-TIPS**, thermal heating delineates a progressive 1602/1595 cm^{-1} intensity inversion (Figure 5, indicated by arrow). In the diagnostic 1600 cm^{-1} region, the spectrum displays a single band at 1602 cm^{-1} at −170 °C accompanied by a very weak signal at 1591 cm^{-1}. With the heating of the sample from room temperature up to 130 °C, a band at 1595 cm^{-1} appears and becomes the strongest. Overall the thermal heating leads to a progressive 1602/1595 cm^{-1} intensity inversion, and importantly, the cycle is reversible (i.e., the spectrum is completely recovered by cooling the sample from 130 °C to room temperature). Our recent studies on a viologen sample with similar singlet and triplet biradical forms showed that its triplet form displaced at lower frequency compared with its singlet biradical.[25b] Thus, for **OZ-TIPS**, we can assign the 1602 cm^{-1} band at low temperatures to its singlet biradical species and the downshifted band at 1595 cm^{-1} at 130 °C to its triplet species. By heating, therefore, we promote a singlet-to-triplet intersystem crossing, which is in consistent with the VT NMR, ESR, and SQUID measurements, as discussed above.

To further confirm the assignment, UCAM-B3LYP/6-31G* theoretical calculations of the Raman spectra were conducted

for the relevant singlet and triplet species of **HZ-TIPS** and **OZ-TIPS** (Figure 6). The main two bands of the theoretical

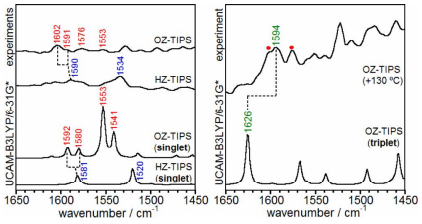

Figure 6. Left: Theoretical UCAM-B3LYP/6-31G* and experimental Raman spectra (in **OZ-TIPS**, the experimental spectrum corresponds to that at −170 °C). Right: UCAM-B3LYP/6-31G* theoretical Raman spectrum of **OZ-TIPS** in its first triplet excited state together with the experimental spectrum at +130 °C. The rest of the bands of the singlet species are denoted as red circles.

spectrum of **HZ-TIPS** at 1581 and 1520 cm^{-1} (difference of 61 cm^{-1}) correlate with the experimental ones at 1590 and 1534 cm^{-1} (difference of 56 cm^{-1}). The band at 1581 cm^{-1} can be described as a CC stretching mode located in the central benzene ring, which represents a motion of the parallel CC bonds of this ring bearing a quinoidal pattern (seen in Figure 7

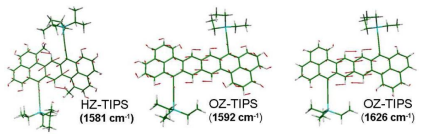

Figure 7. Theoretical vibrational eigenvectors associated with the most relevant bands of the theoretical spectra.

is its theoretical vibrational eigenvector). This 1581 cm^{-1} band splits into two components in **OZ-TIPS** at 1592 and 1580 cm^{-1} (difference of 12 cm^{-1}), which might be related with the experimental bands at 1602 and 1591 cm^{-1} (difference of 11 cm^{-1}). The vibrational eigenvector of the 1592 cm^{-1} theoretical band can be described as a CC stretching placed at the two innermost fused benzene rings in Figure 7. In contrast to that at 1581 cm^{-1} in **HZ-TIPS**, the **OZ-TIPS** mode describes an aromatic-like motion in which the six CC bonds of each benzene vibrate with significant amplitude (in the quinoidal mode this motion is restricted to the parallel quinoidal CC bonds).

Figure 6 also compares the Raman spectrum of **OZ-TIPS** at +130 °C with the UCAM-B3LYP/6-31G* theoretical one of its triplet species. In the 1600 cm^{-1} region, the theoretical spectrum only predicts one intense band at 1626 cm^{-1}. As a result, this theoretical band must be assigned to the sole band that increases its intensity with the heating, that is, the band at 1595 cm^{-1}. The normal mode associated with this band in Figure 7 resembles that associated with the 1592 cm^{-1} band of the open-shell singlet species of **OZ-TIPS**. Therefore, the bands at 1602 and 1591 cm^{-1} measured at −170 °C in **OZ-TIPS** are due to the singlet open shell species. The Raman band of the triplet appears nearby, at 1595 cm^{-1}, but it selectively shows enhancement with the increase of the temperature due to the singlet−triplet equilibrium.

DFT Calculations on the Ground-State Electronic Structures. Unrestricted symmetry-broken DFT calculations using the UCAM-B3LYP method[26] were conducted to further understand the ground-state electronic structures. The $\Delta E_{S\text{-}T}$ values were calculated to be 8.1 and 4.4 kcal/mol for **HZ-TIPS** and **OZ-TIPS**, respectively (triplet above singlet), and the computed energy differences between the closed-shell singlet and the open-shell singlet biradical states were −3.7 and −11.3 kcal/mol for **HZ-TIPS** and **OZ-TIPS**, respectively, suggesting that both molecules may contain a certain degree of the singlet biradical property in the ground state. More informative singlet biradical characters y_0 of 0.159 and 0.434 were obtained for **HZ-TIPS** and **OZ-TIPS**, respectively, to represent their biradical natures between the closed-shell and pure diradical states (0 to 1). While **HZ-TIPS** was predicted to have some lower degree of singlet biradical character in the ground state, our experimental data suggested its closed-shell electronic structure. Such difference between theory and experiment has been observed for other PAHs, especially for those having borderline biradical characters.[27] However, the trends that increasing the conjugated units leads to a decrease of $\Delta E_{S\text{-}T}$ and an increase in the y_0 values are in good agreement with observations in the related systems.[10,11,25b] The calculated singly occupied molecular orbital (SOMO) profiles of the α and β spin of **OZ-TIPS** shown in Figure 8 revealed a typical

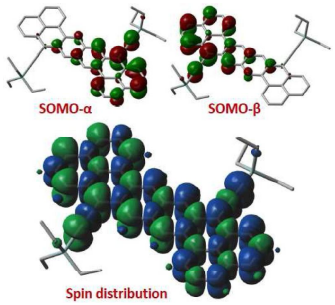

Figure 8. Calculated (UCAM-B3LYP) SOMOs for the α and β electrons and spin density distribution of the singlet biradical of **OZ-TIPS**. Blue and green surfaces represent α and β spin density, respectively. To simplify calculation, the triisopropylsilyl groups are replaced by triethylsilyl units.

disjoint feature, indicating a large singlet biradical character for this molecule. The spin densities in **OZ-TIPS** are evenly distributed throughout the whole octazethrene and ethynylene moieties (Figure 8), which is different from that of the bisphenalenyls, in which the spin density is mainly delocalized at the two terminal phenalenyl units.[10]

TPA Spectroscopic Measurements and Evaluation of the Singlet Biradical Character *y*. As a general rule, we have found that the third-order NLO response reflects variations in the electronic structure as well as the conformational geometry of the molecules, giving rise to the underlying static and dynamic polarizability.[28] In contrast with **HZ-TIPS**, **OZ-TIPS**

has an unusual ground-state structure with an open-shell configuration, which should be one of the most attractive issues in understanding the TPA–structure correlation between these derivatives. The large TPA activities of bis(phenalenyl) hydrocarbons with benzene and naphthalene spacers possessing an intermediate singlet biradical character have been reported.[2] To characterize NLO properties, the TPA values of **HZ-TIPS** and **OZ-TIPS** were measured by using a wavelength-scanning open aperture *Z*-scan method in the wavelength range from 1200 to 1650 nm, where one-photon absorption contribution is negligible. In relevance to the structure-correlation of radical character, while the TPA cross-section of the closed-shell system **HZ-TIPS** was determined to be 920 GM at 1250 nm, **OZ-TIPS** possessing a singlet biradical character exhibited an enhancement of TPA cross section value of 1200 GM at 1250 nm (Figure 9 and Figure S13 in SI). Such an enhancement on the third-order NLO property can be explained by the larger singlet biradical character of **OZ-TIPS**.

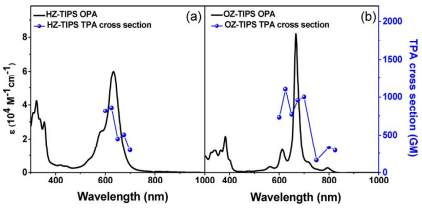

Figure 9. OPA (black solid line and left vertical axis) and TPA spectra (blue symbols and right vertical axis) of (a) **HZ-TIPS** and (b) **OZ-TIPS** in chloroform. TPA spectra are plotted at $\lambda_{ex}/2$.

On the basis of the OPA and TPA data and the $\Delta E_{S\text{-}T}$ value obtained from the SQUID measurement, the singlet biradical character *y* value of **OZ-TIPS** was evaluated to be 0.56 by using the following equation

$$y = 1 - \sqrt{1 - \left(\frac{E_{S_{1u},S_{1g}} - E_{T_{1u},S_{1g}}}{E_{S_{2g},S_{1g}}}\right)^2}$$

where $E_{S_{1u},S_{1g}}$ and $E_{S_{2g},S_{1g}}$ correspond to the energy of the lowest-energy peaks in the one- and two-photon absorption spectra (795 nm = 1.60 eV and 800 nm = 1.55 eV, respectively, in the case of **OZ-TIPS**), and $E_{T_{1u},S_{1g}}$ corresponds to the energy gap between triplet and singlet ground states (3.87 kcal/mol = 0.168 eV for **OZ-TIPS**).[27]

Electrochemical Properties. Cyclic voltammetry was performed to investigate the redox behaviors of **HZ-TIPS** and **OZ-TIPS** (Figure 10, and the data are collected in Table 1). Excellent electrochemical amphotericity was observed for both **HZ-TIPS** and **OZ-TIPS**. **HZ-TIPS** undergoes two reversible oxidations with half-wave potential ($E_{ox}^{1/2}$) at 0.17 and 0.69 V and two reversible reductive waves with half-wave potential ($E_{red}^{1/2}$) at −1.48 and −1.86 V (vs Fc^+/Fc). **OZ-TIPS** shows three reversible oxidation waves with ($E_{ox}^{1/2}$) at 0.02, 0.22, and 0.61 V and three reversible reductive waves with $E_{red}^{1/2}$ at −1.30, −1.56, and −1.82 V (vs Fc^+/Fc). A low electrochemical energy band gap (E_g^{EC}) was determined as 1.13 eV for **OZ-TIPS**, 0.33 eV lower than that of **HZ-TIPS**. For

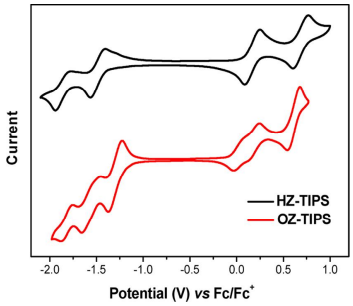

Figure 10. Cyclic voltammograms of **HZ-TIPS** and **OZ-TIPS** in DCM with 0.1 M Bu_4NPF_6 as supporting electrolyte, Ag/AgCl as reference electrode, Au disk as working electrode, Pt wire as counter electrode, and scan rate at 50 mV/s.

comparison, **HZ-DI** has a much smaller E_g^{EC} (0.99 eV) than **HZ-TIPS** (1.46 eV), and the same trend was observed for their optical energy gaps (E_g^{Opt}), i.e, E_g^{Opt} = 1.16 eV for **HZ-DI** and 1.82 eV for **HZ-TIPS** (Table 1). Considering that both **HZ-DI** and **HZ-TIPS** have the same heptazethrene core, such a difference in the energy gap should account for their different ground states. This observation provided further evidence that a small energy gap is a crucial precondition for the formation of a singlet open-shell ground state.[10,11]

X-ray Crystallographic Analysis. Single crystals of **HZ-TIPS** and **OZ-TIPS** suitable for crystallographic analysis were successfully grown from solution and their structure and 3D packing structure determined at 90 K are shown in Figure 11.[29,30] Both molecules are completely flat with point symmetry and exhibit large bond length alternation for the *p*-xylene framework in **HZ-TIPS** and the 2,6-naphthodimethene framework in **OZ-TIPS**. Importantly, the *exo*-methylene double bonds, C2C15 [1.398(2) Å] in **HZ-TIPS** and C3C6 [1.4088(19) Å] in **OZ-TIPS**, are both significantly longer than those in typical olefins (1.33–1.34 Å), suggesting the contribution of biradical character. The slightly but distinctly longer *exo*-methylene bond in **OZ-TIPS** is in accordance with their different singlet biradical character.

Interestingly, both **HZ-TIPS** and **OZ-TIPS** are packed into a 1D infinite chain via intermolecular π–π interactions, with an average π-stacking distance of 3.38 and 3.35 Å, respectively. Such distance is larger than those in the phenalenyl dimer[9] and in the 1D polymer chain of Kubo's bisphenalenyls,[10] in which intermolecular covalent π-bonding is believed to form between the phenalenyl radicals. Thus, the intermolecular interactions in our systems are dominated by π–π interactions with very less covalent character. Such difference may originate from the closed-shell structure of **HZ-TIPS** and the homogeneous spin distribution in **OZ-TIPS**.

Photostability Test. Compounds **HZ-TIPS** and **OZ-TIPS** remained unchanged in the solid state and in chloroform solution for at least 3 months when stored at 4 °C under nitrogen protection and in the absence of light. In contrast, solid **HZ-DI** decomposed in 1 week under the same conditions. The half-lives of **HZ-TIPS** and **OZ-TIPS** in chloroform upon ambient light irradiation in air at room temperature were found to be as long as 4 days and 34 h, respectively (Figure S14–18 in

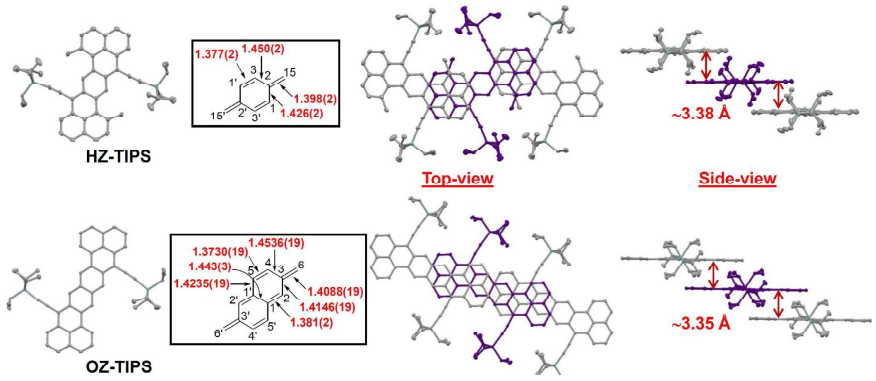

Figure 11. X-ray single-crystal structures of **HZ-TIPS** and **OZ-TIPS**, with bond length labeled for the central *p*-xylylene and 2,6-naphthodimethane units, and their top view and side view packing structures. Hydrogen atoms are omitted for clarity.

SI). The decomposition is likely due to addition of one or two oxygen molecules onto the heptazethrene or octazethrene backbone, as indicated by MALDI-TOF mass spectrometry (Figure S19–S20 in SI). The relatively good photostability of **OZ-TIPS** comes from the large extended delocalization of the biradicals and the kinetic blocking of the most reactive sites by TIPS groups.

3. CONCLUSION

In summary, kinetically blocked heptazethrene (**HZ-TIPS**) and octazethrene (**OZ-TIPS**) were prepared by a new synthetic approach. The attachment of the TIPS group at the most reactive site efficiently stabilizes the otherwise unstable biradicals. Both compounds show good stability both in the solid state and in solution due to kinetic blocking, which is important for their practical applications. Their electronic structures in the ground state were systematically investigated by a series of experimental methods assisted by DFT calculations. Steady-state absorption spectroscopic measurements disclosed the distinguished difference of the band structure between the open-shell **OZ-TIPS** and the closed-shell **HZ-TIPS**. Transient absorption and fluorescence spectra provided further information on the excited state lifetime, which again showed obvious difference between the open-shell and closed-shell structure. VT NMR, ESR, and SQUID were used to probe the magnetic properties, and the observed paramagnetism for the open-shell **OZ-TIPS** can be explained by the thermally excited singlet-to-triplet transition, which is an important feature of the singlet biradicaloids. More importantly, the singlet–triplet energy gap can be evaluated by VT ESR and SQUID experiments. FT-Raman spectroscopy was used to further probe the ground-state electronic structure. The quinoidal resonance form and the aromatic biradical resonance form can be nicely distinguished in their vibrational spectra, and even the singlet–triplet transition can be followed by the VT Raman measurements. Unrestricted symmetry-broken DFT calculations were used to understand the electronic structure and singlet biradical character. X-ray crystallographic analysis provided further information about the bond length, which is closely related to the ground-state electronic structure. Both compounds form a closely packed 1D infinite chain in single crystals via $\pi-\pi$ stacking, indicating their potential applications for ambipolar field effect transistors and spintronics. In addition, both compounds show large TPA cross sections, which is in agreement with theoretical predictions on the open-shell singlet biradicaloids. The large TPA response and good stability of these new compounds indicate their potential applications in nonlinear optics. By collecting all these experimental data and theoretical calculations, a clear picture of the ground state structure can be figured out: the **HZ-TIPS** has a closed-shell ground state while the higher order **OZ-TIPS** has an open-shell singlet biradical ground state. Remarkably, the singlet biradical character y = 0.56 for **OZ-TIPS** was obtained by a combination of the OPA, TPA, and SQUID data.

In contrast to our previously reported open-shell heptazethrene diimide (**HZ-DI**),[17] the **HZ-TIPS** has a closed-shell ground state, although it has the same heptazethrene core. This can be explained by the relatively large energy gap of the latter, indicating that a small energy gap is crucial for an open-shell ground state structure. It is noteworthy that the first stable octazethrene derivative **OZ-TIPS** was synthesized, which has been pursued by chemists for a long time. The design concept and the new synthetic strategy starting from the corresponding diketone likely can be applied to the synthesis of other stable open-shell polycyclic hydrocarbons or hybrid structures. The characterization methods reported here can be regarded as a comprehensive and systematical approach to investigate singlet biradicaloids in the future.

4. EXPERIMENTAL SECTION

The synthetic details and the general characterization methods (e.g., NMR and MS) are described in the Supporting Information.

Steady-state UV–vis absorption and fluorescence spectra were recorded on a Shimadzu UV-1700 spectrometer and a RF-5301 fluorometer, respectively.

The electrochemical measurements were carried out in anhydrous DCM with 0.1 M Bu_4NPF_6 as the supporting electrolyte at a scan rate of 0.05 V/s at room temperature under the protection of nitrogen. A gold disk was used as working electrode, platinum wire was used as

counting electrode, and Ag/AgCl (3 M KCl solution) was used as reference electrode. The potential was externally calibrated against the ferrocene/ferrocenium couple.

Continuous wave X-band ESR spectra were obtained with a Bruker ELEXSYS E500 spectrometer using a variable-temperature Bruker liquid nitrogen cryostat.

A superconducting quantum interference device magnetometer MPMS-XL was used for the magnetic characterization. The temperature-dependent magnetic susceptibility (χ_{mol}) was measured for the **HZ-TIPS** and **OZ-TIPS** samples under a constant magnetic field of 1000 Oe in the temperature range of 5−380 K.

FT−Raman spectra were measured using an FT−Raman accessory kit (FRA/106−S) of a Bruker Equinox 55 FT−IR interferometer. A continuous-wave Nd−YAG laser working at 1064 nm was employed for excitation, at a laser power in the sample not exceeding 30 mW. A germanium detector operating at liquid nitrogen temperature was used. Raman scattering radiation was collected in a back-scattering configuration with a standard spectral resolution of 4 cm^{-1}. 2000 scans were averaged for each spectrum. A variable-temperature cell Specac P/N 21525, with interchangeable pairs of quartz windows, was used to record the FT-Raman spectra at different temperatures. The variable temperature cell consists of a surrounding vacuum jacket (0.5 Torr), and combines a refrigerant Dewar and a heating block as the sample holder. It is also equipped with a copper constantan thermocouple for temperature monitoring between −170 and 150 °C. Samples were inserted into the heating block part or the Dewar/cell holder assembly in the form of pure solids dispersed in KBr pellets, and Raman spectra were recorded after waiting for thermal equilibrium in the sample. The samples in KBr pellets were prepared in an oxygen and water-free bag.

The femtosecond time-resolved transient absorption spectrometer used for this study consisted of a femtosecond optical parametric amplifier (Quantronix, Palitra-FS) pumped by a Ti:sapphire regenerative amplifier system (Quantronix, Integra-C) operating at 1 kHz repetition rate and an accompanying optical detection system. The generated OPA pulses had a pulse width of ∼100 fs and an average power of 1 mW in the range 450−800 nm, which were used as pump pulses. White light continuum (WLC) probe pulses were generated using a sapphire window (2 mm thick) by focusing of small portion of the fundamental 800 nm pulses, which were picked off by a quartz plate before entering into the OPA. The time delay between pump and probe beams was carefully controlled by making the pump beam travel along a variable optical delay (Newport, ILS250). Intensities of the spectrally dispersed WLC probe pulses were monitored by miniature spectrograph (OceanOptics, USB2000+). To obtain the time-resolved transient absorption difference signal (ΔA) at a specific time, the pump pulses were chopped at 25 Hz and absorption spectra intensities were saved alternately with or without pump pulse. Typically, 6000 pulses were used to excite samples and to obtain the TA spectra at a particular delay time. The polarization angle between pump and probe beam was set at the magic angle (54.7°) using a Glan-laser polarizer with a half-wave retarder to prevent polarization-dependent signals. The cross-correlation fwhm in the pump−probe experiments was less than 200 fs, and the chirp of WLC probe pulses was measured to be 800 fs in the 400−800 nm regions. To minimize chirp, all reflection optics were used in the probe beam path, and a quartz cell of 2 mm path length was employed. After completing each set of fluorescence and TA experiments, the absorption spectra of all compounds were carefully checked to rule out the presence of artifacts or spurious signals arising from, for example, degradation or photo-oxidation of the samples in question.

Time-resolved fluorescence lifetime experiments were performed by the TCSPC technique. As an excitation light source, we used a homemade cavity-dumped Ti:sapphire oscillator, which provides a high repetition rate (200−400 kHz) of ultrashort pulses [100 fs at full width at half-maximum (fwhm)] pumped by a continuous wave (cw) Nd-YVO_4 laser (Coherent, Verdi). The output pulse of the oscillator was frequency-doubled by a 1 mm thickness of a second harmonic crystal (barium borate, BBO, CASIX). The fluorescence was collected by a microchannel plate photomultiplier (MCP-PMT, Hamamatsu, R3809U-51) with a thermoelectric cooler (Hamamatsu, C4878) connected to a TCSPC board (Becker & Hickel SPC-130). The overall instrumental response function was about 25 ps (fwhm). A vertically polarized pump pulse by a Glan-laser polarizer irradiated samples, and a sheet polarizer, set at an angle complementary to the magic angle (54.7°), was placed in the fluorescence collection path to obtain polarization-independent fluorescence decays.

The two-photon absorption spectrum was measured in the NIR region using the open-aperture Z-scan method with 130 fs pulses from an optical parametric amplifier (Light Conversion, TOPAS) operating at a repetition rate of 3 kHz generated from a Ti:sapphire regenerative amplifier system (Spectra-Physics, Hurricane). After passing through a 10 cm focal length lens, the laser beam was focused and passed through a 1 mm quartz cell. Since the position of the sample cell could be controlled along the laser beam direction (z axis) using the motorcontrolled delay stage, the local power density within the sample cell could be simply controlled under constant laser intensity. The transmitted laser beam from the sample cell was then detected by the same photodiode as used for reference monitoring. The on-axis peak intensity of the incident pulses at the focal point, I_0, ranged from 40 to 60 GW cm^{-2}. For a Gaussian beam profile, the nonlinear absorption coefficient can be obtained by curve fitting of the observed open-aperture traces $T(z)$ with the following equation

$$T(z) = 1 - \frac{\beta I_0 (1 - e^{-\alpha_0 l})}{2\alpha_0 [1 + (z/z_0)^2]}$$

where α_0 is the linear absorption coefficient, l is the sample length, and z_0 is the diffraction length of the incident beam. After the nonlinear absorption coefficient has been obtained, the TPA cross section $\sigma^{(2)}$ of one solute molecule (in units of GM, where 1 GM = 10^{-50} cm^4 s $photon^{-1}$ $molecule^{-1}$) can be determined by using the following relationship

$$\beta = \frac{10^{-3} \sigma^{(2)} N_A d}{h\nu}$$

where N_A is Avogadro's constant, d is the concentration of the compound in solution, h is Planck's constant, and ν is the frequency of the incident laser beam.

Theoretical calculations were carried out by using the Gaussian 09 suite of programs. The initial geometry optimization of **HZ-TIPS** and **OZ-TIPS** was performed with the UCAM-B3LYP level of theory on the singlet state and the Handy and co-workers' long-range corrected version of B3LYP 6-31G*, and all electron basis sets were employed for all atoms.[26a,31] The resulting DFT solution (singlet "closed-shell": zero spin density on all atoms) was further tested for its stability with the STABLE=OPT keyword.[26b] A spin symmetry broken DFT solution was found with lower energy. Then the Guess=Read keyword was used to perform the optimization at the UCAM-B3LYP level (singlet open shell). Frequency calculations were conducted to ensure that these structures are indeed local minima. To simplify calculation, the triisopropylsilyl groups are replaced by triethylsilyl units.

■ ASSOCIATED CONTENT

Supporting Information

Synthetic procedures and characterization data of all new compounds, steady-state and time-resolved fluorescence spectra, Z-scan curves, photostability test details, and crystallographic data. This material is available free of charge via the Internet at http://pubs.acs.org.

■ AUTHOR INFORMATION

Corresponding Author

dongho@yonsei.ac.kr; osuka@kuchem.kyoto-u.ac.jp; casado@uma.es; msedingj@nus.edu.sg; chmwuj@nus.edu.sg

Notes

The authors declare no competing financial interest.

■ ACKNOWLEDGMENTS

J.W. acknowledges the financial support from the BMRC-NMRC grant (no. 10/1/21/19/642), MOE Tier 2 grant (MOE2011-T2-2-130), and A*STAR IMRE core funding (IMRE/10-1P0509). The work at Yonsei University was supported by WCU (World Class University) programs (*R*32-2010-10217-0) and an AFSOR/APARD grant (no. FA2386-09-1-4092). K.-W.H. acknowledges the financial support from KAUST. We thank Ji'En Wu and Yanhui Han for their kind assistance on the NMR analysis and Prof. Yuan-Chung Cheng for useful discussion.

■ REFERENCES

(1) (a) Rajca, A. *Chem. Rev.* **1994**, *94*, 871−893. (b) Morita, Y.; Suzuki, K.; Sato, S.; Takui, T. *Nat. Chem.* **2011**, *3*, 197−204. (c) Lambert, C. *Angew. Chem., Int. Ed.* **2011**, *50*, 1756−1758. (d) Sun, Z.; Wu, J. *J. Mater. Chem.* **2012**, *22*, 4151−4160. (e) Sun, Z.; Ye, Q.; Chi, C.; Wu, J. *Chem. Soc. Rev.* **2012**, DOI: 10.1039/c2cs35211G.

(2) Kamada, K.; Ohta, K.; Kubo, T.; Shimizu, A.; Morita, Y.; Nakasuji, K.; Kishi, R.; Ohta, S.; Furukawa, S.; Takahashi, H.; Nakano, M. *Angew. Chem., Int. Ed.* **2007**, *46*, 3544−3546.

(3) (a) Chikamatsu, M.; Mikami, T.; Chisaka, J.; Yoshida, Y.; Azumi, R.; Yase, K. *Appl. Phys. Lett.* **2007**, *91*, 043506. (b) Chase, D. T.; Fix, A. G.; Kang, S. J.; Rose, B. D.; Weber, C. D.; Zhong, Y.; Zakharov, L. N.; Lonergan, M. C.; Nuckolls, C.; Haley, M. M. *J. Am. Chem. Soc.* **2012**, *134*, 10349−10352. (c) Nishida, J.; Tsukaguchi, S.; Yamashita, Y. *Chem.—Eur. J.* **2012**, *18*, 8964−8970.

(4) Yazyev, O.; Katsnelson, M. I. *Phys. Rev. Lett.* **2008**, *100*, 047209.

(5) Morita, Y.; Nishida, S.; Murata, T.; Moriguchi, M.; Ueda, A.; Satoh, M.; Arifuku, K.; Sato, K.; Takui, T. *Nat. Mater.* **2011**, *10*, 947−951.

(6) (a) Son, Y. W.; Cohen, M. L.; Louie, S. G. *Nature* **2006**, *444*, 347−349. (b) Son, Y. W.; Cohen, M. L; Louie, S. G. *Phys. Rev. Lett.* **2006**, *97*, 216803. (c) Kim, W. Y.; Kim, K. S. *Nat. Nanotechnol.* **2008**, *3*, 408−412.

(7) (a) Thiele, J.; Balhorn, H. *Chem. Ber.* **1904**, *37*, 1463. (b) Flynn, C. R.; Michl, J. *J. Am. Chem. Soc.* **1974**, *96*, 3280−3288. (c) Montgomery, L. K.; Huffman, J. C.; Jurczak, E. A.; Grendze, M. P. *J. Am. Chem. Soc.* **1986**, *108*, 6004−6011. (d) Chase, D. T.; Rose, B. D.; McClintock, S. P.; Zakharov, L. N.; Haley, M. M. *Angew. Chem., Int. Ed.* **2011**, *50*, 1127−1130. (e) Zeng, Z.; Sung, Y. M.; Bao, N.; Tan, D.; Lee, R.; Zafra, J. L.; Lee, B. S.; Ishida, M.; Ding, J.; Lopez Navarrete, J. T.; Li, Y.; Zeng, W. D.; Kim, D.; Huang, K.-W.; Webster, R. D.; Casado, J.; Wu, J. *J. Am. Chem. Soc.* **2012**, DOI: 10.1021/ja3050579.

(8) (a) Kolc, J.; Michl, J. *J. Am. Chem. Soc.* **1970**, *92*, 4147−4148. (b) Iwashita, S.; Ohta, E.; Higuchi, H.; Kawai, H.; Fujiwara, K.; Ono, K.; Takenaka, M.; Suzuki, T. *Chem. Commun.* **2004**, 2076−2077. (c) Shimizu, A.; Tobe, Y. *Angew. Chem., Int. Ed.* **2011**, *50*, 6906−6910.

(9) (a) Reid, D. H. *Chem. Ind.* **1956**, 1504−1505. (b) Gerson, F. *Helv. Chim. Acta* **1966**, *49*, 1463−1472. (c) Goto, K.; Kubo, T.; Yamamoto, K.; Nakasuji, K.; Sato, K.; Shiomi, D.; Takui, T.; Kubota, M.; Kobayashi, T.; Yakusi, K.; Ouyang, J.-Y. *J. Am. Chem. Soc.* **1999**, *121*, 1619−1620. (d) Itkis, M. E.; Chi, X.; Cordes, A. W.; Haddon, R. C. *Science* **2002**, *296*, 1443−1445.

(10) (a) Ohashi, K.; Kubo, T.; Masui, T.; Yamamoto, K.; Nakasuji, K.; Takui, T.; Kai, Y.; Murata, I. *J. Am. Chem. Soc.* **1998**, *120*, 2018−2027. (b) Kubo, T.; Sakamoto, M.; Akabane, M.; Fujiwara, Y.; Yamamoto, K.; Akita, M.; Inoue, K.; Takui, T.; Nakasuji, K. *Angew. Chem., Int. Ed.* **2004**, *43*, 7474−6479. (c) Kubo, T.; Shimizu, A.; Sakamoto, M.; Uruichi, M.; Yakushi, K.; Nakano, M.; Shiomi, D.; Sato, K.; Takui, T.; Morita, Y.; Nakasuji, K. *Angew. Chem., Int. Ed.* **2005**, *44*, 6564−6568. (d) Shimizu, A.; Uruichi, M.; Yakushi, K.; Matsuzaki, H.; Okamoto, H.; Nakano, M.; Hirao, Y.; Matsumoto, K.; Kurata, H.; Kubo, T. *Angew. Chem., Int. Ed.* **2009**, *48*, 5482−5486. (e) Shimizu, A.; Kubo, T.; Uruichi, M.; Yakushi, K.; Nakano, M.; Shiomi, D.; Sato, K.; Takui, T.; Hirao, Y.; Matsumoto, K.; Kurata, H.; Morita, Y.; Nakasuji, K. *J. Am. Chem. Soc.* **2010**, *132*, 14421−14428. (f) Shimizu, A.; Hirao, Y.; Matsumoto, K.; Kurata, H.; Kubo, T.; Uruichi, M.; Yakushi, K. *Chem. Commun.* **2012**, *48*, 5629−5631.

(11) Konishi, A.; Hirao, Y.; Nakano, M.; Shimizu, A.; Botek, E.; Champagne, B.; Shiomi, D.; Sato, K.; Takui, T.; Matsumoto, K.; Kurata, H.; Kubo, T. *J. Am. Chem. Soc.* **2010**, *132*, 11021−11023.

(12) (a) Bendikov, M.; Duong, H. M.; Starkey, K.; Houk, K. N.; Carter, E. A.; Wudl, F. *J. Am. Chem. Soc.* **2004**, *126*, 7416−7417. (b) Jiang, D.-E.; Dai, S. *J. Phys. Chem. A* **2008**, *112*, 332−335.

(13) (a) Jiang, D.-E.; Sumpter, B. G.; Dai, S. *J. Chem. Phys.* **2007**, *127*, 124703. (b) Yao, J.; Chi, C.; Wu, J.; Loh, K.-P. *Chem.—Eur. J.* **2009**, *15*, 9299−9302. (c) Zhang, K.; Huang, K.-W.; Li, J.; Luo, J.; Chi, C.; Wu, J. *Org. Lett.* **2009**, *11*, 4854−4857. (d) Li, J.; Zhang, K.; Zhang, X.; Huang, K.-W.; Chi, C.; Wu, J. *J. Org. Chem.* **2010**, *75*, 856−863. (e) Zhang, X.−J.; Li, J.; Qu, H.; Chi, C.; Wu, J. *Org. Lett.* **2010**, *12*, 3946−3949. (f) Li, J.; Jiao, C.; Huang, K.-W.; Wu, J. *Chem.—Eur. J.* **2011**, *17*, 14672−14680. (g) Li, J.; Chang, J.; Tan, P.; Jiang, H.; Chen, X.; Chen, Z.; Zhang, J.; Wu, J. *Chem. Sci.* **2012**, *3*, 846−850.

(14) (a) Nakano, M.; Kishi, R.; Takebe, A.; Nate, M.; Takahashi, H.; Kubo, T.; Kamada, K.; Ohta, K.; Champagne, B.; Botek, E. *Comput. Lett.* **2007**, *3*, 333−338. (b) Yoneda, K.; Nakano, M.; Fukui, H.; Minami, T.; Shigeta, Y.; Kubo, T.; Botek, E.; Champagne, B. *ChemPhysChem* **2011**, *12*, 1697−1707.

(15) (a) Clar, E.; Lang, K. F.; Schulz-Kiesow, H. *Chem. Ber.* **1955**, *88*, 1520−1527. (b) Staab, H. A.; Nissen, A.; Ipaktschi, J. *Angew. Chem., Int. Ed. Engl.* **1968**, *7*, 226−226. (c) Mitchell, R. H.; Sondheimer, F. *Tetrahedron* **1970**, *26*, 2141−2150. (d) Umeda, R.; Hibi, D.; Miki, K.; Tobe, Y. *Org. Lett.* **2009**, *11*, 4104−4106. (e) Wu, T. C.; Chen, C. H.; Hibi, D.; Shimizu, A.; Tobe, Y.; Wu, Y. T. *Angew. Chem., Int. Ed.* **2010**, *49*, 7059−7062. (f) Sun, Z.; Huang, K.-W.; Wu, J. *Org. Lett.* **2010**, *12*, 4690−4693.

(16) Clar, E.; Macpherson, I. A. *Tetrahedron* **1962**, *18*, 1411−1416.

(17) Sun, Z.; Huang, K.-W.; Wu, J. *J. Am. Chem. Soc.* **2011**, *133*, 11896−1199.

(18) Erünliü, R. K. *Liebigs Ann. Chem.* **1969**, *721*, 43−47.

(19) Merlet, S.; Birau, M.; Wang, Z. Y. *Org. Lett.* **2002**, *4*, 2157−2159.

(20) Bailey, R. J.; Card, P. J.; Shechter, H. *J. Am. Chem. Soc.* **1983**, *105*, 6096−6103.

(21) (a) Weil, T.; Vosch, T.; Hofkens, J.; Peneva, K.; Müllen, K. *Angew. Chem., Int. Ed.* **2010**, *49*, 9068−9093. (b) Anthony, J. *Angew. Chem. Int. Ed.* **2008**, *47*, 452−483.

(22) Motta, S. D.; Negri, F.; Fazzi, D.; Castiglioni, C.; Canesi, E. V. *J. Phys. Chem. Lett.* **2010**, *1*, 3334−3339.

(23) Koide, T.; Furukawa, K.; Shinokubo, H.; Shin, J.-Y.; Kim, K. S.; Kim, D.-H.; Osuka, A. *J. Am. Chem. Soc.* **2010**, *132*, 7246−7247.

(24) Bleaney, B.; Bowers, K. D. *Proc. R. Soc. London Ser. A* **1952**, *214*, 451−465.

(25) (a) Ortiz, R. P.; Casado, J.; Hernández, V.; Navarrete, J. T. L.; Viruela, P. M.; Ortí, E.; Takimiya, K.; Otsubo, T. *Angew. Chem., Int. Ed.* **2007**, *46*, 9057−9061. (b) Casado, J.; Patchkovskii, S.; Zgierski, M. Z.; Hermosilla, L.; Sieiro, C.; Moreno Oliva, M.; López Navarrete, J. T. *Angew. Chem., Int. Ed.* **2008**, *47*, 1443−1447. (c) González, S. R.; Ie, Y.; Aso, Y.; López Navarrete, J. T.; Casado, J. *J. Am. Chem. Soc.* **2011**, *133*, 16350−16353.

(26) (a) Yanai, T.; Tew, D.; Handy, N. *Chem. Phys. Lett.* **2004**, *393*, 51−57. (b) Seeger, R.; Pople, J. A. *J. Chem. Phys.* **1977**, *66*, 3045−3050.

(27) Kamada, K.; Ohta, K.; Shimizu, A.; Kubo, T.; Kishi, R.; Takahashi, H.; Botek, E.; Champagne, B.; Nakano, M. *J. Phys. Chem. Lett.* **2010**, *1*, 937−940.

(28) Pawlicki, M.; Collins, H. A.; Denning, R. G.; Anderson, H. L. *Angew. Chem., Int. Ed.* **2009**, *48*, 3244−3266.

(29) Crystallographic data for **HZ-TIPS**: $C_{52}H_{60}Si_2$, M_w = 741.18; monoclinic; space group C_2/c; a = 18.548(6), b = 19.178(6), c = 13.920(5) Å, β = 122.838(4)°; V = 4160(2) Å^3; Z = 4; ρ_{calcd} = 1.183 Mg/m^3; R_1 = 0.0480 ($I > 2\sigma(I)$), wR_2 = 0.1398 (all data). CCDC No. 875408. X-ray-quality crystal was obtained by slow evaporation of the solution in toluene/heptane.

(30) Crystallographic data for **OZ-TIPS**: $C_{54}H_{58}Si_2$, M_w = 763.18; triclinic; space group $P\bar{1}$; a = 8.410(3) Å, b = 9.846(4) Å, c = 14.020(6) Å, α = 73.046(5)°, β = 77.078(5)°, γ = 87.083(5)°; V = 1082.1(8) Å^3; Z = 1; ρ_{calcd} = 1.171 Mg/m^3; R_1 = 0.0345 ($I > 2\sigma(I)$), wR_2 = 0.0947 (all data). CCDC No. 875409. X-ray-quality crystal was obtained by slow evaporation of the solution in toluene/THF/heptane.

(31) (a) Lee, C.; Yang, W.; Parr, R. G. *Phys. Rev. B* **1988**, *37*, 785−789. (b) Becke, A. D. *J. Chem. Phys.* **1993**, *98*, 5648−5652. (c) Ditchfie, R. W.; Hehre, J.; Pople, J. A. *J. Chem. Phys.* **1971**, *54*, 724−728. (d) Hehre, W. J.; Ditchfie, R.; Pople, J. A. *J. Chem. Phys.* **1972**, *56*, 2257−2261. (e) Harihara, P. C.; Pople, J. A. *Theor. Chim. Acta* **1973**, *28*, 213−222.

THE JOURNAL OF CHEMICAL PHYSICS **140**, 054706 (2014)

Zethrene biradicals: How pro-aromaticity is expressed in the ground electronic state and in the lowest energy singlet, triplet, and ionic states

José Luis Zafra,[1] Rafael C. González Cano,[1] M. Carmen Ruiz Delgado,[1] Zhe Sun,[2] Yuan Li,[2] Juan T. López Navarrete,[1] Jishan Wu,[2] and Juan Casado[1,a)]
[1]*Department of Physical Chemistry, University of Málaga, Campus de Teatinos s/n, Málaga 29071, Spain*
[2]*Department of Chemistry, National University of Singapore, 3 Science Drive 3, Singapore 117543*

(Received 28 October 2013; accepted 16 January 2014; published online 4 February 2014)

A analysis of the electronic and molecular structures of new molecular materials based on zethrene is presented with particular attention to those systems having a central benzo-quinoidal core able to generate *Kekulé* biradicals whose stability is provided by the aromaticity recovery in this central unit. These *Kekulé* biradicals display singlet ground electronic states thanks to double spin polarization and have low-energy lying triplet excited states also featured by the aromaticity gain. Pro-aromatization is also the driving force for the stabilization of the ionized species. Moreover, the low energy lying singlet excited states also display a profound biradical fingerprint allowing to singlet exciton fission. These properties are discussed in the context of the size of the zethrene core and of its substitution. The work encompasses all known long zethrenes and makes use of a variety of experimental techniques, such as Raman, UV-Vis-NIR absorption, transient absorption, *in situ* spectroelectrochemistry and quantum chemical calculations. This study reveals how the insertion of suitable molecular modules (i.e., quinoidal) opens the door to new intriguing molecular properties exploitable in organic electronics. © *2014 AIP Publishing LLC*. [http://dx.doi.org/10.1063/1.4863557]

I. INTRODUCTION

Zethrene molecules refer to a family of Z-shaped polycyclic hydrocarbons in which two phenalenes are head-to-head fused together with or without a benzenoid spacer.[1–3] They can be also regarded as dibenzo-acenes. The smallest member of this family contains a total of six condensed rings where two phenalenes are fused directly and was originally named as zethrene (**Z**), although the term "zethrene" is used to refer to the whole family of Z-shaped quinoidal hydrocarbons. The next parent zethrene is that with seven rings (heptazethrene, **HZ**) where the additional fused benzene goes between the two phenalenes, a ring which features a *para*-benzoquinoidal or *para*-benzoquinodimethane subunit (Scheme 1). Higher order zethrenes with more benzenoid rings are called octazethrene (**OZ**), nonazethrene (**NZ**), and so on. These molecular subunits are key syntons to develop *Kekulé* biradicals[4–7] given their pro-aromatic character which might eventually favour the sacrifice of one of the π-conjugated double bonds generating the biradical state (see Scheme 1).

In *Kekulé* biradicals, there is always a resonance form with all electrons paired in a singlet closed-shell configuration which contributes to stabilize the singlet ground electronic state with the parent triplet configuration of the biradical always residing very close in energy to the ground electronic singlet.[8] Singlet-triplet conversion within small energy gaps is an advantageous property in organic electronics[9] and spintronics:[10] for example, they can behave as switchable systems in response to soft external stimuli (temperature or magnetic excitations).

Wu *et al.* have recently reported new routes for the synthesis of several zethrene derivatives.[11–13] These compounds have two main structural characteristics: (i) their central acene cores are composed of heptazethrenes and octazethrenes (see Fig. 1); (ii) these cores are substituted at the terminal phenalene groups either with electron-acceptor or protecting groups in order to stabilize the biradical forms and to increase solubility and processability. In this way, they were able to prepare soluble heptazethrene diimide (**HZ-DI**)[11,12] and triisopropylsilylethynyl (TIPS)-substituted heptazethrene[13] (**HZ-TIPS**) and octazethrene[13] (**OZ-TIPS**) derivatives (see Fig. 1). In this paper, we will study all these zethrenes together and will attempt to elucidate which electronic configuration, either closed-shell quinoidal or open-shell (biradical) aromatic (Scheme 1), better describes their ground electronic state. We will also interrogate about the structure of the corresponding low-energy lying triplet excited states and of the ionized species (anions and cations). We will extend the study of the excited states to those required to explain their particular photophysical behavior. The information derived from this study might help to mechanistically understand the magnetic, electro-optical, and charge transfer properties of the new zethrene compounds pursuing to envisage new applications.

Raman spectroscopy, in its different modalities, has been shown to be a unique tool to evaluate the ground electronic state of polyconjugated molecules[14] and to discern between the molecular structures of singlet and triplet in *Kekulé* biradicals.[15–19] Typical CC stretching modes of the benzene ring are especially active in the Raman mechanism and hence their associated band frequencies represent valuable

a)Author to whom correspondence should be addressed. Electronic mail: casado@uma.es

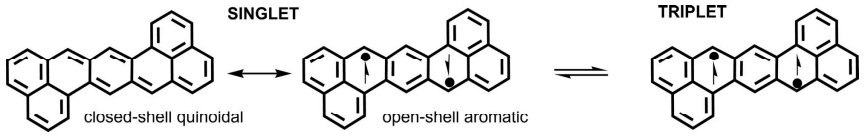

SCHEME 1. Aromatic-to-quinoidal balance in the formation of a *Kekulé* biradical and the singlet-triplet equilibrium in the prototypical case of unsubstituted heptazethrene, **HZ**.

spectroscopic observables to follow the quinoidal-to-aromatic structural change in the benzene moieties of the zethrene core (see Scheme 1).

In this paper, we carry out a comparative study of the molecular properties mentioned above for these two families of substituted zethrenes (Fig. 1) focusing on the character of the ground electronic state. To this end, we will discuss the experimental Raman spectra, the absorption electronic spectra, the transient absorption spectra (using microsecond flash-photolysis), and the *in situ* UV-Vis-NIR absorption spectra for the electrochemically generated charged species, together with the *ex situ* Raman spectra of anions and cations. To guide the spectroscopic analysis, the experimental data will be complemented with quantum chemical calculations.

II. EXPERIMENTAL

A. Synthesis

The synthesis of **HZ-DI** with two solubilising 3,7-dimethyloctyl substituents was accomplished with the same protocol for the synthesis of the related 2,6-diisopropylphenyl-substituted heptazethrene diimide analog[11,12] and this new heptazethrene diimide derivative can be obtained in much higher overall yield. The detailed synthetic procedures and characterization data are shown in the supplementary material.[35] The syntheses of the TIPS substituted heptazethrene (**HZ-TIPS**) and octazethrene (**OZ-TIPS**) derivatives were already reported by us.[13]

B. Raman spectroscopy

FT-Raman spectra of 1064 nm were obtained in an FT-Raman accessory kit (FRA/106–S) of a Bruker Equinox 55 FT–IR interferometer. A continuous-wave Nd–YAG laser working at 1064 nm was employed for excitation. A germanium detector operating at liquid nitrogen temperature was used. Raman scattering radiation was collected in a back-scattering configuration with a standard spectral resolution of 4 cm^{-1}. Scans (1000–3000) were averaged for each spectrum. Raman spectra with the excitation lasers at 532, 633, and 785 nm were collected by using the 1 × 1 camera of a Bruker Senterra Raman microscope by averaging spectra during 50 min with a resolution of 3–5 cm^{-1}. A CCD camera operating at −50 °C was used for the Raman detection.

C. Optical and spectroelectrochemical characterization

UV-vis-NIR spectra were recorded in a 1 cm path-length quartz cell on a 845x UV-visible Agilent spectrophotometer. *In situ* UV-Vis-NIR spectroelectrochemical studies were conducted on a Cary 5000 spectrophotometer from Varian operating in a maximal 175–3300 nm range. A C3 epsilon potentiostat from BASi was used for the electrolysis using a thin layer cell from a demountable omni cell from Specac. In this cell a three electrodes system was coupled to conduct *in situ* spectroelectrochemistry. A Pt gauze was used as the working electrode, a Pt wire was used as the counter electrode, and a Ag wire was used as the pseudo-reference electrode. The spectra were collected a constant potential electrolysis and the potentials were changed in interval of 100 mV. The electrochemical medium used was 0.1 M $(C_4H_9)_4NPF_6$ in fresh distilled CH_2Cl_2, at room temperature with sample concentrations of 10^{-3} M.

D. Flash-photolysis characterization

Transient absorption spectra were measured in fresh 10^{-3} M solutions in degassed tetrahydrofuran by means of a laser

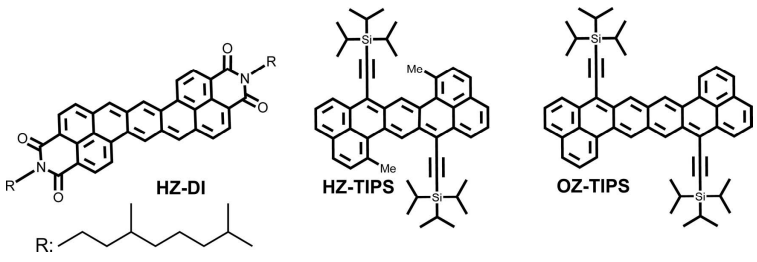

FIG. 1. Chemical structures of the studied zethrenes formulated in their closed-shell quinoidal forms.

flash-photolysis system from Luzchem with a pulsed Nd:YAG laser, using 355 nm and 532 nm as excitation wavelengths. A Lo255 Oriel xenon lamp was employed as the detecting light source. The apparatus is completed with a 77200 Oriel monochromator, and an Oriel photomultiplier (PMT) system. The oscilloscope was a TDS-640A Tektronix. The energy single pulses were of approximately 15 mJ.

E. Theoretical calculations

Quantum-chemical calculations were done in the framework of the density functional theory. Simulations were performed in the gas-phase to obtain the equilibrium structures and the electronic properties of the ground electronic state (S_0), and first excited triplet states (T_1). The B3LYP[20,21] and CAM-B3LYP[22] exchange-correlational functionals and the 6-31G(d,p)[23,24] basis set were used in all calculations, as implemented in the Gaussian´09 package.[25] To simulate the open-shell ground-state structures by DFT we used the broken-symmetry option with the key guess = mix keyword and the unrestricted wavefunctions at the (U)B3LYP or (U)CAM-B3LYP levels. The unrestricted methodologies were also used for the open-shell radicals (radical cation and anions) and triplet states. The time-dependent DFT (TD-DFT) approach[26,27] was used to obtain the relevant excited states transitions (i.e., energies and oscillator strengths) and for the optimization of the lowest excited singlet states.

III. RESULTS AND DISCUSSION

A. Singlet-triplet energy gap discussion

We have carried out quantum chemical calculations at the (U)CAM-B3LYP/3-21G** level to get insights on the energy balance involved in the formation of the biradicals. Fig. 2 displays the absolute energy differences between the open- and closed-shell singlets and between the open-shell (biradical) singlets and triplets of the diimide and TIPS-functionalized zethrenes. As an extension, these energy data have been obtained for other members of the zethrene series, zethrene (**Z**), heptazethrene (**HZ**), and octazethrene (**OZ**) whose chemical structures are shown in Fig. 2.

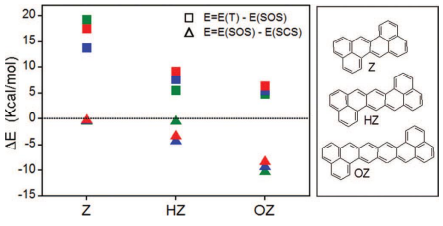

FIG. 2. (U)CAM-B3LYP/3-21G** energy differences (ΔE, see inset) between the singlet open shell (SOS), triplets (T), and singlet closed shell (SCS) states for the unsubstituted zethrenes (red symbols), diimide substituted zethrenes (blue symbols), and TIPS substituted zethrenes (green symbols). See Table S1 for the total formation energies.[35]

In the unsubstituted series, the singlet biradical is stabilized starting from the heptazethrene. On the other hand, terminal substitution with diimides favours the singlet biradical configuration since their strong participation in the overall acene molecular π-conjugation. In contrast, the substitution of heptazethrene with TIPS groups stabilizes the closed-shell quinoidal structure since these groups are not much involved in the π-conjugation and only produce a kinetic stabilization.[13] We have recently addressed the effects of the acceptor strength in the formation of the biradical structures in tetracyanoquinodimethane quinoidal oligothiophenes and learnt that the electron-withdrawing effect of these acceptors reduces the bond length alternation pattern of the conjugated sequence, weakens the conjugated double bonds and facilitates its rupture to form an open-shell biradical.[15–19] This explanation might be the case for the electron-withdrawing diimide substitution.

The enlargement of the acene backbone progressively stabilizes the open-shell biradical since the involvement of more rings that get aromatic. Thus, for octazethrenes independently of the substitution, the singlet biradical is more stable than its closed-shell structure.

In these *Kekulé* biradicals, the open-shell singlet is more stable than the triplet (independently of the substitution pattern and of the acene length). This is contrary to the Hund´s rules which tell us that high spin states are always preferred. This suggests that the stabilizing mechanism of the singlet biradical is double spin polarization (DSP) which, in essence, describes a preferred conjugation of the two radical centers (SOMO orbitals) towards the bridge (doubly occupied orbitals: HOMO, HOMO-1, etc.) in the singlet format.[8,28,29] Overall, the energy stabilization by aromatization favours the stabilization of the biradical over the closed-shell form, while the DSP mechanism always prefers the singlet over the triplet.

B. Raman spectra and molecular structures

Fig. 3 displays the optimized geometries for the ground electronic state (S_0) and triplet excited state (T_1) of some representative heptazethrenes.

It is observed that **HZ-TIPS** has a quinoidal pattern in the central benzene in line with its closed-shell character. However, **HZ-DI** already shows certain aromatization of this central ring revealing the biradical fingerprint in the ground electronic state. For comparison, the optimized geometry of the first triplet excited state of **HZ-DI** is also displayed in Fig. 3 where the aromatic character within the central ring is accentuated. For the **HZ**, the structural description of the S_0 and T_1 is similar to that of **HZ-DI**.

Fig. 4 discloses the Raman spectra of **HZ-DI** in solid state obtained with different excitation wavelengths together with its electronic absorption spectra. The benzenoid CC stretching frequency region in the Raman spectrum is central to discern between singlets and triplets (Scheme 1).[13,18] Among the many benzene rings in these zethrenes, we must indicate that those CC stretching modes of the benzenes where π-conjugation is maximal (the central core) are greatly intensified and therefore we mostly detect them in the Raman

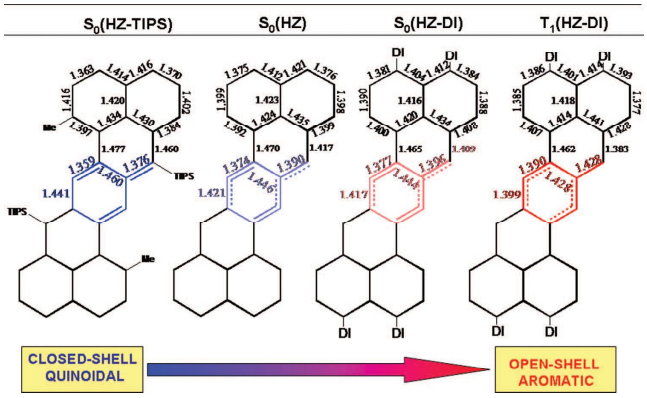

FIG. 3. (U)CAMB3LYP/3-21G** optimized geometries for the singlet ground electronic state (S_0) of **HZ-TIPS**, **HZ**, and **HZ-DI** together with that of the triplet excited state (T_1) of **HZ-DI**.

spectral region of 1600 cm^{-1}. In addition, these modes contain the following structure-spectroscopic relationships: (i) for benzene rings bearing an aromatic structure, the CC Raman bands usually appear at 1600 cm^{-1} (or higher) and (ii) for benzene rings disclosing a quinoidal structure, these CC bands are shifted to lower frequencies, up to 1580–1570 cm^{-1} for well defined benzo-quinoidal units. These vibrational assignments for **HZ-TIPS** and **OZ-TIPS** can be consulted in detail in Ref. 13.

We notice that by exciting with the 633 nm laser in Fig. 4 (and similarly with the 785 nm one) the Raman spectrum is simplified in consonance with the resonance effect with the strongest electronic absorption band. In this spectrum, the most intense Raman band in the benzene region is at 1590 cm^{-1} accompanied by a small shoulder at 1595 cm^{-1}. The 532 nm laser, however, excites the high energy side of the main electronic absorption, giving rise to an additional band at 1610 cm^{-1}. The Raman bands at 1595 cm^{-1} can be related to the benzenoid rings possessing a transitional structure between full quinoidal and full aromatic. However, the bands at 1610 cm^{-1} must be correlated to the well-defined aromatic-like molecular segments. In accordance with the energetic and structural description in the above section, the ground electronic state of **HZ-DI** discloses an open-shell biradical structure that imparts a partial aromatization of its central part, hence the 1595 cm^{-1} feature, midway between full aromatic and full quinoidal, is well associated with the CC stretching of this pseudo-aromatic moiety. The 1610 cm^{-1} band relates with a more accentuated aromatic structure and might be associated with the **HZ-DI** triplet biradical in equilibrium with the singlet biradical at room temperature. Although the triplet has a small or very small population we can obtain its Raman

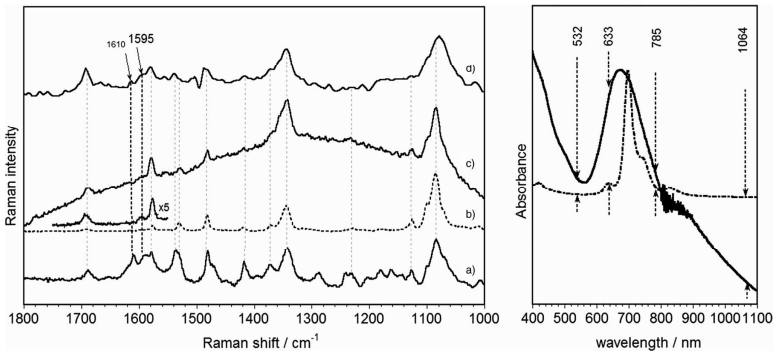

FIG. 4. (Left) Raman spectra of **HZ-DI** with different excitation wavelength: (a) 532 nm, (b) 633 nm, (c) 785 nm, and (d) 1064 nm. (Right) Electronic absorption spectra of **HZ-DI** in CH_2Cl_2 solution (broken line) and in solid state (solid line).

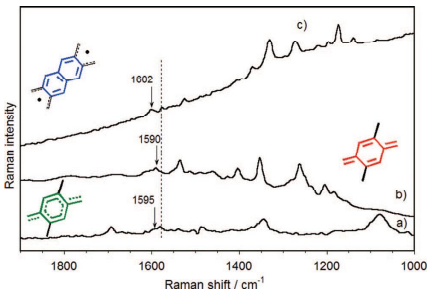

FIG. 5. FT-Raman spectra of 1064 nm in solid state of (a) **HZ-DI**, (b) **HZ-TIPS**, and (c) **OZ-TIPS**. Insets as deduced for the theoretical geometries in Fig. 3 represent the molecular structure of the central core.

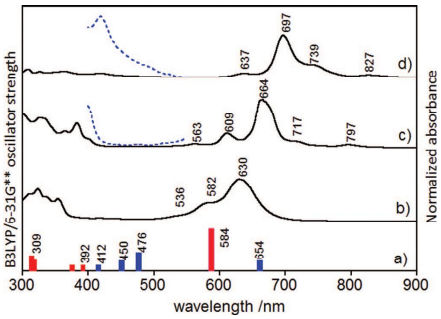

FIG. 6. (a) (U)CAM-B3LYP/6-31G** TD-DFT theoretical spectra of **HZ-TIPS**: absorption of the singlet closed-shell ($S_0 \rightarrow S_n$ transitions) in red; absorption of the triplet excited state ($T_1 \rightarrow T_n$ transitions) in blue. UV-Vis absorption spectra in CH_2Cl_2 of (b) **HZ-TIPS**, (c) **OZ-TIPS**, and (d) **HZ-DI**. Zooms of the 400–550 nm region in dotted blue lines.

spectrum due to the resonant Raman effect with the triplet absorptions existing in the 532 nm region (see below). The 1698 cm^{-1} Raman band related with the C=O stretching mode of the diimide group must be mentioned. This mode usually has weak or very weak Raman intensity and its detection here as a medium intensity band reveals the involvement of the diimide acceptors in the total π-electron conjugation such as already mentioned.

Fig. 5 displays the FT-Raman spectra of the three zethrenes. For **OZ-TIPS**, the most intense band in this region is at 1602 cm^{-1} while for **HZ-TIPS** is at 1590 cm^{-1}. This, from a structural point of view, denotes the aromatic character of the naphthyl core in **OZ-TIPS** and the much more quinoidal character of the central benzene in **HZ-TIPS** in consonance with the biradical character of the singlet ground electronic state of **OZ-TIPS** and with the closed-shell shape for **HZ-TIPS**. Interestingly, the Raman band at 1595 cm^{-1} in **HZ-DI** is in between those of **HZ-TIPS** and **OZ-TIPS** reaffirming its transitional character from a benzo-quinoidal to a benzo-aromatic form of the ground electronic state of the diimide derivative.

C. UV-Vis absorption spectra and excited states

Fig. 6 displays the absorption spectra of **HZ-TIPS**, **OZ-TIPS**, and **HZ-DI** in dichloromethane. For **HZ-TIPS**, we have carried out TD-DFT excited state calculations in order to distinguish the contributions of the singlet and triplet in the electronic absorption spectra. Since **HZ-TIPS** has a non biradical singlet ground electronic state, TD-DFT performs with good accuracy for its closed-shell wavefunction.

The spectrum of **HZ-TIPS** displays the main features at 536, 582, and 630 nm which are spaced by vibrational energies (1474 and 1309 cm^{-1}) allowing to interpret them as vibronic components of the most active $S_0 \rightarrow S_1$ one-electron transition (theoretically predicted at 584 nm). TD-DFT calculations reproduce an excitation at 390 nm (3.16 eV) with zero oscillator strength or dark excited state (i.e., same symmetry than the ground electronic state) which is candidate to originate a two-photon absorption feature in the two-photon absorption experiment at half this energy. Fig. 6 also displays the theoretical absorption excitations of the triplet which always appear around 400–500 nm, in the high energy side of main singlet-singlet absorption band. No bands are assignable to triplet absorptions in the experimental spectrum of **HZ-TIPS**.

OZ-TIPS displays the same three vibrational components of the strong $S_0 \rightarrow S_1$ excitation at 563, 609, and 664 nm which are spaced by a vibrational component around 1350 cm^{-1}. The band at 717 nm, which is new in comparison to **HZ-TIPS**, might be assignable to a new vibronic component at 1112 cm^{-1}. The main vibronic component at 1350 cm^{-1} and the satellite at 1112 cm^{-1} correspond to the main bands of the Raman spectrum of **OZ-TIPS** (see Fig. 5) supporting the assignment as a double vibronic progression of the $S_0 \rightarrow S_1$ band (see Figure S1 for the theoretical vibronic spectrum).[35] At longer wavelengths, 797 nm, a weak absorption is detected which might be related with a absorption to a excited state of the same symmetry than the ground electronic state (dark state, see Sec. III D). A mechanism for the activation of two-photon excitations in the one-photon spectrum goes through the vibrational mixing of the two electronic states of the same symmetry by the action of a totally symmetric vibrational mode such as the totally symmetric CC stretching mode strongly active at 1350 cm^{-1} in the Raman spectrum.[30,31]

Due to the singlet open-shell biradical character of the S_0 of **OZ-TIPS**, its triplet excited state is much closer to the S_0 and, as a result, it should be more populated at room temperature. We enlarge the absorption spectral profile of **OZ-TIPS** in the 400–500 nm triplet region (see Fig. 6) where we see the existence of new weak absorptions that can be tentatively assigned to a small but significant population of the triplet species.

D. Flash-photolysis and triplet excited states

In order to get further insight on the singlet-triplet balance in these zethrenes, Fig. 7 displays the flash-photolysis

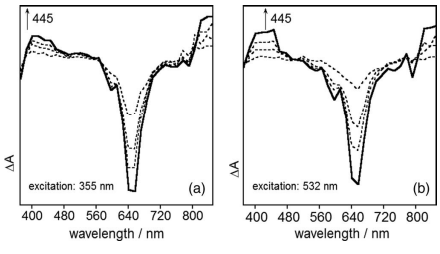

FIG. 7. Microsecond transient spectra after flash-photolysis at (a) 355 nm and at (b) 532 nm in THF at room temperature for **HZ-TIPS**.

spectra of **HZ-TIPS** obtained after laser pulses at 355 and 532 nm followed by recording the transient absorption spectra in the microsecond regime.

Two main features are observed in these spectra: (i) the depletion, or photo-bleaching, of the ground electronic state absorption and (ii) the growing of an absorption at 445 nm that arises at the expenses of the ground state absorption (isosbestic point at 550 nm). There are bands at longer wavelengths than 800 nm which nicely compare with the absorption spectra of the radical anion of **HZ-TIPS**. The 445 nm transient band nicely correlates with the most intense theoretical transition predicted at 476 nm for the main excitation of the triplet species of **HZ-TIPS** in Fig. 6.

In our previous publication,[13] we discussed the nanosecond transient absorption spectra of **HZ-TIPS**, which, surprisingly, display identical shape as those recorded now in microsecond time regime revealing the generation of triplet species in a highly efficient nanosecond process after light excitation. This mechanism cannot be a simple intersystem crossing which, given its inherent non-allowed nature, would require long time scales.[32] Indeed, we might ascribe it to singlet exciton fission which is able to efficiently produce triplet species in pico- and nano-seconds by exciting on the most intense one-photon allowed band [(a) in Fig. 8(a), 1 ^{1}Ag $\rightarrow$ 1 ^{1}Bu].[33] Singlet exciton fission was first reported in anthracene to account for the low fluorescence quantum yield in solid state.[34] In singlet exciton fission, the initial excitation is followed by conical intersection [(b) in Fig. 8(a), 1 ^{1}Bu $\rightarrow$ 2 ^{1}Ag] which populates the second singlet excited state, 2 ^{1}Ag. This state might have a pseudo-aromatic structure similar to that of the first triplet excited state (see Fig. 3), by which internal conversion [(c) in Fig. 8(a)] can efficiently yield triplets. In contrast to **HZ-TIPS**, the same microsecond transient absorption experiments for **OZ-TIPS** and **HZ-DI** do not yield any distinguishable spectra in the Vis region. However, like **HZ-TIPS**, **OZ-TIPS** gives rise to a triplet-like spectrum after nanosecond flash-photolysis.[13] This means that the same singlet exciton fission mechanism is likely operating in **OZ-TIPS**, however, due to its smaller singlet-triplet gap, the formed triplets deactivate very quickly and elude microsecond detection.

E. UV-Vis-NIR spectroelectrochemistry

These compounds disclose amphoteric redox behaviour in their cyclic voltammograms (see Figure S2)[35] which consist of reversible oxidation and reduction processes.[11,12] Fig. 9 displays the absorption spectra of **HZ-TIPS** obtained under controlled electrolysis in a 0.1 M tetrabutyl hexafluorophosphate solution in dichloromethane. Reduction of **HZ-TIPS** gives rise to four new absorptions in the Vis-NIR region with a spectroscopic pattern characteristic of radical anions with double bands well displaced into the near-IR region. The existence in the cyclic voltammetry of a first one-electron reduction, well separated from the second reduction process, further supports the assignment of the spectra to the anion species.[11,12] Similar to the reduction, one-electron oxidation gives way to the generation of the radical cation of **HZ-TIPS** with an absorption spectrum very similar to that of its parent anion. These spectral features are new marks of the quinoidal closed-shell character of **HZ-TIPS** and its pro-aromatic property which makes the molecule to adopt an aromatic form to stabilize the excess, either anodic or cathodic. This is nicely

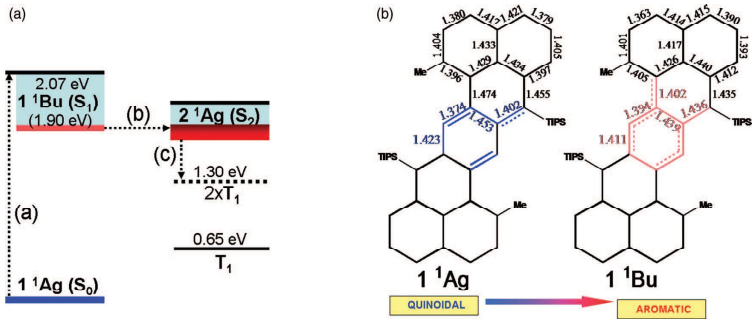

FIG. 8. (a) TD-DFT//CAM-B3LYP/6-31G** vertical for the relevant excited states involved in the singlet fission process for **HZ-TIPS.** The adiabatic energy for the 1^{1}Bu state is shown in parenthesis. (b) Optimized geometries for the 1 ^{1}Ag singlet ground electronic state and the 1 ^{1}Bu first singlet excited state at the same level of theory.

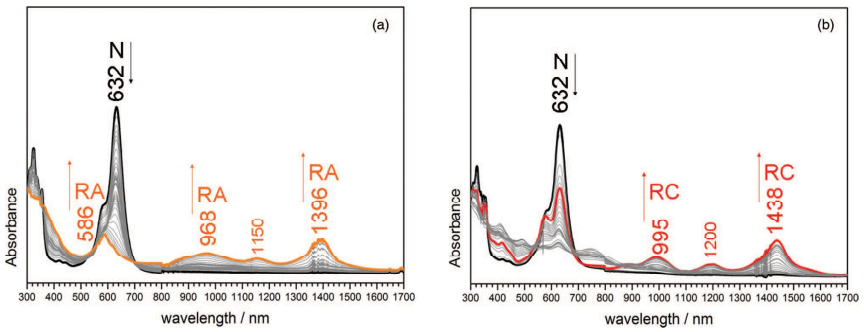

FIG. 9. *In situ* UV-Vis-NIR absorption spectroelectrochemistry of **HZ-TIPS**: (a) one-electron reduction and (b) one-electron oxidation. N: neutral, RA: radical anion, and RC: radical cation. Each spectrum corresponds to that obtained after stepwise variation of 100 mV from 0 V (versus an Ag wire as the pseudo-reference electrode).

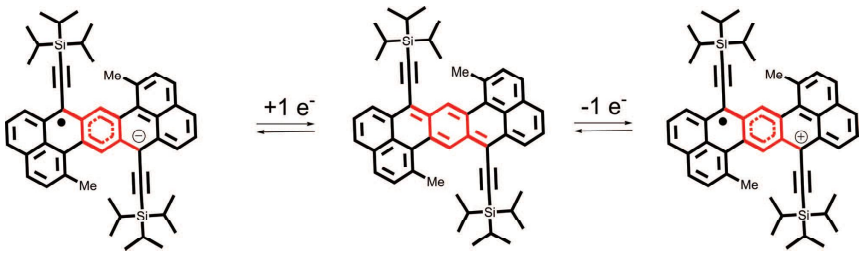

SCHEME 2. Single electron redox processes in **HZ-TIPS**. Structures deduced from the optimized geometries at the (U)CAM-B3LYP/6-31G** level of theory (Fig. S3 in the supplementary material).[35]

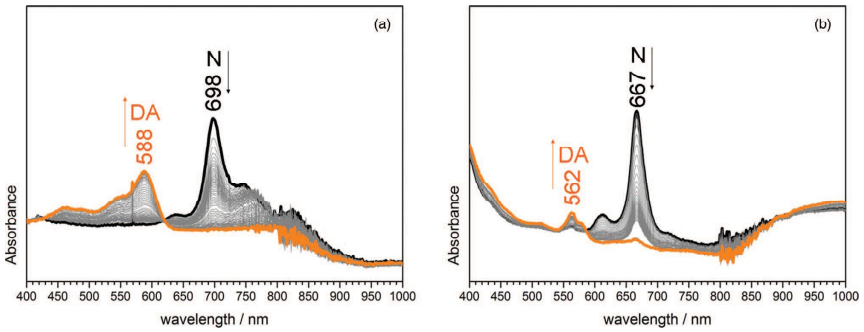

FIG. 10. *In situ* UV-Vis-NIR absorption reduction spectroelectrochemistry of (a) **HZ-DI** and (b) **OZ-TIPS**. N: neutral and DA: dianion. Each spectrum corresponds to that obtained after stepwise variation of 100 mV from 0 V (versus an Ag wire as the pseudo-reference electrode).

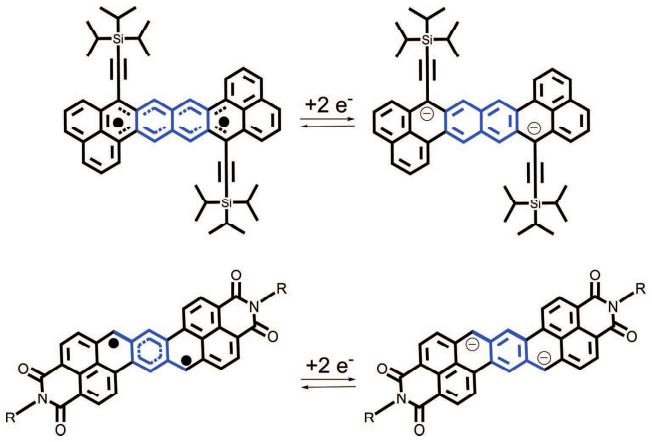

SCHEME 3. Double electron reduction processes in **OZ-TIPS** and **HZ-DI**. Structures deduced from the optimized geometries at the (U)CAM-B3LYP/6-31G** level of theory (Figure S4).[35]

described in the Scheme 2 for the optimized structures of the radical anion and cation deduced by (U)CAM-B3LYP/6-31G** calculations (see Figure S3).[35]

Fig. 10 displays the absorption spectra recorded during the reduction of **OZ-TIPS** and **HZ-DI**. Reduction of both compounds results in the decrease of the absorption of the neutral compound and in the appearance of a well defined band that, in contrast to the radical anion of **HZ-TIPS**, is displaced at shorter wavelengths as it is typical upon direct formation of dianions. This spectroelectrochemical result is in accordance with the detection in the cyclic voltammetry of **OZ-TIPS** of two closely consecutive one-electron reductions overall yielding the dianion.[11,12] The driving force for the formation of the dianionic species in **OZ-TIPS** comes from the further aromatization of the initial pseudo-aromatic naphthyl core in the neutral biradical. In **HZ-DI**, together with the complete aromatization of the pseudo-aromatic phenyl core in the singlet biradical ground electronic state, the formation of the dianion is further helped by the electron acceptor character of the diimide groups (see Scheme 3 and Figure S4[35]).

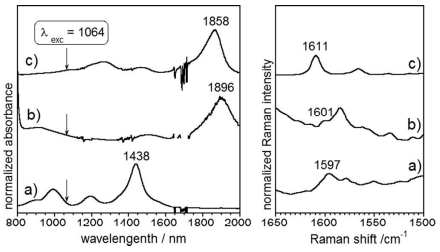

FIG. 11. (Left) UV-Vis-NIR absorption spectra after oxidation in dichloromethane with $FeCl_3$ of (a) **HZ-TIPS**, (b) **HZ-DI,** and (c) **OZ-TIPS**. (Right) FT-Raman spectra of 1064 nm of the same radical cations.

Fig. 11 displays the UV-Vis-NIR absorption spectra of the radical cations of the three zethrene compounds together with their FT-Raman spectra.

The FT-Raman spectra of the three cationic samples allow us to explore their molecular shapes and to corroborate the theoretical structures of the ionized species as deduced by calculations. We have assigned the relevant benzenoid CC stretching mode in the three cationic samples to the Raman bands at 1597 cm^{-1} in **HZ-TIPS**, at 1601 cm^{-1} in **HZ-TIPS**, and at 1611 cm^{-1} in **OZ-DI**. These bands evolve from those in the neutral at 1590, 1595, and 1602 cm^{-1}, respectively, revealing in each case the additional aromatization of the central core upon electron extraction. In the case of the cation of **HZ-DI**, due to the electron-withdrawing effect of the diimide groups, the charge defect is more confined in the middle of the molecule what provokes a greater aromatization in this central benzene than in the case of the TIPS analogue. In the case of the Raman spectrum of the radical cation of **OZ-TIPS** aromatization on oxidation covers the central naphthyl moiety which gives rise to the higher frequency Raman band.

IV. CONCLUSION

Zethrenes are new acene derivatives with promising applications in organic electronics. We have presented a complete analysis of the electronic and molecular structures of the longer available zethrenes. Long zethrenes, due to their quinoidal central core, can promote the formation of *Kekulé* biradicals: here, we interrogate about the competition between the quinoidal closed-shell and the aromatic open-shell biradical forms as a function of the functionalization of the

zethrene and of the dimension of the core. The study encompasses a variety of experimental techniques, such as Raman, UV-Vis-NIR absorption, transient absorption, and *in situ* spectroelectrochemistry in combination with quantum chemical calculations. We conclude that the tendency to aromatization, or pro-aromaticity of the quinoidal module, leads to the creation of *Kekulé* neutral biradicals stabilized in their open-shell singlet forms by double-spin polarization. The pro-aromatic character is also the driving force for the stabilization of the ionized species, either by oxidation or reduction, nicely explaining the redox amphotericity. For the neutral biradicals, there is an energy close triplet excited state, also formed by aromatization of the central core. This triplet has been characterized by Raman spectroscopy and by transient absorption spectroscopy. Interestingly, our study reveals that these triplets are formed not only by thermal access from the singlet ground electronic state but also by exciting the singlet excited state manifold in the context of singlet exciton fission, which is another manifestation of the biradicaloid character, now in the excited state. This study can help to understand the intrinsic physics and chemistry of these peculiar molecular platforms and guide new chemical designs in order to develop new electro-optical and photovoltaics applications.

ACKNOWLEDGMENTS

The work at the University of Málaga was supported by MINECO through project reference CTQ2012-33733 and by the Junta de Andalucía through research project P09-FQM-4708. J.L.Z. acknowledges MINECO for a personal grant. R.C.G.C. acknowledges the Junta de Andalucía for a personal doctoral grant. M.C.R.D. thanks the MICINN for a "Ramón y Cajal" research contract. The work in Singapore was supported by MOE Tier 2 grant (MOE2011-T2-2-130).

[1]E. Clar, K. F. Lang, and H. Schluz-Kiesow, Chem. Ber. **88**, 1520 (1955).
[2]R. Umeda, D. Hibi, K. Miki, and Y. Tobe, Org. Lett. **11**, 4104 (2009).
[3]T. C. Wu, C. H. Chen, D. Hibi, A. Shimizu, Y. Tobe, and Y. T. Wu, Angew. Chem., Int. Ed. **49**, 7059 (2010).
[4]A. E. Chichibabin, Chem. Ber. **40**, 1810 (1907).
[5]L. K. Montgomery, J. C. Huffman, E. A. Jurczak, and M. P. Grendze, J. Am. Chem. Soc. **108**, 6004 (1986).
[6]Z. Sun, Q. Ye, C. Chi, and J. Wu, Chem. Soc. Rev. **41**, 7857 (2012).
[7]Z. Sun and J. Wu, J. Mater. Chem. **22**, 4151 (2012).
[8]W. T. Borden, *Diradicals* (Wiley, New York, 1982).
[9]A. Iwasaki, L. Hu, R. Suizu, K. Nomura, H. Yoshikawa, K. Awaga, Y. Noda, K. Kanai, Y. Ouchi, K. Seki, and H. Ito, Angew. Chem., Int. Ed. **48**, 4022 (2009).
[10]B. O. Jahn, H. Ottosson, M. Galperin, and J. Fransson, ACS Nano **7**, 1064 (2013).
[11]Z. Sun, K.-W. Huang, and J. Wu, J. Am. Chem. Soc. **133**, 11896 (2011).
[12]Z. Sun, K.-W. Huang, and J. Wu, Org. Lett. **12**, 4690 (2010).
[13]Y. Li, W.-K. Heng, B. Sun Lee, N. Aratani, J. L. Zafra, N. Bao, R. Lee, Y. Mo Sung, Z. Sun, K.-W. Huang, R. D. Webster, J. T. López Navarrete, D. Kim, A. Osuka, J. Casado, J. Ding, and J. Wu, J. Am. Chem. Soc. **134**, 14913 (2012).
[14]C. Castiglioni, M. Tommasini, and G. Zerbi, Philos. Trans. R. Soc. London, Ser. A **362**, 2425 (2004).
[15]R. Ponce Ortiz, J. Casado, V. Hernandez, J. T. Lopez Navarrete, P. M. Viruela, E. Orti, K. Takimiya, and T. Otsubo, Angew. Chem., Int. Ed. **46**, 9057 (2007).
[16]S. R. González, Y. Ie, Y. Aso, J. T. López Navarrete, and J. Casado, J. Am. Chem. Soc. **133**, 16350 (2011).
[17]R. Ponce Ortiz, J. Casado, S. Rodríguez González, V. Hernández, J. T. López Navarrete, P. M. Viruela, E. Ortí, K. Takimiya, and T. Otsubo, Chem. Eur. J. **16**, 470 (2010).
[18]J. Casado, S. Patchkovskii, M. Z. Zgierski, L. Hermosilla, C. Sieiro, M. Moreno Oliva, and J. T. López Navarrete, Angew. Chem., Int. Ed. **47**, 1443 (2008).
[19]J. Casado, R. Ponce Ortiz, and J. T. López Navarrete, Chem. Soc. Rev **41**, 5672 (2012).
[20]C. T. Lee, W. T. Yang, and R. G. Parr, Phys. Rev. B **37**, 785 (1988).
[21]A. D. Becke, J. Chem. Phys. **98**, 5648 (1993).
[22]T. Yanai, D. P. Tew, and N. C. Handy, Chem. Phys. Lett. **393**, 51 (2004).
[23]W. J. Hehre, R. Ditchfie, and J. A. Pople, J. Chem. Phys. **56**, 2257 (1972).
[24]M. M. Francl, W. J. Pietro, W. J. Hehre, J. S. Binkley, M. S. Gordon, D. J. Defrees, and J. A. Pople, J. Chem. Phys. **77**, 3654 (1982).
[25]M. J. Frisch, G. W. Trucks, H. B. Schlegel *et al.*, GAUSSIAN 09, Revision C.01, Gaussian, Inc., Wallingford, CT, 2009.
[26]E. Runge and E. K. U. Gross, Phys. Rev. Lett. **52**, 997 (1984).
[27]H. H. Heinze, A. Gorling, and N. Rosch, J. Chem. Phys. **113**, 2088 (2000).
[28]W. T. Borden, H. Iwamura, and J. A. Berson, Acc. Chem. Res. **27**, 109 (1994).
[29]P. Karafiloglou, J. Chem. Educ. **66**, 816 (1989).
[30]S. Di Motta, F. Negri, D. Fazzi, C. Castiglioni, and E. V. Canesi, J. Phys. Chem. Lett. **1**, 3334 (2010).
[31]S. Ito, T. Minami, and M. Nakano, J. Phys. Chem. C **116**, 19729 (2012).
[32]R. S. Becker, *Theory and Interpretation of Fluorescence and Phosphorescence* (Wiley Interscience, New York, 1969).
[33]M. B. Smith and J. Michl, Chem. Rev. **110**, 6891 (2010).
[34]S. Singh, W. J. Jones, W. Siebrand, B. P. Stoicheff, and W. G. Schnider, J. Chem. Phys. **42**, 330 (1965).
[35]See supplementary material at http://dx.doi.org/10.1063/1.4863557 for synthetic procedures and structural characterizations of the new chemical compounds, the cyclic voltammograms, the details of the quantum chemical calculations, and a complete list of authors for Refs. 9, 13, and 25.

JACS
JOURNAL OF THE AMERICAN CHEMICAL SOCIETY
Article
pubs.acs.org/JACS

Stable Tetrabenzo-Chichibabin's Hydrocarbons: Tunable Ground State and Unusual Transition between Their Closed-Shell and Open-Shell Resonance Forms

Zebing Zeng,[†] Young Mo Sung,[‡] Nina Bao,[§] Davin Tan,[∥] Richmond Lee,[∥] José L. Zafra,[⊥] Byung Sun Lee,[‡] Masatoshi Ishida,[‡] Jun Ding,[§] Juan T. López Navarrete,[⊥] Yuan Li,[†] Wangdong Zeng,[†] Dongho Kim,*[,‡] Kuo-Wei Huang,*[,∥] Richard D. Webster,*[,#] Juan Casado,*[,⊥] and Jishan Wu*[,†,▽]

[†]Department of Chemistry, National University of Singapore, 3 Science Drive 3, 117543, Singapore

[‡]Spectroscopy Laboratory for Functional π-Electronic Systems and Department of Chemistry, Yonsei University, Seoul 120-749, Korea

[§]Department of Materials Science & Engineering, National University of Singapore, 119260, Singapore

[∥]Division of Chemical and Life Sciences and Engineering and KAUST Catalysis Center, King Abdullah University of Science and Technology (KAUST), Thuwal 23955-6900, Saudi Arabia

[⊥]Department of Physical Chemistry, University of Malaga, Campus de Teatinos s/n, 229071 Malaga, Spain

[#]Division of Chemistry & Biological Chemistry, School of Physical & Mathematical Sciences, Nanyang Technological University, 21 Nanyang Link, 637371, Singapore

[▽]Institute of Materials Research and Engineering, A*Star, 3 Research Link, 117602, Singapore

Supporting Information

ABSTRACT: Stable open-shell polycyclic aromatic hydrocarbons (PAHs) are of fundamental interest due to their unique electronic, optical, and magnetic properties and promising applications in materials sciences. Chichibabin's hydrocarbon as a classical open-shell PAH has been investigated for a long time. However, most of the studies are complicated by their inherent high reactivity. In this work, two new stable benzannulated Chichibabin's hydrocarbons **1-CS** and **2-OS** were prepared, and their electronic structure and geometry in the ground state were studied by various experiments (steady-state and transient absorption spectra, NMR, electron spin resonance (ESR), superconducting quantum interference device (SQUID), FT Raman, X-ray crystallographic etc.) and density function theory (DFT) calculations. **1-CS** and **2-OS** exhibited tunable ground states, with a closed-shell quinoidal structure for **1-CS** and an open-shell biradical form for **2-OS**. Their corresponding excited-state forms **1-OS** and **2-CS** were also chemically approached and showed different decay processes. The biradical **1-OS** displayed an unusually slow decay to the ground state (**1-CS**) due to a large energy barrier (95 ± 2.5 kJ/mol) arising from severe steric hindrance during the transition from an orthogonal biradical form to a butterfly-like quinoidal form. The quick transition from the quinoidal **2-CS** (excited state) to the orthogonal biradicaloid **2-OS** (ground state) happened during the attempted synthesis of **2-CS**. Compounds **1-CS** and **2-OS** can be oxidized into stable dications by $FeCl_3$ and/or concentrated H_2SO_4. The open-shell **2-OS** also exhibited a large two-photon absorption (TPA) cross section (760 GM at 1200 nm).

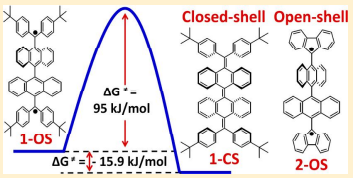

I. INTRODUCTION

Open-shell polycyclic aromatic hydrocarbons (PAHs) refer to a type of hydrocarbons with one or more than one π-electrons that are not tightly paired into the bonding molecular orbital in the ground state, which is different from the typical PAHs with a closed-shell electronic structure. Open-shell PAHs are of fundamental importance in understanding the nature of chemical bonding and the basic chemical and physical phenomena of π-conjugated systems. Recent experimental and theoretical studies have revealed that open-shell PAHs could show unique electronic, optical, and magnetic properties and thus have promising applications in materials science.[1] In the case of biradical PAHs, the two unpaired or weakly bonded electrons can be either in a low-spin singlet or in a high-spin triplet state. The substances with a singlet ground state can exhibit paramagnetic property via a thermally excited transition from singlet to triplet state if the singlet−triplet energy gap (ΔE_{S-T}) is sufficiently small.[2] Open-shell PAHs with intermediate biradical characters are theoretically predicted to

Received: May 24, 2012
Published: August 14, 2012

   dx.doi.org/10.1021/ja3050579 | J. Am. Chem. Soc. 2012, 134, 14513−14525

have enhanced second hyperpolarizability and a large two-photon absorption (TPA) cross section as compared to the corresponding closed-shell and pure diradical systems,[3] and this has been experimentally proven by several open-shell singlet molecules such as Kubo's bisphenalenyls[4] and Osuka's *meso*-diketo hexaphyrin.[5] Therefore, open-shell PAHs could be used as new efficient nonlinear optical (NLO) chromophores for future photonics applications such as optical switching, three-dimensional memory, optical limiting, and photodynamic therapy.[6] Open-shell PAHs usually also exhibit multiple-stage amphoteric redox behavior, which makes them promising materials for low threshold-voltage ambipolar field effect transistors[7] and energy storage devices (e.g., lithium ion batteries).[8] In addition, certain open-shell PAHs can be regarded as graphene nanoflakes with unique magnetic properties and have potential applications for organic spintronics.[9]

Despite all of their intriguing properties and promising applications, the open-shell nature of these molecules has rendered them vulnerable to degradation reactions; therefore, instability remains a key obstacle for their practical applications. Recent progress in synthetic method has led to the successful synthesis and characterization of several types of stable open-shell PAHs: (1) *o*-quinodimethane[10] and *p*-quinodimethane derivatives;[11] (2) phenalenyls,[12] bisphenalenyl[13] and trisphenalenyls;[14] (3) teranthene;[15] and (4) zethrenes.[16] In most cases, both thermodynamic stabilization by π-electron delocalization and kinetic stabilization by blocking of the most reactive sites carrying high-spin density are necessary to obtain stable materials.

Among various known open-shell PAHs, Chichibabin's hydrocarbon possessing a characteristic resonance structure between a closed-shell quinonoid form and an open-shell biradical (Chart 1) has been most extensively studied regarding its ground-state electronic structure and physical properties.[17] Because of the recovery of two aromatic sextet rings in the biradical form, the Chichibabin's hydrocarbon exhibits large biradical character in the ground state. However, Chichibabin's hydrocarbon reacts avidly with oxygen, yielding polymeric peroxide. In addition, it also tends to dimerize and oligomerize to give paramagnetic species. All of these make it challenging to offer a clear-cut conclusion on its ground-state electronic structure.[18] Although some derivatives of Chichibabin's hydrocarbons have been prepared,[19] side reactions such as oxidation, dimerization, polymerization, and decomposition usually cannot be avoided due to the high chemical reactivity of unpaired electrons. Therefore, great attention has been focused on synthesizing and studying long lifetime and stable Chichibabin's hydrocarbons.[20]

Chart 1. Resonance Structures of Chichibabin's Hydrocarbon, Tetrabenzo-Chichibabin's Hydrocarbons, and Its Derivatives 1-CS/1-OS and 2-CS/2-OS

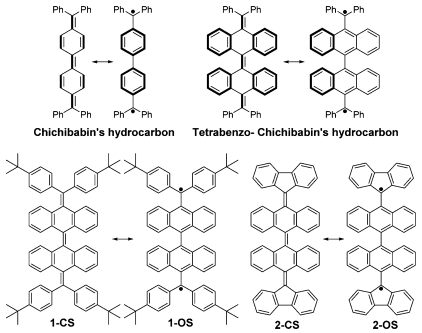

Like other open-shell PAHs, the stabilization of the highly reactive Chichibabin's hydrocarbon can be achieved by either a thermodynamic approach (aromatic stabilization and π-electron delocalization) or kinetic means (steric protection), or by both approaches. As shown in Chart 1, our new strategy toward thermodynamic stabilization of the Chichibabin's hydrocarbon is by benzannulation of the central biphenyl unit with four aromatic benzene rings, and thus tetrabenzo-Chichibabin's hydrocarbon is generated. Such a design can possibly also enhance the kinetic stability due to the steric blocking by the two anthracene units in the case that the biradical form dominates its ground state. Therefore, the tetrabenzo-Chichibabin's hydrocarbon is expected to be more stable due to compensation by both thermodynamic and kinetic stabilization. To improve its solubility and also to further block the reactive sites where dimerization can happen, *tert*-butyl groups are introduced onto the *para*-position of the four phenyl rings in **1-CS**/**1-OS** (Chart 1). It will be of interest to study the inherent electronic structure of this novel hydrocarbon, which can be drawn as a resonance structure between a quinoidal form (**1-CS**) and an open-shell biradical form (**1-OS**). In addition, it has been reported that the stability of a radical center can be improved by delocalization through a fluorenyl moiety.[21] Thus, herein the di(4-*tert*-butylphenyl)-methene groups in **1-CS**/**1-OS** are further replaced by two fluorenyl units, and the obtained molecule can also be drawn as a closed-shell quinoidal form (**2-CS**) or an open-shell biradical (**2-OS**) (Chart 1). The interesting question is whether such substitution will change the ground-state electronic structure of the tetrabenzo-Chichibabin's hydrocarbon. Moreover, considering the large steric hindrance arising from the two anthracene units, the geometric structures of both compounds are also of interest, which could be significantly different from the flat geometry of the parent Chichibabin's hydrocarbon.[17c] In this Article, we report the detailed studies on their synthesis, their ground-state electronic and geometric structures, and transition between their closed-shell and open-shell resonance forms by various experiments assisted by theoretical calculations. Their redox behavior and oxidized species were also investigated. In particular, the dication of the fluorenyl-containing tetrabenzo-Chichibabin's hydrocarbon **2-CS**/**2-OS** provides a new candidate for a study on charged antiaromatic species.[22] In addition, transient absorption and two-photon absorption measurements were conducted to further understand the photophysical properties and NLO response of these types of possibly open-shell hydrocarbons.

II. RESULTS AND DISCUSSION

Synthesis and Structural Characterization of 1-CS/1-OS. The synthetic route toward **1-CS**/**1-OS** is shown in Scheme 1. Treatment of the bianthraquinone **3**[23] with CBr_4/PPh_3 afforded the 11,11,11′,11′-tetrabromo-10,10-bianthraquinodimethane **4** in 90% yield. Subsequently, the tetrabenzo-Chichibabin's hydrocarbon, 11,11,11′,11′-tetrakis(4-*tert*-butyl-

dx.doi.org/10.1021/ja3050579 | J. Am. Chem. Soc. 2012, 134, 14513−14525

Scheme 1. Synthesis of Compound 1-CS and Generation of Its Intermediate Biradical 1-OS[a]

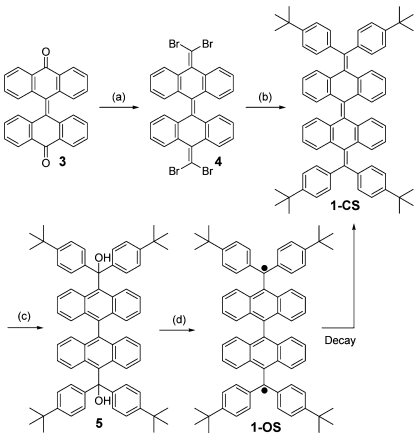

[a]Reaction conditions: (a) CBr_4, PPh_3, toluene, reflux, 36 h, 90%; (b) 4-*tert*-butylphenylboronic acid, $Pd(PPh_3)_4$, Cs_2CO_3–K_2CO_3, toluene/H_2O/EtOH, reflux, 48 h, 90%; (c) DDQ/CH_3SO_3H, CH_2Cl_2, room temperature, 12 h, 75%; (d) $SnCl_2$, dichloromethane, nearly quantitative yield from **5** to **1-OS**.

phenyl)-10,10-bianthraquinodimethane (**1-CS**), was conveniently synthesized as a white solid in 90% yield by a 4-fold Suzuki coupling reaction between 4-*tert*-butylphenylboronic acid and the intermediate bromide **4**. Careful choice of the catalyst ($Pd(PPh_3)_4$) and base (a mixture of Cs_2CO_3 and K_2CO_3) was essential to achieve a clean and high-yield reaction.

The steady-state absorption and emission spectra of compound **1-CS** in dichloromethane (DCM) are shown in Figure 1a. Compound **1-CS** displays an intense absorption band in the UV–visible region with absorption maximum at 349 nm (log ε = 5.54; ε: molar extinction coefficient in M^{-1} cm^{-1}), along with a shoulder absorption at 298 nm. Such a band structure is similar to that for the known bisanthraquinone,[24] indicating that the molecule likely has a closed-shell ground state as do normal acenequinones. Compound **1-CS** shows a broad emission band with emission maximum at 436 nm, with a fluorescence quantum yield of 12%. **1-CS** also exhibited clear and sharp ^1H NMR resonances at room temperature even at elevated temperatures (e.g., 100 °C), which further confirmed its closed-shell structure in the ground state. Single crystals were grown by slow diffusion of methanol into a solution of **1-CS** in DCM at room temperature. X-ray crystallographic analysis revealed that **1-CS** existed in a highly contorted, quinoidal structure (Figure 1b).[25] The lengths of the exo methylene bond and the bond between the two anthracene units, as labeled in Figure 1b, are 1.342 and 1.349 Å, respectively, which are quite close to those in typical olefins (1.33–1.34 Å). Thus, there is no doubt that **1-CS** is a closed-shell species. In contrast to the planar geometry observed for the parent Chichibabin's hydrocarbon from its X-ray crystallographic structure,[17c] the central bisanthracene units in **1-CS** are

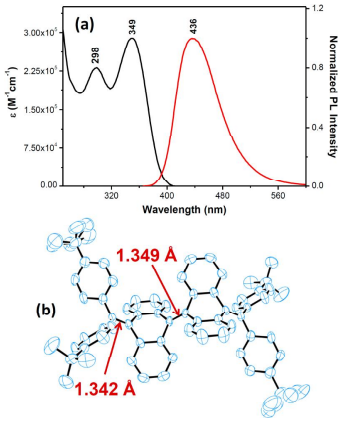

Figure 1. (a) UV–vis absorption spectrum and normalized emission spectrum of compound **1-CS** in DCM. (b) ORTEP plot of the single-crystal structure of **1-CS** with part of the C=C bond labeled with length.

highly twisted due to steric repulsion, and the four additional benzene rings attached to the biphenyl center behave like the wings of a butterfly; thus, the whole molecule looks like a butterfly in the crystal state. The closed-shell ground-state structure of **1-CS** can be ascribed to the loss of two aromatic sextet rings when converted from a quinoidal form to a biradical form (shown in Chart 1), which makes the quinoidal form thermodynamically more stable.

Our intention was to conduct an intramolecular oxidative cyclodehydrogenation reaction of **1-CS** so that a fused, more conjugated hydrocarbon can be generated. The ring cyclization reaction was performed under the well-developed conditions using $FeCl_3$[26] or the 2,3-dichloro-5,6-dicyano-1,4-benzoquinone (DDQ)/CH_3SO_3H system[27] in DCM. Interestingly, no desired ring-closed or even partially cyclized product was found. Alternatively, an unexpected diol **5** was separated in good yield after quenching the reaction with saturated sodium bicarbonate (Scheme 1). This unexpected result indicated that the Scholl-type reaction of **1-CS** when treated with DDQ/H^+ or $FeCl_3$ predominantly generated its dication likely at the exo methylene sites, which is stabilized by charge delocalization through the two phenyl rings and the anthracene units (vide infra). Thus, quenching of the dication with water afforded the diol **5**. The biradical **1-OS** then can be easily generated in nearly quantitative yield by reduction of the diol **5** with $SnCl_2$ in various solvents (e.g., toluene, chloroform, DCM, THF, etc.) (Scheme 1), and MALDI-TOF mass spectroscopy revealed the loss of two –OH groups after reduction. Interestingly, the biradical **1-OS** turned out to be an unstable intermediate, and it relaxed back to the ground-state quinoidal form **1-CS** at an unusually slow rate, which will be discussed in detail in the next section.

Unusually Slow Decay from Open-Shell 1-OS to Closed-Shell 1-CS. The freshly generated biradical **1-OS** by reduction of **5** with excess $SnCl_2$ in toluene displayed a broad

long-wavelength absorption band between 680 and 1050 nm with maximum at 834 nm, together with a strong absorption band centered at 507 nm (Figure 2a). This long-wavelength

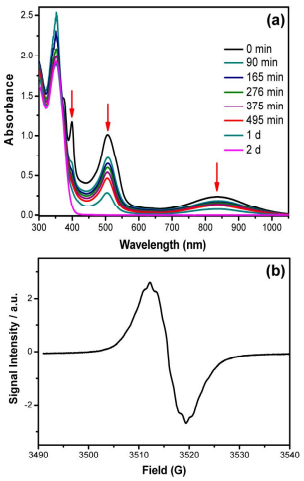

Figure 2. (a) Change of UV−vis absorption spectra of the freshly generated **1-OS** biradical with time. (b) ESR spectrum of **1-OS** in chloroform recorded at room temperature.

absorption spectrum is characteristic of typical open-shell PAHs with unpaired electrons. The existence of the biradical was further proved by the strong electron spin resonance (ESR) signal (g = 2.0029) showing unresolved hyperfine coupling, obtained for the fresh **1-OS** solution generated in chloroform (Figure 2b), indicating a paramagnetic character of the biradical at room temperature.

The time-dependent UV−vis−NIR absorption spectra of the newly generated biradical underwent a slow decay process (Figure 2a). That is, the absorption spectrum of the biradical **1-OS** slowly decreased with time (indicated by the arrow) and reached zero absorbance in 2 days (at the three major absorbances), and the final absorption spectrum after decay was identical to that of **1-CS**. This slow relaxation process was also followed by ^{1}H NMR measurements (Figure S1 in the Supporting Information), which clearly confirmed a transition from an unstable biradical form (**1-OS**) to a stable quinoidal form (**1-CS**). The plot of the absorbance ($\ln(A_t)$) at 834 nm of the freshly prepared **1-OS** in toluene with time revealed a monoexponential decay from the biradical **1-OS** to the quinoidal form **1-CS** at 298 K, with a half-life of around 495 min (Figure 3a). The decay reaction rate constant (k) under this condition was determined to be 0.0014 min^{-1}. To further determine the thermodynamic parameters for this decay process, same decay experiments were conducted at least three times at different temperatures in toluene, and thus the average decay reaction rate constants at respective temperature were obtained (Figure S2 in the Supporting Information). The

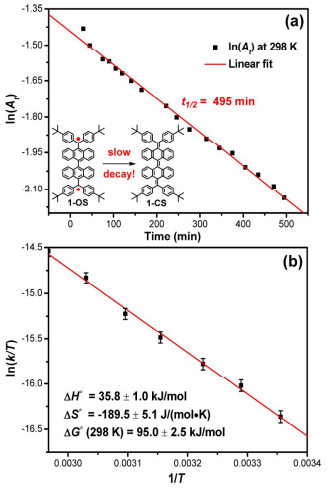

Figure 3. (a) Monoexponential decay of the absorbance at 834 nm of the freshly generated **1-OS** biradical with time at 298 K. R^2, 0.9934; standard error, 0.00786. (b) $\ln(k/T) \approx 1/T$ plot for the decay of **1-OS** at variable temperatures (298−337 K), based on thermodynamic data obtained by fitting the data with Eyring equation.

value of $\ln(k/T)$ was plotted with $1/T$, and a straight line was obtained (Figure 3b). The data were fit by the Eyring equation:

$$\ln\left(\frac{k}{T}\right) = -\frac{\Delta H^{\ddagger}}{R}\cdot\frac{1}{T} + \ln\left(\frac{k_B}{h}\right) + \frac{\Delta S^{\ddagger}}{R}$$

in which k is the reaction rate constant, T is the absolute temperature, $\Delta H^{\ddagger}$ is the enthalpy of activation, R is the gas constant, k_B is the Boltzmann constant, h is the Planck constant, and the $\Delta S^{\ddagger}$ is the entropy of activation. The thermodynamic parameters for such an unusual decay process then were obtained, with $\Delta H^{\ddagger}$ = 38.5 ± 5.1 kJ mol^{-1} and $\Delta S^{\ddagger}$ = −189.5 ± 0.6 J mol^{-1} K^{-1}. Accordingly, the Gibbs energy of activation $\Delta G^{\ddagger}$ ($\Delta H^{\ddagger} - T\Delta S^{\ddagger}$) was determined as 95.0 ± 2.5 kJ mol^{-1} at 298 K. The result means that such a transition from the biradical form to the quinoidal form requires overcoming a high energy barrier. The large negative $\Delta S^{\ddagger}$ value also indicates a conversion from a disordered structure to a highly ordered conformation (i.e., the highly contorted butterfly structure for **1-CS**).

DFT calculations (UCAM-B3LYP/6-31G*)[28] were then conducted to provide a further understanding of such an unusual decay process. The optimized geometries of the **1-CS** and **2-OS** are shown in Figure 4. Molecule **1-CS** also has a butterfly-like geometry with a typical quinoidal character, which is consistent with its single-crystal structure. For **1-OS**, it possibly exists as a singlet or a triplet biradical. In comparison to the quinoidal **1-CS**, both the singlet and the triplet **1-OS** show longer bond lengths for the exo methylene bonds and the bond between the two anthracene units (labeled with arrow), indicating a distinct open-shell character of **1-OS**. In addition, the biradical **1-OS** adopts an orthogonal geometry for the

dx.doi.org/10.1021/ja3050579 | J. Am. Chem. Soc. 2012, 134, 14513−14525

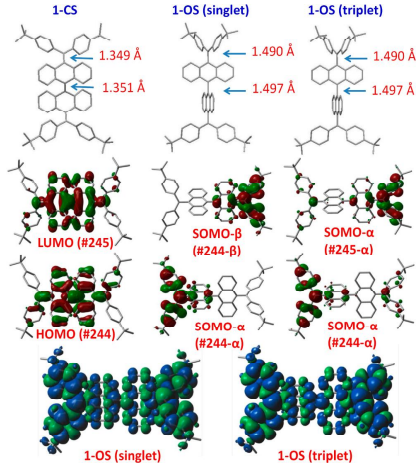

Figure 4. Calculated geometric structures (with part of the bonds labeled with length in Å) and the frontier molecular orbitals of the closed-shell **1-CS** and open-shell **1-OS** both in singlet and in triplet states. The bottom shows the spin density distribution of the singlet and triplet **1-OS**.

bisanthracene core with a dihedral angle of nearly 90°, indicating a transition from a quinoidal structure in **1-CS** to a benzenoid form in **1-OS**. This results in a large negative change of entropy from a disordered to an ordered conformer during the transition from **1-OS** to **1-CS**, which agrees well with the large negative $\Delta S^{\ddagger}$ value determined experimentally.

Calculations also revealed that the Gibbs energies of the singlet and triplet biradical form **1-OS** are located 18.4 and 15.9 kJ/mol higher than for the closed-shell **1-CS**, indicating that the quinoidal resonance form dominates the ground-state electronic and geometric structure and the **1-OS** can be regarded as a metastable excited state (see energy diagram in Figure 5). The

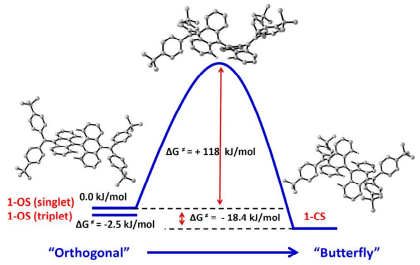

Figure 5. Calculated energy diagram for the **1-CS**, **1-OS** (singlet), and **1-OS** (triplet) and schematic representation of a transition from a higher-energy orthogonal biradical form to a lower-energy butterfly conformer through a high-energy transition state.

decay process mimics the monoexponential fluorescence decay of a chromophore from the excited state to the ground state. In addition, the energy level for the triplet **1-OS** is slightly lower (2.5 kJ/mol) than that of the singlet **1-OS**; thus the orthogonal biradical favors a triplet state, which is also consistent with the observed paramagnetic signal for the newly generated biradical **1-OS**. Upon conversion from the free-rotated orthogonal biradical to the lower-energy butterfly like quinoidal form, the molecule must overcome a high energy barrier to reach a transition state, in which the zigzag edges of the anthracene units are in close proximity with each other and with the four 4-*tert*-butylphenyl rings so that a conversion to a contorted butterfly conformation is possible (Figure 5). A considerable energy barrier of 118 kJ/mol was calculated, which is close to the experimental activation energy value (95 ± 2.5 kJ/mol) measured in solution at 298 K. It is worth noting that, in most cases, the conversion between different electronic configurations that are very close in energy in the ground electronic state occurs at very short time-scale and cannot be easily detected. However, in this case, because of a high activation energy needed for the intersystem crossing from **1-OS** to **1-CS**, an unusually slow decay process was observed experimentally.

1-CS displays the largest coefficients for the highest occupied molecular orbital (HOMO) and the lowest unoccupied molecular orbital (LUMO) along the quinoidal bisanthraquinodimethane moiety (Figure 4), indicating an extended π-electron delocalization despite its highly contorted structure. The two unpaired electrons (α and β spin) in the singlet **1-OS** show a disjointed singly occupied molecular orbital (SOMO), SOMO-α and SOMO-β, with orbital coefficients mainly localized at the terminal diphenylmethene units (Figure 4), indicating a large biradical character for **1-OS**. The spin-density distribution also presents a central symmetry with the terminal diphenylmethene units having the largest density, while there is still significant spin density distributed on the anthracene units (Figure 4). This suggested that the spins are delocalized, which can explain the good chemical stability of the intermediate biradical against oxidation and dimerization/oligomerization. The SOMO-α and SOMO-β profiles and the spin-distribution of the triplet **1-OS** indicate that the two spins are independent from each other, indicating a weak radical−radical coupling.

Synthesis and Characterizations of 2-CS/2-CS. To further tune the ground-state electronic and geometric structure of the tetrabenzo-Chichibabin's hydrocarbon, the two di(4-*tert*-butylphenyl)methene groups in **1-CS** were replaced by two fluorenyl units. The synthesis of **2-OS** was based on a similar synthetic concept as shown in Scheme 2. The 10,10′-dibromo-9,9′-bianthryl **6**[29] was treated with 2 equiv of *n*-BuLi followed by reaction with 9*H*-fluoren-9-one to give the precursor diol **7** in 65% yield. Subsequent reduction of **7** with $SnCl_2$ and purification of the crude product by routine column chromatography on silica gel afforded a deep red solid, which was identified as the biradical **2-OS**.

MALDI-TOF mass spectrum of this product agrees well with the molecular weight of compound **2-OS**. It is noteworthy that the absorption spectral patterns with vibronic splitting observed in the region of 300−400 nm are characteristic of that of anthracene.[30] In addition, a long absorption tail into the near-infrared region is attributed to the lowest energy transition with a small HOMO−LUMO energy gap of 1.28 eV. This steady-state optical property of **2-OS** suggests a representative open-shell biradical electronic structure as we expected (cf., Scheme 2). In this regard, this compound in THF-d_8 solvent did not

Scheme 2. Synthetic Route of Compounds 2-OS and 2-CS[a]

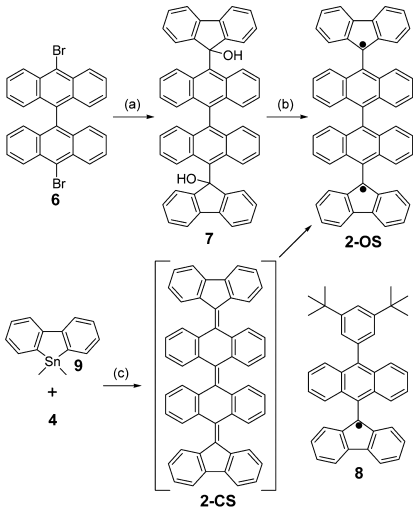

[a]Reaction conditions: (a) (1) *n*-BuLi/THF; (2) 9*H*-fluoren-9-one, 65%; (b) $SnCl_2$, CH_2Cl_2, room temperature, 82%; (c) $Pd(PBu^t_3)_4$, CuI, CsF, toluene.

show any NMR signals at room temperature even after cooling to −100 °C, indicating the presence of a considerable paramagnetic species. Strong ESR signal was detected for the sample in various solutions and in the solid state. For example, the solution of **2-OS** in 2-methyl tetrahydrofuran (2-Me−THF) showed a well-resolved quintet ESR spectrum with g = 2.0027 at 153 K (Figure 7a). Simulations indicated that most of the hyperfine structure resulted from two sets of two equivalent protons with hyperfine coupling constants of 4.1 and 3.2 G. Superconducting quantum interference device (SQUID) measurements were conducted for **2-OS** in the powder form at 5−380 K. The product of magnetic susceptibility χ and temperature T is plotted as a function of temperature in Figure 7b and the magnetic susceptibility can be well fitted with Bleaney−Bowers equation. The singlet−triplet gap was estimated to be $2J/k_B$ = 166 K (1.4 kJ/mol), indicating that the ground state for **2-OS** is triplet (paramagnetic). Thus, all of these experiments confirmed that the obtained compound was the biradical **2-OS** instead of the closed-shell form **2-CS**. Interestingly, **2-OS** displayed extremely high stability, and there was no obvious decomposition when the solution or solid was stored under ambient air and light conditions for months, which could be attributed to thermodynamic stabilization of the fluorenyl moieties and kinetic stabilization by the anthracene units.

To further understand the nature of the biradical in **2-OS**, an anthryl-substituted fluorenyl monoradical **8** (Scheme 2) was also prepared for comparison (see detailed synthesis in the Supporting Information). The UV−vis absorption spectrum (Figure 6) and the ESR spectrum (Figure 7) of compound **8**

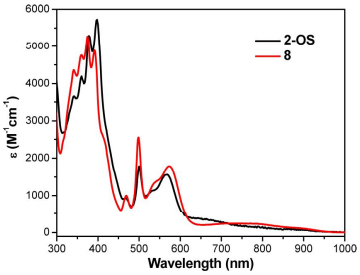

Figure 6. UV−vis−NIR absorption spectrum of **2-OS** and compound **8** in DCM.

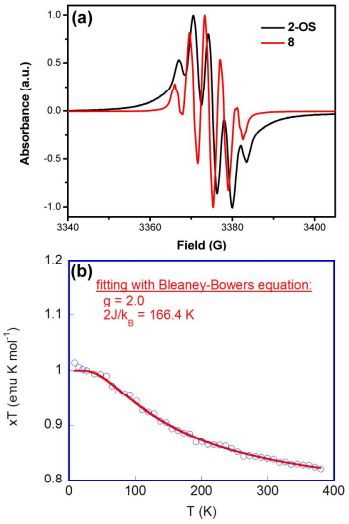

Figure 7. (a) CW ESR spectra of **2-OS** and **8** in 2-Me−THF at 153 K. (b) χT versus T curve for the powder of **2-OS** in the SQUID measurements and the fitting plot via the Bleaney−Bowers equation.

are very similar to that of **2-OS**, indicating that there is very weak dipole coupling between the two radicals. This is presumably due to the large mean internal radical-to-radical distance and the orthogonal arrangement of the two anthracene units in **2-OS** (vide infra). The small singlet−triplet energy gap (1.4 kJ/mol) obtained from the SQUID measurement also indicates a weak coupling between the two radicals, and both the singlet and triplet diradicals could exist at room temperature.

The existence of such a stable biradical character also implied that it may represent the ground-state structure of the **2-CS**/**2-OS**. To confirm this hypothesis, the synthesis of the closed-shell structure **2-CS** was also attempted (Scheme 2). This was

dx.doi.org/10.1021/ja3050579 | J. Am. Chem. Soc. 2012, 134, 14513−14525

done by the Still coupling reaction between compound **4** and 9,9-dimethyl-9-stannafluorene **9**[31] in the presence of Pd-(PBu^t_3)$_4$ as catalyst. However, the biradical form **2-OS** was generated instead of the closed-shell **2-CS**. This suggested that the closed-shell form **2-CS** was formed as an unstable intermediate compound, which quickly underwent relaxation to its more stable open-shell biradical form **2-OS**. The product **2-OS** could not be separated in its pure form by this method due to the contamination with other side-products including a ring-opening oligomer of **9**, which was identified by X-ray single-crystal analysis (Figure S3 in the Supporting Information). However, the formation of **2-OS** can be unambiguously identified by MALDI-TOF mass spectrum and UV−vis absorption measurement, which are identical to those for pure **2-OS**. Therefore, the ground state of **2-CS**/**2-OS** can be defined as the open-shelled biradical, which is in contrast to the **1-CS**/**1-OS** pair.

Similar theoretical calculations were also conducted for **2-CS**/**2-OS** (Figure 8). The closed-shell form of **2-CS** adopted a

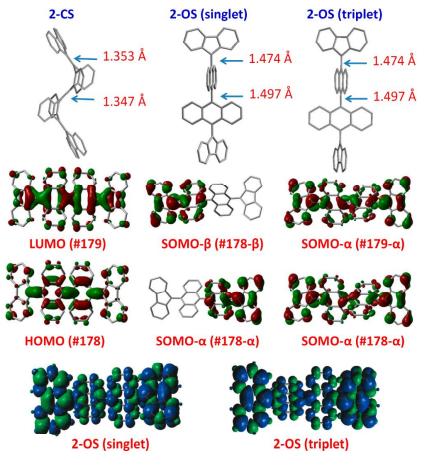

Figure 8. Calculated geometric structures (with part of the bonds labeled with length in Å) and the frontier molecular orbitals of the closed-shell **2-CS** and open-shell **2-OS** both in singlet and in triplet states. The bottom shows the spin density distribution of the singlet and triplet **2-OS**.

contorted butterfly conformation with characteristic bond lengths (as labeled with arrows, 1.353, 1.347 Å, respectively) for a quinoidal hydrocarbon, similar to **1-CS**. The open-shell **2-OS** structures show an orthogonal geometry due to steric congestion, similar to those for **1-OS** as well. DFT calculations showed that the diradical states (singlet and triplet **2-OS**) had lower energies than its closed-shell form (**2-CS**) by 23.4−25.9 kJ/mol, and the energy of the triplet state was slightly lower energy than the singlet biradical state by 2.5 kJ/mol, which is consistent with the SQUID measurement (ΔE_{S-T} = −1.4 kJ/mol). The frontier molecular orbital profiles of **2-CS** revealed that the electrons are mainly delocalized through the π-extended quinodimethane part at the middle of the molecule for both HOMO and LUMO. In contrast to **2-CS**, the SOMOs of the α and β spins in **2-OS** exhibit an extended delocalization to the fluorenyl unit, especially for the singlet state. Thus, **2-OS** showed large spin density at the fluorenyl moiety (Figure 8). The large spin delocalization through the fluorenyl anthryl methene unit should account for the high stability of the biradical.

Electrochemical Properties of 1-CS/2-OS and Their Dication 1-CS^{2+}/2-OS^{2+}. Cyclic voltammetry was performed to investigate electrochemical properties of **1-CS** and **2-OS**. **1-CS** in DCM exhibited one chemically irreversible reductive wave with half-wave potential E_{red} at −1.27 V (vs Fc^+/Fc), and the first oxidative scan revealed an intense irreversible oxidation wave above 0.73 V (Figure 9a). However, the reverse scan from the high oxidation state back to −0.6 V showed two closely overlapped quasi-reversible reduction waves. The second and third circle scans showed that the same redox waves existed. This observation suggested that subsequent chemical reaction

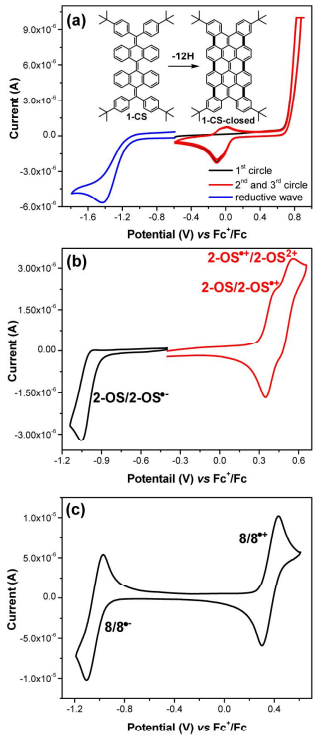

Figure 9. Cyclic voltammograms of **1-CS** (a), **2-OS** (b), and compound **8** (c) in dry DCM with 0.1 M Bu_4NPF_6 as supporting electrolyte, Ag/AgCl as reference electrode, Au disk as working electrode, Pt wire as counter electrode, and a scan rate at 100 mV/s.

dx.doi.org/10.1021/ja3050579 | J. Am. Chem. Soc. 2012, 134, 14513−14525

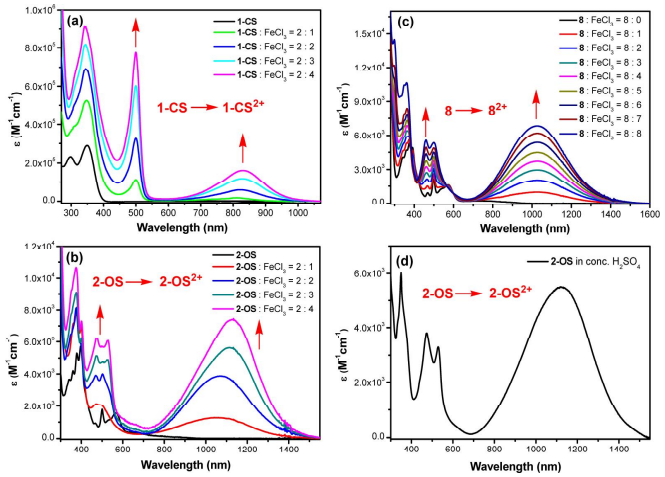

Figure 10. UV−vis−NIR absorption spectra of **1-CS** (a), **2-OS** (b), and compound **8** (c) upon oxidative titration with $FeCl_3$ in dry DCM, and absorption spectrum of **2-OS** in concentrated H_2SO_4 (d).

might happen after the oxidation of **1-CS** at high potential (>0.73 V) so that a new redox active species with lower oxidation potential was generated. Electrolysis of the **1-CS** in DCM was then conducted at 1.0 V using a large Pt plate electrode, and the mixture was monitored by MALDI-TOF mass spectroscopy. Interestingly, the mass spectrum of the mixture revealed the existence of the starting material and a species with a loss of 12 hydrogen atoms (Figure S4 in the Supporting Information). Thus, an intramolecular oxidative cyclodehydrogenation likely occurred at the high oxidation potentials, which gave the fully fused hydrocarbon **1-CS-closed** (inserted structure shown in Figure 9a) via the loss of 12 hydrogen atoms.[32] Compound **2-OS** exhibited two reversible oxidation waves with half-wave potentials $E_{ox}^1 = 0.38$ V and $E_{ox}^2 = 0.52$ V (vs Fc^+/Fc), and one quasi-reversible reduction wave with a half-wave potential $E_{red} = -0.98$ (vs Fc^+/Fc) (Figure 9b). The energy levels of the HOMO and LUMO were determined to be −5.10 and −3.87 eV, respectively, from the onset potentials of the oxidation and reduction waves. Thus, a low electrochemical energy gap (E_g^{EC}) of 1.23 eV was determined for **2-OS**, which was consistent with its optical energy gaps ($E_g^{Opt} = 1.28$ eV). Such a small energy gap promoted **2-OS** to adopt open-shell biradical in the ground state. These two oxidative waves suggest that compound **2-OS** can be oxidized to its monoradical cation and dication after removal of one and two unpaired electrons. For comparison, the monoradical **8** showed one reversible oxidation wave at $E_{ox} = 0.37$ V and one reversible reduction wave at $E_{red} = -1.04$ V (Figure 9c), with the HOMO and LUMO energy levels being −5.10 and −3.84 eV, respectively.

The low oxidation potentials observed for **1-CS** and **2-OS** allowed us to approach their cationic species (monoradical cation and dication) by chemical oxidation. Instead of using highly reactive and expensive oxidants such as super acid SbF_5/SO_2ClF, which are usually used for generating aromatic or antiaromatic carbocations of hydrocarbons at very low temperature.[33] We found that mild oxidants such as $FeCl_3$ could be used for the oxidation of **1-CS**/**2-OS** into their corresponding dications in nearly quantitative yield at room temperature. Chemical oxidative titration of compounds **1-CS** and **2-OS** by $FeCl_3$ was conducted in dry DCM, and the progress was monitored by UV−vis−NIR spectroscopy (Figure 10a and b). Both compounds can be oxidized by $FeCl_3$ into stable cationic species, and the absorbance reached a saturation state when 2 equiv of $FeCl_3$ was used, indicating formation of stable dications. This is consistent with the previous observation that attempted cyclodehydrogenation of **1-CS** with $FeCl_3$ followed by quenching with aqueous solution gave the diol **5**. A new sharp and intense absorption band at 500 nm and a broad absorption band centered at 832 nm were observed for the dication **1-CS**$^{2+}$. Similarly, for **2-OS**, titration with $FeCl_3$ finally led to a well-resolved band with maximum at 528 and 475 nm, and a new broad band with maximum at 1130 nm for the dication **2-OS**$^{2+}$. It should be noted that in both cases, the broad bands were bathochromically shifted obviously during the titration before reaching the final state, indicating the existence of both monoradical cation and dication at the intermediate stage. Under the same condition, compound **8** can be progressively oxidized by $FeCl_3$ into its monocation (Figure 10c), and a broad band centered at 1027 nm together with a well-resolved band at 500/458 nm were observed. The band structure was similar to that for **2-OS**$^{2+}$ due to their similar chemical structure.

Although the preparation of the parent 9-fluorenyl cation in sulfuric acid was difficult due to rapid decomposition and polymerization to unidentifiable products,[34] we found that the oxidation of **2-OS** in concentrated sulfuric acid gave a stable dication **2-OS**$^{2+}$, which permitted UV−vis−NIR absorption and

dx.doi.org/10.1021/ja3050579 | J. Am. Chem. Soc. 2012, 134, 14513−14525

^{1}H NMR spectroscopic measurements. As shown in Figure 10d, the UV−vis−NIR spectrum of compound **2-OS** in concentrated H_2SO_4 is nearly identical to the dication **2-OS**$^{2+}$ generated from oxidation of **2-OS** with $FeCl_3$, indicating that the dication species was indeed formed upon mixing **2-OS** with concentrated H_2SO_4. The ^{1}H NMR spectrum of **2-OS**$^{2+}$ was then recorded in D_2SO_4, and well-resolved aromatic proton resonances appeared after 2 h, which could be clearly assigned to the desired dication **2-OS**$^{2+}$ (Figure S5). It was worthy to note that the protons on the fluorenyl unit showed obvious shift to the high field, indicating an antiaromatic nature of the cyclopentadienyl cation. The dication solution in sulfuric acid was quite stable and showed no change after storage at room temperature for several weeks. However, oxidation of the **1-CS** and compound **8** with concentrated H_2SO_4 led to a complicated mixture due to decomposition of the starting materials.

Subsequently, DFT (UCAM-B3LYP) calculations were conducted to further understand the stability of the dications **1-CS**$^{2+}$ and **2-OS**$^{2+}$. In both cases, high HOMO coeficients are mainly found at the anthracene units, while the LUMO coeficients are mainly localized at the diphenylmethane or fluorenyl moieties (Figure 11). The Mulliken charge density

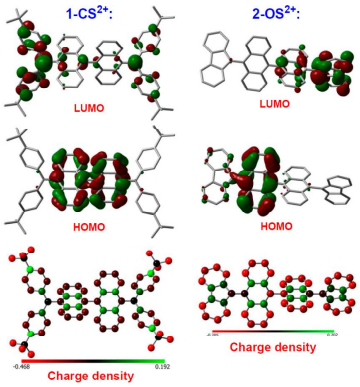

Figure 11. Calculated frontier molecular orbital profiles and the Mulliken charge density distribution of **1-CS**$^{2+}$ and **2-OS**$^{2+}$.

distribution indicated that the positive charges are mainly localized at the methane cation site but also delocalized through the anthracene units and the diphenyl or fluorenyl moieties. Such a charge delocalization should account for the good stability of the dications **1-CS**$^{2+}$ and **2-OS**$^{2+}$.

FT Raman Spectra of 1-CS/2-OS and Their Dications. To scrutinize the intrinsic structure of **1-CS**/**2-OS** in neutral state and their corresponding dications **1-CS**$^{2+}$/**2-OS**$^{2+}$, FT Raman experiments were conducted and provided further structure−property relationships between the closed-shell and open-shell species.[35] FT-Raman spectra of **1-CS** and **2-OS** in their neutral states are shown in Figure 12, and there is a large difference between the two spectra in the 1600 cm^{-1} region. The spectrum of **1-CS** has clear signatures of benzo-quinoidal rings (i.e., band at 1596 cm^{-1}) together with a band at a

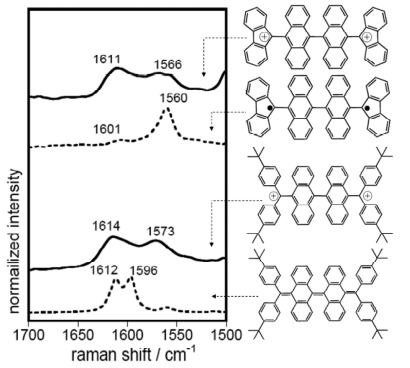

Figure 12. 1064 nm FT-Raman spectra of neutral and oxidized **1-CS** (bottom: dotted and solid lines, respectively) and of neutral and oxidized **2-OS** (top: dotted and solid lines, respectively).

position close to that of usual conjugated C═C bond stretches (i.e., band at 1612 cm^{-1}), which indicates that the structure of **1-CS** is compatible with a closed-shell electronic configuration. The spectrum of **2-OS**, however, with the strongest band at 1560 cm^{-1}, reveals its anthracene-like structure originated from the stabilization of the open-shell aromatized species. The evolution from a closed-shell structure in **1-CS** to an open-shell structure in **2-OS** as delineated by the Raman spectra can be interpreted by the larger stabilization energy of the radical center in a planar cyclopentadienyl moiety in **2-OS**, a structural motif that is not possible in **1-CS**.

The unique absorbance tail of **2-OS** from 500 nm to the near-infrared (Figure 6), likely due to the open-shell structure, allows us to use resonance Raman spectroscopy to get further insights onto the electronic configuration by comparing the Raman spectra of **2-OS** recorded with the 633 and 1064 nm excitation wavelengths, which correspond to on-resonance and off-resonance experiments, respectively (Figure S6 in the Supporting Information). The spectra of **2-OS** under different excitation wavelengths are essentially identical, highlighting that there is a sole electronic configuration describing the ground electronic state. On the other hand, the VT FT-Raman spectra for **1-CS** and **2-OS** in the solid state (Figure S7 in the Supporting Information) showed that between −170 and +120 °C the Raman spectra are almost unaltered, revealing the absence of any relevant thermal interpopulation between low energy lying states; that is, **1-CS** and **2-OS** are robust singlet and triplet ground electronic states, respectively. For **2-OS**, the thermal invariance of the Raman spectra might indicate almost iso-energetic singlet and triplet states or a rather small singlet−triplet energy gap, which is in accordance with both theoretical calculations and experimental measurements.

These two samples were oxidized to their corresponding dications by $FeCl_3$ in dry DCM, and the FT-Raman spectra of the oxidized species in solution are also shown in Figure 12. These two spectra correspond to resonance Raman spectra as the 1064 nm laser of the Raman experiment excites the characteristic electronic absorptions of both dicationic species (Figure 10). This is important because it discards interference

by other species. Conversely to the case of the neutral systems, the two spectra now became similar (Figure 12), suggesting that both species shared a similar geometrical structure in their charged ground electronic states. The appearance of the intense band in the two oxidized species around 1570 cm^{-1} can be assigned to the anthracene-like structure of the two molecular cores, which was in accordance with the formation of the corresponding carbocations either in the fluorenyl center in **2-OS** or in the diphenylmethene center in **1-CS**. Thus, our Raman spectroscopic measurements clearly revealed the ground-state electronic structures of **1-CS**/**2-OS** and their dications, which were consistent with the previous studies by other approaches.

Femtosecond Transient Absorption and Two-Photon Absorption Spectroscopic Measurements. To date, the excited-state dynamics of open-shell organic molecules has been still rarely investigated because of the limited number of systems with stable radical-associated molecules suitable for testing these effects. A few hybrid derivatives possessing the stable heteroatomic spin center on N−O units (e.g., TEMPO and α-nitronylnitroxide) have been characterized by transient absorption spectroscopy.[36] In contrast to the spin-localized heteroatomic systems, the spin-delocalized pure PAHs would exhibit the different relaxation nature in their excited states. The effect of open-shell electronic structure of **2-OS** on the excited-state photophysical properties is of interest. Therefore, we carried out the femtosecond transient absorption (TA) measurements to investigate the excited-state dynamics of **1-CS** and **2-OS** (Figures S8,S9 in the Supporting Information). For compound **1-CS** in toluene at room temperature, the broad excited-state absorption (ESA) signals around 700 nm become narrower and hypsochromically shifted to 670 nm within an initial 15 ps time decay, probably due to the conformational change through the internal conversion process from the higher excited state. The two decay-associated spectra at early time-evolution and the longer one indicate the TA spectra before and after vibrational relaxation process, respectively. The decay time constants probed at various wavelengths are fitted by two exponential functions of 7 and 96 ps. The singlet excited-state lifetime of **1-CS** estimated to be 96 ps is relatively shorter presumably due to the structural flexibility resulting from the contorted butterfly geometry.

In the case of **2-OS**, the broad ESA signal was observed in the whole visible region. The decay profile probed at 736 nm was estimated to be 24 ps by fitting with a single exponential function. As compared to the closed-shell **1-CS**, the open-shell derivative **2-OS** had a more short-lived excited-state lifetime. While the structure-dependent radical-induced quenching mechanism[36b] through enhanced intersystem crossing (ISC) and/or internal conversion (IC) in doublet radical−chromophore dyads has been reported, the fast decay kinetic profile of **2-OS** is considered to reflect an acceleration of the nonradiative IC rates arising from the smaller energy gap between the lowest excited state and the open-shell ground state. The non-fluorescent property of **2-OS** is also consistent with the short excited-state lifetimes. Considering the relatively rigid orthogonal structure of **2-OS** containing aromatized anthracene units, the unpaired electrons associated with the molecule contributed to the ultrafast relaxation dynamics.

To investigate the NLO properties of the biradical **2-OS**, two-photon absorption measurements were conducted by using the open-aperture Z-scan method with 130 fs pulses in the NIR region from 1200 to 1500 nm where one-photon absorption (OPA) contribution is negligible. As shown in Figure 13 (and Figure S10 in the Supporting Information), although **2-OS** had

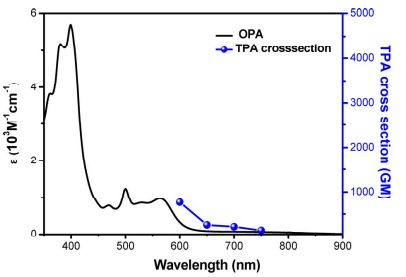

Figure 13. OPA (black solid line and left vertical axis) and TPA spectra (blue symbols and right vertical axis) of **2-OS** in chloroform. TPA spectra were plotted at $\lambda_{ex}/2$.

a rather small OPA absorption coefficient, it showed a large TPA cross section in the wavelength region with the maximum value as 760 GM at 1200 nm. In comparison with typical hydrocarbon chromophores, which only exhibited a small TPA value at the long wavelength, a relatively larger cross section for compound **2-OS** was obtained, and was comparable to the achieved value of other open-shell PAH molecules (300−890 GM)[4] in the same region of photoexcitation. This result can be reasonably understood by the unusual ground-state electronic structure of **2-OS** with distinct biradical character. The measurement on the closed-shell **1-CS** however was limited by its too short absorption wavelength, which was out of the range of the photoexcitation wavelength of our facilities.

III. CONCLUSION

In summary, two new stable tetrabenzo-Chichibabin's hydrocarbons were synthesized by a new strategy, and their electronic structure and geometry in the ground state were investigated by various experiments assisted by DFT calculations. Their ground-state structures were tunable, with **1-CS** as a closed-shell hydrocarbon and **2-OS** as an open-shell biradical. Such a difference can be explained by an enhanced thermodynamic stabilization of the biradicaloid resonance form when the di(4-*tert*-butylphenyl)methene groups in **1-CS** were replaced by fluorenyl units in **2-OS**. The extremely high stability of the biradical **2-OS** can be ascribed to thermodynamic stabilization by delocalization and kinetic blocking by the anthracene units. Their excited states were also approachable by chemical means, and an unusually slow transition from the orthogonal **1-OS** to a highly contorted butterfly like **1-CS** was observed, which can be explained by a very large energy barrier arising from steric repulsion during the transition. A quinoidal form **2-CS** represented the excited state of **2-OS**, and it quickly relaxed back to the ground state during chemical synthesis. The nature of the biradical in **2-OS** was confirmed as two weakly coupled radicals with a triplet ground state and a small singlet−triplet energy gap (ΔE_{S-T} = −1.4 kJ/mol). Both compounds can be oxidized into stable dications by chemical oxidation. FT Raman spectroscopy also provided further structural information, such as a quinoidal form for **1-CS** and a benzenoid form for **2-OS**, **1-CS**$^{2+}$, and **2-OS**$^{2+}$, which was consistent with other

experimental data. The open-shell **2-OS** has a shorter singlet excited lifetime than that of closed-shell **1-OS**, which can be considered to reflect a radical-induced acceleration of the nonradiative internal conversion rates. Moreover, the open-shell **2-OS** exhibited a large TPA cross-section value (760 GM) at long wavelength (1200 nm), indicating promising potential applications of open-shell PAHs in nonlinear optics.

IV. EXPERIMENTAL SECTION

Steady-state UV−vis absorption and fluorescence spectra were recorded on a Shimadzu UV-1700 spectrometer and a RF-5301 fluorometer, respectively. The electrochemical measurements were carried out in anhydrous DCM with 0.1 M Bu_4NPF_6 as the supporting electrolyte at a scan rate of 100 mV/s at room temperature under the protection of nitrogen. A gold disk was used as working electrode, platinum wire was used as counting electrode, and Ag/AgCl (3 M KCl solution) was used as reference electrode. The potential was externally calibrated against the ferrocene/ferrocenium couple. Continuous wave X-band ESR spectra were obtained with a Bruker ELEXSYS E500 spectrometer using a variable-temperature Bruker liquid nitrogen cryostat. Quantitative ESR experiments were conducted by over-modulating the EPR signals and comparing the signal intensities of **8** and **2-OS** with the long-lived radical anion produced by the one-electron reduction of vitamin K1[37] obtained under identical instrumental and experimental conditions. The integrated ESR signals of 1 mM solutions of each radical were obtained separately in a silica flat cell. The observation that compounds **8** show integrated signal intensities similar to that of $VK1^{\bullet-}$ confirms that they are the primary radicals, and the signal is not due to minor impurities. The signal intensity of **2-OS** is 1.77 times that of **8**, indicating the existence of diradicals containing both singlet and triplet species. A SQUID system (Quantum Design, ST) was used for the magnetic characterization in the temperature range of 5−380 K. The powder of **2-OS** powder (9 mg) was sealed in a plastic tube. Magnetic susceptibility was measured under a constant magnetic field of 3000 Oe in the temperature range of 5−380 K. The signal of sample holder and plastic tube was deducted by measuring the sample holder and plastic tube under same conditions. For the analysis of the raw SQUID data, we assumed that the magnetic susceptibility of the **2-OS** sample consists of three components, diamagnetic signal, paramagnetic impurity, and signal of singlet−triplet (which can be described with the Bleaney−Bowers equation).

FT−Raman spectra were measured using an FT-Raman accessory kit (FRA/106-S) of a Bruker Equinox 55 FT-IR interferometer. A continuous-wave Nd-YAG laser working at 1064 nm was employed for excitation, at a laser power in the sample not exceeding 30 mW. A germanium detector operating at liquid nitrogen temperature was used. Raman scattering radiation was collected in a back-scattering configuration with a standard spectral resolution of 4 cm^{-1}. 2000 scans were averaged for each spectrum. A variable-temperature cell Specac P/N 21525, with interchangeable pairs of quartz windows, was used to record the FT-Raman spectra at different temperatures. The variable-temperature cell consists of a surrounding vacuum jacket (0.5 Torr) and combines a refrigerant Dewar and a heating block as the sample holder. It is also equipped with a copper constantan thermocouple for temperature monitoring between −170 and 150 °C. Samples were inserted into the heating block part or the Dewar/cell holder assembly in the form of pure solids dispersed in KBr pellets, and Raman spectra were recorded after waiting for thermal equilibrium in the sample. The samples in KBr pellets were prepared in an oxygen- and water-free bag.

The femtosecond time-resolved transient absorption spectrometer used for this study consisted of a femtosecond optical parametric amplifier (Quantronix, Palitra-FS) pumped by a Ti:sapphire regenerative amplifier system (Quantronix, Integra-C) operating at 1 kHz repetition rate and an accompanying optical detection system. The generated OPA pulses had a pulse width of ∼100 fs and an average power of 1 mW in the range 450−800 nm, which were used as pump pulses. White light continuum (WLC) probe pulses were generated using a sapphire window (2 mm thick) by focusing of small portion of the fundamental 800 nm pulses, which were picked off by a quartz plate before entering into the OPA. The time delay between pump and probe beams was carefully controlled by making the pump beam travel along a variable optical delay (Newport, ILS250). Intensities of the spectrally dispersed WLC probe pulses were monitored by miniature spectrograph (OceanOptics, USB2000+). To obtain the time-resolved transient absorption difference signal (ΔA) at a specific time, the pump pulses were chopped at 25 Hz, and absorption spectra intensities were saved alternately with or without pump pulse. Typically, 6000 pulses were used excite samples and to obtain the TA spectra at a particular delay time. The polarization angle between pump and probe beam was set at the magic angle (54.7°) using a Glan-laser polarizer with a half-wave retarder to prevent polarization-dependent signals. The cross-correlation fwhm in the pump−probe experiments was less than 200 fs, and chirp of WLC probe pulses was measured to be 800 fs in the 400−800 nm regions. To minimize chirp, all reflection optics were used in the probe beam path, and a quartz cell of 2 mm path length was employed. After each set of fluorescence and TA experiments was completed, the absorption spectra of all compounds were carefully checked to rule out the presence of artifacts or spurious signals arising from, for example, degradation or photo-oxidation of the samples in question.

The two-photon absorption spectrum was measured in the NIR region using the open-aperture Z-scan method with 130 fs pulses from an optical parametric amplifier (Light Conversion, TOPAS) operating at a repetition rate of 3 kHz generated from a Ti:sapphire regenerative amplifier system (Spectra-Physics, Hurricane). After passing through a 10 cm focal length lens, the laser beam was focused and passed through a 1 mm quartz cell. Because the position of the sample cell could be controlled along the laser beam direction (z axis) using the motorcontrolled delay stage, the local power density within the sample cell could be simply controlled under constant laser intensity. The transmitted laser beam from the sample cell was then detected by the same photodiode as used for reference monitoring. The on-axis peak intensity of the incident pulses at the focal point, I_0, ranged from 40 to 60 GW cm^{-2}. For a Gaussian beam profile, the nonlinear absorption coefficient can be obtained by curve fitting of the observed open-aperture traces $T(z)$ with the following equation:

$$T(z) = 1 - \frac{\beta I_0 (1 - e^{-\alpha_0 l})}{2\alpha_0 [1 + (z/z_0)^2]}$$

where α_0 is the linear absorption coefficient, l is the sample length, and z_0 is the diffraction length of the incident beam. After the nonlinear absorption coefficient has been obtained, the TPA cross section $\sigma^{(2)}$ of one solute molecule (in units of GM, where 1 GM = 10^{-50} cm^4 s $photon^{-1}$ $molecule^{-1}$) can be determined by using the following relationship:

$$\beta = \frac{10^{-3}\sigma^{(2)} N_A d}{h\nu}$$

where N_A is the Avogadro constant, d is the concentration of the compound in solution, h is the Planck constant, and ν is the frequency of the incident laser beam.

Theoretical calculations were carried out by using the Gaussian 09 program. The initial geometry optimizations of **1-CS**/**1-OS** and **2-CS**/**2-OS** were performed with the UCAM-B3LYP/6-31G* level of theory.[28,38] The resulting DFT solution (i.e., singlet "closed-shell": zero spin density on all atoms) was further tested for its stability with the STABLE=OPT keyword. A spin symmetry broken DFT solution was found with lower energy for **2-OS**. Next, the Guess=Read keyword was used to perform the optimization at the same level. Frequency calculations were conducted to ensure that these structures are indeed local minima (see the Supporting Information for a summary of the computation results).

Synthesis of Tetrabenzo-Chichibabin's Hydrocarbon 1-CS. A mixture of **4** (500 mg, 0.72 mmol), 4-*tert*-butylphenylboronic acid (1.302 g, 7.23 mmol), K_2CO_3 (1.0 g, 7.23 mmol), Cs_2CO_3 (940 mg, 2.89 mmol), and $Pd(PPh_3)_4$ (330 mg, 0.029 mmol) in the mixed solvents of toluene (100 mL), ethanol (1 mL), and water (3.6 mL)

was degassed and purged with argon three times. The mixture was heated to 130 °C for 48 h. After being cooled, the reaction mixture was concentrated in vacuum and then diluted with DCM (200 mL), and washed with water (100 mL) and brine (100 mL). The combined organic extracts were dried over anhydrous Na_2SO_4 and filtered, and the solvent was removed in vacuo. The residue was then purified by column chromatography (silica gel, DCM/hexane = 1:10) to afford the desired product (600 mg, 90%) as a white solid. ^{1}H NMR ($CDCl_3$, 500 MHz): δ ppm 7.41 (d, J = 8.5 Hz, 8H, Ar), 7.32 (d, J = 8.5 Hz, 8H, Ar), 7.15 (d, J = 7.5 Hz, 4H, Ar), 7.08 (d, J = 7.5 Hz, 4H, Ar), 6.87 (t, 4H, J = 7.0 Hz, Ar), 6.82 (t, 4H, J = 7.0 Hz, Ar), 1.32 (s, 36H, CH_3). ^{13}C NMR ($CDCl_3$, 75 MHz): δ ppm 149.41, 139.98, 139.64, 138.89, 137.59, 135.07, 132.14, 129.28, 128.64, 128.24, 125.46, 125.08, 124.74, 34.47, 31.38. High-resolution mass spectrum (HR MS) (EI): caldc for $C_{70}H_{68}$, 908.5321; found, m/z = 908.5329 (error = +0.9 ppm).

Synthesis of Tetrabenzo-Chichibabin's Hydrocarbon 2-OS. Under a nitrogen atmosphere, a solution of 7 (105 mg, 0.147 mmol) in dry DCM (30 mL) was added to $SnCl_2$ (139 mg, 0.735 mmol). The mixture was stirred overnight at room temperature under a nitrogen atmosphere. The solvent was removed under reduced pressure. The residue was then purified by column chromatography (silica gel, chloroform/hexane = 1:20) to give compound **2-OS** as a red solid (82 mg, 82%). HR MS (APCI): calcd for $C_{54}H_{32}$, 680.2504; found, m/z = 680.2506 (error = +0.3 ppm). No NMR signal was observed at room temperature even at low temperature (−100 °C). The purity was further determined by HPLC analysis with a silica column by using different eluents. Under variable conditions, only one elution peak was observed, indicating high purity of this compound (Figure S10 in the Supporting Information).

■ ASSOCIATED CONTENT

Ⓢ Supporting Information

Synthetic procedures and characterization data of all other new compounds. TA spectra and Z-scan curves. Crystallographic data. This material is available free of charge via the Internet at http://pubs.acs.org.

■ AUTHOR INFORMATION

Corresponding Author

chmwuj@nus.edu.sg; dongho@yonsei.ac.kr; kuowei.huang@kaust.edu.sa; casado@uma.es; webster@ntu.edu.sg

Notes

The authors declare no competing financial interest.

■ ACKNOWLEDGMENTS

J.W. acknowledges financial support from the BMRC-NMRC grant (no. 10/1/21/19/642), MOE Tier 2 grant (MOE2011-T2-2-130), and IMRE Core funding (IMRE/10-1P0509). The work at Yonsei University was supported by WCU (World Class University) programs (R32-2010-10217-0) and an AFSOR/APARD grant (no. FA2386-09-1-4092). K.-W.H. acknowledges financial support from KAUST. The work at the University of Málaga was supported by the Ministerio de Educación y Ciencia (MEC) of Spain and by FEDER funds (project CTQ2009-10098 and to the Junta de Andalucía for the research project PO9-4708). We thank Dr. Tan Geok-Kheng for crystallographic analysis.

■ REFERENCES

(1) (a) Rajca, A. *Chem. Rev.* **1994**, *94*, 871−893. (b) Morita, Y.; Suzuki, K.; Sato, S.; Takui, T. *Nat. Chem.* **2011**, *3*, 197−204. (c) Lambert, C. *Angew. Chem., Int. Ed.* **2011**, *50*, 1756−1758. (d) Sun, Z.; Wu, J. *J. Mater. Chem.* **2012**, *22*, 4151−4160. (e) Sun, Z.; Ye, Q.; Chi, C.; Wu, J. *Chem. Soc. Rev.* **2012**, in press, DOI: 10.1039/C2CS35211G.

(2) Iwamura, H.; Koga, N. *Acc. Chem. Res.* **1993**, *26*, 346−351.

(3) (a) Nakano, M.; Kishi, R.; Takebe, A.; Nate, M.; Takahashi, H.; Kubo, T.; Kamada, K.; Ohta, K.; Champagne, B.; Botek, E. *Comput. Lett.* **2007**, *3*, 333−338. (b) Nakano, M.; Kishi, R.; Ohta, S.; Takahashi, H.; Kubo, T.; Kamada, K.; Ohta, K.; Botek, E.; Champagne, B. *Phys. Rev. Lett.* **2007**, *99*, 033001. (c) Nakano, M.; Minami, T.; Yoneda, K.; Muhammad, S.; Kishi, R.; Shigeta, Y.; Kubo, T.; Rougier, L.; Champagne, B.; Kamada, K.; Ohta, K. *J. Phys. Chem. Lett.* **2011**, *2*, 1094−1101. (d) Yoneda, K.; Nakano, M.; Fukui, H.; Minami, T.; Shigeta, Y.; Kubo, T.; Botek, E.; Champagne, B. *ChemPhysChem* **2011**, *12*, 1697−1707.

(4) Kamada, K.; Ohta, K.; Kubo, T.; Shimizu, A.; Morita, Y.; Nakasuji, K.; Kishi, R.; Ohta, S.; Furukawa, S.; Takahashi, H.; Nakano, M. *Angew. Chem., Int. Ed.* **2007**, *46*, 3544−3546.

(5) Koide, T.; Furukawa, K.; Shinokubo, H.; Shin, J.-Y.; Kim, K. S.; Kim, D.-H.; Osuka, A. *J. Am. Chem. Soc.* **2010**, *132*, 7246−7247.

(6) (a) Pathenopoulos, D. A.; Rentzepis, P. M. *Science* **1989**, *245*, 843−845. (b) Zhou, W.; Kuebler, S. M.; Braun, K. L.; Yu, T.; Cammack, J. K.; Ober, C. K.; Perry, J. W.; Marder, S. R. *Science* **2002**, *296*, 1106−1109. (c) Pawlicki, M.; Collins, H. A.; Denning, R. G.; Anderson, H. L. *Angew. Chem., Int. Ed.* **2009**, *48*, 3244−3266. (d) Frederiksen, P. K.; Jøgensen, M.; Ogilby, P. R. *J. Am. Chem. Soc.* **2001**, *123*, 1215−1221.

(7) Chikamatsu, M.; Mikami, T.; Chisaka, J.; Yoshida, Y.; Azumi, R.; Yase, K. *Appl. Phys. Lett.* **2007**, *91*, 043506.

(8) Morita, Y.; Nishida, S.; Murata, T.; Moriguchi, M.; Ueda, A.; Satoh, M.; Arifuku, K.; Sato, K.; Takui, T. *Nat. Mater.* **2011**, *10*, 947−951.

(9) (a) Son, Y. W.; Cohen, M. L.; Louie, S. G. *Nature* **2006**, *444*, 347−349. (b) Son, Y. W.; Cohen, M. L.; Louie, S. G. *Phys. Rev. Lett.* **2006**, *97*, 216803. (c) Kim, W. Y.; Kim, K. S. *Nat. Nanotechnol.* **2008**, *3*, 408−412.

(10) (a) Kolc, J.; Michl, J. *J. Am. Chem. Soc.* **1970**, *92*, 4147−4148. (b) Iwashita, S.; Ohta, E.; Higuchi, H.; Kawai, H.; Fujiwara, K.; Ono, K.; Takenaka, M.; Suzuki, T. *Chem. Commun.* **2004**, 2076−2077. (c) Shimizu, A.; Tobe, Y. *Angew. Chem., Int. Ed.* **2011**, *50*, 6906−6910.

(11) (a) Thiele, J.; Balhorn, H. *Chem. Ber.* **1904**, *37*, 1463. (b) Flynn, C. R.; Michl, J. *J. Am. Chem. Soc.* **1974**, *96*, 3280−3288. (c) Chase, D. T.; Rose, B. D.; McClintock, S. P.; Zakharov, L. N.; Haley, M. M. *Angew. Chem., Int. Ed.* **2011**, *50*, 1127−1130.

(12) (a) Reid, D. H. *Chem. Ind.* **1956**, 1504−1505. (b) Gerson, F. *Helv. Chim. Acta* **1966**, *49*, 1463−1472. (c) Goto, K.; Kubo, T.; Yamamoto, K.; Nakasuji, K.; Sato, K.; Shiomi, D.; Takui, T.; Kubota, M.; Kobayashi, T.; Yakusi, K.; Ouyang, J.-Y. *J. Am. Chem. Soc.* **1999**, *121*, 1619−1620. (d) Itkis, M. E.; Chi, X.; Cordes, A. W.; Haddon, R. C. *Science* **2002**, *296*, 1443−1445.

(13) (a) Ohashi, K.; Kubo, T.; Masui, T.; Yamamoto, K.; Nakasuji, K.; Takui, T.; Kai, Y.; Murata, I. *J. Am. Chem. Soc.* **1998**, *120*, 2018−2027. (b) Kubo, T.; Sakamoto, M.; Akabane, M.; Fujiwara, Y.; Yamamoto, K.; Akita, M.; Inoue, K.; Takui, T.; Nakasuji, K. *Angew. Chem., Int. Ed.* **2004**, *43*, 7474−6479. (c) Kubo, T.; Shimizu, A.; Sakamoto, M.; Uruichi, M.; Yakushi, K.; Nakano, M.; Shiomi, D.; Sato, K.; Takui, T.; Morita, Y.; Nakasuji, K. *Angew. Chem., Int. Ed.* **2005**, *44*, 6564−6568. (d) Shimizu, A.; Uruichi, M.; Yakushi, K.; Matsuzaki, H.; Okamoto, H.; Nakano, M.; Hirao, Y.; Matsumoto, K.; Kurata, H.; Kubo, T. *Angew. Chem., Int. Ed.* **2009**, *48*, 5482−5486. (e) Shimizu, A.; Kubo, T.; Uruichi, M.; Yakushi, K.; Nakano, M.; Shiomi, D.; Sato, K.; Takui, T.; Hirao, Y.; Matsumoto, K.; Kurata, H.; Morita, Y.; Nakasuji, K. *J. Am. Chem. Soc.* **2010**, *132*, 14421−14428. (f) Shimizu, A.; Hirao, Y.; Matsumoto, K.; Kurata, H.; Kubo, T.; Uruichi, M.; Yakushi, K. *Chem. Commun.* **2012**, *48*, 5629−5631.

(14) Kubo, T.; Yamamoto, K.; Nakasuji, K.; Takui, T.; Murata, I. *Angew. Chem., Int. Ed. Engl.* **1996**, *35*, 439−441.

(15) Konishi, A.; Hirao, Y.; Nakano, M.; Shimizu, A.; Botek, E.; Champagne, B.; Shiomi, D.; Sato, K.; Takui, T.; Matsumoto, K.; Kurata, H.; Kubo, T. *J. Am. Chem. Soc.* **2010**, *132*, 11021−11023.

(16) (a) Sun, Z.; Huang, K.-W.; Wu, J. *J. Am. Chem. Soc.* **2011**, *133*, 11896−1199. (b) Li, Y.; Heng, W.-K.; Lee, B. S.; Aratani, N.; Zafra, J. L.; Lee, R.; Young, M. S.; Sun, Z.; Huang, K.-W.; Webster, R. D.;

Lopez Navarrette, J. T.; Kim, D.; Osuka, A.; Casado, J.; Ding, J.; Wu, J. *J. Am. Chem. Soc.* **2012**, DOI: 10.1021/ja304618v.

(17) (a) Chichibabin, A. E. *Chem. Ber.* **1907**, *40*, 1810. (b) Sloan, G. J.; Vaughan, W. R. *J. Org. Chem.* **1957**, *22*, 750−761. (c) Morozova, D. I.; Dyatkina, E. M. *Russ. Chem. Rev.* **1968**, *37*, 377−391. (d) Montgomery, L. K.; Huffman, J. C.; Jurczak, E. A.; Grendze, M. P. *J. Am. Chem. Soc.* **1986**, *108*, 6004−6011. (e) Porter, W. W., III; Vaid, T. P.; Rheingold, A. L. *J. Am. Chem. Soc.* **2005**, *127*, 16559−16566.

(18) (a) Bent, H. E.; Gould, R. G., Jr. *J. Am. Chem. Soc.* **1935**, *57*, 1217. (b) Platz, M. S. In *Diradical*; Borden, W. T., Ed.; Wiley: New York, 1982; pp 195−258. (c) McConnell, H. M. *J. Chem. Phys.* **1960**, *33*, 1868−1869.

(19) (a) Popp, F.; Bickelhaupt, F.; Maclean, C. *Chem. Phys. Lett.* **1978**, *55*, 327−330. (b) Sartorius, R.; Brauer, H.-D. *Angew. Chem., Int. Ed. Engl.* **1972**, *11*, 531−532.

(20) Ballester, M.; Pascual, I.; Carreras, C.; Vidal-Gancedo, J. *J. Am. Chem. Soc.* **1994**, *116*, 4205−4210.

(21) (a) Koelsch, C. F. *J. Am. Chem. Soc.* **1957**, *79*, 4439−4441. (b) Theilacker, W.; Schulz, H.; Baumgarte, U.; Drossier, H. G.; Rohde, W.; Thater, F.; Uffman, H. *Angew. Chem.* **1957**, *69*, 332. (c) Kuhn, R.; Neugebauer, F. A. *Monatsh. Chem.* **1964**, *95*, 322−333. (d) Ballester, M.; Riera-Figueras, J.; Castaner, J.; Badfa, C.; Monso, J. M. *J. Am. Chem. Soc.* **1971**, *93*, 2215−2225.

(22) (a) Mills, N. S.; Malandra, J. L.; Burns, E. E.; Green, A.; Unruh, K. E.; Kadlecek, D. E.; Lowery, J. A. *J. Org. Chem.* **1997**, *62*, 9318−9322. (b) Mills, N. S. *J. Am. Chem. Soc.* **1999**, *121*, 11690−11696. (c) Mills, N. S.; Benish, M. M.; Ybarra, C. *J. Org. Chem.* **2002**, *67*, 2003−2012. (d) Mills, N. S.; Tirla, C.; Benish, M. A.; Rakowitz, A. J.; Bebell, L. M.; Hurd, C. M. M.; Bria, A. L. M. *J. Org. Chem.* **2005**, *70*, 10709−10716. (e) Mills, N. S.; Llagostero, K. B.; Tirla, C.; Gordon, S.; Carpenetti, D. *J. Org. Chem.* **2006**, *71*, 7940−7946.

(23) (a) Clar, E. *Chem. Ber.* **1948**, *81*, 52−63. (b) Kuroda, H. *J. Chem. Soc.* **1960**, 1856−1857. (c) Arabei, S. M.; Pavich, T. A. *J. Appl. Spectrosc.* **2000**, *67*, 236−244.

(24) Zhang, K.; Huang, K.-W.; Li, J.; Luo, J.; Chi, C.; Wu, J. *Org. Lett.* **2009**, *11*, 4854−4857.

(25) Crystallographic data for **1-CS**: The asymmetric unit contains two molecules of $C_{35}H_{34}$ (**1-CS**) and three dichloromethane solvent, $C_{73}H_{74}Cl_6$. Triclinic, space group *P*-1; a = 11.7349(19) Å, b = 15.925(3) Å, c = 19.034(3) Å, α = 99.153(4)°, β = 103.775(4)°, γ = 105.180(3)°; V = 3239.8(9) Å^3; Z = 2; ρ_{calcd} = 1.193 Mg/m^3; R_1 = 0.1258 ($I > 2\sigma(I)$), wR_2 = 0.3605 (all data). The *t*-butyl group and the DMC had very large thermal parameters, indicating large thermal motion or loose packing. One of the *t*-butyl groups was treated as disorder to account for the thermal parameters. Restraints in bond distances were applied to the atoms of the *t*-butyl groups and the DCM. These restraints were applied so that the final refinement cycles can converge and result in reasonable bond geometry.

(26) Wu, J.; Pisula, W.; Müllen, K. *Chem. Rev.* **2007**, *107*, 718−747.

(27) (a) Zhai, L.; Shukla, R.; Rathore, R. *Org. Lett.* **2009**, *11*, 3437−3440. (b) Zhai, L.; Ruchi, S.; Shriya, H. W.; Rathore, R. *J. Org. Chem.* **2010**, *75*, 4748−4760. (c) Navale, T. S.; Thakur, K.; Rathore, R. *Org. Lett.* **2011**, *13*, 1634−1637.

(28) Yanai, T.; Tew, D.; Handy, N. *Chem. Phys. Lett.* **2004**, *393*, 51−57.

(29) Müller, U.; Baumgarten, M. *J. Am. Chem. Soc.* **1995**, *117*, 5840−5850.

(30) Teki, Y.; Miyamoto, S.; Nakatsuji, M.; Miura, Y. *J. Am. Chem. Soc.* **2001**, *123*, 294−305.

(31) Ikuhiro, N.; Masaki, S.; Tamejiro, H. *Angew. Chem., Int. Ed.* **2009**, *48*, 7573−7576.

(32) The electrolysis has been conducted for a long time (>1 week). However, 100% conversion was still not achievable. The separation of the cyclodehydrogenation product (possibly **1-CS-closed**) from the starting materials was not so successful at the moment because of their nearly same polarity on silica gel column. Further studies on the cyclodehydrogenation reaction of **1-CS** by electrochemical, chemical, and photochemical methods are underway in our laboratories.

(33) (a) Olah, G. A.; Schlosberg, R. H. *J. Am. Chem. Soc.* **1968**, *90*, 2726−2727. (b) Montgomery, L. K.; Huffman, J. C.; Jurczak, E. A.; Grendze, M. P. *J. Am. Chem. Soc.* **1986**, *108*, 6004−6011. (c) Malandra, J. L.; Mills, N. S.; Kadlecek, D. E.; Lowery, J. A. *J. Am. Chem. Soc.* **1994**, *116*, 11622−11623. (d) Dahl, B. J.; Mills, N. S. *J. Am. Chem. Soc.* **2008**, *130*, 10179−10186. (e) Piekarski, A. M.; Mills, N. S.; Yousef, A. *J. Am. Chem. Soc.* **2008**, *130*, 14883−14890.

(34) (a) Deno, N. C.; Jaruzelski, J. J.; Schriesheim, A. *J. Org. Chem.* **1954**, *19*, 155−167. (b) Deno, N. C.; Jaruzelski, J. J.; Schriesheim, A. *J. Am. Chem. Soc.* **1955**, *77*, 3044−3051. (c) Olah, G. A.; Prakash, G. K. S.; Liang, G.; Westerman, P. W.; Kunde, K.; Chandrasekhar, J.; Schleyer, P. v. R. *J. Am. Chem. Soc.* **1980**, *102*, 4485−4492.

(35) (a) Casado, J.; Patchkovskii, S.; Zgierski, M. Z.; Hermosilla, L.; Sieiro, C.; Moreno Oliva, M.; López Navarrete, J. T. *Angew. Chem., Int. Ed.* **2008**, *47*, 1443−1446. (b) Ortiz, R. P.; Casado, J.; Hernandez, V.; Navarrete, J. T. L.; Viruela, P. M.; Ortí, E.; Takimiya, K.; Otsubo, T. *Angew. Chem., Int. Ed.* **2007**, *46*, 9057−9061. (c) Ortiz, R. P.; Casado, J.; Rodríguez González, S.; Hernández, V.; Navarrete, J. T. L.; Viruela, P. M.; Ortí, E.; Takimiya, K.; Otsubo, T. *Chem.-Eur. J.* **2010**, *16*, 470−484. (d) Casado, J.; Navarrete, J. T. L. *Chem. Rec.* **2011**, *11*, 45−53.

(36) (a) Karpiuk, J.; Grabowskiv, Z. R. *Chem. Phys. Lett.* **1989**, *160*, 451−456. (b) Giacobbe, E. M.; Mi, G, Q.; Colvin, M. T.; Cohen, B.; Ramana, A.; Scott, A. M.; Yeganeh, S.; Marks, T. J.; Ratner, M. A.; Wasielewski, M. R. *J. Am. Chem. Soc.* **2009**, *131*, 3700−3712. (c) Colvin, M. T.; Smeigh, A. L.; Giacobbe, E. M.; Conron, S. M. M.; Ricks, A. B.; Wasielewski, M. R. *J. Phys. Chem. A* **2011**, *115*, 7538−7538. (d) Colvin, M. T.; Giacobbe, E. M.; Cohen, B.; Miura, T.; Scott, A. M.; Wasielewski, M. R. *J. Phys. Chem. A* **2010**, *114*, 1741−1748. (e) Ishii, K.; Hirose, Y.; Fujitsuka, H.; Ito, O.; Kobayashi, N. *J. Am. Chem. Soc.* **2001**, *123*, 702−708.

(37) Hui, Y.; Chng, E. L. K.; Chng, C. Y. L.; Poh, H. L.; Webster, R. D. *J. Am. Chem. Soc.* **2009**, *131*, 1523−1534.

(38) (a) Lee, C.; Yang, W.; Parr, R. G. *Phys. Rev. B* **1988**, *37*, 785−789. (b) Becke, A. D. *J. Chem. Phys.* **1993**, *98*, 5648−5652. (c) Ditchfie, R. W.; Hehre, J.; Pople, J. A. *J. Chem. Phys.* **1971**, *54*, 724−728. (d) Hehre, W. J.; Ditchfie, R.; Pople, J. A. *J. Chem. Phys.* **1972**, *56*, 2257−2261. (e) Harihara, P. C.; Pople, J. A. *Theor. Chim. Acta* **1973**, *28*, 213−222.